The transmission of chromatin and DNA lesions by sperm and their fate in the zygote

Alwin Derijck & Godfried van der Heijden

Alwin Derijck & Godfried van der Heijden

The transmission of chromatin and DNA lesions by sperm and their fate in the zygote

Thesis Radboud University Nijmegen 2007

ISBN: 978-90-9022243-1

Lay out:
Alwin Derijck & Godfried van der Heijden

Cover concept:
Godfried van der Heijden

Cover illustration:
Alwin Derijck

The cover depicts a germline genome skipping on the somatic sea through time.

Printed by:
PrintPartners Ipskamp B.V., Enschede

The transmission of chromatin and DNA lesions by sperm and their fate in the zygote

Een wetenschappelijke proeve op het gebied van de Medische Wetenschappen

Proefschrift

Ter verkrijging van de graad van doctor
aan de Radboud Universiteit Nijmegen
op gezag van de Rector Magnificus prof. mr. S.C.J.J. Kortmann,
volgens het besluit van het College van Decanen
in het openbaar te verdedigen op donderdag 1 november 2007
des namiddags om 14:00 uur precies

door

Alwin Adrianus Hendricus Antonius Derijck & **Godfried Willibrord van der Heijden**

Geboren op 22 augustus 1978 te Roosendaal en Nispen

Geboren op 9 mei 1977 te Geldrop

Promotor:
prof. dr. J.A.M. Kremer

Co-promotor:
dr. P. de Boer

Manuscriptcommissie:
prof. dr. B. Wieringa (voorzitter)
prof. dr. A. Geurts van Kessel
dr. W.M. Baarends (Erasmus MC Rotterdam)

CONTENTS

Section 1

Introduction

Relevance

In 2005 of all Dutch children conceived, around one in 40 originated from artificial reproductive techniques (ART). The main reason for using ART to procreate is obvious: infertility does not allow and subfertility hampers natural conception. The causes of hampered fertility are numerous and can stem from either the female, the male or both. In case of male sub- and infertility there is evidence that sperm contains an increased level of DNA lesions and a higher incidence of aberrant chromatin conformations.
Research presented in this thesis is aimed at investigating the paternal contribution to the zygote, particularly the chromatin composition of the nucleus and the incidence of double strand DNA breaks and their interaction with maternally driven chromatin remodeling and DNA repair. Therefore a division between the transmission of sperm chromatin and the transmission of DNA breaks has been made in this thesis. Part of our work was focused on effects of sperm DNA damage on long term genomic stability.

Introduction

We all were zygotes once. Just prior to this state we could be traced back to two gametes, an oocyte and a spermatozoon, which were produced by our parents, who were also zygotes once. Sexually reproductive organisms form germ cells that fuse and give rise to a newborn, which will in turn produce germ cells. This repetitive cycle ensures our existence, as a species, through time (Fig. 1).

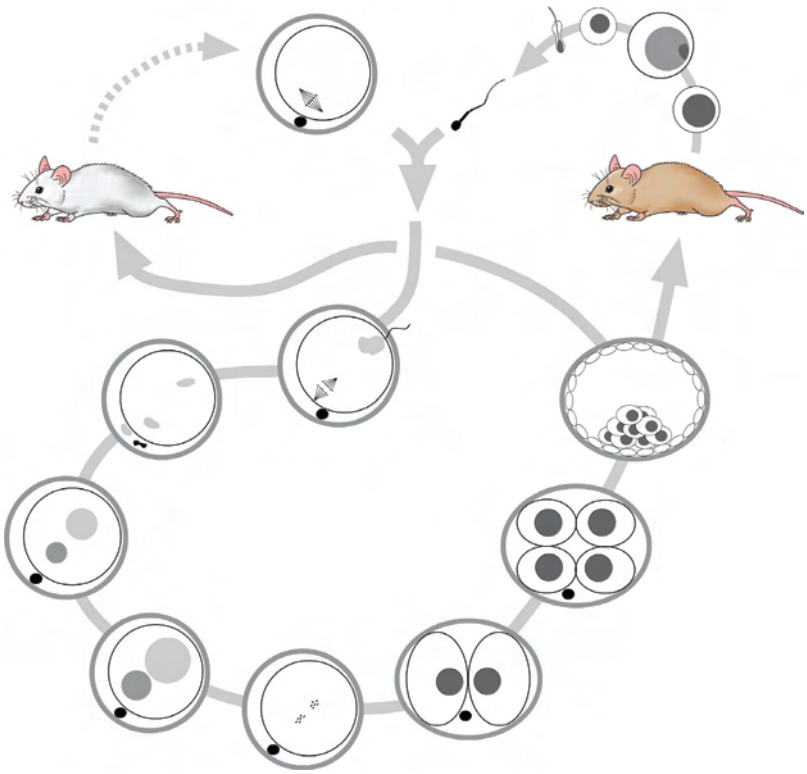

Figure 1 Perennial propagation of genomes

Gametogenesis results in production of oocytes (upper left) or sperm (upper right). Fusion of these gametes yields a 1-cell embryo, the zygote. During most of the first cell cycle the parental pronuclei remain separate. Fusion of the genomes occurs after chromosome condensation. During pre-implantation development successive cleavage divisions occur. Eventually, after implantation and gestation, a newborn is produced. Depending on the sex of the newborn it will produce oocytes or sperm.

Section 1.1 Male germ line

In the male gonad, the testis, a continues production of sperm takes place. Spermatogenesis, the differentiation and maturation process by which stem cell spermatogonia eventually yield sperm, can be divided in three distinct phases: i) mitotic proliferation, ii) meiosis iii) spermiogenesis (Fig. 2A). In mice the time between the first differentiation step of a spermatogonia until the release of the sperm into the lumen of the seminiferous tubules is approximately 34.5 days[1]. Constant proliferation of germ cells for continuity of spermatogenesis is provided by the first part. After a final round of DNA replication primary spermatocytes enter into meiosis. During meiosis reciprocal exchange of genetic material between the parental homologs takes place, after which two subsequent divisions occur (Fig. 2B). The first division reduces the ploidy of the germ cell, which is necessary to cope with ploidy doubling at fertilization, and yields two secondary spermatocytes each containing a haploid set of chromosomes consisting of two chromatids. The second division is mechanistically mitotic and separates the homologous sister chromatids. Eventually each germ cell that enters and survives meiosis gives rise to four haploid spermatids that subsequently start spermiogenesis, during which nuclear and cytoplasmic changes are established.

Meiosis

Meiosis in the male mouse has an approximate duration of 300 hours. During these 12 days the parental chromosomes recombine and the reduction of ploidy takes place. Recombination between the homologous chromosomes is facilitated by the synaptonemal complex (SC), a proteinaceous structure that is assembled in between the homologous chromosomes[2, 3] (Fig. 2C). The SC functions as a platform for recombination nodules, which are protein complexes involved in the repair of meiotic double strand breaks leading to recombination. They consist of proteins connected with homologous recombination (HR) and mismatch repair (MMR)[4, 5].
Synapsis of chromosomes is primarily based on DNA sequence homology. The heteromorphic sex chromosomes of the male germ cell exhibit homologous synapsis in the pseudo autosomal region (PAR), where sequence homology is conserved only. In the labora-

tory mouse this region is around 0.7 Megabase (Mb)[6] while the X and Y chromosome contain around 165 and 60 Mb respectively. After assembly of the SCs of autosomal bivalents, the sex chromosomes become temporarily synapsed over a greater distance than the PAR. This heterologous synapsis can extend to 70% of the length of the Y chromosome. An incomplete SC is observed in this domain and as meiosis progresses the incomplete SC disassembles, though a fully assembled SC remains present at the PAR, where recombination will occur. The analysis of prophase I in mice carrying chromosomal translocations revealed that non-homologous sequences are sometimes able to synapse. In this situation the formation of a complete SC occurs through synaptic adjustment. Study of this phenomenon in the *T70H/T1WA* translocation mouse (described in section 2.1) clearly showed a positive effect of the quantity of surrounding homologous sequences on heterologous synapsis of interspliced domains[7, 8].
To study meiotic progression in detail, the morphology of the SC is a valuable tool to determine first meiosis prophase sub stages. Prophase of meiosis I is divided in four phases characterized by the preparation for and appearance, presence and disappearance of the SC (Fig. 2C). Staining of SC proteins therefore is frequently used to determine the classical first meiotic prophase sub-stages of a primary meiocyte, namely leptotene, zygotene pachytene and diplotene.

MSUD/MSUC/MSCI

Meiotic pairing, hence synapsis of chromosomes is based on sequence homology. In several phyla mechanisms have evolved that check pairing and inactivate chromatin domains or specific DNA sequences. This type of quality assurance mechanism has as a common denominator: it is triggered by perturbations of the alignment of "homologous" DNA. In mammals (human and mouse) and nematodes (*Caenorhabditis elegans*), this control mechanism is referred to as Meiotic Silencing of Unpaired Chromatin or MSUC. MSUC induces silencing at a transcriptional level[11, 12]. In mammals MSUC is thought to hamper meiotic differentiation by termination of gene transcription, eventually resulting in apoptosis[12]. Through the action of MSUC germ cells with an aberrant chromosomal constitution in principle can be removed on basis of failure of synapsis, although

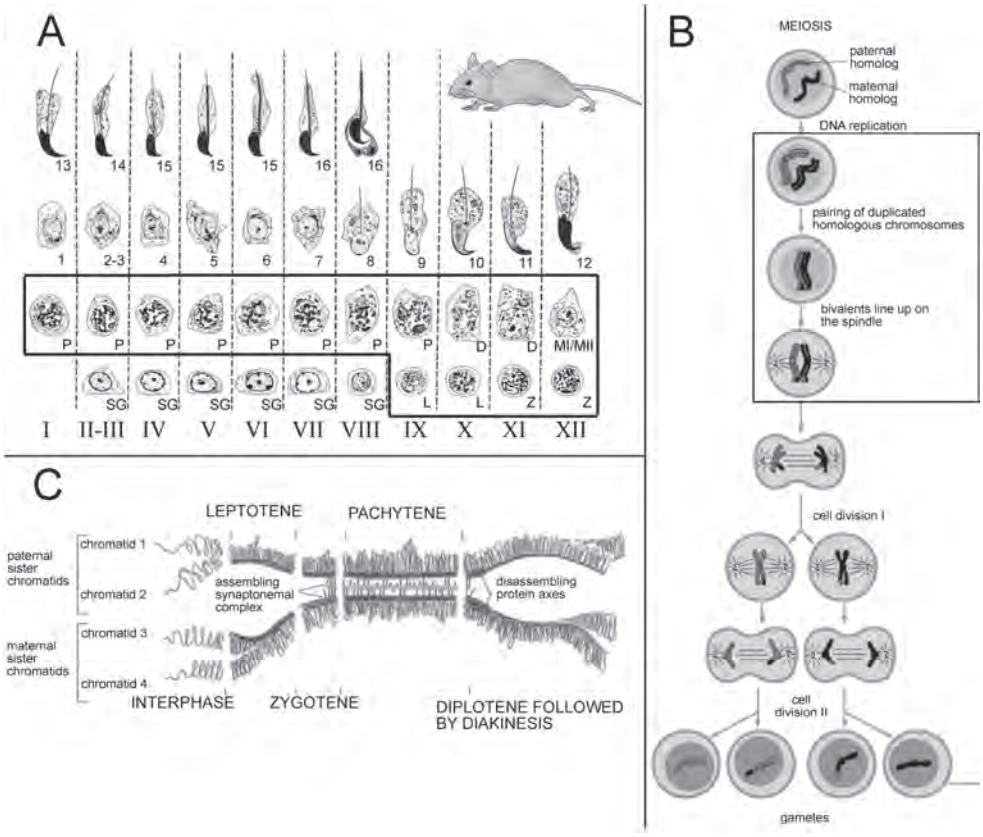

Figure 2 Overview of spermatogenesis, meiosis and prophase I
A. Schematic representation of spermatogenesis (mouse), which encompasses mitotic proliferation and differentiation of spermatogonia (SG), a final round of replication (pre-L), meiosis and spermiogenesis. Meiosis is indicated in the box and comprises the stages leptotene (L), zygotene (Z), pachytene (P), diplotene (D) and the meiotic divisions (MI/MII). Spermiogenesis is divided in 16 stages, based on the formation of the acrosome. A total of twelve differently composed germ cell populations in seminiferous tubules can be observed (roman numerals). is adapted from [9].
B. Pairing, recombination and subsequent cell divisions during meiosis. Figure adapted from[10].
C. The meiotic sub stages of prophase I coincide with the status of the synaptonemal complex. Figure adapted from[10].

through the existence of germ cells as symplasts, this could be circumvented in individual cases. This control mechanism is bypassed when heterologous synapsis is achieved[7, 13, 14].
In nematodes, MSUC also inactivates transcription of unsynapsed domains but does not always induce apoptosis. Other differences between mammalian and nematode MSUC show the two mechanisms to be distinct but with some striking similarities[12].
A different meiotic defense mechanism is functional in the slime mold *Neurospora crassa*. This organism, like mammals and nematodes, silences DNA sequences that remain unpaired. However, identical but paired DNA sequences are also silenced [15]. Silencing in *N. crassa* is a post transcriptional phenomenon and its strategy (termed Meiotic Silencing of Unpaired DNA, MSUD) is therefore functionally different from MSUC. Because MSUD can detect abnormalities at the level of DNA pairing it is able to silence specific DNA sequences such as transposons. Such a mechanism is irreconcilable with the structural variety found in individual mouse and human genomes[16]. MSUC detects abnormalities at the level of chromosome synapsis. Since heterologous synapsis in mammalian meiosis can extend over many megabases[8], it is more likely a defense against aneuploid gametes that could arise from asynapsis or early desynapsis[17].

MSUC would be a priori incompatible with the mammalian male karyotype, in which two highly non-homologous sex chromosomes are present, if adaptation had not occurred. Already in 1898 a dense chromatin mass in the nuclei of mammalian spermatocytes was described[18]. Further study showed that this chromatin mass contained the sex chromosomes[19]. It appeared that during the zygotene–pachytene transition (Fig. 1) the sex chromosomes form a chromatin domain that becomes excluded from autosomal chromatin. After the formation of the XY body, XY-linked transcription ceases. This process has been termed Meiotic Sex Chromosome Inactivation (MSCI) and was described prior to MSUD and MSUC[11]. MSCI and MSUC seem to be the result of an identical molecular cascade: the multitask tumor suppressor protein BRCA1 localizes to unsynapsed regions and attracts the PI3 kinase-like kinase ATR, which in turn phosphorylates histone H2AX[20] (BOX 2). Several proteins and post translational histone modifications (BOX 1) have been described that are enriched in MSUC-subjected domains as well as in

Box 1. Chromatin

The DNA in a cell nucleus is tightly associated with numerous proteins that assist its organization, safeguard its integrity, regulate its accessibility, and facilitate its replication. This DNA-protein amalgam is termed chromatin and its composition is heterogeneous and dynamic[25-27]. The basic recurring chromatin structure and building block is the well defined nucleosome[28, 29].

The nucleosome harbours a protein complex consisting of four different histone proteins (H2A, H2B, H3 and H4) that are each present twice. Approximately 150 base pairs are folded around this protein complex. Initially the general idea was that the nucleosome solely fulfils an organizing role. The discovery that the nucleosomal conformation is transcriptionally repressive changed this idea, apparently the nucleosome not only organizes the DNA but also influences gene transcription. Research of the last two decades showed that the nucleosome is a crucial player in all cellular processes in which nuclear DNA takes part[30, 31].

The main mechanisms by which the nucleosome influences DNA-related processes are the blocking of targeting sequences and the binding of transcriptional regulators. Both ways of influencing DNA-related processes have their own actors: covering or disclosure of a DNA sequence is facilitated by the ATP-dependent chromatin remodeling machinery[32-35], whereas binding sites are formed by histone modifying complexes[36, 37].

Specific amino acids in proteins can be modified by covalent attachment of small groups (acetyl, phosphoryl, methyl) or peptides (ubiquitin, Sumo, Ned). Their attachment to histones can create binding sites for other proteins or change physical properties of the nucleosome. The effect of a modification that will prevail is dictated by its chromatin-context[38-42]. These modifications add another layer of possibilities to fine-tune the molecular machinery implicated in DNA function regulation.

The research aimed at elucidating the function of histone modifications has yielded appreciable understanding of the impact of several modifications in a context and organism specific way. It has lead to

the proposal of the "histone code hypothesis" which states that a certain combination of histone modifications will induce a certain action[43, 44]. Proceeding scientific work indicates that the strictness of the term "code" seems less appropriate than initially thought[39, 40].

While the post-translational modifications mostly decorate the outside of the nucleosome, interior nucleosome-alterations are facilitated by the existence of histone variants[45-47]. The differences between subtypes can be significant or limited to a few amino acid changes. Assembly of a nucleosome with one of these histone variants can change the physical structure of the nucleosome, reflected by the strength by which it binds the DNA, the stability of the nucleosome structure and the rigidity of the chromatin polymer. Also potential modification sites can be added, all depending on which variant is incorporated.

the XY body[12]. Although the molecular mechanisms behind MSUC and MSCI seem highly similar if not identical, they aim at opposite goals. MSUC will induce elimination of meiocytes containing segments of unsynapsed chromatin while MSCI is an absolute necessity for male meiosis[13, 14, 21, 22]. MSCI is solely part of mammalian male meiosis while MSUC functions in meiosis of both sexes[12, 23].
At least one clear difference between MSUC occurring in female meiosis and MSCI exists: during female meiosis unsynapsed and subsequently silenced chromatin is not compartmentalized as the XY body is during male meiosis.
Possibly the molecular action of MSUC/MSCI is diffuse and can affect transcription of surrounding synapsed chromatin. If so this will contribute to demise of wrongfully synapsed primary oocytes but it will be intolerable for normal MSCI-undergoing spermatocytes. Formation of a separate chromatin domain to which MSCI is confined could overcome this. MSCI might be a compartmentalized form of MSUC to which the spermatocyte has adapted[24].

Spermiogenesis

After reduction of ploidy during meiosis, the germ cell enters spermiogenesis, a phase of morphological differentiation and maturation, which eventually renders the sperm. During this last phase of spermatogenesis a nuclear overhaul takes place, eventually replacing nucleosomes (BOX 1) by protamines[48]. Prior to their removal the nucleosomes become hyperacetylated, which lowers the degree of nucleosomal compaction and the strength of the DNA-histone interaction. Likely, histone hyperacetylation facilitates nucleosome removal during spermiogenesis[48]. During nuclear elongation of the spermatid the nucleosomes are gradually replaced by Transition Protein 1 and 2 (TPs), which in turn are subsequently replaced by protamines[48, 49].

The morphology of the spermatid nucleus and the acrosome (a Golgi-like structure that forms anterior of the sperm nucleus) are used to classify the stage of seminiferous tubules. In the mouse a total of 16 distinct types of spermatid nuclear morphology exist. The first eight and last four stages have an overlapping presence in the semi-

niferous tubules (Fig. 2A). Spermatogenesis is therefore subdivided in 12 stages (usually numbered in roman numerals). Since spermatogenesis is a continuous process, every seminiferous tubule at any stage will in time also contain all progenitor stages (Fig. 2A).

The hallmark of sperm chromatin is the packing of DNA with protamines. Protamines were discovered more than a century ago[50] and although the precise packing of the DNA in the sperm nucleus is not conclusively established, a generally accepted congruent model exists. Protamines are relatively small proteins with a high arginine content, which renders them positively charged. The current model proposes that the central polyarginine stretch in the protamine protein binds the minor groove of the DNA helix, thereby neutralizing the negative charge of the DNA[51]. The presence of several cysteine residues allows formation of inter- and intra-protamine disulfide bridges[51]. Since DNA looses its supercoil at the nucleosome to protamine transition, arrays of the DNA-protamine polymer can stack on top of each other. The basic unit of nucleoprotamine is a single toroid structure (donut) that contains 50 kb. An estimated 100-200 of these toroids are grouped together in a globular structure of 500 nm. The 500 nm structures are grouped by two, resulting in a 1000 nm structure[52-54].

The protamine-DNA polymer serves multiple functions. The reduction in size of the sperm nucleus enables the formation of its hydrodynamic shape, facilitating the journey through the reproductive tract. Furthermore, the highly compacted DNA-protamine structure renders sperm radioresistant[55] and makes it less susceptible to other DNA damaging agents like reactive oxygen species. The downside of this streamlined state is the overall shutdown of genomic repair mechanisms after protamine-induced compaction (at stage XII of spermatogenesis, some 2 weeks prior to ejaculation), as the gain in compaction results in loss of DNA accessibility[56, 57]. DNA repair mechanisms engaged in genome maintenance prior to this moment mainly encompass BER while the status of NER is under debate (BOX 3) [58-60].
DNA lesions left unrepaired or acquired during this repair deprived state can be deemed as premutational lesions which are transferred to the zygote upon gamete fusion[61].

Similarities and differences in the sperm nuclei of mice and man

The blueprint of the nuclear anatomy of mouse and human sperm is quite similar. In both species the telomeres are positioned in the periphery of the nucleus whereas the centromeres are contained in the centre[62-64]. In the human the 1000 nm nucleoprotamine fibre travels from the telomere on one side of the chromosome to the centromere and folds back 180°, aligning the fibre of the two arms[53]. In both species individual chromosomes have a favoured intranuclear position[53, 64, 65].

The major difference chromatin-wise, is the degree of protamination. Human sperm stands out in the high amount of nucleosomal DNA when compared to other mammals. An estimated 15% of the genome is contained in a nucleosomal configuration in human sperm whereas this is in the range of 1% for boar, bull and rodents[66-68].

Especially structural domains such as centromeres and telomeres retain a nucleosomal conformation[69-71]. In addition also retroposon and repeat sequences show higher concentrations of nucleosomal DNA. Some studies have assessed the variation in chromatin conformation (nucleosomal or nucleoprotamine) for specific DNA sequences in human sperm. This appeared to be strikingly small, not only in sperm of one individual but also in sperm of more individuals[70, 71].

These data suggest that protamination of the genome is a coordinated process. It is likely that this sequence specific packaging of the genome facilitates the formation of the sperm nucleus, or, if it has a crucial role post sperm penetration, is at least compatible with its formation. Analysis of histone modifications present in human sperm identified acetylated isoforms of histone H4[66]. The relevance of these modifications is unknown. They could be a mere leftover from the hyperacetylation occurring during spermiogenesis but it is tempting to speculate that these modified nucleosomes are instrumental in the transition of the sperm nucleus after gamete fusion. In mouse sperm, modified nucleosomes are also present. The nucleosomal chromatin fraction is concentrated in the chromocentre and specific histone modifications are retained in this region (H4K8ac and H4K12ac)[72]. Possibly this could underlie the rapid decondensa-

tion of the chromocentre after gamete fusion[73].

Common abnormalities in sperm of sub-fertile males

Transgenic mice harboring an avian protamine (Prm) transgene have less compacted chromatin due to an altered chromatin configuration. However, these alterations do not disrupt pronucleus formation and preimplantation development[74]. These early findings already demonstrated the subtlety of chromatin compaction during spermiogenesis and the generation of protamine deficient mouse models confirmed that mouse spermiogenesis is sensitive for alterations of protamine ratios [75]. Heterozygosity for either one of the Prm1 or Prm2 genes results in a total reproductive block[75] and the haploinsufficiency correlated with sperm DNA damage [76]. Preimplantation embryos derived from Protamine 2 deficient sperm after ICSI showed a developmental block. Due to fragmentation of the paternal genome, only a few were able to develop to the blastocyst stage [76]. In man, research on the relation between spermiogenesis and infertility has been performed [reviewed in [77]]. In 1988, the first description of altered protamine ratio's in infertile patients with abnormal seminal parameters was reported [78]. Increased histone content coincides with abnormal protamine ratios[79] and is often caused by reduced levels of protamine 2. Sperm selected for normal morphology and mobility, derived from oligozoo- and asthenozoospermic semen samples, retained altered protamine ratios [80]. Reduced DNA integrity in human sperm with protamine abnormalities confirms the protective role of properly structured sperm chromatine for the genetic integrity of the male gamete[81, 82] and developmental potential after gamete fusion [83, 84].

Mice partially defective for transition nuclear proteins (TP) 1 and 2 showed a progressive decline in sperm nuclear quality with epididymal passage [85]. Chromosomes at first cleavage division derived from TP hampered cauda epididymal sperm showed an increased frequency of chromosome abnormalities further demonstrating that altered spermiogenesis results in an increase of DNA damaged sperm [85]. The decline of sperm quality of these mice was shown to occur in the journey between testis and cauda epididymis [85], a result that was also obtained when using oligospermic carriers of two semi-identical reciprocal translocations in the mouse [86]. Intriguing-

ly, in contrast to the testicular milieu, the epididymal environment is not considered to be hypo-oxygenated[87, 88] warranting interaction with reactive oxygen species. Recently, a similar decline in DNA integrity (i.e. reduced integrity at a more distal site of retrieval) has been observed in man [89].

The etiology of especially human sperm DNA damage is not fully elucidated. Eminently, a correlation with infertility, poor embryo quality and reduced pregnancy rates has been observed [reviewed in [90-92]]. Many assays measuring aspects of sperm chromatin and/or DNA integrity exist. The hallmark of these assays, as is clear from their descriptions (BOX 2), is their qualitative and/or population based nature.

Gamete fusion and everything after

After cytoplasmic fusion of the two highly specialized gametes, the parental chromosomes stay physically separated. Chromatin fusion follows after nuclear "syngamy", at the first cleavage division [93, 94] (a real syngamy does not occur as nuclear envelopes do not fuse but dissolve in one mitotic spindle). The term zygote denotes the cytoplasmic fusion of spermatozoon and oocyte and has distinctive biological differences with a preimplantation embryo [95] although the term 1-cell embryo is commonly used. During the 16-18 hours (in mouse) between cytoplasmic and nuclear fusion, much of the processes that take place serve the purpose to coalesce the two fused gametes into a totipotent 2-cell embryo. For the former sperm nucleus, this mainly concerns chromatin related processes whereas the former oocyte undergoes nuclear and cytoplasmic changes.

Chromatin remodeling at the absolute beginning

Immediately after fusion of the two gametes the transformation of the highly differentiated sperm nucleus begins. The protamines are removed and maternally derived histones are deposited onto the DNA [73, 93, 94, 96]. The precise mechanism by which protamines are removed is unclear. Reduction of the disulfide bridges of the protamines is facilitated by reduced glutathione (GSH) which becomes enriched in the ooplasm during oocyte maturation[93, 94]. Inhibition of the reducing power of glutathione disables decondensation of the sperm nucleus[93].

Chromatin remodeling after gamete fusion has been intensely studied in the African claw frog *Xenopus laevis*. The most abundant nuclear protein present in Xenopus eggs is Nucleoplasmin (Npm2)[97]. This protein is able to bind sperm specific histones present in frog sperm, hence facilitates the decondensation of the sperm nucleus. This function has not been conserved for Npm2 in mouse, likely due to the loss of a specific region (A1 tract) in the N-terminus. However, the presence of such a domain in Npm3 suggests that this protein might be involved in protamine removal and histone deposition. There are indeed indications that this is the case. Preliminary work showed that combined knock down of Npm3 and Nap1 in the zygote results in a failure to load histones on the decondensed DNA[98].
Work on the Drosophila sesame-mutant identified a critical role for HirA protein in early paternal chromatin maturation. HirA is a histone H3.3•H4 specific chaperone that loads this heterodimer onto the paternal DNA, an essential process in reconstituting paternal chromatin [99]. In the mouse zygote, HirA localizes in the decondensing sperm nucleus[73] suggesting an equivalent mechanism.

Protamine removal after gamete fusion is a swift process. At initial decondensation protamines are lost from sperm DNA suggesting this to be a necessity to enable decondensation. This fits the current model for the DNA-protamine polymer[51]. Concurrent with protamine removal, DNA is repacked in histones to uphold a chromatin state capable of protecting the DNA fibre [73]. During finalization of meiosis II, male chromatin morphology is reminiscent of the sperm nucleus: a spherical domain that lacks characteristics of a true nucleus such as the nuclear envelope or nucleolus-like structures. It is approximately three hours after gamete fusion that the male pronucleus (PN) is formed, which has a nuclear envelope and contains non-functional, nucleolus-like structures[73, 100]. The absence of a nuclear envelope around paternal chromatin does not hamper chromatin related processes such as double strand break recognition or post translational modification of histones[73, 101]. Moreover, it is already during this phase that differential maturation of euchromatin versus heterochromatin takes place. In the decondensed sperm chromatin, components of the Polycomb Repressor Complex

BOX 2. Sperm Assays

Nuclear proteins

CMA3
Chromomycin A3 is a compound that binds to DNA in competition with protamines. Hence, increased CMA3 binding, measured by fluorescence, indirectly relates to the amount of DNA bound protamines.

Aniline blue
A dye that stains histones measuring the degree of residual nucleosomes in sperm

Protamine PAGE
Normally fulfilled spermiogenesis results in a fixed ratio between Prm1 and Prm2. Nuclear proteins are isolated from sperm nuclei and separated by polyacrylamide gel electrophoresis (PAGE), which allows for direct quantification of both protamine proteins and the "P1/P2 ratio".

Thiol measurement
Testicular and caput epididymal sperm is fully matured on a protein level. However, during epididymal transfer free thiol (SH) groups in protamines oxidize and form disulphide bridges. This cross-linked state is sturdier and provides better protection for the DNA it enwraps. Hampered protamine cross-linking can be measured by compounds that react with SH groups, like monobromobimane, and provide insight in protamine cross-linking.

DNA damage

SCE
Single Cell Electrophoresis (the Comet Assay) uses the negative charge of DNA to extract small fragments from the nucleus by means of an electric current. After staining the DNA with a fluorescent dye, the fluorescence outside of the nucleus (the comet tail) is measured, giving an arbitrary value of the amount of DNA damage. The neutral variant measures the degree of double strand breaks (DSBs), the alkali variant also includes single strand breaks and al-

kali-labile sites.

TUNEL
Terminal deoxynucleotidyl transferase-mediated dUTP nick end-labeling, is based on the enzymatic addition of fluorescently labelled nucleotides (dUTPs) by the enzyme TdT (Terminal deoxynucleotidyl Transferase) to accessible 3'-OH groups of DNA ends. The measured fluorescence results from DNA ends, or fragments (representing DSBs) but also from single strand breaks. TUNEL has been developed in the apoptosis field (DSBs in abundance) and its sensitivity is entirely inadequate for measuring lower amounts of DSBs per nucleus.

SCSA
Sperm Chromatin Structure Assay, is based on the metachromatic DNA dye Acridine Orange (AO), which fluoresces green when bound to double stranded DNA and red when bound to single stranded DNA and RNA. In SCSA sperm is treated with low pH to denature DNA at the sites of DNA strand breaks, followed by AO staining and fluorescent flow cytometry. The ratio of red and green fluorescence per sperm cell estimates sperm DNA damage and is, on a population basis, indicated by the DFI, or DNA fragmentation index.

SCD
The Sperm Chromatin Dispersion test, also referred to as Halosperm kit, is based upon the principle that normal sperm nuclei after acid denaturation and protein removal, form dispersed DNA loops that extend from the nucleus. Such DNA loops, or halos, do not form in sperm with high amounts of DNA damage.

DBD-FISH
DNA Breakage Detection-FISH. DNA of sperm nuclei trapped in agarose are denatured in an alkaline solution, deproteinized and dehydrated. Areas of single-stranded DNA are generated by the alkaline solution in proportion to the degree of DNA strand breakage. These then act as targets for FISH. Measurement of the amount and surface area of FISH signals provides information on the breakage level in probed areas.

1 (PRC1) localize to the DAPI bright "heterochromatic" chromocentre. During PN formation these proteins remain localized on the rim of the nucleolar-like structure where satellite DNA resides[102].
Histone modifications present in paternal chromatin either stem from sperm derived (transmitted) nucleosomes or from the ooplasm. The latter origin is by far the most prominent one, since a minute quantity of nucleosomes remains in mouse sperm at chromatin remodeling during spermiogenesis. Detailed analysis of histone modifications present in paternal chromatin just after gamete fusion showed that transmission of modified histones does occur, especially in the nucleosome rich chromocentre[72]. In humans, the quantity and therefore the potential of an epigenetic message in paternally inherited nucleosomal chromatin is much greater.
With the exception of mono-methylated histone H3K4 and H4K20, no methylated histone residues have been detected in paternal chromatin during zygotic G1. The hypomethylation of the histones is contrasted by their hyperacetylated state[72, 73, 96]. This probably is a reflection of the volatile character of histone acetylation and the stable nature, thus long-lasting effect, of lysine methylation[39, 40]. During S-phase the paternal chromatin acquires H3K27 methylation and dimethylated H3K9, but at the end of the first cell cycle asymmetry still exists for trimethylated histone H3K9 and H4K20 [103, 104]. These are trademarks of static somatic heterochromatin and therefore likely withheld from paternal chromatin, as part of its reprogramming.
Added to this epigenetic parental asymmetry is the active removal of CpG methyl groups from sperm derived DNA during zygotic G1 and S-phase. Maternal DNA methylation is passively lost through subsequent cell divisions, due to absence of maintenance methyltransferases. The demethylation of the paternal genome is not complete, the modification remains present in heterochromatic regions[103, 105] and some paternally imprinted loci[106]. In parthenogenetic zygotes whith two maternally derived PNs (or gynogenones), active demethylation does not occur[107]. Likely the chromatin composition of the paternal chromatin is permissive for this process. Recently a protein, (Dpc7/Stella) functioning in the protection of the maternal genome and some paternal sequences against active demethylation, was identified. Dpc7/Stella is present in both PNs, so apparently other factors are also involved[108].
After injection of round spermatids, which have a nucleosomal con-

stitution, into oocytes, deviating methylation patterns are observed at the PN stage[109]. Intriguingly, paternal demethylation takes place, but during DNA replication methylation reappears. When elongated spermatids are injected the same phenomenon is observed although less severe[109]. In addition, mouse pre-implantation embryos obtained from round spermatid injection show altered transcription levels[110, 111].

Since both spermatid types contain modified nucleosomes, it is impossible to allot the deviating maternal processing to either nucleosomal chromatin or specific modifications. However, it clearly shows that the chromatin composition of sperm can affect its processing after gamete fusion. Sperm from sub-fertile human males have a deviating nucleosome/protamine ratio[79, 112]. The possibility, that transmission of paternal DNA sequences in a deviant chromatin configuration elicit epigenetic alterations in the early zygote and beyond, exists. The risk for such an event might be elevated when round spermatids that by definition have not properly remodeled their chromatin, are used. By extrapolation sperm obtained via TESE (Testicular Sperm Extraction), could also belong to this category. Unfortunately, the possible risks and consequences of aberrant paternal chromatin for development are unknown as scientific insight is lagging behind on clinical application.

Transcription at the absolute beginning

In mouse, transcriptional activation of the zygotic genome (ZGA) occurs during the first round of replication, approximately 9 hours after gamete fusion. Detailed RNA expression profiling of zygotic transcription confirmed that nascent transcripts are not translated[113]. This does not seem to stem from a global impairment of the spliceosome but could be a consequence of the aberrant nature of zygotic transcripts[113, 114]. Possibly this is a result of the absence of component(s) of the transcriptional machinery, which could lead to premature or delayed terminatation of zygotic transcripts[113]. The function of this mute zygotic transcription is possibly to serve as a preparation of the chromatin template for future transcription[115]. This is not unlikely since during more than two weeks of spermatid and sperm maturation, the transcription machinery does not access paternal chromatin. During the larger part of this period most of

the DNA was in the uniform nucleoprotamine conformation.
Zygotic transcription levels, as determined by BrUTP incorporation, are around 4 to 5 times higher in the male PN than in the female. This is largely attributed to a higher concentration of transcription factors and higher levels of histone acetylation in the paternal PN[116]. A correlation between the latter and unequal parental transcriptional activity is suggested since equalization of histone acetylation levels also equalizes transcription levels[117]. Protein-yielding transcription commences during the 2-cell stage. Analysis of its transcriptome showed the selective activation of genes involved in processes like RNA processing and gene transcription[113, 118-120]. This early "sense of purpose" can be illustrated by the protein transcription intermediate factor 1α (Tif-α), which enters the zygotic PNs during S-phase and co-localizes with BrUTP uptake. Knock down or inhibition of Tif1α results predominantly in an early cleavage stage (2, 3 and 4-cell) arrest and appeared to be the result of deregulation of a specific group of genes rather than a general defect on transcription[121].
The onset of embryonic transcription is solely driven by maternally derived factors, which initiate the first transcriptional wave by a "zygotic clock" [118]. Inhibition of DNA replication does neither affect timing of initiation nor the overall composition of the early zygotic transcriptome. This suggests that the replication machinery is not necessary for the transcription machinery to access the majority of genes[118].

Maternal effect genes and zygotic DNA repair

The zygote predominantly thrives on maternally derived proteins and mRNA which, during early development, are eventually replaced by embryonic ones. [115]. Maternal supplies allow first developmental steps to occur without full transcriptional activation of embryonic genes. Genes encoding factors stored in the oocyte that are necessary for development are termed maternal effect genes. Absence of such maternal factors is detrimental for the embryo and cannot be overcome by transcription of the paternal gene. Embryonic lethality of homozygous null mutations hinders the identification of maternal effect genes as nullizygous germ cells cannot be obtained. A clear example is Brg1, the ATPase subunit of Swi/Snf chromatin remodeling complex. The nullizygous mouse is embryonic lethal.

However, a conditional knock-out mouse that generates oocytes lacking Brg1, enables the functional study of Brg1 during oogenesis and early embryogenesis[122]. Loss of Brg1 does not affect oocyte generation but is essential for early transcription activation. Oocytes lacking Brg1, fertilized with wild-type sperm, arrested at the 2-cell stage, an archetypical phenotype for a maternal effect gene[122].

DNA metabolism comprises a multitude of biochemical processes, DNA repair arguably being the most diverse (presented concisely in BOX 3). In 2002 the first maternal effect for a gene functioning in DNA repair was described[123]. However, the phenotype of embryos derived from oocytes nullizygous for this gene (*Pms2*) does not strictly adhere to the definition of a maternal effect as described previously[123]. The maternal effect of the *Pms2* mutation is revealed after analysis of microsatellite repeat length. Heterozygous progeny, derived from a wild-type father and homozygous null mother contain microsatellite mutations in loci derived from the father. Furthermore, maternal and paternal mosaics for microsatellite loci are obtained. Hence oocytes lacking *Pms2* cause a maternal effect mutator phenotype that at the onset of embryonic transcription is compensated by the wild-type *Pms2* allele from the father. Erstwhile research had already shown that genomic integrity of the zygote is safeguarded by DNA repair factors stored in the oocyte [61, 124-126]. Also, the maternal DNA repair machinery is used in transgenesis[127]. Hence, the zygote can be viewed as a cross-road for the maternal derived repair machinery to collide with paternal derived DNA damage. The outcome influences the mutation status of the prospective embryo and future organism as modified by DNA repair factors stored in the oocyte [61, 128]. Maternal effects of repair genes are normally not noticed and usually solely surface when DNA repair is challenged. Long term effects of repair deprived preimplantation development have been scarcely studied.

Inheritance of epigenetic state and transgenerational instability

Inheritance of classic Mendelian phenotypes follow strict rules resulting in a perfect correspondence between phenotype and a single-locus genotype [129]. At the other end of the scale, an epigenetically

determined phenotype follows a stochastic distribution[130]. There is a certain chance, for a given epigenetic state to result in a particular phenotypic outcome. An allele associated with phenotypic variation in the absence of genetic heterogeneity is referred to as epiallele. An epigenotype is the sum of all DNA and chromatin associated modifications (the latter discussed in Box 1) resulting in a transcriptional state which is mitotically heritable (for review see [131]). An epigenetic state is dynamic, exemplified by variable expression of a gene amongst cells of the same type, a phenomenon known as variegation.

Mitotic inheritance of an epigenetic state on a cellular level is often generically referred to as epigenetic inheritance. In the context of sexual reproduction, this should not be confused with inheritance of an epigenotype across generations. In the primordial germ cells (PGCs), which eventually give rise to the gametes, both DNA methylation and histone modifications are erased [132]. Currently, DNA methylation has been studied most and incomplete erasure at transmission for certain epialleles has been described. The inheritance of such an epiallele and its associated phenotype show a probabilistic nature and have therefore been termed metastable[133]. The inheritance of such alleles across generational boundaries remains an intriguing field of research. Thus far, several examples of transgenerationally inheritable epialleles have been described [reviewed in [134, 135]]. The *Agouti* locus of the mouse is archetypical for the study of transgenerational epigenetic inheritance[136, 137], however evidence for generalization remains flimsy. This most likely is due to the fact that epialleles, such as found at the *Agouti* locus, are associated with a retroviral element. The *Agouti* gene has an IAP insertion (intracisternal A particle) upstream of the gene, providing a cryptic promoter able to induce ectopic expression. The activity of such a retroviral cryptic promoter, under the pressure of evolution, is kept in check by CpG methylation.

Transgenerational instability

Mutations follow a probabilistic pattern and the likelihood of occurrence is influenced by the type of mutation, the genetic background of the organism/cell and its environment (both internal and external). The state in which due to a DNA repair defect the likelihood

of de novo occurrence of a mutation (= mutation rate) is increased compared to the general population, is often referred to as mutator phenotype. DNA damage, whether due to endogenous or exogenous factors, plays a pivotal role in mutation induction. Most mutations arise at the site of DNA damage and are causally related to a specific type of DNA damage, for instance translocations are formed by misrepair of DSBs. Mutations of tandem repeats, like minisatellites and Expanded Simple Tandem Repeats (ESTR), arise in a different manner. Tandem repeats are genomic loci formed by an array of repeated sequences (units) and are located predominantly in non-coding regions (Figure 3). Gain or loss of such units results in a variable array size which can be measured by differences in electrophoretic mobility, enabling calculation of the mutation rate (Figure 3b). The high germline mutation rate has made minisatellites a very useful

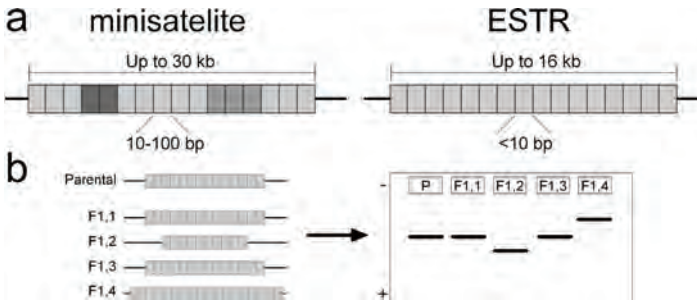

Figure 3.
Tandem repeat sequences and measurement of instability

tool in forensic science and establishment of family relationships (DNA Fingerprint)[138]. Minisatellite mutation shows a bias for gain of repeats and are mainly driven by recombination events between homologous chromosomes during meiosis (human). In contrast to minisatellites, ESTR arrays contain very small repeat units of homogeneous sequence. Longer and more homogeneous arrays show a higher instability. By direct observation, little is known about the mechanism of ESTR mutation. There is no bias for gain or loss of repeat units in ESTR arrays. In addition to germline instability, somatic instability for these repeats has been described, correlating with mitotic activity, i.e. instability was found in bone marrow and spleen, not in brain[139]. Hence, ESTR mutations are suspected to be associated with replication errors. DNA damage augments the mutation rate of tandem repeat sequences by an unknown mechanism, also because the microsatellite changes present as a delayed response

[140]. Such an increase is already found at very mild genomic insult and therefore thought to occur in a non-targeted manner, in contrast to most mutations. DNA damage alters many cellular processes, i.e. DNA repair machinery and cell cycle checkpoints become activated. In addition the transcriptome is (temporarily) altered. Also, an insult like ionizing irradiation causes a general stress response in the cell associated with massive free radical production. These global changes of cellular physiology and not the initial DNA damage, result in an increased likelihood of tandem repeat mutation to occur. The mitotic inheritance of an increased probability for mutation at these particular non-targeted loci foreshadows an epigenetic mechanism.

Transgenerational epigenetic inheritance of ESTR instability was subsequently described. The analysis of first generation offspring sired by irradiated males showed a similar enhanced mutation rate that was transmittable to a second generation [141, 142]. Recently, the elevated ESTR mutation rate was associated with a transmittable increased incidence of mutation in the protein coding gene *hprt*, and of endogenous levels of single and double strand DNA breaks possibly implying a more general transgenerational genomic instability[143]. Hypothesizing, the inheritance of an epigenome with an increased likelihood for replication errors seems likely. The nature of this heritable increase in mutation rate and genome instability remains an enigma and the possible risk to the population cannot be ignored.

BOX 3. DNA repair mechanisms counteracting genome alterations

A plenitude of DNA damages can alter a genome and ultimately result in lasting changes or cellular demise. Cellular processes and environmental hazards effectuate DNA alterations which have been classified and linked to particular repair pathways. A subset is listed in the figure below (adapted from[144]). Abrogation of repair genes results in characteristic sensitivity profiles for particular damaging agents due to the specificity of DNA repair pathways. Repair of DNA damage is pivotal; hence mutations of repair genes often result in cancer predisposition and/or specific clinical syndromes.

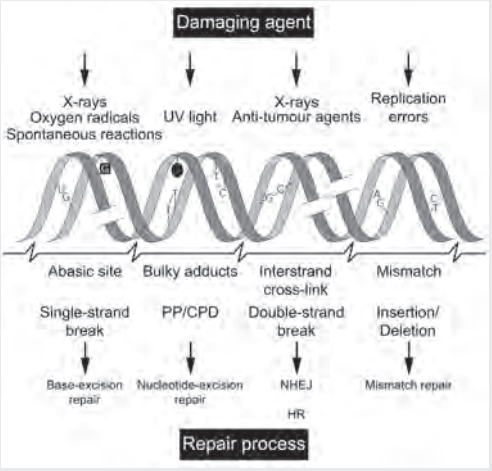

Figure BOX 3. DNA damaging agents resulting in a variety of DNA lesions and the repair processes that act upon them. PP: 6-4 photoproduct, CPD: cyclobutane pyrimidine dimer

<u>BER. Base Excision Repair</u>
Cellular metabolism generates numerous reactive molecules (i.e. reactive oxygen species) resulting in base changes. A battery of DNA glycosylases, each recognizing a spectrum of base changes, removes altered bases leaving an abasic site. Such conversions also occur spontaneously and induce DNA incision resulting in a single strand DNA break (SSB). These SSBs and those generated by irradiation feed into the core BER machinery which fills the gap and seals the break. No human disorders for this repair pathway have been described, however, loss of core BER components (mice) is not compatible with life underlining the importance of this repair pathway.

<u>NER. Nucleotide Excision Repair</u>
UV-induced DNA lesions result in disrupted base-pairing and are recognized by the NER-machinery. Consecutively, a protein complex is formed that culminates in the excision of a stretch of nucleotides

along with the DNA lesion. The created gap is filled by replication factors. The NER pathway consists of two sub-pathways, one acting globally (global genome or GG-NER), the other at transcriptionally active loci (transcription coupled NER or TCR). Extensively studied human disorders are Xeroderma Pigmentosum (GG-NER) and Cockayne syndrome (TCR).

Non Homologous End Joining (NHEJ) and Homologous Recombination (HR)

A double strand DNA break (DSB) is a disastrous form of DNA damage, resulting in loss of genetic information or chromosomal rearrangements. However, during several essential cellular processes, DSBs are a necessary intermediate. For instance, DSBs are generated during genomic rearrangements at VDJ genes, essential for antibody diversity and ultimately immunity. Another form of regulated DSBs forms the foundation of sexual reproduction as they enable meiotic cross-overs resulting into gametes with a unique genetic content. NHEJ resolves DSBs at the VDJ-gene locus, while HR is responsible for repair of meiotic DSBs.

Repair of exogenously induced DSBs, i.e. by irradiation or chemical compounds, is less categorical. A family of kinases (PIKK) recognizes DSBs and reacts by phosphorylating the variant histone H2AX. This serves as a binding platform mustering a myriad of proteins involved in cell cycle regulation and DNA repair[145-147]. Like a molecular assembly line, these proteins start processing and repairing the DSB.

NHEJ acts by ligating ("gluing") opposing ends very shortly after break occurrence. The DNA-PK holoenzyme, existing of Ku70-Ku80 heterodimer and DNA-PKcs, binds and juxtaposes DNA ends. They are ligated by means of XRCC4, DNA ligase IV and XLF and several other factors depending on the type of DNA ends. This "simple" ligation mechanism makes this repair route more error prone. NHEJ functions independent of cell cycle phase. During S/G2 its counterpart HR becomes active.

HR resolves DSBs by using the homologous DNA sequence on the sister chromatid. DNA ends are converted to single strand DNA and ultimately coated by Rad51 protein. In conjunction with a family of proteins (Rad52 epistasis family) the homologous sister sequence is located and used for repair of the DSB, generating a recombina-

tion intermediate. Via an intricate mechanism, partly facilitated by Rad54/Rad54B proteins, this structure is resolved. HR is less liable to misrepair DSBs then NHEJ but can only function properly in the context of replicated DNA.
Chromosome duplication via DNA replication is a laborious process that poses a threat on the conservation of the genetic code. It requires absolute accuracy and the process itself is liable to interruption in the form of stalled or disrupted replication forks. HR specifically functions in reactivating and re-establishing replication forks, arguably the most import task for this repair pathway.
There are numerous clinical manifestations of defects in DSB repair and related cell cycle regulation. Many impose cancer predisposition and other complications like neurological disorders, immunodeficiency and infertility. Genes associated with these disorders are extensively studied in mice[148]. The clinical disorder scid, for severe combined immunodeficiency, serves as an example of a natural occurring mutation in both mouse and man. It is caused by a truncating mutation of the NHEJ protein DNA-PKcs effectively abrogating the enzymatic activity of the DNA-PK holoenzyme.
For extensive reviews on mechanistic details of DSB repair the reader is referred to [149, 150].

MMR. Mismatch Repair

Despite the proofreading activity and high fidelity of replicative DNA polymerases (alpha and delta), erroneous nucleotide incorporations resulting in a mismatch (i.e. A-G or T-C) occur. In addition, stretches of dinucleotide repeats (microsatellites, not to be confused with minisatellites) elicit polymerase slippage and concurrently generate insertion/deletion loops. Human disease genes of this pathway have thus far been linked to hereditary forms of colorectal cancer (HNPCC). Gene targeting of a particular MMR gene, Pms2, has been shown to invoke a maternal effect on microsatellite instability in the mouse.

Section 1.4 Thesis outline

The practical work of this thesis is divided in three different sections. The main focus of section 2 is chromatin, section 3 focuses on DNA repair and section 4 describes the utilization of findings described in section 2 and 3 in answering more clinical questions

Section 2
Histone biology of the male germline pre and post gamete fusion

Section 2.1 focuses on the sex chromosomes during meiosis and describes a hitherto unknown phenomenon that takes place in the sex body during pachytene and diplotene of meiosis.
Findings presented in Section 2.2 show that during mouse spermiogenesis, the heterochromatin of elongating spermatids retains nucleosomal chromatin. These nucleosomes carry post-translational modifications and are transmitted to the zygote.
Section 2.3 demonstrates that also in humans, nucleosomal chromatin is transmitted to the zygote, contributing to the paternal zygotic chromatin.
At fertilization the sperm nucleus undergoes extensive chromatin remodeling. In Section 2.4 we have studied the dynamics of this process in the mouse. Furthermore we describe significant differences between the parental pronuclei in the early zygote.

Section 3
Maternal effects on DNA repair

In Section 3.1 we show that the phosphorylation of histone H2AX at serine 139 (γH2AX), in somatic cells a signal for mainly DNA double strand breaks, also occurs in the zygote. The dynamics of zygotic γH2AX during G1 and its relation to DNA double strand breaks was determined by sperm irradiation and treatment of zygotes with DNA damaging drugs.
Section 3.2 corroborates and extends the findings of section 3.1. The contribution of the two major pathways in repair of DNA double strand breaks, namely Non Homologous End Joining and Homologous Recombination, are assessed by the use repair deficient mouse models. The two pathways are not independent, and differences in likelihood of repair in male and female pronuclei were revealed.

Section 3.3 addresses the question whether offspring sired by irradiated male mice via mature sperm with irradiation induced DNA breaks, show an increased genetic instability at an expanded simple tandem repeat. Using reciprocal crosses, the existence of a maternal effect on ESTR instability was established.

Section 4
Fundamental biological answers on clinical questions

In section 3.1 we determined that DNA double strand breaks present in the fertilizing sperm are marked by γH2AX shortly after gamete fusion. In section 4.1 we use this principle, combined with heterologous ICSI, to determine the amount of DNA double strand breaks present in human sperm from fertile and infertile probands. Furthermore, this method was used to examine the fate of immotile sperm after fertilization.
In section 2.4 we described parental asymmetries regarding histone lysine methylation. In section 4.2 we utilized these findings to determine the genetic composition of monopronuclear mouse and human zygotes.

References

1. de Rooij,D.G. & Grootegoed,J. A. Spermatogonial stem cells. *Curr. Opin. Cell Biol.* **10**, 694-701 (1998).

2. de,B.E. & Heyting,C. The diverse roles of transverse filaments of synaptonemal complexes in meiosis. *Chromosoma* **115**, 220-234 (2006).

3. Revenkova,E. & Jessberger,R. Shaping meiotic prophase chromosomes: cohesins and synaptonemal complex proteins. *Chromosoma* **115**, 235-240 (2006).

4. Ashley,T. & Plug,A. Caught in the act: deducing meiotic function from protein immunolocalization. *Curr. Top. Dev. Biol.* **37**, 201-239 (1998).

5. Keeney,S. Mechanism and control of meiotic recombination initiation. *Curr. Top. Dev. Biol.* **52**, 1-53 (2001).

6. Perry,J., Palmer,S., Gabriel,A., & Ashworth,A. A short pseudoautosomal region in laboratory mice. *Genome Res.* **11**, 1826-1832 (2001).

7. de Boer,P., Searle,A.G., van der Hoeven,F.A., de Rooij,D.G., & Beechey,C.V. Male pachytene pairing in single and double translocation heterozygotes and spermatogenic impairment in the mouse. *Chromosoma* **93**, 326-336 (1986).

8. Peters,A.H., Plug,A.W., & de,B. P. Meiosis in carriers of heteromorphic bivalents: sex differences and implications for male fertility. *Chromosome. Res.* **5**, 313-324 (1997).

9. Russell,L.D., Ettlin,R.A., Hikim,A.P.S., & Clegg,E.D. *Histopathological Evaluation of the Testis*(Cache River Press, Clearwater, FL, 1990).

10. Alberts ,B. *et al. Molecular Biology of the Cell*(Garland Science,2002).

11. Handel,M.A. & Hunt,P.A. Sex-chromosome pairing and activity during mammalian meiosis. *Bioessays* **14**, 817-822 (1992).

12. Turner,J.M. Meiotic sex chromosome inactivation. *Development*(2007).

13. Baarends,W.M. *et al.* Silencing of unpaired chromatin and histone H2A ubiquitination in mammalian meiosis. *Mol. Cell Biol.* **25**, 1041-1053 (2005).

14. Turner,J.M. *et al.* Silencing of unsynapsed meiotic chromosomes in the mouse. *Nat. Genet.* **37**, 41-47 (2005).

15. Shiu,P.K., Raju,N.B., Zickler,D., & Metzenberg,R. L. Meiotic silencing by unpaired DNA. *Cell* **107**, 905-916 (2001).

16. Khaja,R. *et al.* Genome assembly comparison identifies structural variants in the human genome.

Nat. Genet. **38**, 1413-1418 (2006).

17. Schimenti,J. Synapsis or silence. *Nat. Genet.* **37**, 11-13 (2005).

18. Lenhossek,M. Untersuchungen uber spermatogenese. *Arch. Mikrosk. Anat. Entwicklungsmech* **51**, 215-318 (1898).

19. Painter ,T.S. Studies in mammalian spermatogenesis III. The fate of the chromatin-nucleolus in the opossum. *J. Exp. Zool.* **19**, 197 (1924).

20. Turner,J.M. *et al.* BRCA1, histone H2AX phosphorylation, and male meiotic sex chromosome inactivation. *Curr. Biol.* **14**, 2135-2142 (2004).

21. Speed,R.M. Abnormal RNA synthesis in sex vesicles of tertiary trisomic male mice. *Chromosoma* **93**, 267-270 (1986).

22. Turner,J.M., Mahadevaiah,S. K., Ellis,P.J., Mitchell,M.J., & Burgoyne,P.S. Pachytene asynapsis drives meiotic sex chromosome inactivation and leads to substantial postmeiotic repression in spermatids. *Dev. Cell* **10**, 521-529 (2006).

23. Bean,C.J., Schaner,C.E., & Kelly,W.G. Meiotic pairing and imprinted X chromatin assembly in Caenorhabditis elegans. *Nat. Genet.* **36**, 100-105 (2004).

24. Handel,M.A. The XY body: a specialized meiotic chromatin domain. *Exp. Cell Res.* **296**, 57-63 (2004).

25. Tremethick,D. Chromatin: the dynamic link between structure and function. *Chromosome. Res.* **14**, 1-4 (2006).

26. Polo,S.E. & Almouzni,G. Chromatin assembly: a basic recipe with various flavours. *Curr. Opin. Genet. Dev.* **16**, 104-111 (2006).

27. Luger,K. & Hansen,J.C. Nucleosome and chromatin fiber dynamics. *Curr. Opin. Struct. Biol.* **15**, 188-196 (2005).

28. Luger,K., Mader,A.W., Richmond,R.K., Sargent,D.F., & Richmond,T.J. Crystal structure of the nucleosome core particle at 2.8 A resolution. *Nature* **389**, 251-260 (1997).

29. Kornberg,R.D. & Lorch,Y. Twenty-five years of the nucleosome, fundamental particle of the eukaryote chromosome. *Cell* **98**, 285-294 (1999).

30. Workman,J.L. Nucleosome displacement in transcription. *Genes Dev.* **20**, 2009-2017 (2006).

31. Ehrenhofer-Murray,A.E. Chromatin dynamics at DNA replication, transcription and repair. *Eur. J. Biochem.* **271**, 2335-2349 (2004).

32. Saha,A., Wittmeyer,J., & Cairns,B.R. Chromatin remodelling: the industrial revolution of DNA around histones. *Nat. Rev. Mol. Cell Biol.* **7**, 437-447 (2006).

33. Smith,C.L. & Peterson,C.L. ATP-dependent chromatin remodeling. *Curr. Top. Dev. Biol.* **65**, 115-148 (2005).

34. de,l.S., I, Ohkawa,Y., & Imbalzano,A.N. Chromatin remodelling in mammalian differentiation: lessons from ATP-dependent remodellers. *Nat. Rev. Genet.* **7**, 461-473 (2006).

35. van Vugt,J.J., Ranes,M., Campsteijn,C., & Logie,C. The ins and outs of ATP-dependent chromatin remodeling in budding yeast: Biophysical and proteomic perspectives. *Biochim. Biophys. Acta* **1769**, 153-171 (2007).

36. Sterner,D.E. & Berger,S.L. Acetylation of histones and transcription-related factors. *Microbiol. Mol. Biol. Rev.* **64**, 435-459 (2000).

37. Trievel,R.C. Structure and function of histone methyltransferases. *Crit Rev. Eukaryot. Gene Expr.* **14**, 147-169 (2004).

38. Peters,A.H. & Schubeler,D. Methylation of histones: playing memory with DNA. *Curr. Opin. Cell Biol.* **17**, 230-238 (2005).

39. Nightingale,K.P., O'neill,L. P., & Turner,B.M. Histone modifications: signalling receptors and potential elements of a heritable epigenetic code. *Curr. Opin. Genet. Dev.* **16**, 125-136 (2006).

40. Kouzarides,T. Chromatin modifications and their function. *Cell* **128**, 693-705 (2007).

41. Hay,R.T. SUMO: a history of modification. *Mol. Cell* **18**, 1-12 (2005).

42. Prigent,C. & Dimitrov,S. Phosphorylation of serine 10 in histone H3, what for? *J. Cell Sci.* **116**, 3677-3685 (2003).

43. Strahl,B.D. & Allis,C.D. The language of covalent histone modifications. *Nature* **403**, 41-45 (2000).

44. Jenuwein,T. & Allis,C.D. Translating the histone code. *Science* **293**, 1074-1080 (2001).

45. Kamakaka,R.T. & Biggins,S. Histone variants: deviants? *Genes Dev.* **19**, 295-310 (2005).

46. Henikoff,S. & Ahmad,K. Assembly of variant histones into chromatin. *Annu. Rev. Cell Dev. Biol.* **21**, 133-153 (2005).

47. Bernstein,E. & Hake,S.B. The nucleosome: a little variation goes a long way. *Biochem. Cell Biol.* **84**, 505-517 (2006).

48. Rousseaux,S. *et al.* Establishment of male-specific epigenetic information. *Gene* **345**, 139-153 (2005).

49. Meistrich,M.L., Mohapatra,B., Shirley,C.R., & Zhao,M. Roles of transition nuclear proteins in spermiogenesis. *Chromosoma* **111**, 483-488 (2003).

50. Miescher ,F. Das Protamin – Eine neue organische Basis aus denSamenf – den des Rheinlachses. *Ber Dtsch Chem* **7**, 376 (1874).

51. Balhorn,R. A model for the structure of chromatin in mammalian sperm. *J. Cell Biol.* **93**, 298-305 (1982).

52. Ward,W.S. & Coffey,D.S. DNA packaging and organization in mammalian spermatozoa: comparison with somatic cells. *Biol. Reprod.* **44**, 569-574 (1991).

53. Mudrak,O., Tomilin,N., & Zalensky,A. Chromosome architecture in the decondensing human sperm nucleus. *J. Cell Sci.* **118**, 4541-4550 (2005).

54. Ward,M.A. & Ward,W.S. A model for the function of sperm DNA degradation. *Reprod. Fertil. Dev.* **16**, 547-554 (2004).

55. van Loon,A.A. *et al.* Induction and repair of DNA single-strand breaks and DNA base damage at different cellular stages of spermatogenesis of the hamster upon in vitro exposure to ionizing radiation. *Mutat. Res.* **294**, 139-148 (1993).

56. Kofman-Alfaro,S. & Chandley,A.C. Radiation-initiated DNA synthesis in spermatogenic cells of the mouse. *Exp. Cell Res.* **69**, 33-44 (1971).

57. Sega,G.A., Sotomayor,R.E., & Owens,J.G. A study of unscheduled DNA synthesis induced by X-rays in the germ cells of male mice. *Mutat. Res.* **49**, 239-257 (1978).

58. Baarends,W.M., van der,L.R., & Grootegoed,J.A. DNA repair mechanisms and gametogenesis. *Reproduction.* **121**, 31-39 (2001).

59. Olsen,A.K., Lindeman,B., Wiger,R., Duale,N., & Brunborg,G. How do male germ cells handle DNA damage? *Toxicol. Appl. Pharmacol.* **207**, 521-531 (2005).

60. Xu,G. *et al.* Nucleotide excision repair activity varies among murine spermatogenic cell types. *Biol. Reprod.* **73**, 123-130 (2005).

61. Generoso,W.M., Cain,K.T., Krishna,M., & Huff,S.W. Genetic lesions induced by chemicals in spermatozoa and spermatids of mice are repaired in the egg. *Proc. Natl. Acad. Sci. U. S. A* **76**, 435-437 (1979).

62. Zalensky,A.O., Breneman,J.W., Zalenskaya,I.A., Brinkley,B.R., & Bradbury,E.M. Organization of centromeres in the decondensed nuclei of mature human sperm. *Chromosoma* **102**, 509-518 (1993).

63. Zalensky,A.O. *et al.* Well-defined genome architecture in the human sperm nucleus. *Chromosoma* **103**, 577-590 (1995).

64. Haaf,T. & Ward,D.C. Higher order nuclear structure in mammalian sperm revealed by in situ hybridization and extended chromatin fibers. *Exp. Cell Res.* **219**, 604-611 (1995).

65. Zalenskaya,I.A. & Zalensky,A. O. Non-random positioning of chromosomes in human sperm nuclei. *Chromosome Res.* **12**, 163-173 (2004).

66. Gatewood,J.M., Cook,G. R., Balhorn,R., Schmid,C.W., & Bradbury,E.M. Isolation of four core histones from human sperm chromatin representing a minor subset of somatic histones. *J. Biol. Chem.* **265**, 20662-20666 (1990).

67. Tanphaichitr,N., Sobhon,P., Taluppeth,N., & Chalermisarachai,P. Basic nuclear proteins in testicular cells and ejaculated spermatozoa in man. *Exp. Cell Res.* **117**, 347-356 (1978).

68. Bench,G.S., Friz,A.M., Corzett,M.H., Morse,D.H., & Balhorn,R. DNA and total protamine masses in individual sperm from fertile mammalian subjects. *Cytometry* **23**, 263-271 (1996).

69. Zalenskaya,I.A., Bradbury,E. M., & Zalensky,A.O. Chromatin structure of telomere domain in human sperm. *Biochem. Biophys. Res. Commun.* **279**, 213-218 (2000).

70. Gardiner-Garden,M., Ballesteros,M., Gordon,M., & Tam,P.P. Histone- and protamine-DNA association: conservation of different patterns within the beta-globin domain in human sperm. *Mol. Cell Biol.* **18**, 3350-3356 (1998).

71. Wykes,S.M. & Krawetz,S.A. The structural organization of sperm chromatin. *J. Biol. Chem.* **278**, 29471-29477 (2003).

72. van der Heijden,G.W. *et al.* Transmission of modified nucleosomes from the mouse male germline to the zygote and subsequent remodeling of paternal chromatin. *Dev. Biol.* **298**, 458-469 (2006).

73. van der Heijden,G.W. *et al.* Asymmetry in Histone H3 variants and lysine methylation between paternal and maternal chromatin of the early mouse zygote. *Mech. Dev.* **122**, 1008-1022 (2005).

74. Rhim,J.A. *et al.* Expression of an avian protamine in transgenic mice disrupts chromatin structure in spermatozoa. *Biol. Reprod.* **52**, 20-32 (1995).

75. Cho,C. *et al.* Haploinsufficiency of protamine-1 or -2 causes infertility in mice. *Nat. Genet.* **28**, 82-86 (2001).

76. Cho,C. *et al.* Protamine 2 deficiency leads to sperm DNA damage and embryo death in mice. *Biol. Reprod.* **69**, 211-217 (2003).

77. Oliva,R. Protamines and male infertility. *Hum. Reprod. Update.* **12**,

417-435 (2006).

78. Balhorn,R., Reed,S., & Tanphaichitr,N. Aberrant protamine 1/protamine 2 ratios in sperm of infertile human males. *Experientia* **44**, 52-55 (1988).

79. Zhang,X., Gabriel,M.S., & Zini,A. Sperm nuclear histone to protamine ratio in fertile and infertile men: evidence of heterogeneous subpopulations of spermatozoa in the ejaculate. *J. Androl* **27**, 414-420 (2006).

80. Mengual,L., Ballesca,J.L., Ascaso,C., & Oliva,R. Marked differences in protamine content and P1/P2 ratios in sperm cells from percoll fractions between patients and controls. *J. Androl* **24**, 438-447 (2003).

81. Aoki,V.W. *et al.* DNA integrity is compromised in protamine-deficient human sperm. *J. Androl* **26**, 741-748 (2005).

82. Aoki,V.W., Emery,B.R., Liu,L., & Carrell,D.T. Protamine levels vary between individual sperm cells of infertile human males and correlate with viability and DNA integrity. *J. Androl* **27**, 890-898 (2006).

83. Tesarik,J., Greco,E., & Mendoza,C. Late, but not early, paternal effect on human embryo development is related to sperm DNA fragmentation. *Hum. Reprod.* **19**, 611-615 (2004).

84. Nasr-Esfahani,M.H. *et al.* Effect of protamine-2 deficiency on ICSI outcome. *Reprod. Biomed. Online.* **9**, 652-658 (2004).

85. Suganuma,R., Yanagimachi,R., & Meistrich,M.L. Decline in fertility of mouse sperm with abnormal chromatin during epididymal passage as revealed by ICSI. *Hum. Reprod.* **20**, 3101-3108 (2005).

86. Baart,E.B. *et al.* Reduced oocyte activation and first cleavage rate after ICSI with spermatozoa from a sterile mouse chromosome mutant. *Hum. Reprod.* **19**, 1140-1147 (2004).

87. Free,M.J., Schluntz,G.A., & Jaffe,R.A. Respiratory gas tensions in tissues and fluids of the male rat reproductive tract. *Biol. Reprod.* **14**, 481-488 (1976).

88. Zheng,H. & Olive,P.L. Influence of oxygen on radiation-induced DNA damage in testicular cells of C3H mice. *Int. J. Radiat. Biol.* **71**, 275-282 (1997).

89. Greco,E. *et al.* Efficient treatment of infertility due to sperm DNA damage by ICSI with testicular spermatozoa. *Hum. Reprod.* **20**, 226-230 (2005).

90. Lewis,S.E. & Aitken,R.J. DNA damage to spermatozoa has impacts on fertilization and pregnancy. *Cell Tissue Res.* **322**, 33-41 (2005).

91. Spano,M., Seli,E., Bizzaro,D., Manicardi,G.C., & Sakkas,D. The significance of sperm nuclear DNA strand breaks on reproductive outcome. *Curr. Opin. Obstet. Gynecol.* **17**, 255-260 (2005).

92. Zini,A. & Libman,J. Sperm DNA damage: importance in the era of assisted reproduction. *Curr. Opin. Urol.* **16**, 428-434 (2006).

93. Wright,S.J. Sperm nuclear activation during fertilization. *Curr. Top. Dev. Biol.* **46**, 133-178 (1999).

94. Sutovsky,P. & Schatten,G. Paternal contributions to the mammalian zygote: fertilization after sperm-egg fusion. *Int. Rev. Cytol.* **195**, 1-65 (2000).

95. Tesarik,J. & Greco,E. A zygote is not an embryo: ethical and legal considerations. *Reprod. Biomed. Online.* **9**, 13-16 (2004).

96. Adenot,P.G., Mercier,Y., Renard,J.P., & Thompson,E.M. Differential H4 acetylation of paternal and maternal chromatin precedes DNA replication and differential transcriptional activity in pronuclei of 1-cell mouse embryos. *Development* **124**, 4615-4625 (1997).

97. Frehlick,L.J., Eirin-Lopez,J. M., & Ausio,J. New insights into the nucleophosmin/nucleoplasmin family of nuclear chaperones. *Bioessays* **29**, 49-59 (2007).

98. McLay,D.W. & Clarke,H.J. Remodelling the paternal chromatin at fertilization in mammals. *Reproduction* **125**, 625-633 (2003).

99. Loppin,B. *et al.* The histone H3.3 chaperone HIRA is essential for chromatin assembly in the male pronucleus. *Nature* **437**, 1386-1390 (2005).

100. Adenot,P.G., Szollosi,M.S., Geze,M., Renard,J.P., & Debey,P. Dynamics of paternal chromatin changes in live one-cell mouse embryo after natural fertilization. *Mol. Reprod. Dev.* **28**, 23-34 (1991).

101. Derijck,A.A. *et al.* gamma-H2AX signalling during sperm chromatin remodelling in the mouse zygote. *DNA Repair (Amst)* **5**, 959-971 (2006).

102. Puschendorf ,M. *et al.* Suv39h and Polycomb group proteins specify constitutive heterochromatin in mouse pre-implantation embryos in a parent-of-origin dependent manner. *Submitted*(2007).

103. Santos,F., Peters,A.H., Otte,A.P., Reik,W., & Dean,W. Dynamic chromatin modifications characterise the first cell cycle in mouse embryos. *Dev. Biol.* **280**, 225-236 (2005).

104. Kourmouli,N. *et al.* Heterochromatin and tri-methylated lysine 20 of histone H4 in animals. *J. Cell Sci.* **117**, 2491-2501 (2004).

105. Yamazaki,T., Yamagata,K., &

Baba,T. Time-lapse and retrospective analysis of DNA methylation in mouse preimplantation embryos by live cell imaging. *Dev. Biol.* **304**, 409-419 (2006).

106. Reik,W. & Walter,J. Genomic imprinting: parental influence on the genome. *Nat. Rev. Genet.* **2**, 21-32 (2001).

107. Mayer,W., Smith,A., Fundele,R., & Haaf,T. Spatial separation of parental genomes in preimplantation mouse embryos. *J. Cell Biol.* **148**, 629-634 (2000).

108. Nakamura,T. *et al.* PGC7/Stella protects against DNA demethylation in early embryogenesis. *Nat. Cell Biol.* **9**, 64-71 (2007).

109. Kishigami,S. *et al.* Epigenetic abnormalities of the mouse paternal zygotic genome associated with microinsemination of round spermatids. *Dev. Biol.* **289**, 195-205 (2006).

110. Hayashi,S., Yang,J., Christenson,L., Yanagimachi,R., & Hecht,N.B. Mouse Pre-implantation Embryos Developed from Oocytes Injected with Round Spermatids or Spermatozoa Have Similar but Distinct Patterns of Early mRNA Expression. *Biol. Reprod.*(2003).

111. Ziyyat,A. & Lefevre,A. Differential gene expression in pre-implantation embryos from mouse oocytes injected with round spermatids or spermatozoa. *Hum. Reprod.* **16**, 1449-1456 (2001).

112. Ramos,L. *et al.* Incomplete nuclear transformation of human spermatozoa in oligo-asthenoteratospermia: characterisation by indirect immunofluorescence and thiol status. *Submitted*(2007).

113. Zeng,F. & Schultz,R.M. RNA transcript profiling during zygotic gene activation in the preimplantation mouse embryo. *Dev. Biol.* **283**, 40-57 (2005).

114. Peaston,A.E. *et al.* Retrotransposons regulate host genes in mouse oocytes and preimplantation embryos. *Dev. Cell* **7**, 597-606 (2004).

115. Schultz,R.M. The molecular foundations of the maternal to zygotic transition in the preimplantation embryo. *Hum. Reprod. Update.* **8**, 323-331 (2002).

116. Aoki,F., Worrad,D.M., & Schultz,R.M. Regulation of transcriptional activity during the first and second cell cycles in the preimplantation mouse embryo. *Dev. Biol.* **181**, 296-307 (1997).

117. Wiekowski,M., Miranda,M., & DePamphilis,M.L. Requirements for promoter activity in mouse oocytes and embryos distinguish paternal pronuclei from maternal and zygotic nuclei. *Dev. Biol.* **159**, 366-378 (1993).

118. Hamatani,T., Carter,M.G., Sharov,A.A., & Ko,M.S. Dynamics of global gene expression changes during mouse preimplantation development. *Dev. Cell* **6**, 117-131 (2004).

119. Zeng,F., Baldwin,D.A., & Schultz,R.M. Transcript profiling during preimplantation mouse development. *Dev. Biol.* **272**, 483-496 (2004).

120. Wang,Q.T. *et al.* A genome-wide study of gene activity reveals developmental signaling pathways in the preimplantation mouse embryo. *Dev. Cell* **6**, 133-144 (2004).

121. Torres-Padilla,M.E. & Zernicka-Goetz,M. Role of TIF1alpha as a modulator of embryonic transcription in the mouse zygote. *J. Cell Biol.* **174**, 329-338 (2006).

122. Bultman,S.J. *et al.* Maternal BRG1 regulates zygotic genome activation in the mouse. *Genes Dev.* **20**, 1744-1754 (2006).

123. Gurtu,V.E. *et al.* Maternal effect for DNA mismatch repair in the mouse. *Genetics* **160**, 271-277 (2002).

124. Brandriff,B. & Pedersen,R.A. Repair of the ultraviolet-irradiated male genome in fertilized mouse eggs. *Science* **211**, 1431-1433 (1981).

125. Matsuda,Y., Yamada,T., & Tobari,I. Studies on chromosome aberrations in the eggs of mice fertilized in vitro after irradiation. I. Chromosome aberrations induced in sperm after X-irradiation. *Mutat. Res.* **148**, 113-117 (1985).

126. Matsuda,Y., Seki,N., Utsugi-Takeuchi,T., & Tobari,I. Changes in X-ray sensitivity of mouse eggs from fertilization to the early pronuclear stage, and their repair capacity. *Int. J. Radiat. Biol.* **55**, 233-256 (1989).

127. Perry,A.C. Hijacking oocyte DNA repair machinery in transgenesis? *Mol. Reprod. Dev.* **56**, 319-324 (2000).

128. Bishop,J.B., Kodell,R.L., Whorton,E.B., & Domon,O.E. Dominant lethal test response with IMS and TEM using different combinations of male and female stocks of mice. *Mutat. Res.* **121**, 273-280 (1983).

129. Risch,N.J. Searching for genetic determinants in the new millennium. *Nature* **405**, 847-856 (2000).

130. Blewitt,M.E., Chong,S., & Whitelaw,E. How the mouse got its spots. *Trends Genet.* **20**, 550-554 (2004).

131. Bernstein,B.E., Meissner,A., & Lander,E.S. The mammalian epigenome. *Cell* **128**, 669-681 (2007).

132. Surani,M.A., Hayashi,K., & Hajkova,P. Genetic and epigenetic

regulators of pluripotency. *Cell* **128**, 747-762 (2007).

133. Rakyan,V.K., Blewitt,M. E., Druker,R., Preis,J.I., & Whitelaw,E. Metastable epialleles in mammals. *Trends Genet.* **18**, 348-351 (2002).

134. Peaston,A.E. & Whitelaw,E. Epigenetics and phenotypic variation in mammals. *Mamm. Genome* **17**, 365-374 (2006).

135. Whitelaw,N.C. & Whitelaw,E. How lifetimes shape epigenotype within and across generations. *Hum. Mol. Genet.* **15 Spec No 2**, R131-R137 (2006).

136. Morgan,H.D., Sutherland,H. G., Martin,D.I., & Whitelaw,E. Epigenetic inheritance at the agouti locus in the mouse. *Nat. Genet.* **23**, 314-318 (1999).

137. Blewitt,M.E., Vickaryous,N. K., Paldi,A., Koseki,H., & Whitelaw,E. Dynamic reprogramming of DNA methylation at an epigenetically sensitive allele in mice. *PLoS. Genet.* **2**, e49 (2006).

138. Jeffreys,A.J., Wilson,V., & Thein,S.L. Individual-specific 'fingerprints' of human DNA. *Nature* **316**, 76-79 (1985).

139. Yauk,C.L., Dubrova,Y.E., Grant,G.R., & Jeffreys,A.J. A novel single molecule analysis of spontaneous and radiation-induced mutation at a mouse tandem repeat locus. *Mutat. Res.* **500**, 147-156 (2002).

140. Barber,R.C. *et al.* Germline mutation rates at tandem repeat loci in DNA-repair deficient mice. *Mutat. Res.* **554**, 287-295 (2004).

141. Dubrova,Y.E., Plumb,M., Gutierrez,B., Boulton,E., & Jeffreys,A.J. Transgenerational mutation by radiation. *Nature* **405**, 37 (2000).

142. Barber,R., Plumb,M.A., Boulton,E., Roux,I., & Dubrova,Y. E. Elevated mutation rates in the germ line of first- and second-generation offspring of irradiated male mice. *Proc. Natl. Acad. Sci. U. S. A* **99**, 6877-6882 (2002).

143. Barber,R.C. *et al.* Radiation-induced transgenerational alterations in genome stability and DNA damage. *Oncogene* **25**, 7336-7342 (2006).

144. Hoeijmakers,J.H. Genome maintenance mechanisms for preventing cancer. *Nature* **411**, 366-374 (2001).

145. Thiriet,C. & Hayes,J.J. Chromatin in need of a fix: phosphorylation of H2AX connects chromatin to DNA repair. *Mol. Cell* **18**, 617-622 (2005).

146. Lowndes,N.F. & Toh,G.W. DNA repair: the importance of phosphorylating histone H2AX. *Curr. Biol.* **15**, R99-R102 (2005).

Section 2

Histone biology of the male germline pre and post gamete fusion

Section 2.1

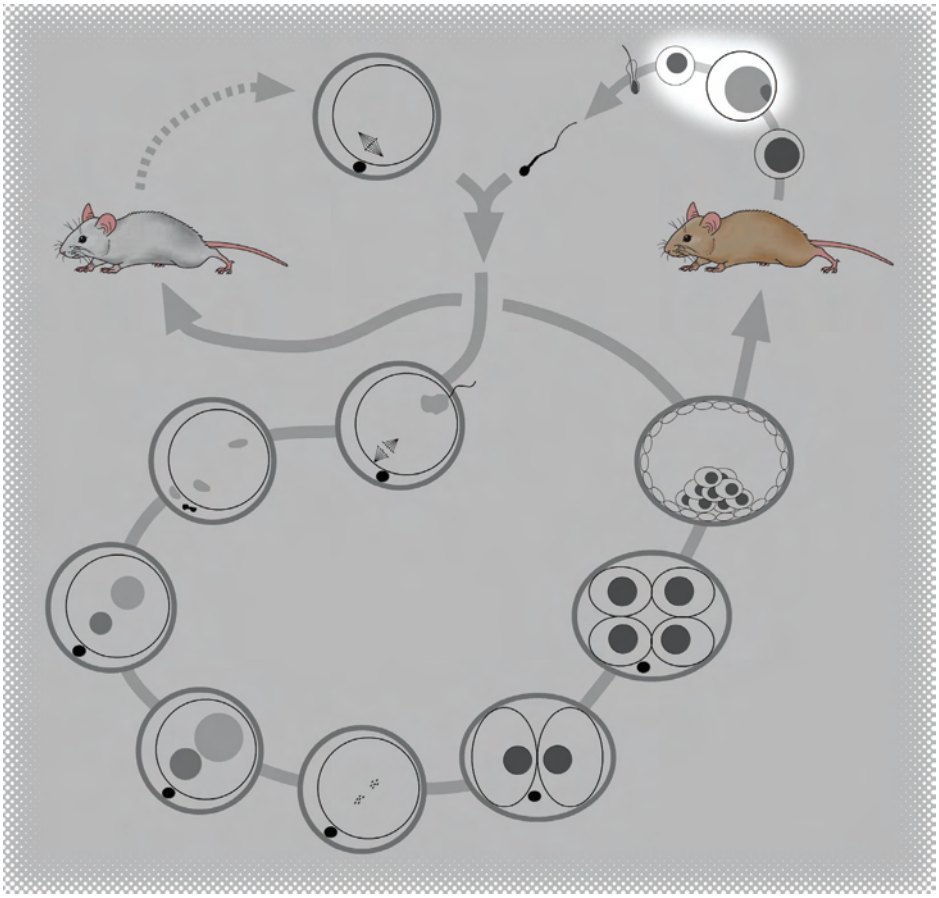

Nature Genetics 2007 February; 39(2):251-8

Chromosome-wide nucleosome replacement and H3.3 incorporation during mammalian meiotic sex chromosome inactivation

Godfried W. van der Heijden[1*], Alwin A.H.A. Derijck[1*], Eszter Pósfai[2], Maud Giele[1], Pawel Pelczar[2], Liliana Ramos[1], Derick G. Wansink[3], Johan van der Vlag[4#], Antoine H.F.M Peters[2#], Peter de Boer[1]

[1]Department of Obstetrics and Gynaecology, Radboud University Nijmegen Medical Centre, P.O. Box 9101, 6500 HB Nijmegen, The Netherlands. [2]Friedrich Miescher Institute for Biomedical Research, Maulbeerstrasse 66, CH 4058 Basel, Switzerland. [3]Department of Cell Biology, Nijmegen Centre for Molecular Life Sciences, Radboud University Nijmegen Medical Centre, P.O. Box 9101, 6500 HB Nijmegen, The Netherlands. [4]Nephrology Research Laboratory, Nijmegen Centre for Molecular Life Sciences, The Netherlands.

[*] *These authors contributed equally*

[#] *These authors contributed equally*

Abstract

In mammalian males, the first meiotic prophase is characterized by formation of a separate chromatin domain called the sex body[1]. In this domain the X and Y chromosomes are partially synapsed and transcriptionally silenced, a process termed meiotic sex chromosome inactivation (MSCI)[2, 3]. Likewise, unsynapsed autosomal chromatin present during pachytene is also silenced (Meiotic Silencing of Unsynapsed Chromatin, MSUC)[2, 4, 5]. Although MSCI and MSUC are both dependent on ATR-mediated histone H2A.X phosphorylation and cause repressive H3 lysine 9 dimethylation[4], the underlying mechanisms of silencing are unidentified. Here, we demonstrate an extensive replacement of nucleosomes within unsynapsed chromatin, depending on and initiated shortly after MSCI/MSUC induction. Nucleosomal eviction results in the exclusive incorporation of the H3.3-variant which to date has primarily been associated with transcriptional activity. Nucleosomal exchange causes loss and subsequent selective re-acquisition of specific histone modifications. This process therefore provides means for epigenetic reprogramming of sex chromatin presumably required for gene silencing in the male mammalian germ line.

Results and Discussion

The nucleosome core particle comprises an octamer of four histone proteins (H2A, H2B, H3 and H4) each present twice, around which 146 basepairs of DNA are folded. By functioning as a carrier of post-translational modifications (PTMs), that regulate gene transcription and chromatin architecture, the nucleosome is at the centre of chromatin dynamics and epigenetic memory[6]. A further diversification of chromatin is enabled by the utilisation of histone variants[7]. The canonical H3.1 and H3.2 proteins are expressed during S phase and deposited during replication by a DNA replication-dependent (RD) nucleosome assembly pathway[8]. Besides H3.1/H3.2, two H3 variants exists. CENP-A, a highly specialised variant is only present at the centromere. Mammalian H3.3 only differs from H3.1/H3.2 at five/four amino acid positions and is expressed throughout the cell cycle. It is deposited by a DNA replication-independent (RI) nucleosome assembly pathway[8-10].

Pachytene spermatocytes, characterised by fully synapsed homologous autosomal chromosomes, have been reported to undergo extensive changes in chromatin configuration[1, 5, 11-13]. Chromosome-wide RD nucleosome assembly is completed after pre-meiotic S phase. Loss of H3.1/H3.2 therefore becomes a marker for nucleosome eviction. To study nucleosomal dynamics during mouse meiosis, we performed immunofluorescence analysis using an antibody that, on basis of one amino acid difference in the N-tail, specifically detects H3.1/H3.2 but not H3.3[9]. In early pachytene spermatocytes, H3.1/H3.2 levels are equal in autosomal and sex body chromatin. At later stages however, we observed a progressive disappearance of H3.1/H3.2 in the XY body, eventually resulting in complete loss of H3.1/H3.2 from the sex chromosomes for the remainder of spermatogenesis (Fig. 1a). To establish whether this was also reflected in the overall levels of histones and in nucleosome structure, we used antibodies directed against the C-terminus of H3 (detecting H3.1, H3.2 and H3.3) and an antibody that specifically recognizes nucleosomes[14]. Signal intensities of both antibodies underwent a transient reduction at sex chromatin of pachytene up to early diplotene (Fig. 1b and supplementary Fig. 1) and returned to autosomal levels when the XY axial elements obtained their bulged appearance, a typical feature of mid-late diplotene spermatocytes[15]. These data suggest

that *de novo* RI-nucleosome assembly of nucleosomes and H3.3 incorporation takes place during MSCI.

To investigate whether H3.1/H3.2 removal and *de novo* nucleosome deposition occur simultaneously, we localised the H3.3•H4-specific chaperone HirA[16]. Concomitant with H3.1/H3.2 removal, a relative increase of signal in the XY body was observed (Fig. 1c) suggesting that H3.1/H3.2 removal coincides with *de novo* H3.3•H4 deposition. HirA levels in the XY body were equal to or lower than autosomal levels in mid-late diplotene spermatocytes (Fig. 1c; supplementary Table 1).
RI-nucleosome assembly by HirA is predicted to yield H3.3-containing nucleosomes[16]. As no specific antibody against unmodified H3.3 is available, we examined the H3.3 specific phospho-epitope (H3.3S31ph). This modification is prominently present during mitosis in human cells[17] and meiosis of the urochordate Oikopleura dioica[18]. At diakinesis (Fig. 1d) and meiosis II, the antibody H3.3S31ph decorates all chromosomes but levels are much higher in sex chromosomes, confirming the enrichment of H3.3-containing nucleosomes in XY chromatin. In contrast, phosphorylation of serine S28, which occurs also during mitosis and meiosis in H3.1/H3.2 and in H3.3, showed a similar labelling index for autosomal and XY chromatin (Fig. 1d).
To establish whether H3.1/H3.2 depletion is conserved in humans we performed a double staining, combining antibodies against H3.1/H3.2 and the synaptonemal complex protein 3 (SYCP3) on human spermatocytes. As in mice, loss of H3.1/H3.2 from sex chromosomes at pachytene was observed (Fig. 1e).

To estimate the onset and duration of H3.1/H3.2 removal, we carried out double stainings with an anti-γH2A.X antibody which stains the sex chromosomes from the zygotene-pachytene transition on[19]. This event preceded H3.1/H3.2 loss (Fig. 2a). The histone H1 testis variant (H1t) is present from mid pachytene onwards[20]. A strong H1t signal always correlated with lack of H3.1/H3.2 staining (Fig. 2b). To more precisely determine the timing of remodeling (Fig. 2c), we selected pachytene spermatocytes, as defined by complete synaptonemal complexes (SCs), and scored for the H3.1/H3.2 status of the sex body (Fig. 2d). Ten percent of 246 spermatocytes

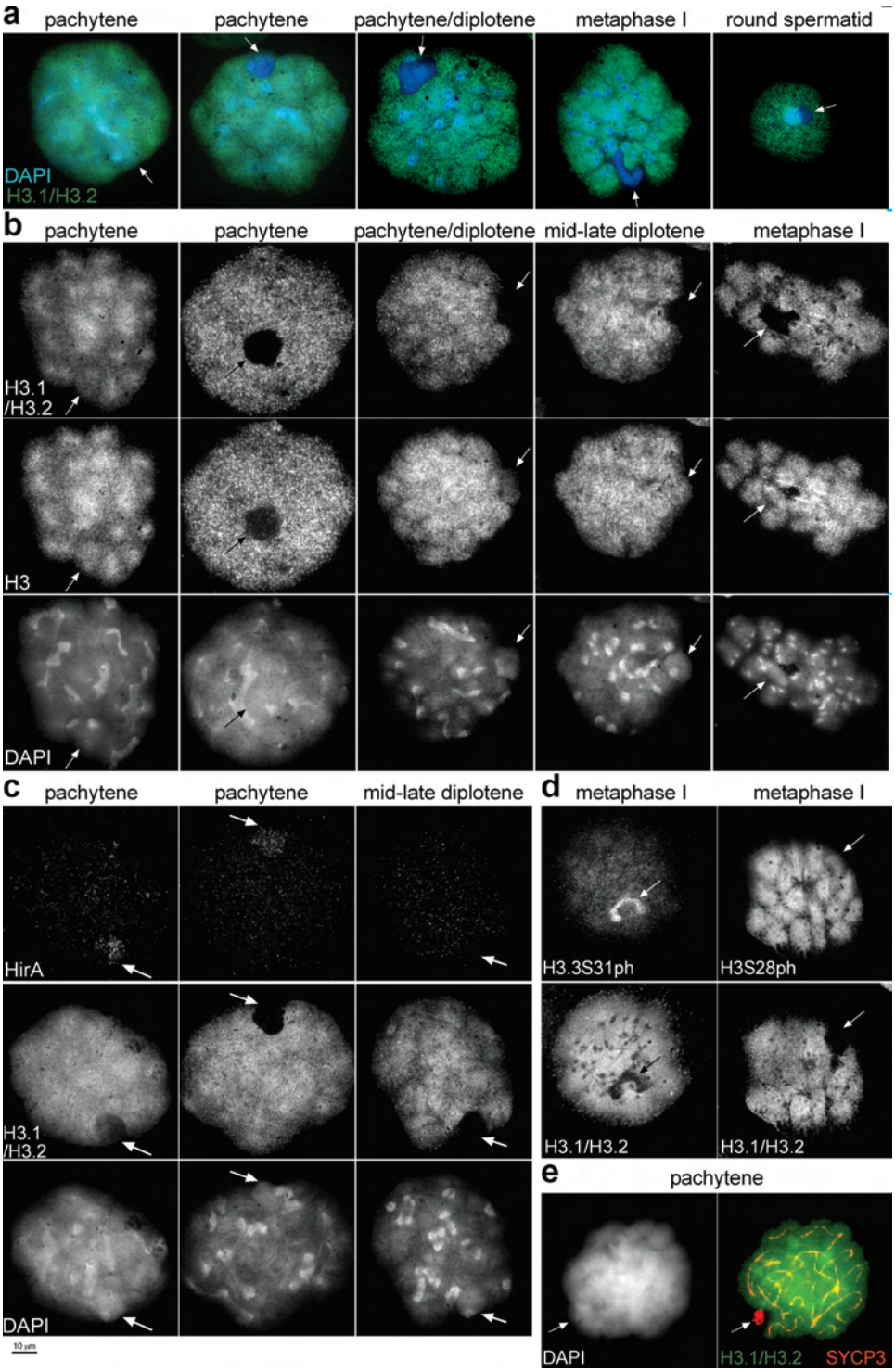
a
pachytene
pachytene
pachytene/diplotene
metaphase I
round spermatid
DAPI
H3.1/H3.2
b
pachytene
pachytene
pachytene/diplotene
mid-late diplotene
metaphase I
H3.1
/H3.2
H3
DAPI
c
pachytene
pachytene
mid-late diplotene
HirA
H3.1
/H3.2
DAPI
10 µm
d
metaphase I
metaphase I
H3.3S31ph
H3S28ph
H3.1/H3.2
H3.1/H3.2
e
pachytene
DAPI
H3.1/H3.2
SYCP3

Figure 1 Gradual removal of H3.1/H3.2 in the XY body in spermatocytes during meiotic prophase I
Arrows indicate sex chromosomes.
a, Spermatocytes in progressing stages of prophase I, metaphase I and a round spermatid stained by anti-H3.1/H3.2 (green) and DAPI (blue). A gradual loss of H3.1/H3.2 from the XY body is observed, resulting in sex chromatin lacking H3.1/H3.2.
b, Spermatocytes in progressing stages of prophase I and metaphase I stained by anti-H3.1/H3.2 (upper panels), anti-H3 (middle panels) and DAPI (lower panels). Whereas loss of H3.1/H3.2 is persistent, anti-H3 staining only shows a temporal decrease in signal.
c, Localisation of the replication independent (RI) nucleosome assembly histone chaperone HirA in pachytene and diplotene spermatocytes (upper panels) combined with H3.1/H3.2 (middle panels) and DAPI (lower panels) staining. HirA is enriched in the XY body in pachytene and early diplotene spermatocytes and reduces to autosomal levels or lower in mid-late diplotene spermatocytes.
d, Presence of H3.3 was confirmed by localisation of the H3.3-specific modification phosphoS31. Metaphase I spermatocytes stained for H3.3S31ph and H3S28ph are depicted on the left and right respectively. Histone H3.3-specific phosphorylation of S31 is enriched in XY chromatin whereas phosphorylation of H3.1/H3.2/H3.3 on S28 is equally present at XY and autosomal chromatin.
e, Localisation of H3.1/H3.2 (green) in a human pachytene spermatocyte. SYCP3 (red) labels lateral elements of the synaptonemal complex and axial elements of the sex chromosomes, DAPI labels DNA. Loss of H3.1/H3.2 from the XY chromatin, as identified by typical SYCP3 configuration, is observed during prophase I.
Bar represents 10 μm.

showed no difference in signal intensity between the XY body and autosomal bivalents, 42% a decreased signal and 48% exhibited a complete loss of H3.1/H3.2 from the sex chromatin. Given that in mice the pachytene stage lasts for 6.6 days (159 hrs), these quantifications show that the decrease in H3.1/H3.2 labeling is first detectable approximately 16 hrs after the zygotene-pachytene transition. It is however anticipated that the actual replacement process starts somewhat earlier. Histone H3.1/H3.2 removal was completed at 3.5 days, coinciding with up regulation of autosomal transcription[3]

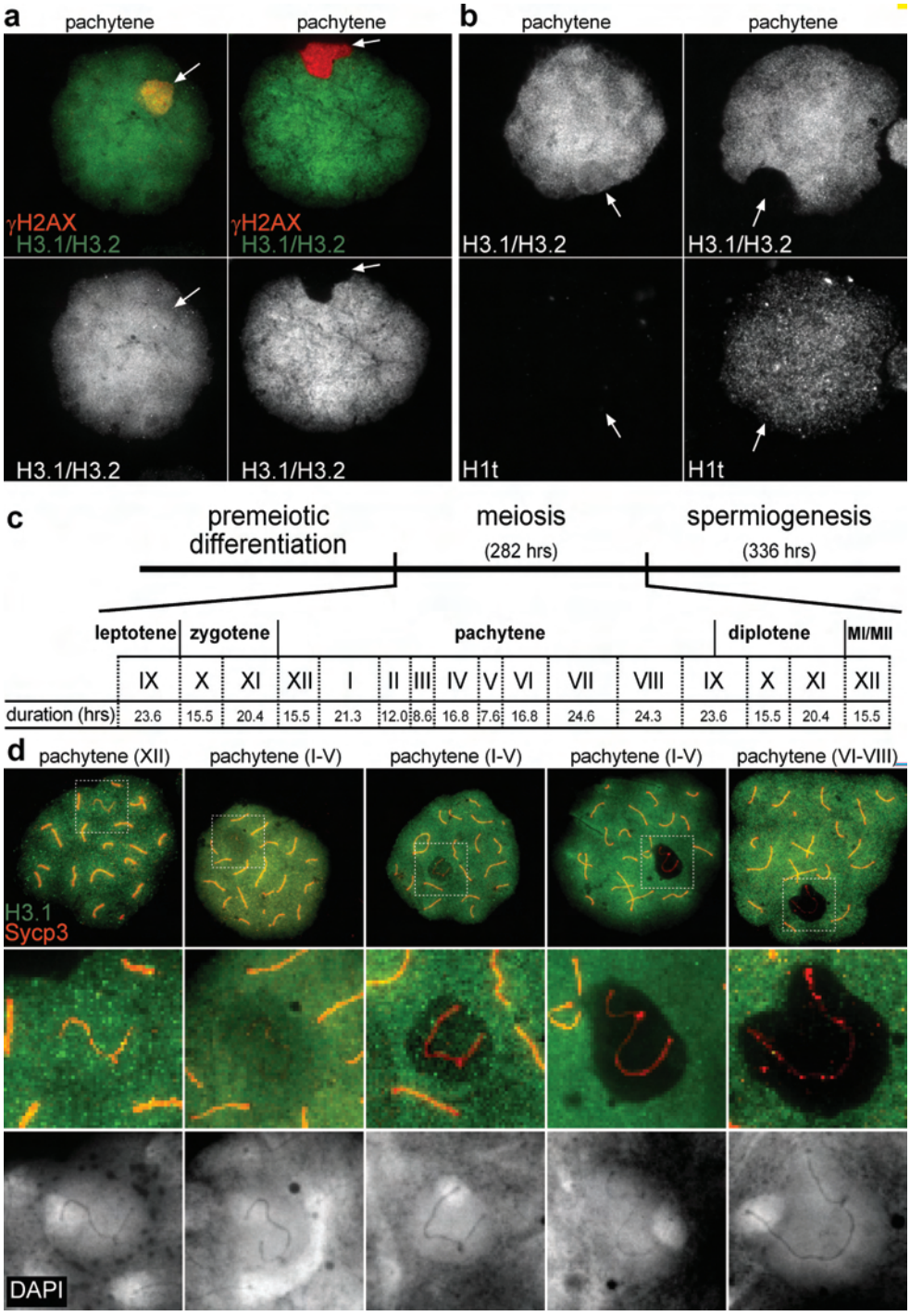
a
pachytene
pachytene
γH2AX
H3.1/H3.2
γH2AX
H3.1/H3.2
H3.1/H3.2
H3.1/H3.2
b
pachytene
pachytene
H3.1/H3.2
H3.1/H3.2
H1t
H1t
c
premeiotic differentiation
meiosis
(282 hrs)
spermiogenesis
(336 hrs)
leptotene
zygotene
pachytene
diplotene
MI/MII
IX X XI XII I II III IV V VI VII VIII IX X XI XII
duration (hrs) 23.6 15.5 20.4 15.5 21.3 12.0 8.6 16.8 7.6 16.8 24.6 24.3 23.6 15.5 20.4 15.5
d
pachytene (XII)
pachytene (I-V)
pachytene (I-V)
pachytene (I-V)
pachytene (VI-VIII)
H3.1
Sycp3
DAPI

Figure 2 Timing of onset and duration of H3.1/H3.2 removal. Arrows indicate sex chromosomes
a, Localisation of γH2A.X (red) and H3.1/H3.2 (green) in pachytene spermatocytes. Phosphorylation of H2A.X at S139 in the XY body precedes loss of H3.1/H3.2.
b, Localisation of H1t and H3.1/H3.2 in pachytene spermatocytes. Loss of H3.1/H3.2 precedes full expression of H1t.
c, Schematic representation of spermatogenesis. Sequence of epithelial stages (roman numerals) and their duration (hours) is based on Oakberg[21]. The pachytene to diplotene transition is adapted based on Dietrich and de Boer[15].
d, Determination of the start and completion of H3.1/H3.2 removal. We stained spermatocytes with anti-H3.1/H3.2 (green), anti-Sycp3 (red) and DAPI. Pachytene spermatocytes were identified on the basis of synaptonemal complex morphology (n=246). Between brackets the corresponding stages of the seminiferous epithelium.

(supplementary Table 2). In terms of Oakberg's scheme of stages of the seminiferous epithelium, we conclude that removal of H3.1/H3.2 takes place during stages I-V (Fig. 2c)[21].

To address the kinetics of *de novo* H3.3 incorporation into XY chromatin during MSCI, we generated two transgenic mouse models, one with a V5-tagged H3.3 gene, the other with a HA-tagged H3.1 gene (supplementary Fig. 2) and studied the spatial and temporal appearance of the tagged histones. In both a high- and a low-expressing transgenic line (supplementary Fig. 2), the meiotic H3.3-V5 signal became visible in chromatin of the X chromosome at mid-pachytene, after desynapsis of the axial elements of the XY chromosomes had initiated (Fig. 3a-e; supplementary Table 3). This was later than detection of HirA in the XY body (Fig. 1c, supplementary Table 1), probably as a result of a lower sensitivity of the H3.3-V5 staining. The intensity of the signal progressively increased and the staining extended to chromatin of the Y chromosome during late pachytene. For autosomal chromatin, we observed a concomitant rise that may relate to increasing levels of autosomal transcription observed at this stage[3]. The H3.3-V5 signal reached its maximal intensity at the diplotene stage in both autosomal and sex chromatin (Fig. 3f-j). In round spermatids, both sex chromosomes could be easily recognised

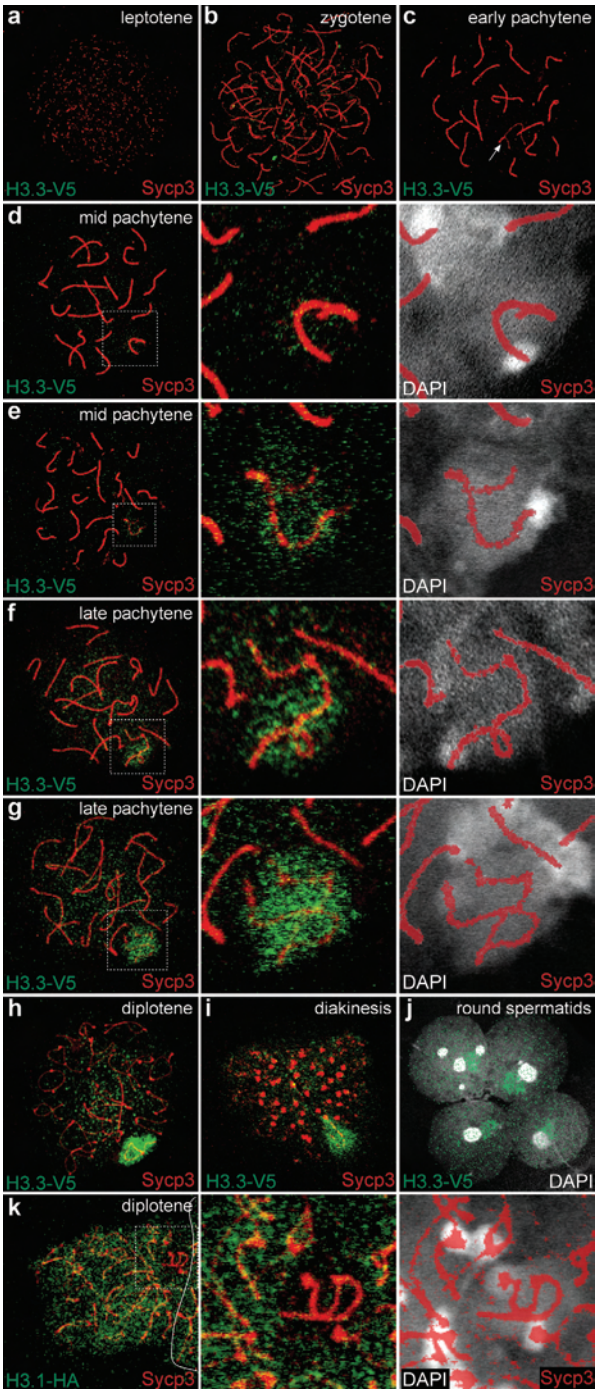

Figure 3 Progressive incorporation of H3.3 at sex chromosomes and autosomes during murine meiotic prophase All H3.3-V5 images are from the high-expressing transgenic line TgN(H3.3-V5)1Apet. Spermatocytes were staged based on morphological criteria of chromosome axial and lateral elements (supplementary Tables 3), visualized by anti-Sycp3 (red). DNA was stained by DAPI (white). (**a-d**) From leptotene onwards, H3.3-V5 (green) only became visible throughout chromatin in midpachytene spermatocytes. (**d-g**) For the sex chromosomes, H3.3-V5 incorporation was first detected at X-linked chromatin, later during late-pachytene also at Y-linked chromatin. (**h-i**) H3.3-V5 labeling increased upto diplotene stage and remained detectable during both meiotic divisions. (**j**) H3.3-V5 labeled X and Y territories[4, 12, 13] in haploid round spermatids. (**k**) H3.1-HA staining (green) at XY chromosomes was lost in diplotene spermatocytes of transgenic line TgN(H3.1-HA)1Apet.

by their H3.3 accumulation (Fig. 3j). The behaviour of HA-tagged H3.1 supports the findings with the anti H3.1/H3.2 monoclonal, though with a reduced sensitivity for stages before late pachytene due to a low expression level of the transgene (Fig. 3k).

Structural differences between H3.1, H3.2 and H3.3 containing nucleosomes are expected to be small[8], suggesting that the replacement of H3.1/H3.2 by H3.3 as such is not the prime aim of the observed nucleosomal exchange. H3.1/H3.2 eviction may follow from the need to remove certain histone PTMs carried by the H3•H4 dimers. To test this hypothesis, we studied the temporal dynamics of methylated forms of H3 and H4 in the XY body from early pachytene spermatocytes up to round spermatids.
All thirteen modifications (H3K4me1,2,3; H3K9me1,2,3; H3K27me1,2,3; H3K79me2; H4K20me1,2,3) were detected in varying degrees of intensity in early pachytene XY chromatin (Table 1, Fig. 4 and supplementary Fig. 3). Loss of H3.1/H3.2 coincided with loss of all histone PTMs, with the exception of the mono-methylated forms of H3K9 and H4K20.
Four patterns of histone lysine methylation dynamics from early pachytene to haplophase could be distinguished (Table 1): A) the mark was lost and reappeared gradually during stages VI-XII, (6 cases, e.g. H3K9me3 in Fig. 4a); B) the mark was lost and reappeared at haplophase (2 cases, e.g. H3K79me2 in Fig. 4b); C) the mark accumulated during nucleosome replacement, was absent in mid-late diplotene (stages X-XI) and reappeared during the meiotic divisions or haplophase (2 cases, e.g. H4K20me1 in Fig. 4c); D) the mark was lost from the sex chromosomes (3 cases, e.g. H4K20me3 in Fig. 4d). The temporary absence of certain histone modifications as a consequence of nucleosome replacement clarifies variations between reported staining patterns of these methylated lysine residues during pachytene [5, 11-13]. Moreover, it is conceivable that it largely precludes H2A.Z from being incorporated into sex chromatin during pachytene and diplotene while autosomal chromatin is amenable[13].
In conclusion, nucleosomal replacement during pachytene causes loss of almost all studied H3 and H4 associated methyl marks and leads to a selective reappearance of specific histone modifications in later meiotic and post-meiotic stages.

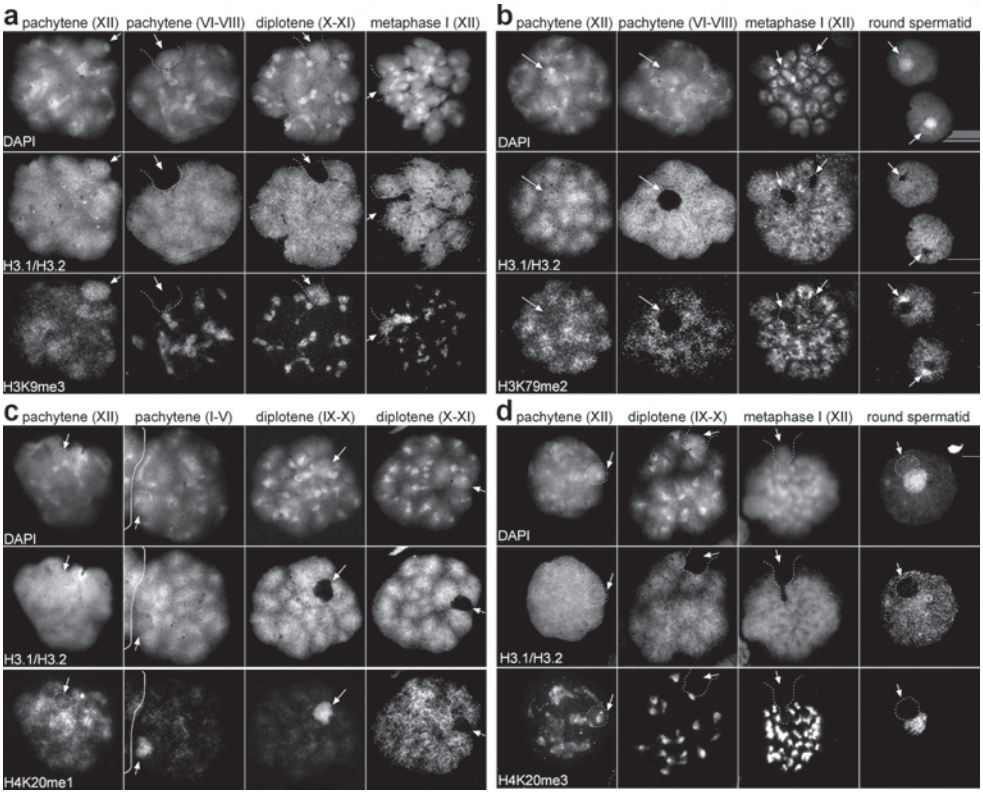

Figure 4 Dynamics in histone lysine methylation patterns in relation to nucleosomal exchange at the XY body (a-d). Progressing stages of spermatogenesis are shown from left to right. Nuclei were stained with DAPI (upper panels), antibodies against H3.1/H3.2 (middle panels) and the indicated post-translational histone modification (lower panels). Arrows and dotted white lines indicate position and shape of sex chromosomes.

a, H3K9me3: prior to H3.1/H3.2 removal, H3K9me3 was enriched in the sex body. Loss of H3.1/H3.2 depleted most of this mark though some signal remained present in the heterochromatic region of the X chromosome. By stages X/XI, a prominent signal had accumulated in the XY chromatin, which persisted throughout the meiotic divisions and haplophase (supplementary Fig. 3).

b, H3K79me2: in stage XII pachytene spermatocytes H3K79me2 was present in XY chromatin although less prominently than in the autosomes. A complete loss of signal was observed with H3.1/H3.2 removal. A signal accentuating the sex chromatin reappeared in round spermatids.

c, H4K20me1: in stage XII pachytene spermatocytes H4K20me1 levels of sex chromatin were reduced compared to autosomes. During nucleosome replacement, levels of this mark increased vastly, to be absent in stage X/XI diplotene and to reappear in round spermatids (supplementary Fig. 3).
d, H4K20me3: H4K20me3 was prominently present in X heterochromatin and the pseudo-autosomal region and faintly throughout the euchromatin of the sex chromosomes in stage XII pachytene spermatocytes[29]. A complete loss of signal was observed in concert with H3.1/H3.2 removal. No return of this mark was observed up to the round spermatid stage.

Table 1. Temporal dynamics of histones and histone PTMs in sex chromatin during pachytene, diplotene, the meiotic divisions and in round spermatids

Staining pattern	Antibody	Early pachytene (stages XII)	Mid pachytene to mid diplotene (stages VI-X)	Mid to late diplotene (stages X-XI)	Meiotic divisions (stage XII)	Round spermatids#
	H3.1/H3.2	+	-	-	-	-
	H3	+	+/-	+	+	+
A	H3K4me1	+/-	+/-*	+/-	+	+/-
	H3K4me2	+/-	-	-	+	+/-
	H3K4me3	+/-	-	-	+/-	+
	H3K9me2	+	+*	+	+	+
	H3K9me3	+	+*	+	+	+
	H4K20me2	+/-	-	+/-*	+/-	-
B	H3K27me1	+	-	-	-	+
	H3K79me2	+	-	-	-	+
C	H3K9me1	+/-	+/-Δ	-	-	+/-
	H4K20me1	+/-	+Δ	-	+/-	+
D	H3K27me2	+	-	-	-	-
	H3K27me3	+/-	-	-	-	-
	H4K20me3	+	-	-	-	-

Corresponding stages of the seminiferous epithelium are denoted between brackets.
+ = abundant; +/- = faintly present; - = not present.
* de novo appearance of histone PTM after temporary previous absence.
Δ *de novo* appearance during stages I-V. # Period of appearance of histone modifications in sex chromatin of round spermatids differed between marks.

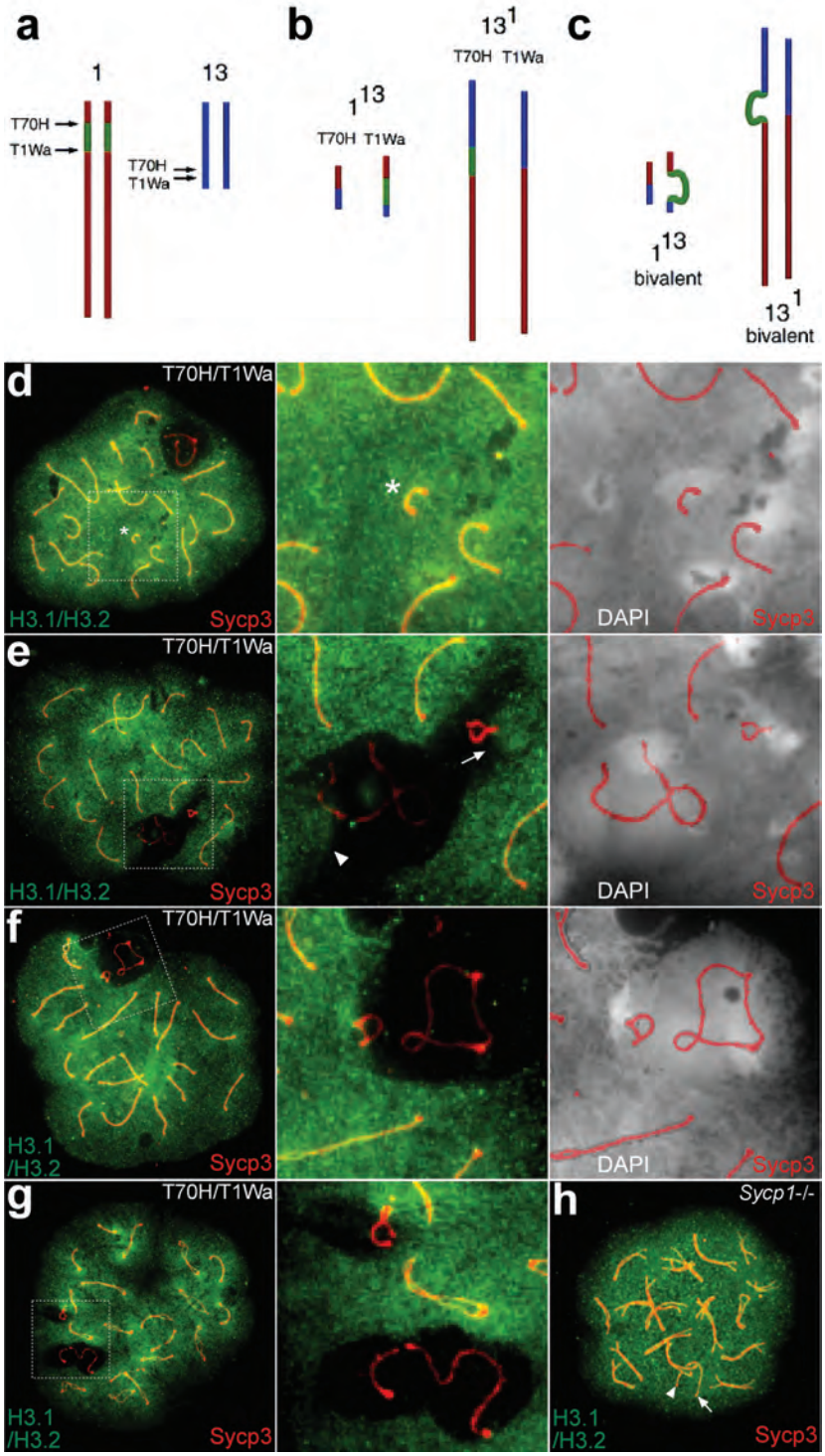
a
1
13
T70H
T1Wa
T70H
T1Wa
b
1^{13}
T70H T1Wa
13^{1}
T70H T1Wa
c
1^{13}
bivalent
13^{1}
bivalent
d
T70H/T1Wa
H3.1/H3.2
Sycp3
DAPI
Sycp3
e
T70H/T1Wa
H3.1/H3.2
Sycp3
DAPI
Sycp3
f
T70H/T1Wa
H3.1
/H3.2
Sycp3
DAPI
Sycp3
g
T70H/T1Wa
H3.1
/H3.2
Sycp3
h
Sycp1-/-
H3.1
/H3.2
Sycp3

Figure 5 Localisation of H3.1/H3.2 in asynapsed autosomal chromatin of the T(1;13)70H and T(1;13)Wa translocation containing spermatocytes and Sycp1$^{-/-}$ spermatocytes Nuclei were stained for H3.1/H3.2 (green), Sycp3 (red) and DAPI. Second and third column are higher magnifications except for h.
a, Localisation of *T70H* and *T1Wa* breakpoints.
b, Double translocation heterozygosity leads two semi-identical "homologous" chromosomes 1^{13} and 13^{1}.
c, During early meiotic prophase I, the non-homologous segments (green) are initially asynapsed. In the 13^{1} bivalent, this segments readjusts during late zygotene, early pachytene while in the 1^{13} bivalent, it frequently remains totally or partially asynapsed (diagram reproduced from[19]).
d, When full heterologous synapsis was accomplished a horse shoe-like synaptonemal complex was produced (indicated by asterisk). No loss of H3.1/H3.2 was observed from the 1^{13} bivalent.
e, Synapsis on one end of the 1^{13} bivalent yielded a fork conformation. H3.1/H3.2 removal was observed in the asynapsed regions. Synapsed chromatin of the same bivalent retained H3.1/H3.2 (indicated with arrow). In spermatocytes carrying a partially synapsed 1^{13} bivalent, an incomplete loss of H3.1/H3.2 in the XY chromatin was more frequently observed (indicated with arrowhead).
f, Synapsis occurring on both ends of the 1^{13} bivalent resulted in the loop conformation. H3.1/H3.2 was only lost in the intermediate asynapsed region but not in synapsed extremities of the bivalent.
g, Loss of H3.1/H3.2 was also observed when the sex chromosomes and the 1^{13} bivalent were localised in separate domains. Such separation was a rare event (3 out of 221 pachytene/diplotene spermatocytes).
h, In *Sycp1*$^{-/-}$ diplotene-like spermatocytes no loss of H3.1/H3.2 was observed from the sex chromosomes (arrow indicates X, arrowhead indicates Y).

To asses whether nucleosome replacement is a sex chromosome-specific trait, or whether asynapsed autosomal segments also display this event, we analysed primary spermatocytes from mice that are double heterozygous for two semi-identical reciprocal translocations[22]. In such *T(1;13)70H/T(1;13)1Wa* spermatocytes, translocation bivalents (Fig. 5a-c) often contain asynapsed autosomal chromosome segments that are subjected to MSUC[5] and positioned adjacent to the XY bivalent. Localisation of Sycp3 and H3.1/H3.2 did reveal eviction of H3.1/H3.2 in such asynapsed autosomal regions (Fig.

5d-f). Loss of H3.1/H3.2 also occurred when asynapsed autosomal and sex chromatin were localized in separate domains indicating that nucleosomal replacement is a general feature of MSUC and independent of sex body formation (Fig. 5g). Intriguingly, in ~40% of late pachytene and early diplotene spermatocytes we observed a residual H3.1/H3.2 signal in asynapsed autosomal segments and/or adjacent sex chromosomes (Fig. 5e; supplementary Table 4). Thus, the capacity for nucleosomal replacement seems to be limited in spermatocytes. Since sex bodies containing asynapsed autosomal chromatin show increased levels of transcription[23], nucleosomal replacement is likely a prerequisite for proper gene silencing in the context of MSCI/MSUC.

According to recent reports, MSUC/MSCI is initiated in late zygotene cells by targeting of the PI3-kinase ATR via BRCA1 to asynapsed chromatin[24, 25] that subsequently phosphorylates H2A.X (γH2A.X)[19], and ultimately leads to sex body formation in early pachytene spermatocytes. Timely induction of MSCI/MSUC by ATR targeting to asynapsed chromatin depends on the capacity of cells to monitor the state of synapsis at the zygotene-pachytene transition[2, 26]. For example, in *Sycp1*$^{-/-}$ spermatocytes that fail to finalise synaptonemal complex formation, staining patterns of ATR and γH2A.X are invariant between sex chromosomes and autosomes, and between zygotene, pachytene and diplotene stages[26]. Accordingly, such mutants fail to form sex bodies. To determine whether nucleosome replacement depends on MSUC and MSCI induction, we probed *Sycp1*$^{-/-}$ zygotene, pachytene and diplotene-like spermatocytes[26] with anti-H3.1/H3.2 and anti-Sycp3 antibodies. As illustrated in Fig 5h; supplementary Table 4, we failed to obtain any evidence for nucleosome exchange at XY or autosomal chromatin.

Together, the presented data on H3.1/H3.2 eviction in wild-type, *T(1;13)70H/T(1;13)1Wa*, and *Sycp1*$^{-/-}$ spermatocytes and on H3.3 incorporation in transgenic H3.3-V5 spermatocytes demonstrate nucleosome replacement to be a general feature of MSUC, initiated shortly after MSUC induction in early pachytene cells.
A function of γH2A.X in DNA double strand break repair is to attract chromatin remodelers[27] and an analogous role for γH2AX in MSUC is therefore likely (as elimination of H2A.X results in fail-

ure to induce MSCI[28]). The accumulation in the XY body[1] of DNA repair proteins, such as Mre11 and Rad50 could therefore be connected to MSUC induced nucleosome replacement. Hence, we propose that during MSUC these repair proteins facilitate chromatin remodeling, rather than being instrumental in DNA repair.
In summary, we describe massive chromatin remodeling of the sex chromosomes to be a feature of human and mouse male meiotic prophase I. The unique chromatin composition obtained in this process potentially serves a role in MSCI and postmeiotic functioning of the sex chromosomes when a selective gene reactivation of MSCI subjected genes occurs[12].

Acknowledgements
We thank T. Jenuwein, A. Schulmeister, F van Leeuwen, C. Heyting, P.B. Moens, P.D. Adams and H.G. Stunnenberg for providing antibody reagents; J.-F. Spetz, A. Kelly and M. Puschendorf for their help in the generation and initial characterization of H3.1-HA and H3.3-V5 transgenic mice; C. Heyting, A. Pastink and E. de Boer for male meiotic preparations of *Sycp1*$^{-/-}$ knock out mice and W.M. Baarends, C. Logie, and P.J. Wang for critical reading of the manuscript. Research in the AHFMP laboratory is supported by the Novartis Research Foundation and the NoE network "The Epigenome" (LSHG-CT-2004-503433).

Methods

Mice

Initial observations were made in male F1(CBA/B6) mice. Homozygous T(1;13)70H male mice on a Swiss random bred background were used for collecting all data presented here. Male *T(1;13)70H/T(1;13)1Wa* double heterozygous mice, also on a Swiss random bred background, were used to study translocation chromosome involved autosomal asynapsis[22]. Procedures involving animals were approved by the animal ethics committee of the Radboud University Nijmegen Medical Centre and conformed to the Dutch Council for Animal Care and the NIH guidelines. Generation, handling and housing of transgenic H3.3-V5 and H3.1-HA animals was conform the Swiss Animal Protection Ordinance, chapter 1. Human testicular tissue was obtained as remnant material from a diagnostic testicular biopsy with informed consent.

Surface spread preparations

Nuclear spreads were obtained as described in Peters et al., with some modifications introduced in Baart et al.[25, 30]. Briefly, a suspension of spermatogenic cells was obtained that was treated with a hypotonic buffer (17 mM sodium citrate, 50 mM sucrose, 30 mM Tris.HCl pH 8.2). After centrifugation the pellet was carefully resuspended in a 100 mM sucrose solution and applied over a PFA coated glass slide (1% PFA, 0.15% Triton-X-100, pH 9,2-9,5). The slides were kept for 2 hours in a humidified atmosphere. After 1.5 hours the box was opened and slides were washed with 0,08% photoflow (Kodak).

Fluorescent immunostaining

Surface spread slides were stained according to the protocol described in Baart et al[25]. Briefly, slides were blocked for 1 hour at 37°C. After blocking, primary antibodies diluted in blocking solution were applied. Priming for 40 minutes at 37°C was followed by overnight incubation at 4°C. The next day slides were washed after which nuclei were blocked for 1 hour at 37°C. Secondary antibodies were diluted in blocking solution and incubated for 2 hours at 37°C. After washing in PBS, slides were incubated with DAPI and mounted with Vectashield.

Antibodies

The monoclonal antibody #34 was used to localise H3.1/H3.2 at a dilution of 1:1500 [9]. The monoclonal antibody #32 recognizes nucleosomes and was used at a dilution of 1:2000[14]. Polyclonal rabbit Pan-H3 (ab1791; 1:500) and H3.3S31ph (ab2889; 1:20) antibodies were purchased from Abcam. Polyclonal rabbit D34, which recognizes HirA was used in 1:100 (P.

Adams). Polyclonal rabbit Sycp3 was used in a 1:400 dilution (C. Heyting). The mouse monoclonal antibody against gH2A.X was purchased from Upstate Biotechnology (# 05-636; clone JBW301;1:10.000). Polyclonal rabbit antibody against Histone H1t was used in a 1:100 dilution (P. Moens). Polyclonal rabbit antibodies against H3K9me1,2,3; H3K27me1,2,3 were diluted 1:250; H4K20me1 was diluted 1:1000, H4K20me2 was diluted 1:50 and H4K20me3 was diluted 1:250 (T.Jenuwein). Rabbit polyclonal antibodies for H3K4me1,2,3 were purchased from Abcam (catalogue nr and dilutions ab8895, 1:100; ab7766 1:100; ab8580 1:1500, respectively). Polyclonal rabbit antibody was used to detect H3K79me2 in a 1:500 dilution (F. van Leeuwen). V5 antibody (Invitrogen, 46-0705) and HA antibody (Roche, 3F10) were used in a 1:500 and a 1:100 dilution respectively. To uncover the epitopes for the pan-H3; H3K79me2, H3.3S31ph, V5 and HA antibodies, slides were first incubated in 4 M HCl for 6 minutes prior to blocking, after which slides were extensively washed in PBS. Primary antibodies were detected by labelling with Molecular Probes A11001 fluor 488 goat anti-mouse IgG (H+L), A11012 fluor 594 goat anti-rabbit IgG (H+L). Both were used in a 1:500 dilution.

Analysis and image capture

A minimum of hundred pachytene/diplotene nuclei or round spermatid nuclei were analysed per staining. All stainings except those with the nucleosome antibody were performed in combination with the H3.1/H3.2 antibody. As immunofluorescence stainings were co-stainings in combination with DAPI, the identification of first meiotic prophase stages relied on DAPI staining pattern, in particular the morphology of the sex body. The assumption was made that pachytene had commenced when a sex body could be identified with DAPI. More precise staging was based on anti-staining of the axial elements of the XY chromosomes by DAPI with Dietrich and de Boer and Ashley et al., as references[15, 31]. The DAPI staining characteristics of centric heterochromatin that change over prophase I, constituted the other criterion[31] (Fig.1 and supplementary Fig. 1). The pachytene-diplotene transition could not be precisely determined with this approach. Diakinesis and metaphase I (stage XII) were grouped as metaphase I. Images were collected on a Zeiss axioplan fluorescence microscope. Pictures were captured by a Zeiss AxioCam MR camera on Axiovision 3.1 software (Carl Zeiss). Adobe Photoshop 7.0 was used to reduce background when necessary.

Spermatocytes from H3.3-V5 and H3.1-HA transgenic mice where co-stained with anti-Sycp3 ad either anti-V5 or anti-HA antibodies. Staging criteria for sub stages of pachytene are described in Supplementary Table 3.

Extended discussion of

Chromosome-wide nucleosome replacement and H3.3 incorporation during mammalian meiotic sex chromosome inactivation

Godfried W. van der Heijden, Alwin A.H.A. Derijck, Peter de Boer

In section 2.1 we describe chromosome wide-replacement of nucleosomes in the XY body. The timing of this event suggests involvement in Meiotic Sex Chromatin Inactivation (MSCI) and therefore also in differentiation of the germ cell downstream of meiosis, since MSCI has been shown to have an epigenetic effect on MSCI-subjected chromatin during haplophase[4, 33]. Qualitative interference with this process is indicated to have a negative effect on the meiotic divisions and spermiogenesis[23]. MSCI is an adaptation, which is utilized during male meiosis, of the general principle of Meiotic Silencing of Unpaired Chromatin (MSUC)[33]

The rate of nucleosome turnover and deposition

The duration of nucleosome turnover as determined by loss of H3.1/H3.2 is approximately 67 hours (Section 2.1, Supplementary Table 2). DNA replication proceeds first meiotic prophase, hence the sex body contains around 446 mega base (mb) of DNA. This implies that on average 6.6 mb is being remodelled hourly. One nucleosome represents 200 bp including linker DNA[34, 35]. Under the assumption that the nucleosome removal rate is linear, this suggests that in stage I-IV pachytene spermatocytes every second roughly nine nucleosomes are removed.

An estimation of the onset of de novo nucleosome deposition can be obtained by calculating the percentage of pachytene spermatocytes without enrichment of tagged-H3.3 in the XY body (17%, Section 2.1, Supplementary Table 3). Tagged-H3.3 is detectable at 27 hours into pachytene (this calculation is analogous to the one used to calculate H3.1/H3.2 loss as described in Section 2.1, Supplementary Table 2. If disappearance of the H3.3•H4 chaperone HirA from the sex body (that coincides with a return to autosomal levels of a-nucleosome and a-panH3 in sex chromatin at stage X) is defined as the endpoint of de novo nucleosome deposition, this process takes

159 hours, corresponding to an average nucleosome assembly rate of approximately 4 per second. This number, however, should be considered a rough estimate since it relies on the assumption that all nucleosomes in the sex chromatin are replaced

The rate of nucleosome turnover and deposition

The duration of nucleosome turnover as determined by loss of H3.1/H3.2 is approximately 67 hours (Section 2.1, Supplementary Table 2). DNA replication precedes first meiotic prophase, hence the sex body contains around 446 mega base (mb) of DNA. This implies that on average 6.6 mb is being remodelled hourly. One nucleosome represents 200 bp including linker DNA[34, 35]. Under the assumption that the nucleosome removal rate is linear, this suggests that in stage I-IV pachytene spermatocytes every second roughly nine nucleosomes are removed.

An estimation of the onset of de novo nucleosome deposition can be obtained by calculating the percentage of pachytene spermatocytes without enrichment of tagged-H3.3 in the XY body (17%, Section 2.1, Supplementary Table 3). Tagged-H3.3 is detectable at 27 hours into pachytene (this calculation is analogous to the one used to calculate H3.1/H3.2 loss as described in Section 2.1, Supplementary Table 2). If disappearance of the H3.3•H4 chaperone HirA from the sex body (that coincides with a return to autosomal levels of a-nucleosome and a-panH3 in sex chromatin at stage X) is defined as the endpoint of de novo nucleosome deposition, this process takes 159 hours, corresponding to an average nucleosome assembly rate of approximately 4 per second. This number, however, should be considered a rough estimate since it relies on the assumption that all nucleosomes in the sex chromatin are replaced

The XY body, a highly active domain

It is well established that heterochromatin is transcriptionally silenced and that silenced genes often show a heterochromatic chromatin signature[36]. It is therefore understandable that the transcriptionally silenced XY body, which during the first half of pachytene also has been described as a condensed structure, has long been regarded as a heterochromatic, static chromatin domain[1, 37]. The XY body, however, appears to be far from static and only temporarily heterochromatic.

The XY body is formed in early pachytene spermatocytes and dissolves in mid-diplotene spermatocytes[1, 37], a lifetime of around 187 hours (for a recent review see[33]). During its existence, nucleosome removal and/or deposition stretches over an estimated 171 hours (onset of removal occurs at stage I while finalization of deposition occurs in stage X). Thus, during a significant part of its existence the XY body undergoes chromatin remodelling.

Timing and initiation of XY body formation and MSCI

During early prophase I, Spo11 induces double strand breaks, which are crucial for synapsis and recombination of the homologous chromosomes and the pseudo autosomal region (PAR)[38, 39]. The induced double strand breaks are processed by Rad51 and its meiotic specific homologue Dmc1[40]. During zygotene most of these breaks are repaired and, in the context of SC completion, Rad51 and Dmc1 are lost from the synapsed regions[41-43]. Rad51 binds Brca1 and Brca1, in turn, binds Atr[24, 44]. This explains the large overlap of these proteins observed in the incomplete SC of unsynapsed regions. When autosomal synapsis is finalised (stage XI-XII) these markers are progressively lost from the autosomes but remain present in the eventually largely unsynapsed sex chromatin and, if present, in unsynapsed autosomal chromatin. During early prophase I, phosphorylation of H2AX is mainly governed by Atm[45]. A sharp increase in *Atr* mRNA is observed during early pachytene, this coincides with the spread of ATR throughout chromatin loops in the sex body[25, 45]. The ability of $Atm^{-/-}$; $Spo11^{-/-}$ spermatocytes to form ectopic sex body-like structures, to which Atr localises and where H2AX phosphorylation occurs, strongly indicates that Atr mediates this second wave of H2AX phosphorylation, which is linked to initiation of MSUC. The sex chromosomes, but also autosomal segments that fail to undergo synapsis, still possess double strand breaks as indicated by the presence of Rad51/Dmc1 foci at their axial elements[42]. Possibly the presence of double strand breaks interferes with or delays the formation of the SC in heterologous domains. As a consequence, unsynapsed heterologous domains will be detected and subjected to MSUC after the zygotene-pachytene transition.

During early pachytene the sex chromosomes have migrated to the periphery of the nucleus. The importance of this migration is indicated by the observation that in spermatocytes that have a telo-

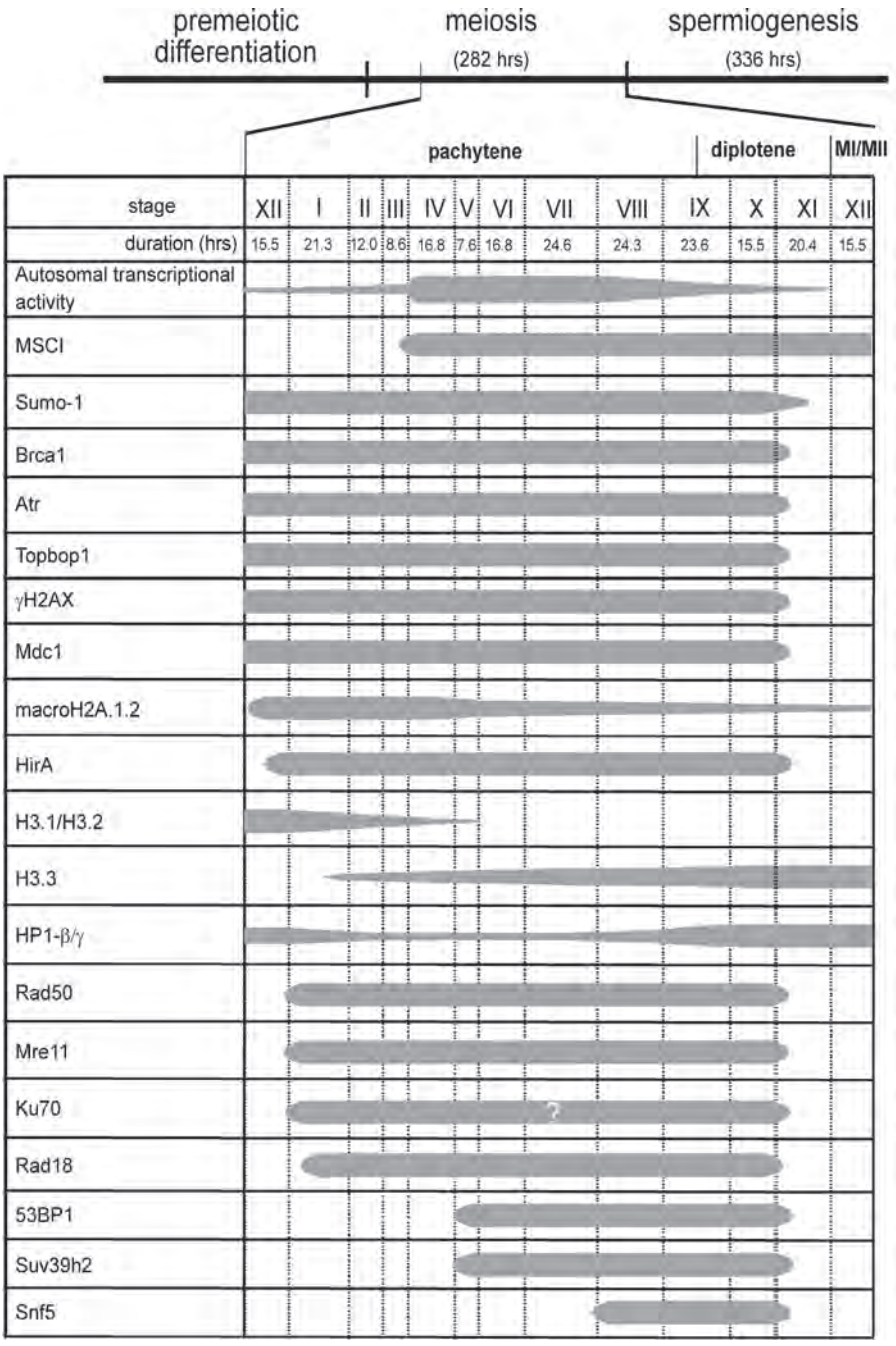

Figure 1 Dynamics of processes and proteins present in the XY body

mere-telemore attraction of the X chromosome centromeric region and an autosomal one, prevents migration and the sex body is not formed[46].

From leptotene on till mid-pachytene, global levels of transcription are low but by no means promiscuous[2, 3, 5]. Deletion of the meiosis-specific histone H3K4 methyl transferase results in transcriptional deregulation and subsequent demise of spermatocytes[47]. A burst of autosomal transcriptional activity occurs during mid pachytene (stage IV)[3, 48]. This coincides with the full establishment of MSCI as nicely shown by the H2AX and Brca1 KO mouse models. In these models abrogation of MSCI results in an upregulation of sex linked genes at mid pachytene (around stage IV)[24, 28]. Incomplete silencing of sex linked genes seems to result in meiotic failure[4, 49].

The order of MSCI induction and subsequent autosomal transcriptional upregulation therefore likely reflects the adaptation of autosomal transcription to MSCI. In other words, the rise of autosomal transcription at stage IV is only possible when in the same nucleus inactivation of the sex chromosomes has occurred.

Mechanism of MSCI/MSUC induced silencing

During establishment of MSCI numerous proteins accumulate in the XY body (Fig. 1, Table 1). Striking is the abundance of proteins functional in DNA repair. In concordance with the transcriptional inactivity of the XY body is the absence of RNA Pol II, splicing machinery and histone modifications that are linked to gene transcription from this domain, as is the presence of several transcriptional repressors and repressive modifications (Tables 1-3). It is hitherto unclear which downstream processes establish actual transcriptional silencing. Recent studies have shown that the cessation of transcription induced by MSCI is not caused by phosphorylation of H2AX, as has been speculated previously. Deletion of Parp-2 reduces poly(ADP-ribose) (pAR) levels of the XY chromatin, a modification that occurs downstream of ATR mediated H2AX phosphorylation. In these gH2AX positive, pAR negative XY bodies, RNA Pol II was observed in the XY body and transcription, as determined by RT-PCR occurred[49].

On the other hand, presence of RNA Pol II in the XY body is not sufficient for transcriptional activation of XY chromatin during prophase I. Spermatocytes in which Scmh1, a component of the Polycomb repressor complex 1 (Prc1), is absent, fail to exclude

RNA Pol II, though MSCI is normally induced[83]. Transcriptional silencing of the XY linked genes during MSCI could be the result of recruitment of transcriptional repressors and exclusion of transcriptional activators (Table 3). Additionally, the intensive nucleosome replacement as described in section 2.1 might be intrinsically repressive. Gene silencing could follow from occupation of the DNA by chromatin remodelling machinery, thereby competing for access with transcription machinery. If nucleosome replacement invokes transcriptional inactivation in the sex body it would be interesting to study the effect of the pAR-modification in this process.

From recent studies on the mechanisms of DNA double strand break repair, a clear link between protein complexes functional in repair of DNA insults and the chromatin remodelling machinery has become apparent[27]. After detection of a (somatic) double strand DNA break, phosphorylation of H2AX by Atm or Atr occurs, which subsequently attracts DNA repair proteins as Mdc1 and 53BP1, while the MRN complex (Mre11/Rad50/Nbs1) and the Ku70-Ku80 heterodimer localize to the unligated ends of the double strand break. The outcome of a competition between Ku70-Ku80 and RPA mediated loading of Rad51 decides which mode of double strand break repair is utilized[85, 86]. Also attracted by γH2AX is the nucleosome remodelling complex INO80, whereas Mre11 recruits the nucleosome remodelling complex RSC. Both complexes have been shown to posses nucleosome evicting capacity[27, 87].

The similarity between the composition of the double strand break repair machinery and proteins that accumulate in the XY body is striking (Fig. 1 and Table 1). It has been suggested that, like the telomere, the XY body functions as a protein reservoir[53]. However, the finding that during the existence of the XY body massive nucleosome replacement occurs suggests a function for several of these proteins in this process.

Clearly, a common denominator between dsDNA repair and nucleosome replacement is chromatin remodelling. Possibly, γH2AX and Mre11 attract chromatin remodelling complexes. In concordance with this is the observation that in the sex body, non-remodelled (α-H3.1/H3.2 positive) domains show decreased levels of γH2AX (Fig. 2). It would therefore be interesting to see whether the INO80 and/or RSC complexes are present in the XY body. Another protein that is present early on in sex chromatin is Mdc1[60]. This protein has

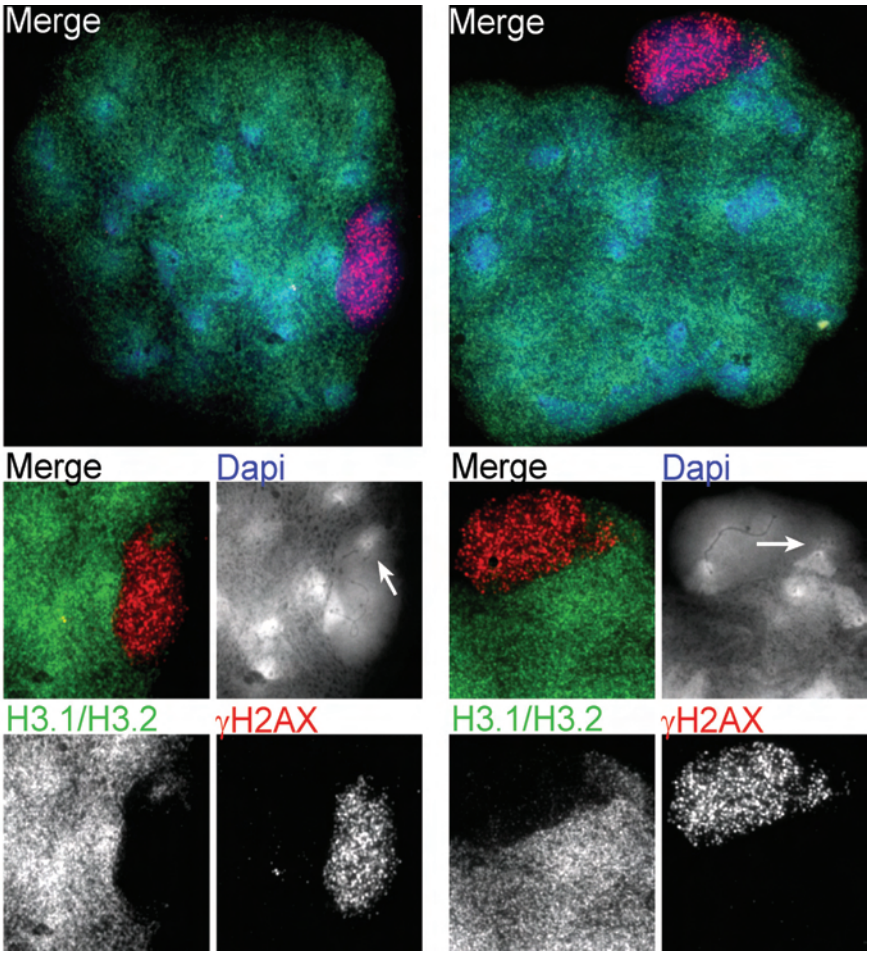

Figure 2 Loss of histone H3.1/H3.2 co-localises to histone gH2AX

Spermatocytes carrying the *T(1; 13)70H and T(1; 13)T1Wa* translocation are stained with a-H3.1/H3.2 antibody (green) and a-gH2AX (red), DNA is labelled with DAPI (blue). The sex body of the spermatocyte on the left contains the 1^{13} chromosome as two univalents. The arrow indicates its Dapi bright heterochromatic segment. Loss of H3.1/H3.2 from this segment is incomplete whereas gH2AX is absent. On the right, the spermatocyte contains the 1^{13} bivalent in a loop conformation. Loss of H3.1/H3.2 is observed from the loop but not yet in the extremities, where the level of gH2AX signal is low.

been described as an amplifier of the dsDNA break distress signal and recruiter of 53BP1[59, 88]. Male meiosis in *Mdc1*$^{-/-}$ mice is severely distorted and has a similar meiotic arrest as the *H2AX*$^{-/-}$ mouse model[59]. It is tempting to speculate that Mdc1, apart from attracting DNA repair proteins, also recruits chromatin remodelling machinery.

The presence of other proteins of which deletion does not infer male meiosis (Table 1) could be the result of their binding characteristics. For example, accumulation of 53BP1 could be a mere consequence its binding capacity for MDC1 and gH2AX, since the mouse model of this protein is fertile[59]. The NHEJ proteins Ku70/Ku80 are enriched in the XY body while another important NHEJ factor, DNA-PKcs, is not[53, 89]. Both the Ku proteins are dispensable for male meiosis as well is NHEJ[57, 58, 90]. Possibly their presence could follow from their association with Mre11[53]. To clarify the role of these proteins in MSCI/MSUC-related nucleosome remodeling a straightforward next step would be to systematically study the dynamics of H3.1/H3.2 status in the XY body or MSUC subjected domains of meiotic mutants.

The molecular mechanism of MSCI/MSUC is diffuse

Although the PAR undergoes synapsis, genes contained in the PAR are silenced and its nucleosomes are replaced. Apparently also synapsed chromatin, which does not attract Brca1, can be subjected to MSCI. Nucleosome remodeling does not affect recombination, the only indication for a difference being the curtailed presence of Mlh1 as a marker for recombination nodules[42]. The capacity to remodel synapsed chromatin was also observed in spermatocytes carrying the T70H/T1WAH translocations. The small 1[13] bivalent contained in these spermatocytes was usually grouped with the XY chromosomes when containing segments of unsynapsed chromatin. Depending on the size of the synapsed segments, the degree of association with the XY chromosomes and the positioning of the synapsed segments, loss of H3.1/H3.2 could occasionally also be observed in there (Fig. 3). This is a strong indication that nucleosome replacement activity is not restricted to Brca1 positive domains. Localisation of Atr (zie table consistent gebruik hoofdletters) as well phosphorylation of H2AX is not excluded from the PAR[2] and as a

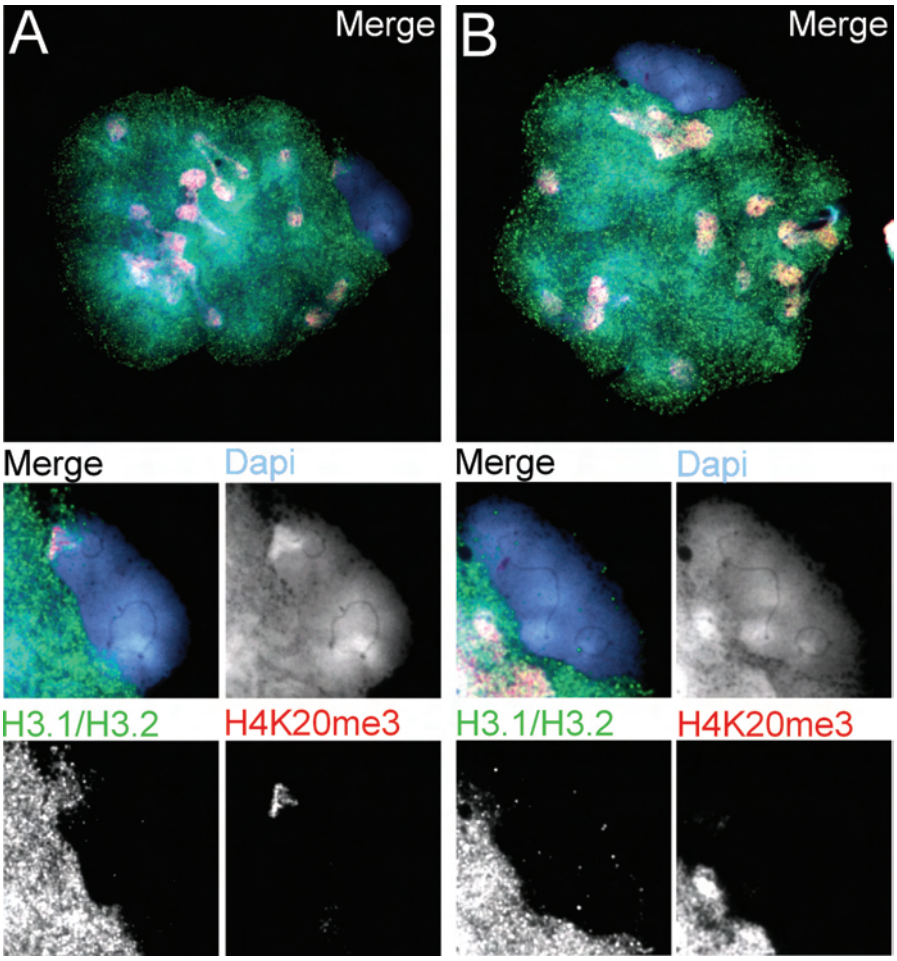

Figure 3 Chromatin remodelling of synapsed domains
Spermatocytes carrying the *T(1; 13)70H* and *T(1; 13)T1Wa* translocation are stained with a-H3.1/H3.2 antibody (green) and a-H4K20me3 (red), DNA is labelled with Dapi (blue).
A) shows a spermatocyte with the 1^{13} bivalent in a loop. The heterochromatic region of the 1^{13} bivalent, which can be recognised by its brighter DAPI staining, stains positive for H3.1/H3.2 and H4K20me3, implying that nucleosome remodeling has not occurred in this segment.
B) shows also shows a spermatocyte with the 1^{13} bivalent in a loop formation (see SC in magnified DAPI image). Loss of H3.1/H3.2 and H4K20me3 has occurred in this domain.

consequence this also accounts for nucleosome replacement[63]. The diffusive character of the molecular mechanism of MSCI emphasizes the necessity of compartmentalization of the XY body during male meiosis[1].

Table 1. proteins enriched in the XY body

Protein	Function	Male phenotype	Reference
Brca1	Breast and ovarian cancer suppression protein	Embryonic lethal; exon 11 deletion combined with P53 heterozygozity pachytene arrest	24
Atr	Ataxia Telangiectasia and Rad3 related; checkpoint kinase	Embryonic lethal	25, 50
Topbp1	Amplifier of ATR kinase activity	ND	51, 52
Mre11	Multifunctional protein; core unit of MRN complex; has DNA nuclease, strand-dissociation and strand-annealing activities	Embryonic lethal	53-55
Nbs1	Member of MRN complex	Embryonic lethal	55, 56
Rad50	Member of MRN complex; ATP-dependent SMC-like protein	Embryonic lethal	54, 55
Ku70/80	Central components of Non-homologous End Joining	Fertile	53, 57, 58
Mdc1	Mediator of Damage Checkpoint	Stage IV arrest	59, 60
53BP1	Mediator of DNA damage checkpoint	Fertile	60, 61

Rad18	Ring domain Ubiquitin ligating enzyme that binds single stranded DNA functional in Translesion DNA Synthesis pathway	ND	62
HirA	H3.3-H4 specific chaparone	Embryonic lethal	63
Snf5	Chromatin remodeller	Embryonic lethal	64
Mael	Homologue of Drosohila HMG protein	ND	64
Parp2	Poly (adp-ribosyl) polymerase-2	Incomplete penetrant hypofertility	49
HP1β/ Cbx1	Heterochromatin Protein 1 β; binds di and trimethylated histone H3 position	Embryonic lethal	13, 65, 66
HP1γ/ Cbx3	Heterochromatin Protein 1 γ; binds di and trimethylated histone H3	Embryonic lethal	13, 66
Suv39h2	H3K9me2,3 HMT	Fertile	67
H2A macro	Histone H2A variant	Fertile	65, 68-70
DMWD	Putative interactor with UBHI and HP1-γ/Cbx3	ND	71
Erk1/2	Ubiquitous serine/threonine protein kinase	Erk1 KO fertile; Erk2 KO Embryonic lethal	72
Pml	Promyelocytic leukaemia protein	Fertile	73

Daxx	Transcriptional repressor; known Sumo substrate	Embryonic lethal	[73]
Xybp/ Rnf19	Ring finger protein; enriched in sex chromatin during zygote/pachytene	ND	[74]
Gcnf/ Nr6a1	Transcriptional repressor	Embryonic lethal	[75]
Dmrt7	DM domain containing transcription factor	Infertile, late pachytene arrest	[76, 77]

Supplementary data section 2.1

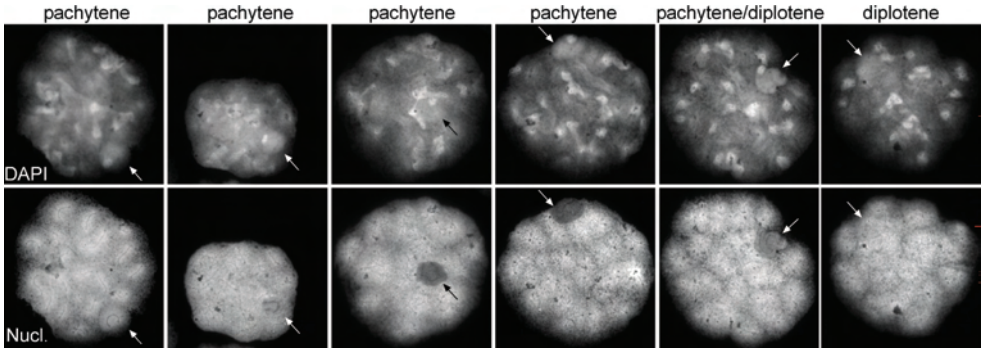

Supplementary Figure 1. Temporary reduction of nucleosome density in the XY body.
Staining with a monoclonal antibody that specifically recognizes nucleosomes shows a temporary decrease of epitope in the XY body during prophase I. Progressing stages of spermatogenesis are shown from left to right. Arrows indicate XY body. The anti-nucleosome antibody #32 is derived from a Lupus mouse. Extensive characterization of #32 with histones, histone peptides, subnucleosome structures and intact native nucleosomes revealed a superior reactivity of #32 with the intact nucleosome. When used in the appropriate dilution, the antibody only reacts with native nucleosomes[14].
Spermatocytes stained with the nucleosome-specific antibody showed a pattern similar to that of H3 staining (Fig. 1b). In early primary spermatocytes identical levels were observed in autosomal and sex chromatin. A temporary decrease of signal was observed in the XY body in later stages. As with the H3 staining, a residual level was always present. During mid-late diplotene, levels in autosomal and XY chromatin were equal again. For staging, see M&M and supplementary data.

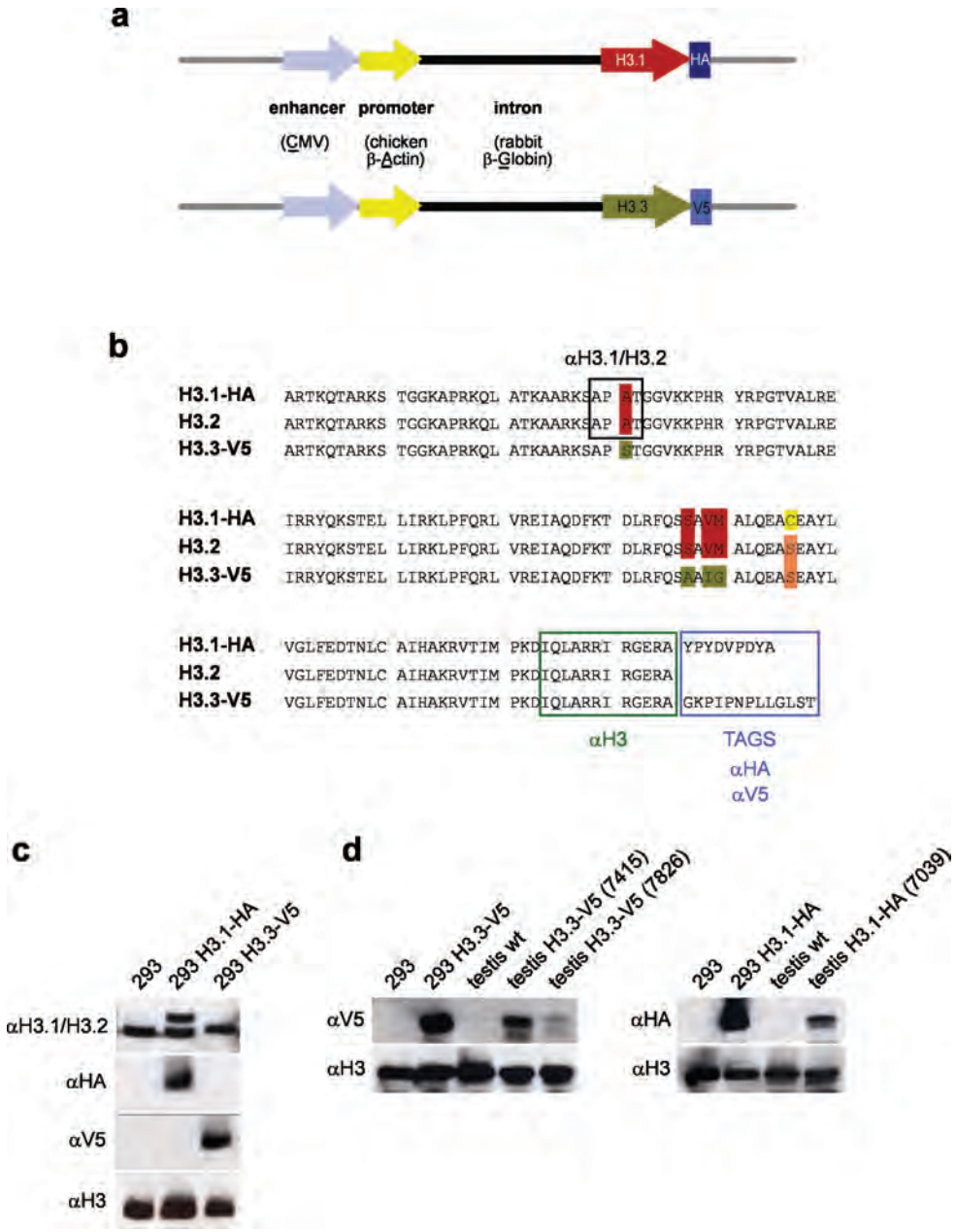

Supplementary Figure 2 Generation and characterization of H3.3-V5 and H3.1-HA transgenic lines

a, Schematic diagram of constructs used to generate transgenic mice. H3.1-HA and H3.3-V5 contain one copy of either the HA or V5 tag and are expressed under transcriptional regulation of the "CAG promoter"

consisting of the Cytomegalovirus (CMV) immediate-early enhancer, chicken b-Actin promoter, and rabbit b-Globin intron. Histone cDNAs were obtained by PCR amplification from total mouse embryonic fibroblast cDNA using transcript specific primers and cloned into pGEM-T-easy plasmids. After addition of the HA or V5-tag via PCR-based cloning strategies, H3-tag open reading frames were cloned into the EcoR1 site of the pCX vector, thereby deleting the EGFP cassette. The final plasmids were linearised with PvuI and HindIII and injected into pronuclear stage zygotes on a C57BL/6-BALB/c x C57BL6 genetic background.

b, Sequence alignment of H3.1, H3.2 and H3.3 proteins. Sequence diversities between different H3 proteins are indicated by different colors. The minimal epitope (APAT) recognized by the a-H3.1/H3.2 antibody is indicated by a box[9]. The panH3 antibody (Abcam 1791) was raised against a synthetic peptide corresponding to 12 amino acids (IQLARRIRGERA) localized at the C-terminus of Histone H3. Following entries were used for sequence alignment: H3.1 accession: P68433; H3.2 accession: P84228; H3.3 accession: P84244.

c, Western blot analyses showing specificity of a-H3.1/H3.2, a-HA, and a-V5 antibodies. Histone-enriched protein preparations were obtained via H_2SO_4 extraction from control Human Embryonic Kidney 293 cells and HEK293 cells either transfected with H3.1-HA or H3.3-V5 expression constructs. Antibodies were used in the following dilutions: a-H3.1/H3.2 (#34), 1:30,000; a-HA (Roche, 3F10), 1:20,000; a-V5 (Invitrogen, 46-0705), 1:75,000; a-H3 (Abcam, 1791) 1:200,000. The panH3 antibody failed to recognize the tagged H3.1 and H3.3 proteins, possibly due to epitope masking. A similar observation was made for a C-terminally GFP-tagged H3.3 variant of *C. elegans*[32].

d, Expression level of H3.3-V5 and H3.1-HA tagged histones in testis of different transgenic mouse lines. Western blot analyses of testis extracts prepared from wild type (C57BL/6) and transgenic animals. Histone preparation and antibody detection as described in **c**. The following transgenic lines were used in this study: H3.3-V5 #1: TgN(H3.3-V5)1Apet; H3.3-V5 #2: TgN(H3.3-V5)2Apet; H3.1-HA #1: TgN(H3.1-HA)1Apet.

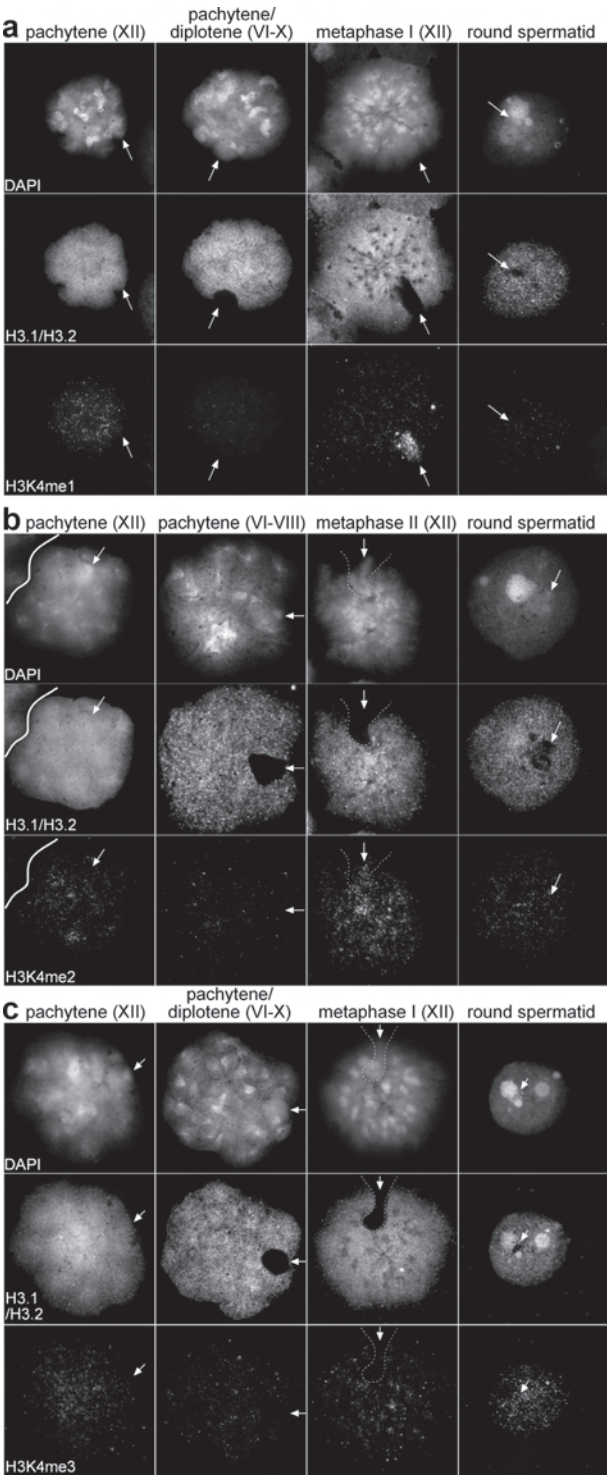
a
pachytene (XII)
pachytene/ diplotene (VI-X)
metaphase I (XII)
round spermatid
DAPI
H3.1/H3.2
H3K4me1
b
pachytene (XII)
pachytene (VI-VIII)
metaphase II (XII)
round spermatid
DAPI
H3.1/H3.2
H3K4me2
c
pachytene (XII)
pachytene/ diplotene (VI-X)
metaphase I (XII)
round spermatid
DAPI
H3.1 /H3.2
H3K4me3

Supplementary Figure 3 Patterns of H3K4 methylation during prophase I

a, Localisation of mono-methylated histone H3 lysine 4 (H3K4me1). The overall faint signal for H3K4me1 throughout the primary spermatocyte was lost during H3.1/H3.2 removal. During diplotene H3K4me1 accumulated in XY chromatin, eventually resulting in its enrichment in the condensed XY chromatin. In round spermatids this mark was faintly present throughout the chromatin.

b, Localisation of di-methylated histone H3 lysine 4 (H3K4me2). As for H3K4me1, levels of this mark dropped during chromatin remodeling and eventually were lost from XY chromatin. XY levels were equal to autosomal levels in condensed meiotic chromosomes. In round spermatids the mark was present in the sex chromatin in a punctuated form.

c, Localisation of tri-methylated histone H3 lysine 4 (H3K4me3). Prior to H3.1/H3.2 loss this mark was faintly present in sex chromatin. The mark disappeared completely from the sex body after H3.1/H3.2 removal. During the meiotic divisions a faint signal was detected on the sex chromosomes when compared to the signal autosomes showed. Histone H3K4me3 was present in the sex chromatin of round spermatids in levels equal to autosomal euchromatin.

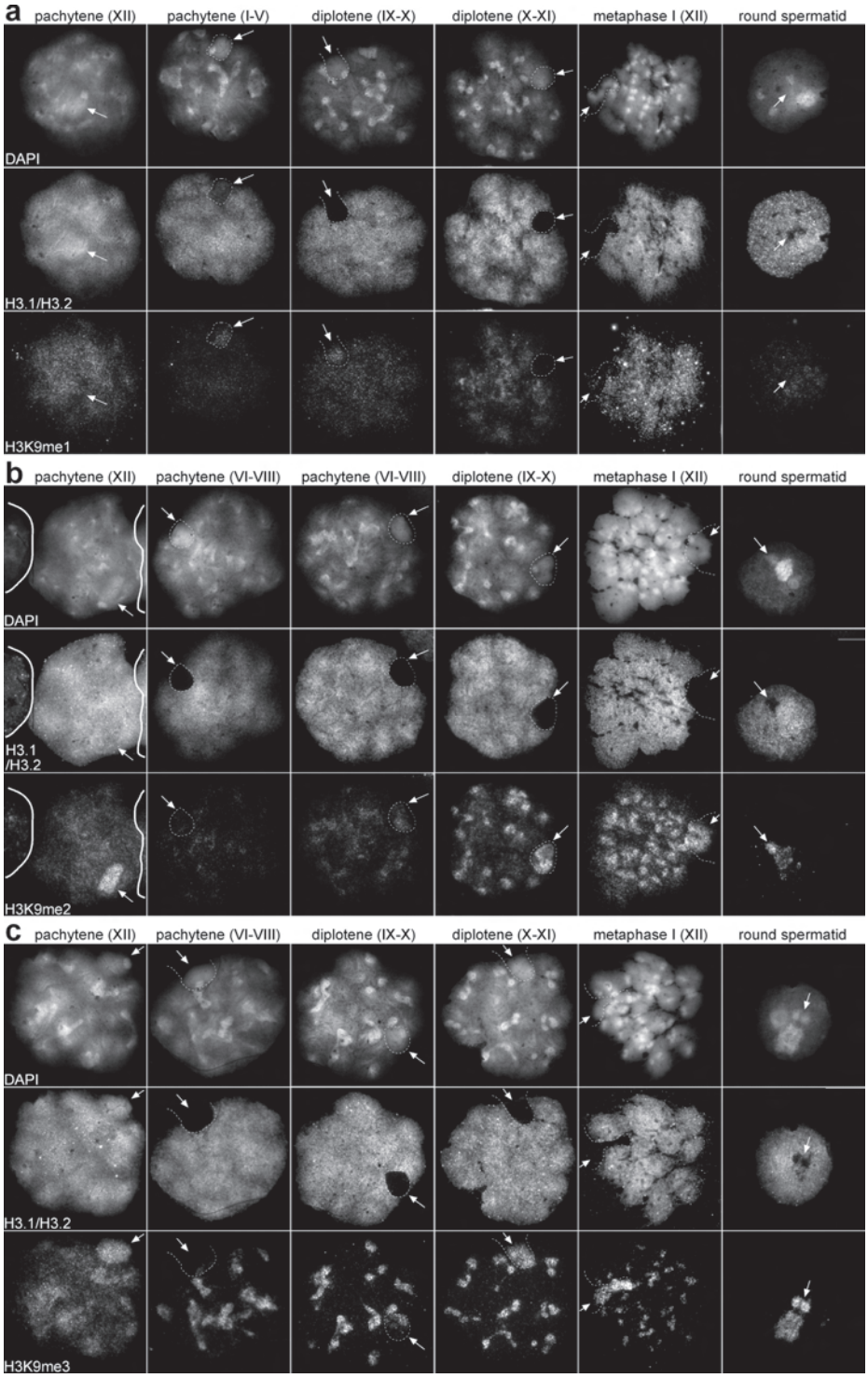
a
pachytene (XII)
pachytene (I-V)
diplotene (IX-X)
diplotene (X-XI)
metaphase I (XII)
round spermatid
DAPI
H3.1/H3.2
H3K9me1
b
pachytene (XII)
pachytene (VI-VIII)
pachytene (VI-VIII)
diplotene (IX-X)
metaphase I (XII)
round spermatid
DAPI
H3.1
/H3.2
H3K9me2
c
pachytene (XII)
pachytene (VI-VIII)
diplotene (IX-X)
diplotene (X-XI)
metaphase I (XII)
round spermatid
DAPI
H3.1/H3.2
H3K9me3

Supplementary Figure 4 Dynamics of mono, di and tri-methylated histone H3 lysine 9 during male prophase I Nuclei were co-stained for H3.1/H3.2. Progressing stages of spermatogenesis are shown from left to right. Arrows/dotted white lines indicate position and form of XY chromatin.

a, Localisation of mono-methylated histone H3 lysine 9 (H3K9me1). XY levels of this mark varied from absent to low prior to H3.1/H3.2 removal. During H3.1/H3.2 loss (stages I-V), an increase of H3K9me1 was observed in the sex body, which persisted to early diplotene. However, in late diplotene (X-XI) this mark had disappeared again (its loss is likely a consequence of conversion to the di and tri-form, which are abundantly present at that stage). Condensed chromosomes exhibited faint staining. During haplophase overall nuclear staining for H3K9me1 was low.

b, Localisation of di-methylated histone H3 lysine 9 (H3K9me2). Prior to H3.1/H3.2 removal enrichment of this mark was observed in XY chromatin. A sharp decrease of H3K9me2 was observed during and after removal of H3.1/H3.2. Signals gradually reappeared during pachytene stages VI-VIII. A further increase of levels was observed throughout diplotene. The condensed sex chromosomes were enriched for H3K9me2 and also in round spermatids this modification was prominent in the sex chromatin.

c, Localisation of tri-methylated histone H3 lysine 9 (H3K9me3). Alike H3K9me2, this mark was enriched in XY chromatin prior to H3.1/H3.2 loss. Except for some faint signals observed in the heterochromatin of the X chromosome, H3K9me3 was lost from the sex body concomitant with H3.1/H3.2 loss. A gradual return of this mark in XY chromatin was observed during stages VI-XI. Condensed sex chromosomes exhibited high levels of H3K9me3 and also in the sex chromatin of round spermatids this mark was abundant.

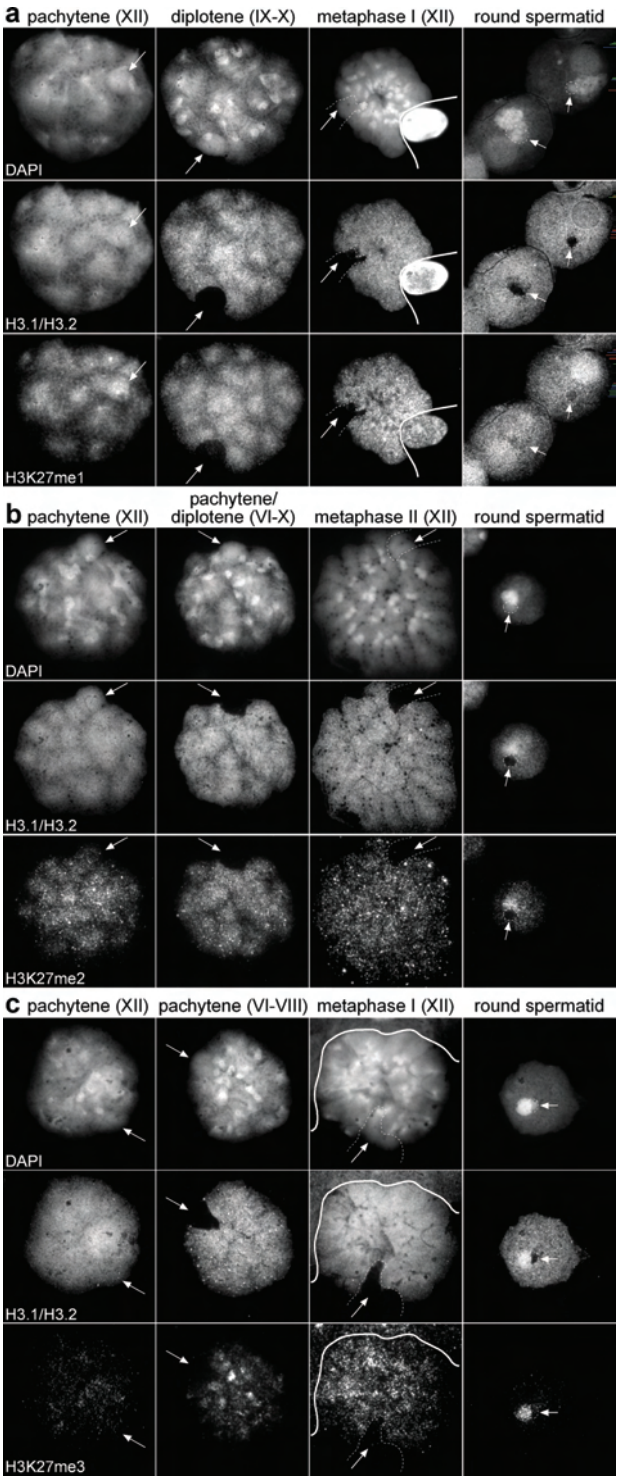
a pachytene (XII)
diplotene (IX-X)
metaphase I (XII)
round spermatid
DAPI
H3.1/H3.2
H3K27me1
b pachytene (XII)
pachytene/
diplotene (VI-X)
metaphase II (XII)
round spermatid
DAPI
H3.1/H3.2
H3K27me2
c pachytene (XII)
pachytene (VI-VIII)
metaphase I (XII)
round spermatid
DAPI
H3.1/H3.2
H3K27me3

Supplementary Figure 5 Dynamics of mono, di and tri-methylated histone H3 lysine 27 during male prophase I Nuclei were co-stained for H3.1/H3.2. Progressing stages of spermatogenesis are shown from left to right. Arrows/dotted white lines indicate position and form of XY chromatin.

a, Localisation of mono-methylated histone H3 lysine 27 (H3K27me1). High levels of H3K27me1 in the XY body were observed prior to H3.1/H3.2 loss. After H3.1/H3.2 loss a faint residual H3K27me1 staining was detected. This might be due to cross reactivity of this antibody with H3K9me1 and H4K20me1 (personal communication T. Jenuwein). Both of these marks were abundantly present in the XY body of pachytene spermatocytes but not when chromatin was condensed, when H3K27me1 was not detected also. In round spermatids H3K27me1 was again present in sex chromatin, though at a lower level than autosomal chromatin.

b, Localisation of di-methylated histone H3 lysine 27 (H3K27me2). H3K27me2 was present in comparable levels in the XY chromosomes and autosomes in early pachytene spermatocytes. Together with H3.1/H3.2 this mark completely disappeared from XY chromatin, its absence from sex chromatin was sustained to round spermatids.

c, Localisation of tri-methylated histone H3 lysine 27 (H3K27me3). Abundance of this modification was lower than H3K27me2 throughout the spermatocyte chromatin. Loss of H3.1/H3.2 resulted in the loss of this mark from the XY chromatin altogether. No return of this modification was observed into round spermatids.

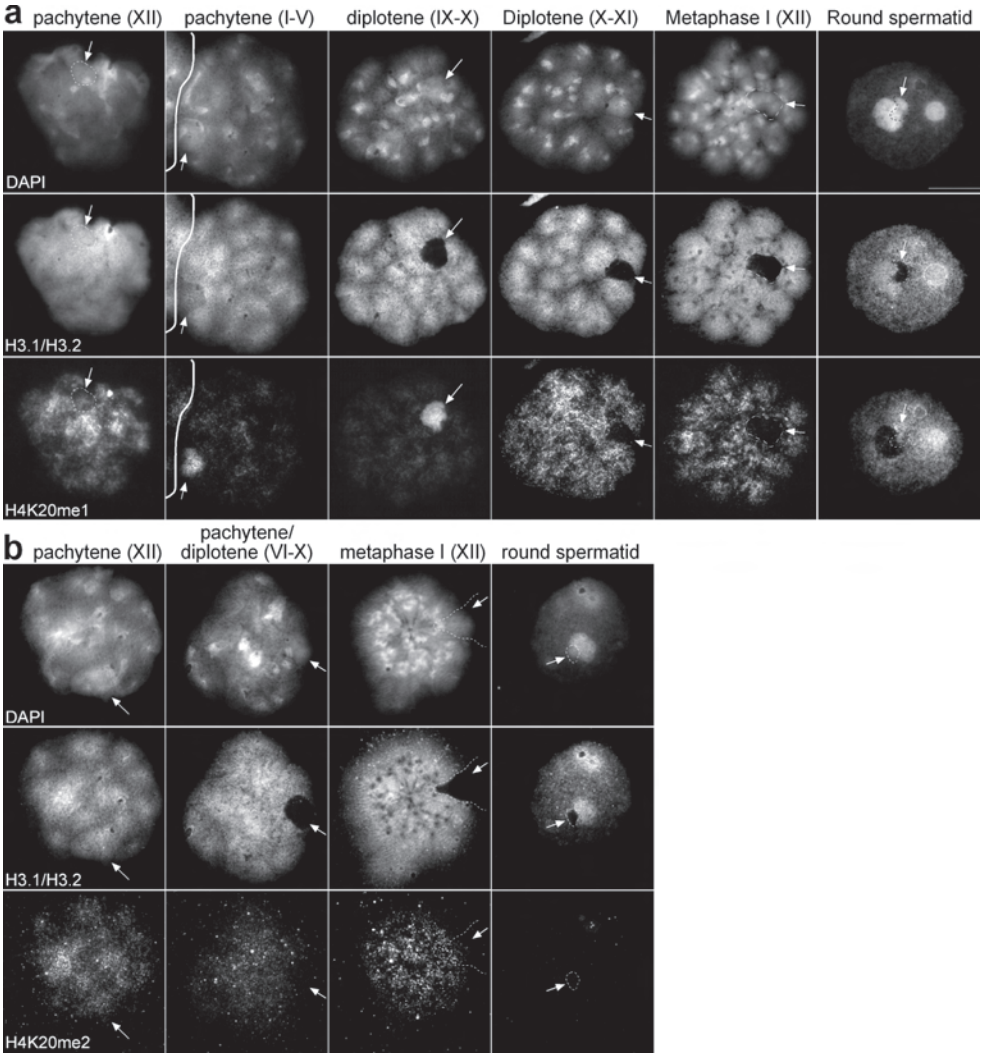

Supplementary Figure 6 Dynamics of mono and di-methylated histone H4 lysine 20 during male prophase I Nuclei were co-stained for H3.1/H3.2. Progressing stages of spermatogenesis are shown from left to right. Arrows/dotted white lines indicate position and form of XY chromatin.

a, Localisation of mono-methylated histone H4 lysine 20 (H4K20me1). Initial levels of H4K20me1 in the XY body were reduced when compared to autosomal levels. A rapid increase was observed at the onset of chromatin remodeling. However, a decline of signal was observed when the axial elements of the XY-chromosomes started to bulge (diplotene,

stages X-XI). Since conversion of H4K20me1 to H4K20me2 is limited and to H4K20me3 not observed at all, its loss suggests the existence of an H4K20me1-demethylase. A reappearance of this mark was observed in the sex chromatin of round spermatids, where it was restricted to euchromatin. Together with our previous observation that H4K20me1 accumulates in sperm chromatin after gamete fusion, when a surge of histone deposition takes place[9], this suggests a function in nucleosome assembly. **b**, Localisation of di-methylated histone H4 lysine 20 (H4K20me2). Signals obtained for H4K20me2 were low in spermatocytes. An overall staining throughout the nucleus prior to H3.1/H3.2 loss was observed. Loss of signal from the XY chromosomes was detected during H3.1/H3.2 removal. In condensed chromosomes this mark became visible again in XY chromatin. However, in round spermatids (sex) chromatin did not exhibit staining.

Supplementary Table 1. Presence of HirA in XY chromatin during prophase I

HirA signal / Stage	Homogeneously stained nucleus	Enriched in XY	Homogeneously stained nucleus, decreased overall levels	Absent in XY body	# analyzed cells
pachytene XII	3	6	-	-	9
pachytene I-V	4	29	-	-	33
pachytene/diplotene VI-X	12	21	-	3	36
diplotene X-XI	-	-	11	12	23

Cells were co-stained with α-HirA and α-H3.1/H3.2 and DAPI.

Table 2a. Duration of substages of meiotic prophase I

Stage	Days	Hours
Leptotene+zygotene	2.5	60
Pachytene	6.6	159.3
Diplotene	2.0	47.7
Diakinesis+M1+M2	0.7	15.5
Meiosis	11.8	282.5

Duration of prophase I stages in days and hours based on Oakberg[20]. The pachytene to diplotene transition is adapted based on Dietrich and de Boer[15].

Table 2b. Theoretical and observed proportion of pachytene and diplotene spermatocytes

Stage	Days	Hours	%	Expected distribution	Observed # analysed cells (%)
Pachytene	6.6	159.3	77	231	246 (82)
Diplotene	2.0	47.7	23	69	54 (18)
Total	8.6	207		300	300

Spermatocytes stained with α-H3.1/H3.2 and α-Sycp3 with fully formed or disassembling synaptonemal complexes were analysed for presence of H3.1/H3.2 in the sex body (n=300). Distribution of analysed cells compared to expected distribution based on relative time intervals of pachytene and diplotene. No significant difference was found.

Table 2c. H3.1/H3.2 status of XY body in pachytene cells

	+	+\-	-
# of cells (%), N=246	25 (10)	103 (42)	118 (48)

+ = H3.1/H3.2 levels in XY body comparable to autosomal chromatin
+\- = H3.1/H3.2 levels in XY body lower than autosomal chromatin
- = No H3.1/H3.2 in the XY body

Table 2d. Duration of H3.1/H3.2 removal

	+	+/-	-
Duration hours (days)	16 (0.66)	67 (2.79)	76 (3.19)

The duration of H3.1/H3.2 removal was calculated by multiplying the frequency of the three H3.1/H3.2 situations of the XY body (Table 2c) by duration of pachytene (Table 2a). Removal of H3.1/H3.2 from XY chromatin starts 16 hours after entry in pachytene, which coincides with the beginning of stage I, and has a duration of 67 hours. The end point of H3.1/H3.2 removal (16+67 = 83 hours after entry in pachytene) coincides with start of stage VI.

Supplementary Table 3. Frequencies of H3.3-V5 incorporation into sex chromosomes during subsequent stages of meiotic prophase and in round spermatids

Table 3a. Number and percentage of analyzed cells at each stage showing H3.3 V5 incorporation

	Sex chromosomes			N	Autosomes
	XY – (%)	X+; Y- (%)	XY+ (%)		
Leptotene	9 (100)			9	-
Zygotene	12 (100)			12	-
early pachytene	13 (100)			13	-
mid pachytene	10 (45,5)	8 (36,6)	4 (18,2)	22	+
late pachytene		4 (9,5)	38 (90,5)	42	+/++
Diplotene			25 (100)	25	++/+++
Diakinesis			4 (100)	4	++/+++
Secondary spermatocytes			7 (100)	7	+/++
round spermatids			36 (100)	36	++

Number and percentage of analyzed cells at each stage showing lack of H3.3-V5 incorporation (XY-), presence of H3.3-V5 at only the X chromosome (X+; Y-) or at both X and Y chromosomes (XY+). The relative intensity of H3.3-V5 labelling at autosomes during each stage is indicated. Analysis were performed on the TgN(H3.3-V5)1Apet transgenic line.

Table 3b. H3.3-V5 status at sex chromosomes during sub-stages of pachytene

	Sex chromosomes			N	%
	XY –	X+; Y-	XY+		
early pachytene	13			13	17
mid pachytene	10	8	4	22	29
late pachytene		4	38	42	54
N	23	12	42		
%	30	16	54		

Staging criteria

Spermatocytes from H3.3-V5 transgenic mice where co-stained with anti-V5 and anti-Scp3 antibodies. Staging of spermatocyctes was based on the morphology of the synaptonemal complex[15, 30]. Pachytene was divided in three sub-stage using the following criteria: Early-pachytene is characterized by complete synapsis of autosomes. Moreover, XY chromosomes contain long thin lateral elements that display synapsis at the pseudoautosomal region. Mid-pachytene is characterized by high levels of non-homologous synapsis between the sex chromosomes (up to 80% of length of Y chromosome has been monitored). During desynapsis of X and Y chromosomes, the axial element of the X chromosome starts to curl. In late-pachytene the axial elements of the XY become longer and curlier in appearance and at synaptonemal complex ends attachment points start to develop. The transition into diplotene is initiated by desynapsis of autosomes.

Supplementary Table 4. Histone H3.1/H3.2 in T70H/T1Wa and Sycp$^{-/-}$ spermatocytes

Table 4a. Spermatocytes containing a synapsed 1[13] bivalent

Complete H3.1/H3.2 loss from XY	Incomplete H3.1/H3.2 loss from XY
54	2

Table 4b. Spermatocytes containing a partly unsynapsed 1[13] bivalent

Complete H3.1/H3.2 loss from XY and unsynapsed bivalent	Incomplete H3.1/H3.2 loss from XY and/or unsynapsed bivalent
29	21

Cells were co-stained with α-Sycp3, α-H3.1/H3.2 and DAPI. Only late pachytene and diplotene spermatocytes were taken into account.

Table 4c. Quantification of H3.1/H3.2 staining in Sycp1$^{-/-}$ spermatocytes

Stage	Homogeneous nuclear H3.1/H3.2 signal
zygotene	28
pachytene	75
diplotene	25

Surface spreads of testicular cells derived from a Sycp1 KO male mice[25] were co-stained with α-Sycp3 and α-H3.1/H3.2 antibodies. Staging of cells occurred via criteria of de Vries et al., 2005[25].

Section 2.2

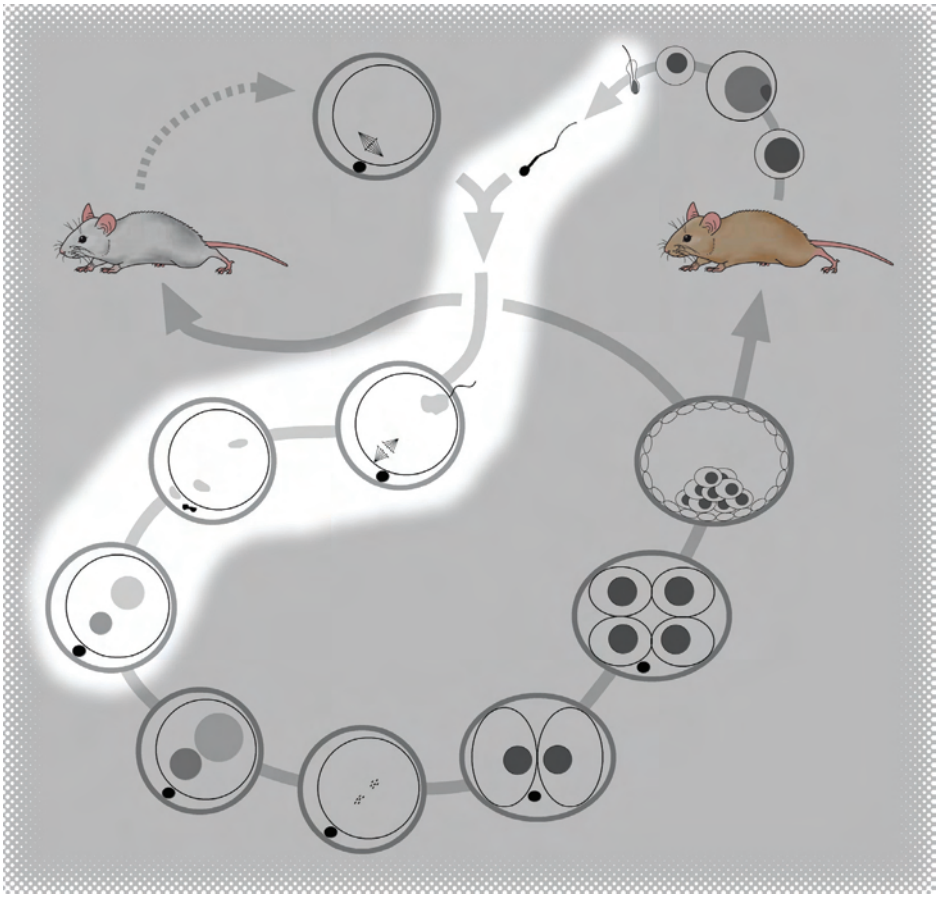

Developmental Biology 2006 October; 298(2):458-69

Transmission of modified nucleosomes from the mouse male germline to the zygote and subsequent remodeling of paternal chromatin

Godfried W. van der Heijden [a,*], Alwin .A.H.A. Derijck [a,*], Liliana Ramos [a], Maud Giele [a], Johan van der Vlag[b], Peter de Boer [a]

[1]*Department of Obstetrics and Gynaecology, Radboud University Nijmegen Medical Centre, P.O. Box 9101, 6500 HB Nijmegen, The Netherlands*
[2]*Nephrology Research Laboratory, Nijmegen Centre for Molecular Life Sciences, Division of Nephrology, Radboud University Nijmegen Medical Centre, Geert Grooteplein 26, 6525 GA Nijmegen, The Netherlands.*

[*] *These authors contributed equally*

Abstract

Rapidly after gamete fusion, the sperm nucleus loses its specific chromatin conformation and the DNA is repopulated with maternally derived nucleosomes. We evaluated the nature of paternally derived nucleosomes and the dynamics of sperm chromatin remodeling in the zygote directly after gamete fusion. We observed histone H4 acetylated at K8 or K12 already prior to full decondensation of the sperm nucleus, suggesting that these marks are transmitted by the spermatozoon. Tracking down the origin of H4K8ac and H4K12ac during spermiogenesis revealed the retention of nucleosomes with these modifications in the chromocentre of elongating spermatids. We show that sperm constitutive heterochromatin is enriched for nucleosomes carrying specific histone modifications which are transmitted to the zygote. Our results suggest an epigenetic mechanism for inheritance of chromosomal architecture. Furthermore, up to pronucleus formation, histone acetylation and phosphorylation build up in a cascade-like fashion in the paternal chromatin. After formation of the pronucleus, a subset of these marks is removed from the heterochromatin, which suggests a reestablishment of the euchromatin-heterochromatin partition.

Introduction

In the condensed sperm nucleus, DNA is present in an inert, sperm-specific constitution, in which it is bound to protamines that facilitates a high density packing [91]. During spermiogenesis, the replacement of histones by protamines is not complete and varies strongly among species. In mouse sperm an estimated 1% of the DNA remains bound to nucleosomes (R. Balhorn, personal communication). The nuclear organization of the sperm genome is well defined, with the telomeres positioned at the outer membrane and centromeric (constitutive) heterochromatin in the centre of the nucleus, in sperm also referred to as the chromocentre [92].

After fusion of mammalian gametes, the start of development is characterized by the resumption of meiosis of the arrested secondary oocyte and the transformation of the sperm nucleus into the male pronucleus (PN) [93, 94]. A sea change in paternal chromatin conformation takes place directly after oocyte penetration, swiftly resulting in the reestablishment of nucleosomal chromatin [9]. During the first hours after gamete fusion, the paternal chromatin is not yet engulfed by a nuclear membrane. It is only after approximately three hours, when the paternal chromatin has expanded once more after a period of recondensation, that the nuclear membrane can be detected and the male PN is defined [95].

Relatively little is known of the pre-PN phase during which the paternal genetic contribution becomes intertwined with maternal processing. The transformation from the sperm-specific chromatin conformation to a somatic-like chromatin architecture is fast. Already in G1, paternal chromatin can be triggered to undergo chromosome contraction [96]. Whether the remaining 1% nucleosomal chromatin plays a facilitating role in this reconfiguration is unknown. In human sperm telomeres and centromeres contain nucleosomal chromatin [97, 98], possibly indicating that preservation of nucleosomal domains is important. The rapid return of "somatic" chromatin characteristics is also illustrated by the biphasic replication pattern observed in the paternal PN during zygotic S-phase, indicating that euchromatin is already distinguished from late replicating heterochromatin [99]. In somatic nuclei, these types of chromatin differ in histone lysine methylation patterns [100]. Paternal zygotic chromatin virtually lacks all of these post translational modifications (PTMs) [9, 29, 79].

It has been reported that prior to full decondensation the pater-

nal chromatin undergoes rapid acetylation of histone H4 at lysine 5 indicating that histone acetylation might play an important role in early zygotic development [101]. To gain a better insight into the nature and dynamics of paternal chromatin remodeling in the early zygote, we evaluated the appearance of histone PTMs that were known to be present during zygotic S phase/G2 phase [102, 103]. We observed a stepwise appearance of maternally derived histone PTMs in the prePN chromatin. In several cases this was followed by a partial or complete removal when the PN had formed, which indicated that these processes are dynamic and follow a developmental program. Furthermore, we identified the chromocentre of the decondensing sperm nucleus as a region enriched for modified nucleosomes. It is well established that during the first hours after gamete fusion, DNA methylation is actively removed from the paternal euchromatin, while being preserved in the heterochromatin [104]. We speculate that nucleosomal chromatin in the sperm chromocentre facilitates the difference in demethylation pattern.
By revealing the localization of these modified nucleosomes in the chromocentre of elongating spermatids and sperm, we demonstrate that nucleosomal chromatin originating from the male germline contributes to the zygote. Our results increase the notion that sperm contributes more than only its genetic content.

Materials and Methods

Gamete Collection and IVF

IVF was performed as described previously [9]. Briefly, sperm was obtained from CBA/B6 F1 mice (6-20-weeks). Caudae epididymis were partially cut open to allow swimming-out of sperm. For capacitation, the sperm suspension was transferred to the bottom of a 5 ml tube with HTF 3% BSA, including 10 μM adenosine. The sperm suspension was incubated at 37°C, 5% CO_2 in air for one hour. At 45 min a sperm count was performed. Female B6/CBA F1 mice (4-12 weeks old) were housed with adjusted light periods set at 9:00 – 21:00 hours. Superovulation was induced by injecting 7.5 U PMSG (Intervet, Boxmeer, The Netherlands) around 18:00 hours and 7.5 U HCG (Intervet) 48 hours later. Females were sacrificed next morning at 9:00 hours. Oocytes were harvested from the ampullae and transferred to 50 μl HTF 0.5% BSA droplets covered with light mineral oil. Sperm was added to these droplets to a final concentra-

tion of $1*10^6$ cells/ml.

Timing of zygote development

The timing of gamete fusion and subsequent zygote development in our IVF setting has been described earlier [9]. Oocyte penetration occurs predominantly 70 min post insemination (pi). For this study zygotes were fixed at four time points pi: 70, 100, 150 and 280 min, respectively. All time periods mentioned in this report are corrected for the 70-min lag phase.

Antibodies

The following antibodies were used: from Upstate Biotechnology (Lake Placid, USA): H3S10ph (06-570; 1:1000 dilution), H3K9K14ac (06-599, 1:500), H3K18ac (07-354; 1:500), H4K5ac (06-759; 1:50), H4K8ac (06-760; 1:1000), H4K12ac (06-761; 1:500) and H4K16ac (06-762; 1:500). Antibodies against protamines: HuP1N, HuP2B (R. Balhorn; 1:1000). Antibodies #32, #34 and # 36 are monoclonal autoantibodies derived from lupus mice: #32 is nucleosome-specific (1:3000) [14], #36 is specific for dsDNA (1:800) [105], and #34 is specific for the replication histone H3 variants H3.1 and H3.2 (1:1500) [9]. Furthermore antibodies against HP1-α (P. Singh; 1:200), HP1-β (P. Singh; 1:100), H3K9me3 and H4K20me3 (T. Jenuwein; 1:250), Hira, (D34, P. Adams; 1:100) and CREST (P. Burgoyne; 1:5000). Secondary abs that were used: Molecular Probes, Oregon, USA: A11001 fluor 488 goat anti-mouse IgG (H+L), A11012 fluor 594 goat anti-rabbit IgG (H+L), Sigma: F6258; anti-rat IgG, FITC-conjugated. All were used in a 1:500 dilution. All secondary abs were tested for non-specific binding, which was never observed.

Immobilization, fixation and immunofluorescence staining of zygotes

Before fixation of the zygotes the zona pellucida was removed using acidic tyrode (pH 2.5) containing 1% BSA. Thereafter, cells were immobilized in a fibrin clot [106]. Fibrinogen was obtained from Calbiochem (cat. nr. 341573) and thrombin was obtained from Sigma (cat. nr. T-6634). Cells were fixed in 2% paraformaldehyde (PFA), 0.15% Triton-X-100 for 30 min. Immunofluorescence (IF) was applied as described before [25].

Preparation of nuclear spreads from the testis and characterization of spermatid stages

Spreads were obtained as described with minor modifications [30]. Testes of CBA/B6 F1 mice (12 weeks old) were dissected and placed in MEMα-

HEPES. After removal of the tunica albuginea, the tubuli were minced between two curved forceps. The cell suspension was transferred to a 10 ml tube filled with MEMα. After a quick spin at 400 rpm (~13.5 g) the supernatant was collected in a clean tube and centrifuged for 10 min at 1000 rpm (~84 g). The supernatant was removed up to ~1 ml, the pellet suspended and MEMα added. This step was repeated twice. After resuspending the pellet, an equal volume of hypobuffer (17 mM sodium citrate; 50 mM sucrose; 30 mM Tris.HCl pH 8.2) was added and cells were incubated for eight min followed by centrifugation as before (~1000 rpm). The supernatant was removed and the pellet was carefully resuspended in 1-2 ml 100 mM sucrose. Ten µl of this suspension was applied to a PFA coated glass slide (1% PFA, 0.15% Triton-X-100, pH 9.2-9.5). The cells were kept for two hours in a humidified atmosphere. After 1.5 hours the box was opened and slides were washed with 0.08% photoflow (Kodak). IF was performed as described above. Because spermatid nuclei were observed outside their cellular organization, spermatid development steps were appointed according to the criteria of Russell et. al., [107]. For every ab tested, at least 150 nuclei were evaluated.

Decondensation of mouse caput sperm

The epididymis was cut open and sperm was allowed to swim out in PBS. The sperm pellet (3000 rpm, eight min in an Eppendorf bench centrifuge) was resuspended in 50 µl PBS (pH 7.0). The suspension was diluted 1:4 in water and drops of 5 µl were placed on a glass slide and dried. 100 µl of decondensing mix (freshly prepared 25 mM DTT, 0.2% Triton X-100, 200 IU heparin/ml (Leo Laboratories) in PBS) was put on top of the dried sperm followed by incubation in a humidified atmosphere for 15-18 min. The speed and degree of decondensation was followed by phase contrast microscopy. When the majority of the nuclei appeared dull grey with roughly twice the surface area of the undecondensed sperm heads, the slide was placed in a coplin jar with 4% PFA in PBS (pH 7) for 15 min. Subsequently, slides were washed in PBS and dried. IF was performed as described above. For every staining at least 150 nuclei were evaluated.

Collection of images

Images were collected with a Zeiss Axioplan fluorescence microscope. Pictures were captured by a Zeiss AxioCam MR camera with Axiovision 3.1 software (Carl Zeiss). Shown images of type a, b, c post-penetration sperm nuclei and PNs are either stacks projected into a single image or a single slide of a stack. Whenever necessary, images where deconvoluted with Metamorph software version 6.

Results

Stepwise appearance of histone modifications in the paternal chromatin

Using specific antibodies, we determined the appearance of acetylated histone H3 and H4 isoforms in paternally derived chromatin of the early zygote at four time points after insemination. As described earlier [9], we could distinguish three types of paternal nuclei in the pre-PN zygote: (1) type a nuclei, which are partially decondensed, hence contain both condensed and decondensed chromatin; (2) type b nuclei, which are fully decondensed; and (3) type c nuclei, which are recondensing (Figs. 1A, 1C, 1D, respectively). Decondensation of sperm chromatin always commenced in the posterior and ventral parts and spread to the tip, which expanded last (Figs. 1A, B).

H4K8ac

Acetylated histone H4 at K8 was consistently observed from the initial stages of sperm chromatin expansion on. Strikingly, in type a nuclei this mark was restricted to the centre region (Figs. 1A, B). In type b nuclei, H4K8ac localized to the chromocentre (Fig. 1C). To confirm this colocalization, we performed double stainings with the kinetochore-specific CREST serum. The kinetochores were indeed embedded in chromatin regions intensely stained by the H4K8ac ab (Figs. 1F-H). This was different from somatic cells, where heterochromatin was characterized by a low abundance of histone acetylation (Figs. 1I-I"). The restricted localization in type a and b nuclei was masked after full decondensation due to increasing levels of maternally derived H4K8ac (Fig. 1D). The global localization of H4K8ac became more restricted after formation of the PN, when the signal disappeared from heterochromatin areas surrounding prenucleoli [108] (Fig. 1E).

H4K12ac

Overall, in the pre-PN phases, a steady increase of the signal for H4K12ac was observed (Figs. 1J-M). In the early decondensing regions, the signal was already detected (Fig. 1J). In type b nuclei a prominent appearance of H4K12ac was observed in the posterior rim and, to a lesser extent, in the chromocentre (Fig. 1K). The signal was always less intense or even absent in the anterior regions of

early type b nuclei (Fig. 1K). A steady increase of signal intensity, however, could be detected in these regions at a later stage (Fig. 1L). During recondensation of the sperm chromatin, H4K12ac was homogeneously present (Fig. 1M). In the PN, H4K12ac, alike H4K8ac, disappeared from the peri-prenucleolar chromatin (Fig. 1N).
Maternally derived, newly incorporated histone H4, acetylated at K5 and K12 [109], provides an opportunity to distinguish deposited maternal nucleosomes from paternal ones that lack these marks. In order to detect chromatin regions populated by paternally derived nucleosomes, we performed double stainings with a nucleosome-specific ab (#32) combined with the H4K12ac ab. Indeed, at the earliest phase of decondensation, we could observe regions containing nucleosomal chromatin that was not acetylated at K12 (Fig. 1O). However, the subsequent appearance of H4K12ac obscured these regions quickly (Fig. 1P).

H3S10ph, H4K16ac, H3K9K14ac and H3K18ac

With regard to time of appearance, di-acetylated histone H3 at K9 and K14 (H3K9K14ac), acetylated histone H3 at K18 (H3K18ac), acetylated histone H4 at K16 (H4K16ac) and phosphorylated histone H3 at S10 (H3S10ph) were distinct from H4K8ac and H4K12ac, since they were not observed in type a nuclei (data not shown). H3S10ph and H4K16ac were first observed at complete decondensation (type b nuclei) around 30 min after gamete fusion. The marks localized to the periphery and chromocentre of the type b decondensing sperm nucleus (Figs. 2A-A' and 2D-D'). In time, the signal for both marks progressed until it covered the entire paternal chromatin (Figs. 2B-B' and E-E'). A rapid decline of signal for the two marks was observed at PN formation. For H3S10ph, the overall signal decreased and bright foci were left (Figs. 2C-C'). Finally, this mark completely disappeared when prenucleoli were pronounced, approximately 210 min after gamete fusion. At this stage, H4K16ac had not vanished totally, but was present in a more granular pattern (Figs. 2F-F'). We observed a synchronized appearance of H3K9K14ac and H3K18ac shortly after H3S10ph and H4K16ac became detectable. These histone PTMs did not concentrate in the chromocentre but were initially observed faintly throughout the sperm chromatin (Figs. 2G-G' and 2J-J'). In type c nuclei these marks were more abundant (Figs. 2H-H' and 2K-K').

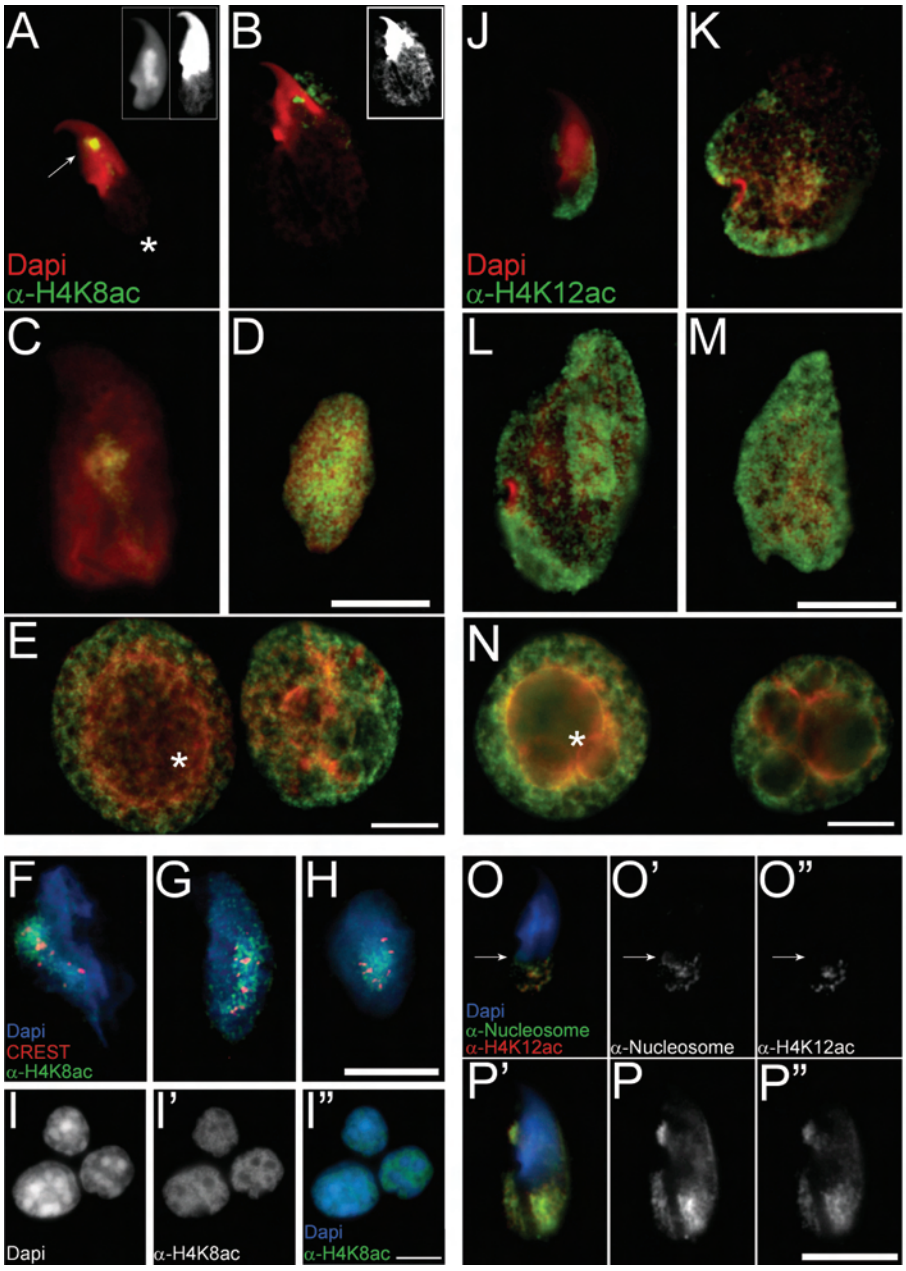

Figure 1 Localization of H4K8ac and H4K12ac in the zygotic male chromatin

A-E Localization of H4K8ac in type a nuclei (A, B; n=19), type b nuclei (C; n=47), type c nuclei (D; n=17) and in the PN (E; n=52) (see results section for the description of a, b and c stages). DAPI is pseudo-coloured

red and H4K8ac is depicted in green. All pictures are cutouts from whole zygote images. Rapidly after the fusion of oocyte and sperm, decondensation of the nucleus starts. This caused the rim of the sperm nucleus to blur (compare DAPI staining inset in A of a sperm nucleus (left) with the decondensing sperm nucleus (right)). This process was always first observed in the posterior and centre regions, indicated in A with an asterisk and an arrow, respectively. The left inset in A also illustrates the localization of the chromocentre. In the PN (E), H4K8ac was reduced in the heterochromatic regions around the prenucleolus (denoted by asterisk). The left PN is the paternal one, the right PN is maternal.

F-H The H4K8ac positive domain embeds the centromeres in type b nuclei. Double staining with the kinetochore CREST ab in red and α-H4K8ac in green. DAPI is pseudo-coloured blue (n=8).

I-I" Enrichment for H4K8ac in heterochromatin is a-typical. In somatic mouse follicle cells, heterochromatin domains are DAPI bright (I). These regions contained low levels of H4K8ac (I').

J-N Localization of H4K12ac in type a sperm nuclei (J; n=28), type b nuclei (K, L; n=43), type c nuclei (M; n=14) and in the early PN (N; n=18). DAPI is pseudo-coloured red and H4K12ac green. Alike H4K8ac, this mark was present as soon as technically could be observed. In contrast to H4K8ac, it spread across the decondensing sperm chromatin immediately (J,K,L). In the PN, H4K12ac was reduced in the heterochromatic regions around the prenucleolus (denoted by asterisk). The left PN is the paternal one, the right PN is maternal.

O-O", P-P" Double staining with a nucleosomal ab (#32) and H4K12ac ab to pinpoint regions populated by paternally derived nucleosomes (n=12). Localization of nucleosomes (O', P) and H4K12ac (O", P") in type a nuclei (O, P', merge with DAPI pseudo coloured blue, the nucleosomal ab in green and H4K12ac in red). The progression of chromatin decondensation was clearly visible when comparing (O), which only underwent some posterior decondensation and (P), where decondensation was clearly more advanced in the posterior region and was also observed in the mid-ventral region. The arrow in O-O" points at a region where nucleosomes are present without H4K12ac acetylation. Bar represents 10 μm.

This increase continued throughout PN formation (Figs. 2I-I' and 2L-L').

Localization of nucleosomes, protamines, modified histones H3 and H4, and HP1 during spermiogenesis

As described above, H4K12ac and especially H4K8ac were observed immediately after gamete fusion. We investigated the possibility of their presence in the sperm nucleus prior to fertilization. To this end, spreads were made from mouse spermatogenic cells and used for IF staining. Since progressive compaction of sperm chromatin during spermiogenesis is likely to interfere with penetration of antibodies, we investigated until which morphological nuclear step IF detection was feasible. By staining with a dsDNA ab (#36), we observed lack of signal in the anterior region of a nuclear morphology, roughly coinciding with step 12 (Supplementary Fig. 1) but not in preceding nuclear forms. The partial penetration of elongated spermatids by the dsDNA ab reflected the progression of nuclear remodeling along the anterior-posterior axis [110]. Since DAPI has a preference for AT-rich sequences, as mouse centric DNA is, these domains were more brightly stained.

Nucleosomes and protamines

Staining of elongating spermatids with a nucleosome-specific ab (#32) visualized the process of their removal. It also revealed a gradually appearing difference between euchromatin and heterochromatin. At morphologies representative for step 9, nucleosomes were generally evenly present (Figs. 3A-A"). In more differentiated spermatids, a selective reduction of the overall signal was observed. Regions with a higher intensity colocalized with the chromocentre, whereas nucleosome levels in the surrounding chromatin were greatly diminished (Figs. 3B-B"). Staining with the dsDNA ab showed a relatively homogeneous signal in elongating spermatids with a corresponding morphology (Supplementary Fig. 1). The higher concentration of nucleosomes in the chromocentre is therefore not due to an elevated DNA concentration.

During further differentiation, a progressive reduction of nucleosomes was observed. However, even in step 11 spermatid nuclei a signal could still be observed in the chromocentre (Figs. 3C-C"). This also applied to the posterior region of the nucleus (Figs. 3C-

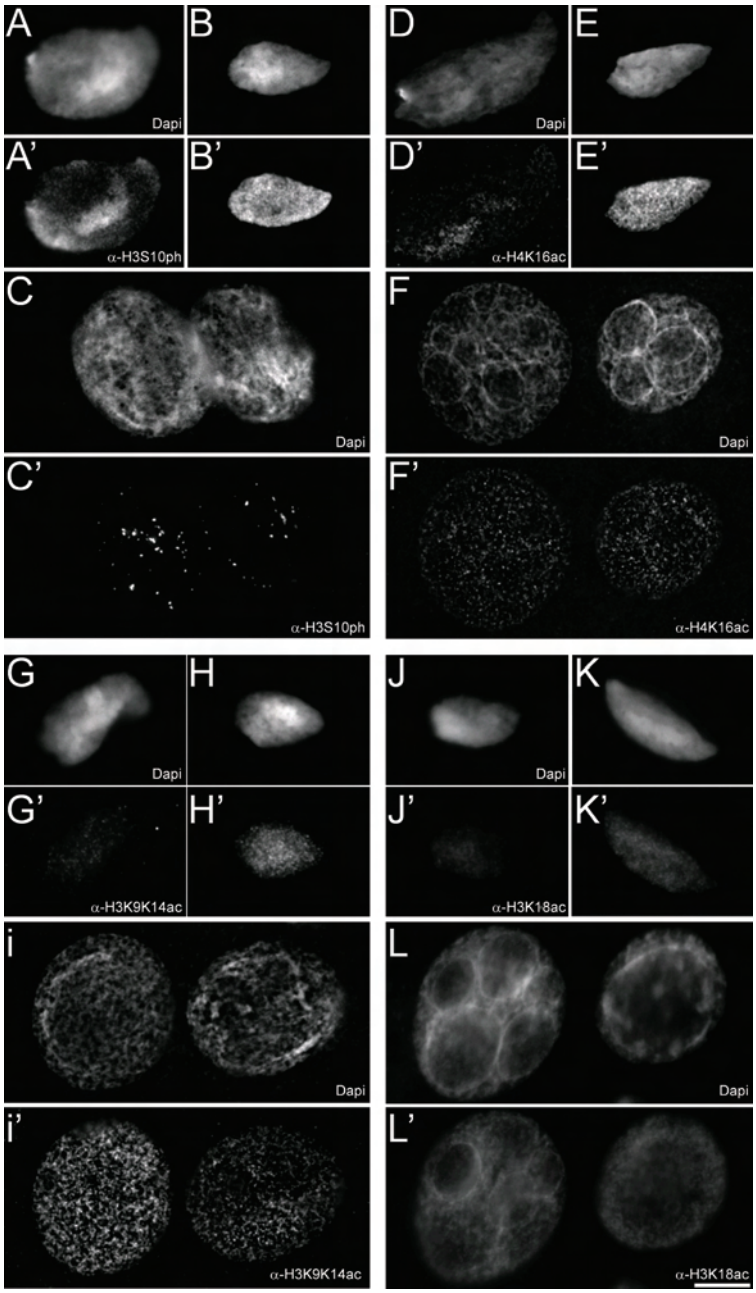

Figure 2 Localization of H3S10ph, H4K16Ac, H3K9K14ac and H3K18ac in the zygotic male chromatin

A-C, A'-C' DAPI and corresponding α-H3S10ph staining in type b sperm nucleus (2A and A'; n=17), type c sperm nucleus (2B and B'; n=16) and in the PN (2C and C'; n=25). H3S10ph had completely disappeared

when prenucleoli had formed.
D-F, E'-F' DAPI and corresponding α-H4K16ac staining in type b sperm nucleus (2D and D'; n=16), type c sperm nucleus (2E and E'; n=13) and in the PN (2F and F'; n=12).
G-I, G'-I' DAPI and corresponding α-H3K9K14ac staining in type b sperm nucleus (2G and G'; n=25), type c sperm nucleus (2H and H'; n=9) and in the PN (3I and I'; n=15).
J-L, J'-L' DAPI and corresponding α-H3K18ac staining in type b sperm nucleus (3J and J'; n=10), type c sperm nucleus (3K and K'; n=7) and in the PN (3L and L'; n=12). In all cases, the left PN is the paternal one, the right PN is maternal. Bar represents 10 μm.

C''). Since chromatin remodeling proceeds in the anterior-posterior axis, this may be expected.
To establish whether the nucleosomes observed in the chromocentre were newly deposited onto the DNA, we investigated whether de novo nucleosome deposition took place. Since DNA replication does not occur during spermiogenesis, all newly deposited nucleosomes will involve the histone chaperone Hira, which specifically deposits histone H3.3-H4 dimers on the DNA [16]. Staining with a Hira-specific ab revealed that this protein is not present in elongating spermatid nuclei, which implies the lack of de novo nucleosome deposition (data not shown).
The presence of nucleosomes in the chromocentre should lead to a lower protamine (Prm) content in this region, since they compete for DNA binding. Indeed, staining with Prm1 and 2-specific abs revealed a reduced signal in the chromocentre (Figs. 3D-D'').

Acetylated isoforms of histone H4
At initial stages of nuclear elongation, a homogeneous localization of H4K5ac, K8ac, K12ac and K16ac throughout the spermatid nucleus was observed (Figs. 4.1A-A'', D-D'' and Supplementary Fig. 2) as has been described for whole mount seminiferous tubuli earlier [110]. At later stages (morphological steps 10-11) however, H4K5ac and H4K16ac were severely reduced or had completely disappeared (Figs. 4.1E-E''; F-F'' and Supplementary Fig. 2). H4K8ac and K12ac exhibited the same behaviour as nucleosomes and were lost from euchromatin but retained in the chromocentre and the posterior

region (Figs. 4.1A-C" and Supplementary Fig. 2).

H3K9me3, H4K20me3 and HP1

In a previous study [9], we did not detect the characteristic heterochromatin marks H3K9me3 and H4K20me3 in pre-PN stage paternal zygotic chromatin. H3K9me3 serves as a binding site for HP1, a protein also able to bind to itself, thereby inducing chromatin compaction [111]. Absence of these marks in type a and b zy-

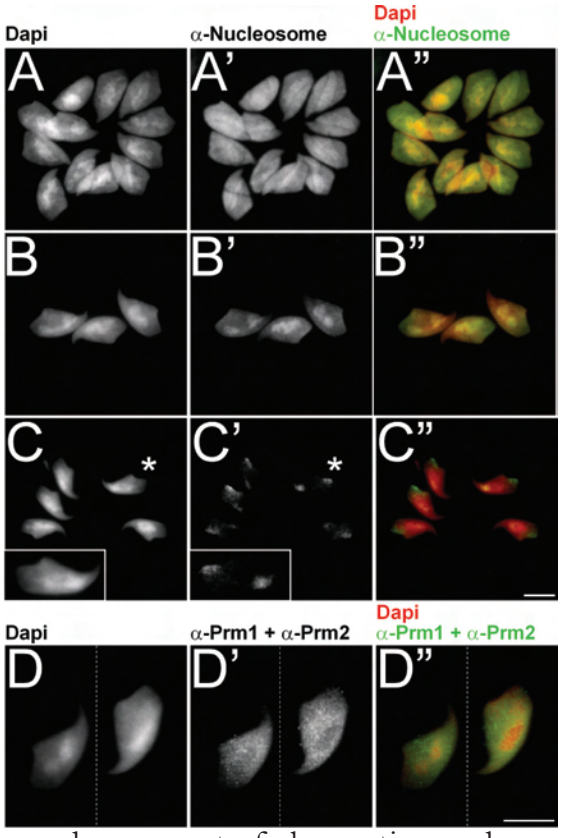

Figure 3 Localization of nucleosomes and protamines in spermatids The left column depicts DAPI, the middle column ab staining and the right column the merged image. DAPI is pseudo-coloured red, the ab signal is in green.

A-C" Localization of nucleosomes by ab #32 in spermatids in advancing stages of condensation. A relative enrichment of nucleosomes in the chromocentre could be observed. In A-A" (morphologies representing steps 9/10) DAPI-bright regions did not necessarily colocalize with bright ab staining. In later stages (morphology step 10), there is a clear colocalization of the two (B-B"). After further advancement of chromatin condensation (morphology step 11) nucleosomes could still be observed in the chromocentre (C-C"). Inset is a magnification of the nucleus marked with an asterisk.

D-D" Localization of both Prm1 and Prm2 in elongating sperm nuclei in morphology step 10. A lower concentration of protamines was observed in the chromocentre, most likely the result of the presence of nucleosomal bound DNA. A mixture of both abs was used. Bar represents 10 μm.

gotic sperm chromatin indicated that these were removed from heter chromatin during spermiogenesis. Since this did not seem to be the case for H4K8ac and K12ac, we determined when these heterochromatin markers were lost from spermatid nuclei. H3K9me3 and H4K20me3 were clearly present in spermatids after the onset of elongation (Figs. 4.1G-G" and Supplementary Fig. 3). A clear colocalization of both marks with the DAPI bright chromocentre was observed. With progression of elongation, intensity levels were reduced. At morphologies around step 11, signals for both marks were highly reduced or virtually absent, following the same dynamics as H4K5ac and H4K16ac. HP1-α was lost from spermatid nuclei prior to the appearance of tri-methylations (data not shown), whereas HP1-β quickly disappeared after the onset of spermatid nuclear elongation (Supplementary Fig. 3), but a faint signal could be observed in spermatids that had progressed to morphology step 12. This fits with the reported presence of HP1-β in mouse sperm as determined by Western blot analysis [112].

Localization of nucleosomes, H4K8ac and H4K12ac in mature sperm

To be certain that nucleosomes and modified histone H4 were also present upon completion of spermiogenesis, we analyzed gametes derived from the caput epididymis. After *in vitro* chromatin decondensation, a prominent signal in the anterior central region of the nucleus was observed for nucleosomes, H4K8ac and H4K12ac (Figs. 4.2A-C). In all cases, the signals colocalized with the chromocentre. These results resemble our observations in late elongating spermatids. Occasionally, the nucleosome-specific ab also stained the rim of the sperm nucleus, possibly reflecting the findings of Pittoggi et. al.[113]. The posterior localization of nucleosomes in spermatid nuclei (Figs. 3C-C") was not observed in sperm nuclei, which may indicate their eventual removal during spermiogenesis.

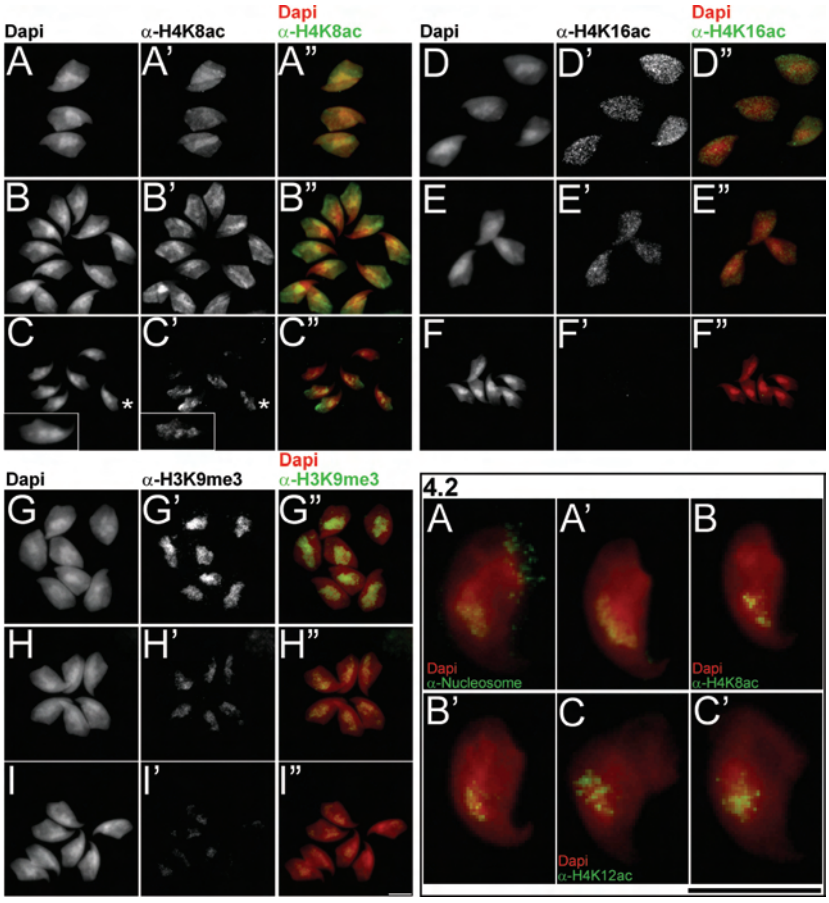

Figure 4.1 Localization of H4K8ac, H4K16ac and H3K9me3 in spermatid nuclei

The left column depicts DAPI, the middle column ab staining and the right column the merged images. DAPI is pseudo-coloured red, the ab signal is in green.

A-C" Localization of H4K8ac in spermatids in advancing stages of elongation. Higher H4K8ac levels were sometimes observed in regions encompassing euchromatin and heterochromatin in morphologies representing step 10, (A-A"). Later on the signal was concentrated in the chromocentre, though the colocalization was not absolute in morphologies representing step 11 (B-B"). In spermatids that experienced further nuclear condensation (morphologies representing step 12 and beyond) signal was mainly observed in the posterior region but also in the more anteriorly localized chromocentre (C-C"). Inset is a magnification of the nucleus marked with an asterisk. A similar pattern was observed for

H4K12ac (Supplementary Fig. 2).
D-F" Localization of H4K16ac in spermatids in advancing stages of elongation. Initially H4K16ac was observed homogeneously throughout the spermatid nucleus (morphologies representing steps 9/10, D-D"). In spite of progressive condensation (E-E"), the signal was slightly reduced, indicating removal of this mark. At a later stage (morphologies representing step 11), when ab penetration was still possible, the mark had disappeared (F-F"). A similar pattern was observed for H4K5ac (Supplementary Fig. 2).
G-I" Localization of H3K9me3 in spermatids in advancing stages of elongation. A clear colocalization of this mark with the chromocentre was observed in all stages (morphologies representing steps 9/10; G-G" and 10; H-H"). Reduction of the signal was apparent with increase of condensation (morphologies representing steps 10/11; I-I"). A similar pattern was observed for H4K20me3 (Supplementary Fig. 3). Bar represents 10 μm.
Figure 4.2. Localization of nucleosomes, H4K8ac and H4K12ac in sperm nuclei
Localization of nucleosomes (A, A'), H4K8ac (B, B') and H4K12ac (C, C') in artificially expanded sperm nuclei derived from the caput epididymis. Signal was observed in the chromocentre. DAPI is pseudo-coloured red, the ab signal is in green. Bar represents 10 μm.

Discussion

Centric DNA in sperm is enriched for nucleosomes

In mouse sperm, about 1% of the DNA is wrapped around nucleosomes (R. Balhorn, personal communication). These nucleosomes are not randomly distributed over the sperm DNA. In a previous report, it was shown that retroposon sequences show enrichment for nucleosomes and that these sequences are localized in the nuclear periphery [113]. Here we describe a clear enrichment of nucleosomal chromatin in centric "heterochromatin" DNA of mouse sperm (Fig. 4.2). Pittogi and coworkers communicated that their fraction of DNA in a nucleosomal conformation did not exceed 0.1% [113]. We propose, therefore, that a major portion of the remaining nucleosomal chromatin in mouse sperm is contained in the centric heterochromatin.

Hypoacetylation of histone H4 correlates with nucleosome retention

During mouse spermiogenesis, histones are stepwise replaced by protamines (for a review [114]). We observed that nucleosome density in euchromatin was declining faster than in the chromocentre where nucleosomes can still be detected when nuclear elongation proceeds (Figs. 3A,B). Since de novo nucleosome assembly does not take place, these nucleosomes must be retained from the original chromatin. A similar pattern of selective preservation during spermiogenesis was observed for two specific acetylated H4 isoforms, H4K8ac and H4K12ac. Whereas H4K5ac and H4K16ac eventually disappeared completely from the spermatid chromatin, H4K8ac and H4K12ac levels were drastically, but not entirely, reduced and restricted to the chromocentre and posterior region (Fig. 4 and Supplementary Fig. 2). Like the retained nucleosomes, these histone PTMs are set prior to the onset of nucleosome eviction since histone acetylation does not take place in condensing spermatids [110]. Hyperacetylation of the nucleosome and especially histone H4 is well documented during spermiogenesis and has been observed in several species [114]. Acetylation partially neutralizes the positive charge of the histone tail and will therefore weaken DNA-nucleosome and nucleosome-nucleosome interactions, inducing a more open chromatin structure [115], which may then facilitate removal of nucleosomes and subsequent replacement by protamines [116]. On the protein level, it has been shown that Brdt, identified as a testis-specific chromatin reorganizer, needs a certain degree of histone acetylation for proper function [117]. If hyperacetylation is beneficial for nucleosome eviction, a hypoacetylated state might help to retain nucleosomes. Notably, nucleosomes in the chromocentre and the posterior region of the spermatids were not hyperacetylated (lacking at least H4K5ac and H4K16ac; Fig. 4F and Supplementary Fig. 2C). However, nucleosomes disappeared from the posterior region of the nucleus, indicating that hypoacetylation alone is not sufficient for retention in the chromocentre. It has been shown that also the higher AT content of centric heterochromatin contributes to intrinsic nucleosome stability [118]. Possibly, the accumulative effect of a lower acetylation level and a more stable nucleosome conformation hampers nucleosome disassembly, resulting in nucleosome retention in the chromocentre.

Potential role of transmitted male nucleosomes

When premature chromosome condensation is induced in G1 pronuclear zygotes, the paternal and maternal chromatin is reconfigured into mitotic chromosomes [96], displaying centric heterochromatin. Apparently, chromosome architecture is already reestablished during zygotic G1. Structural domains as telomeres, centromeres and centric heterochromatin have distinct roles in chromosomal organization. Manipulation of these domains, if at all possible, often results in genome instability [119, 120]. Remarkably, telomeres and centromeres are reported to be arranged into nucleosomal chromatin in human sperm [97, 98]. The localization of telomeres in the nucleosome-rich nuclear periphery in mouse sperm [92] and the presence of the kinetochore-specific CREST signal in the chromocentre of elongating spermatids (data not shown) and shortly after gamete fusion suggest a similar organization in mouse. Hence, also in mouse sperm it seems that structurally important chromosome domains maintain to some degree a nucleosomal chromatin conformation.

The organization of telomeric and centric DNA into nucleosomes could serve as a chromatin blueprint, directing the remodeling machinery by supplying a nucleosomal template. Additionally, the presence of acetylated lysines in the histone tails - e.g., H4K8ac and H4K12ac - could provide an incentive for binding chromatin remodellers via their bromodomains, typically contained in chromatin-associated proteins [121]. It has been that shown that telomere length is pivotal for proper early zygote development [122]. When sperm of 3rd generation telomerase knock out males fertilize wild type oocytes, a high percentage of zygotes fails to undergo cleavage. In these zygotes, the sperm nucleus does not decondense, implying a structural role for telomeres during early sperm chromatin remodeling. The complex nature of centric heterochromatin and centromeres will make it difficult to determine whether this also applies to them. The finding by Santos et. al., [104] that centric DNA is protected from genome-wide active demethylation upon gamete fusion, suggests inherited modified nucleosomal chromatin to act as a protective barrier. In agreement with this is the recent observation that CpG methylation levels of paternal PNs derived from injected round spermatids, which possess only nucleosomal chromatin and have high H4K8ac and H4K12ac levels (data not shown), are much

higher than CpG levels of PNs derived from injected sperm [123].

Acetylation of paternal chromatin post-gamete fusion occurs in a stepwise fashion

Histone PTMs in the paternal chromatin prior to PN formation - i.e., the acetylations investigated here - evolve in three phases.

The transmission of H4K8ac and H4K12ac from the sperm constitutes the first phase. For H4K8ac, we unambiguously showed its transfer from the sperm nucleus to the zygote (Figs. 1A, B and Figs. 4.2B, B'). This is very likely also the case for H4K12ac, since it is present in the chromocentre of caput sperm (Fig. 1J and Figs. 4.2C, C'). The reason why during male chromatin decondensation, the H4K12ac paternal modification cannot be distinguished from modification by the oocyte, is the second phase that involves the deposition of maternally derived histones. Prior to deposition, histone H4 becomes acetylated at K5 and K12 [109]. Therefore, histone deposition will consequently obscure detection of H4K12ac-labelled paternally derived nucleosomes. Our earlier observation that maternal nucleosome deposition commences immediately after decondensation [9] is in concordance with the synchronous accumulation of H4K5ac [101] and H4K12ac (this study). It has been proposed [101] that chromatin of type a sperm nuclei is hyperacetylated as indicated by the presence of H4K5ac. Although this may hold for somatic chromatin in interphase or mitosis, in the decondensing sperm chromatin H4K5ac and H4K12ac are hallmarks of histone deposition and therefore precede subsequent acetylation or deacetylation events.

The third event occurs after full decondensation: H3K9K14ac, H3K18ac, H4K8ac and H4K16ac appear more or less synchronized (Figs. 1C and 2D',G',J'). A steady increase results in their homogeneous presence when recondensation commences (Figs. 1D and 2E',H',K' and for a schematic overview Fig. 5).

A possible function for hyperacetylation of paternal chromatin

Chromatin remodeling in elongating spermatids and in sperm nuclei after gamete fusion does involve similar histone PTMs, notwithstanding that the endpoints are opposite (i.e., from nucleosomes to protamines and vice versa). Both phases are characterized by a temporary hyperacetylated chromatin state. As mentioned earlier, in

spermatid nuclei this is thought to facilitate chromatin remodeling by decreasing nucleosome-DNA and nucleosome-nucleosome interactions. Possibly, the physical changes conferred on nucleosomes by hyperacetylation facilitate fine-tuning of nucleosome position or density after their assembly. In general, acetylation of histone tails is associated with an enhanced transcriptional activity [124]. Transcriptional activity in the male PN starts in mid S phase, about six hours after PN formation [125]. Since histone acetylation has a high turnover [126], a relation between early paternal chromatin acetylation and transcription status is disputable.

Phosphorylation of paternal histone H3 at serine 10, a conserved phenomenon

As in mouse, H3S10ph is also rapidly observed in *Xenopus* sperm after decondensation in egg extract [127], indicating that this phosphorylation event is evolutionary conserved. A function in chromatin condensation at mitosis has frequently been implied for this mark although mutation of S10 does not affect this process [127]. Phosphorylation of S10, therefore, does not cause chromatin condensation but seems to be a consequence [128]. In the paternal zygotic chromatin, H3S10ph is homogeneously present when recondensation has started (Fig. 2B), again correlating chromatin condensation with this mark. An explanation for the appearance of H3S10ph may be found in the fact that the sperm decondenses in a situation where Maturation Promoting Factor (MPF) is still present, until its activity decreases as a consequence of the end of telophase II [129]. At that stage, a rapid maternal H3S10 dephosphorylation is observed (data not shown), while the paternal chromatin is accumulating this mark (Figs. 2A-B'). Maybe the paternal H3S10ph mark symbolises the end of meiotic activity: it is rapidly removed at nuclear expansion due to PN formation (Fig. 2C).

Reestablishing the euchromatin-heterochromatin partition through localized deacetylation

After PN formation, loss of H4K8ac and H4K12ac is specifically observed in the centric chromatin (Figs. 1E and N). A potential role for this partial loss of H4K8ac and H4K12ac might be found in reestablishing the euchromatin-heterochromatin partition. Since the level of nucleosome acetylation has a direct effect on replication

timing of DNA - lower acetylation levels delay and high levels stimulate replication [130] - it is to be expected that these hypoacetylated chromatin domains will undergo delayed DNA replication. Centric DNA is typically late replicating in somatic cells. Although the male PN lacks most important hallmarks of heterochromatin [9, 29, 79], in S phase in the mouse, zygote replication of euchromatin regions is followed by replication of heterochromatin domains [99]. Since methylated CpGs are capable of recruiting HDAC containing complexes [131] the deacetylation of the paternal heterochromatin could be related to the retained CpG methylation in the heterochromatin [104]. Thus, a decrease in acetylation of the zygotic paternal centric chromatin,

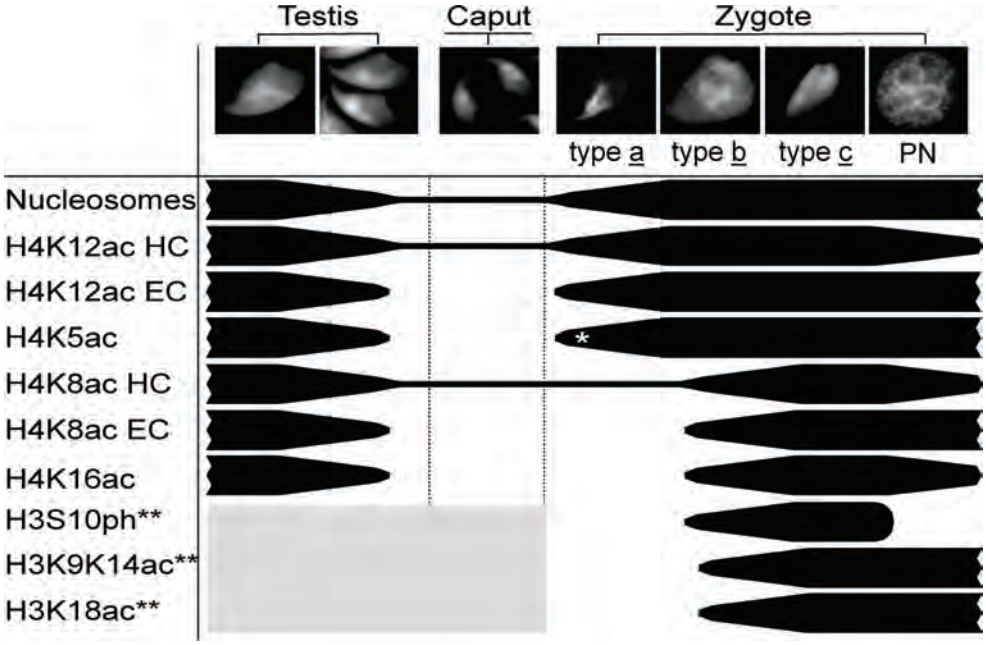

Figure 5 Schematic overview of chromatin dynamics during spermiogenesis and in the early zygote

Presence of nucleosomes and PTMs during spermiogenesis, in sperm from the caput epididymis and in the early zygote up to 280 min post insemination (~3.5 hrs after gamete fusion) is indicated with black bars. HC = heterochromatin, EC = euchromatin. * as shown in Adenot et. al., 1997. ** Since these histone PTMs were not detected in type a sperm nuclei, we did not determine their dynamics in spermiogenesis and caput sperm.

possibly mediated through CpG methylation, will establish a somatic-like replication pattern. This separation in time of euchromatin and heterochromatin replication is expected to allow their further maturation by differential composition of the replication machinery [132].

In summary, we show that centric heterochromatin is inherited from the father and is characterized by the presence of H4K8ac and H4K12ac. We propose this to be of significance for the reconstitution of soma-like male chromosomes after gamete fusion and possibly also for the conservation of CpG methylation. Furthermore, the dynamics of maternally derived histone PTMs indicate a facilitating role of hyperacetylation for chromatin remodeling in the pre-PN paternal chromatin while hypoacetylation of centric heterochromatin observed after PN formation could establish the euchromatin-heterochromatin partition as expressed by replication kinetics.

Acknowledgements

Dr. H. Stunnenberg (Dept. of Molecular Biology, NCMLS, Nijmegen, The Netherlands), Dr. P. Adams (FCCC, Philadelphia, PA), Dr. P. Singh (Division of Tumor Biology, Dept. of Immunology and Cell Biology, Forschungszentrum Borstel, Germany), Dr. T. Jenuwein (IMP, Vienna, Austria), Dr. P. Burgoyne (Division of Stem Cell Research and Developmental Genetics, MRC National Institute for Medical Research, London, UK) and Dr. R. Balhorn (Electronic Engineering Technologies Division, Lawrence Livermore National Laboratory, Livermore, CA) are gratefully acknowledged for their antibodies. We thank Dr. D.G. Wansink (Dept. of Cell Biology, NCMLS, Nijmegen, The Netherlands) for critical reading of the manuscript. This research was financed by the Dutch Ministry of Health, Welfare and Sport.

Supplementary data section 2.2

Supplementary figure 1 Penetration of elongating spermatids for IgG ab (#36) recognizing dsDNA
A) Morphologies representing steps 9/10
B) Morphologies representing steps 10/11
C) Morphologies representing step 11 and beyond

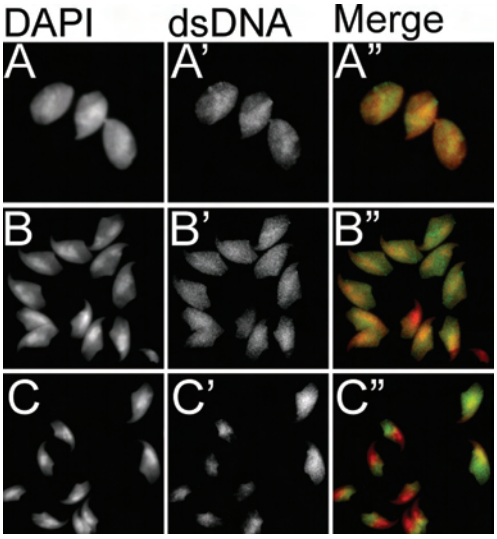

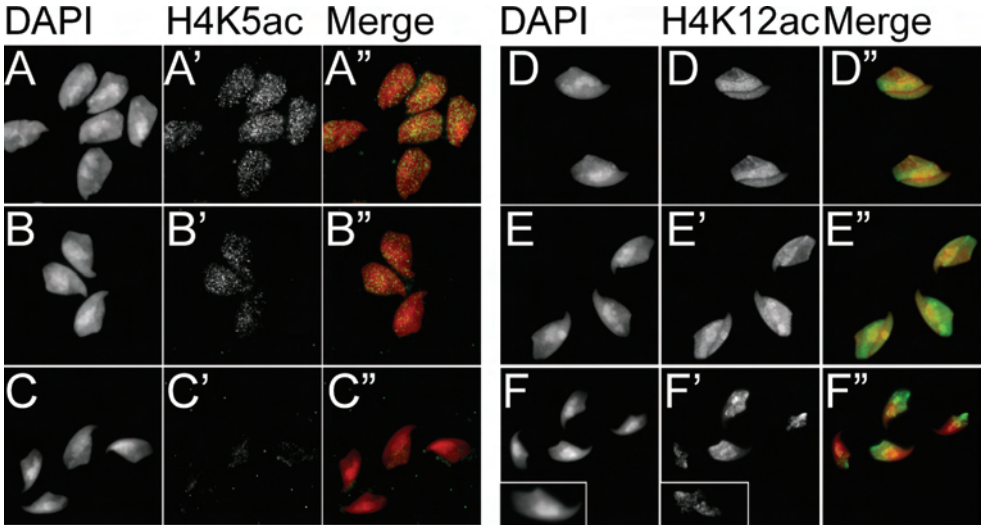

Supplementary Figure 2 Localization of H4K5ac and H4K12ac in spermatids in advancing stages of elongation
A) Morphologies representing steps 9/10
B) Morphologies representing step 10
C) Morphologies representing steps 10/11
D) Morphologies representing step 10
E) Morphologies representing steps 10/11
F) Morphologies representing step 11 and beyond

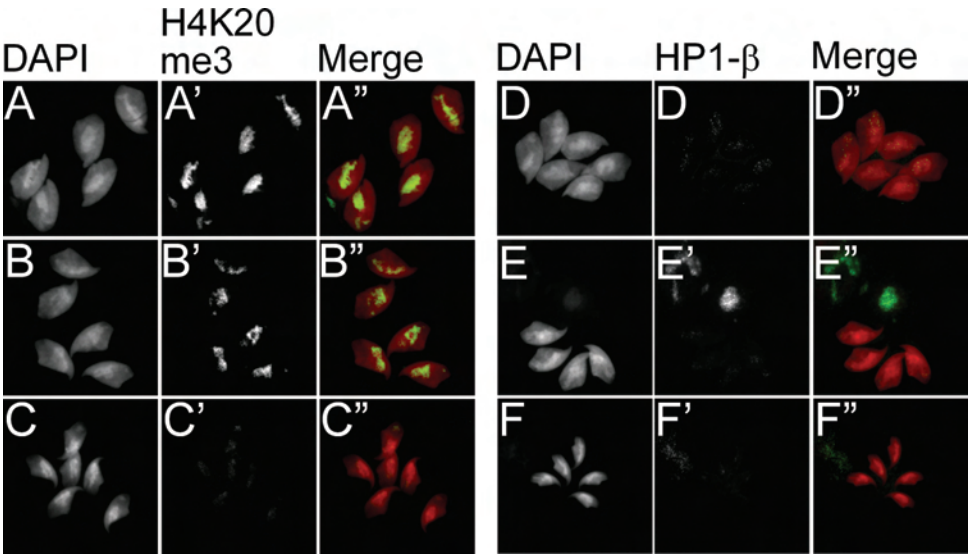

Supplementary Figure 3 Localization of H4K20me3 and HP1-β in spermatids in advancing stages of elongation

A) Morphologies representing steps 9/10
B) Morphologies representing step 10
C) Morphologies representing steps 12 and beyond
D) Morphologies representing steps 9/10
E) Morphologies representing step 10
F) Morphologies representing steps 11 and beyond

Section 2.3

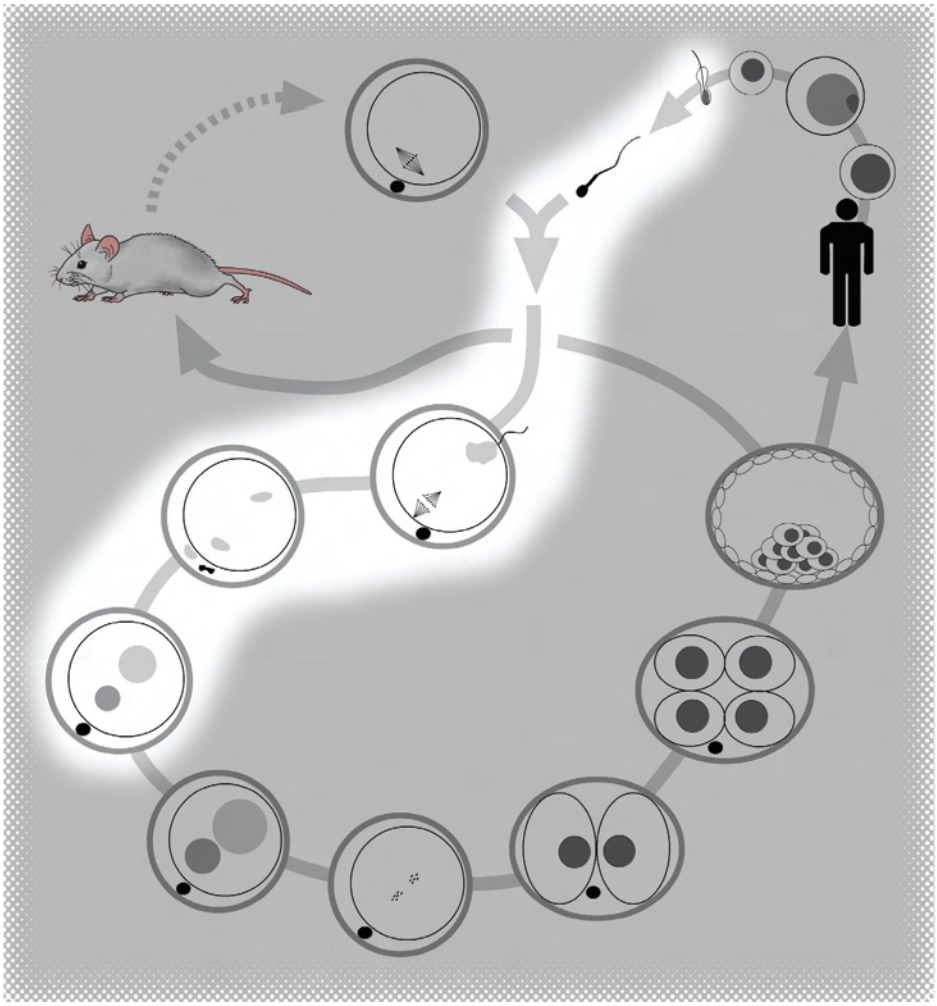

Submitted

Sperm-derived histones contribute to zygotic chromatin in humans

Godfried W. van der Heijden [a,1], Liliana Ramos [a,1], Esther B. Baart [b,2], Ilse M. van den Berg [b], Alwin A.H.A. Derijck [a], Johan van der Vlag [c], Elena Martini [b], Peter de Boer [a,*]

[a] *Department of Obstetrics and Gynaecology, Radboud University Nijmegen Medical Centre, P.O. Box 9101, 6500 HB Nijmegen, The Netherlands*

[b] *Division of Reproductive Medicine, Department of Obstetrics and Gynaecology, Erasmus MC, University Medical Center, Gravendijkwal 230, 3015CE Rotterdam, The Netherlands*

[c] *Nephrology Research Laboratory (279), Nijmegen Centre for Molecular Life Sciences, Division of Nephrology, Radboud University Nijmegen Medical Centre, P.O. Box 9101, 6500 HB, Nijmegen, The Netherlands*

[1] *Both authors contributed equally*

Abstract

About 15% to 30% of the DNA in human sperm is packed in nucleosomes and transmission of this fraction to the embryo potentially serves as a mechanism to facilitate paternal epigenetic programs during embryonic development. However, hitherto it has not been established whether these nucleosomes are removed like the protamines or indeed contribute to paternal zygotic chromatin. To clarify the fate of sperm-derived nucleosomes we have used the deposition characteristics of histone H3 variants from which follows that H3 replication variants present in zygotic paternal chromatin prior to S-phase originate from sperm. We have performed heterologous ICSI by injecting human sperm into mouse oocytes. Probing these zygotes with an antibody highly specific for the H3.1/H3.2 replication variants showed a clear signal in the decondensed human sperm chromatin prior to S-phase. In addition, staining of human multipronuclear zygotes also showed the H3.1/H3.2 replication variants in paternal chromatin prior to DNA replication. These findings reveal that sperm-derived chromatin contributes to paternal zygotic chromatin. Hence, the execution of epigenetic programs originating from transmitted paternal chromatin during subsequent embryonic development is a logical consequence of this observation.

Introduction

A hallmark of spermiogenesis is the transformation of the chromatin of the germ cell. In elongating spermatids nucleosomes are replaced by transition proteins, which are subsequently replaced by protamines. The protamine-based chromatin allows a dense packing of the DNA, which facilitates its protection and transportation to the oocyte (see for a review [114]). The replacement of nucleosomes by protamines is frequently observed throughout the animal kingdom [133], though the degree of this chromatin substitution varies among species. Protamination in mouse and boar is almost complete and only an estimated 1% of the total DNA in mouse sperm cells remains nucleosome bound, whereas in human sperm this is estimated to be about 15% [134-136]. Characterisation of the histones in human sperm identified H2A, H2AX, H2AZ, H2B, H3.1, H3.3, CenH3 and H4 [135, 137]. Analysis of the preferential chromatin conformation (nucleosome and/or protamine based) of several genes and structural elements in human sperm showed limited differences between sperm of one individual, but also between sperm of different individuals [138-140]. This sequence-specific chromatin conformation has been suggested to facilitate transcriptional activation of paternal genes in early embryogenesis and enable the three-dimensional organization of the sperm nucleus [137-139]. However, whether sperm-derived nucleosomes contribute to zygotic chromatin, a necessity to enable such epigenetic programs, or are removed during the extensive chromatin remodelling occurring after gamete fusion [9, 141] has hitherto not been established. However, roles for the maintenance of imprinting, as speculated by [32] has recently been illustrated in Arabidopsis, where, contrary to the zygote proper, a paternal-specific H3.3 isoform is maintained in the endosperm, the plant tissue where imprinting pays a role [142]

Therefore, we set out to detect histones of sperm origin in paternal zygotic chromatin. Since deposition of maternally derived histones takes place immediately after gamete fusion [9], sperm-derived histones, if retained, become indistinguishable from maternal ones. To circumvent this problem we used the difference in deposition characteristics of the histone H3 variants. The histone H3.1/H3.2 (the replication variants) are assembled into nucleosomes when DNA replication occurs, in contrast to histone H3.3, which is only incorporated outside the context of DNA replication [8]. Deposition of

maternal H3.1/H3.2 starts at the onset of zygotic S-phase, which commences approximately 8 hours after insemination in human zygotes [143]. Therefore, all H3.1/H3.2 present in the paternal chromatin prior to S-phase must originate from the male germ line.

Materials and Methods

Sperm decondensation in vitro

Sperm head decondensation was achieved by incubation of sperm sample in PBS containing 0.2% Triton X-100, 100 IU heparin (Leo Laboratories) and 2.5 mM DTT at room temperature. In order to obtain more than 80% decondensed heads per sample, incubation time varied between 10 to 15 minutes. The decondensation process was stopped by immersing the glass slides in 4% paraformaldehyde (PFA) for 15 minutes. Slides were then washed twice in PBS and allowed to dry.

Preparation of Cryo-preserved human sperm for heterologous ICSI

Cryo-straws containing 500 µl sperm suspension were thawed at room temperature and 1000 µl HTF-HEPES was added and gently mixed. The content was transferred to an eppendorf vial and centrifuged for 5 minutes at 500 xg. Subsequently the supernatant was discarded and the pellet was gently dissolved in HTF-HEPES and kept at room temperature.

Preparation of mouse oocytes for heterologous ICSI

B6D2 F1 females (Charles River, Sulzfeld, Germany) were used as oocyte donors and were kept in an adjusted light schedule, set at 9.00 am - 9.00 pm. Superovulation was induced by i.p. injection of 7.5 IU pregnant mare's serum gonadotrophin (PMSG, Intervet, Boxmeer, The Netherlands) around 9 pm, followed by 7.5 IU hCG (Intervet) after 48 h. Oocytes were harvested from the oviducts 13 h after administration of hCG and stored without cumulus cells at 37°C for up to 5 h in complemented Mem-a[144].

Heterologous intra cytoplasmic sperm injection

Microinjection was performed as described in [145] and [144] with some adaptations. The temperature in the injection droplet was kept at 24° C. For each ICSI experiment cryo-preserved sperm samples were freshly prepared (see above). Each injection round a sperm aliquot was transferred

to medium containing 12% polyvinyl pyrrolidone. Sperm were selected for normal morphology and motility. After injection, oocytes were kept on the injection platform for 5 minutes, then gradually warmed to 37°C and placed in culture medium at 37°C, 5% CO_2 in air [144].

Immobilization, fixation and immunofluorescence staining of mouse zygotes

Prior to fixation of the zygotes the zona pellucida was removed with acidic tyrode (pH 2.5) containing 1% BSA. Thereafter, cells were immobilised in a fibrin clot [106]. Fibrinogen was obtained from Calbiochem, cat. nr. 341573; Thrombin was obtained from Sigma, cat. nr. T-6634. Cells were fixed in 2% PFA, 0.15% Triton X-100 for 30 minutes, followed by incubation in ice-cold methanol for 10 minutes. Immunofluorescence was performed as described previously [9].

Antibodies

The monoclonal antibody #34 was used at a dilution of 1:1500 to detect H3.1/H3.2 (for characterisation see [9]). Polyclonal rabbit Pan-H3 (Abcam ab1791) was used at a dilution of 1:500. To unmask the epitope for the pan-H3 antibody slides were first incubated in 4 M HCl for 6 minutes prior to blocking, after which slides were extensively washed in PBS. Primary antibodies were detected by Molecular Probes A11001 fluor 488 goat anti-mouse IgG (H+L) and A11012 fluor 594 goat anti-rabbit IgG (H+L). Both were used in a 1:500 dilution.

Collection and fixation of human polypronuclear zygotes

Polypronuclear zygotes, i.e. zygotes that show three or more pronuclei after insemination instead of the expected two, are considered to be non-diploid and are therefore never transferred to the uterus in a human IVF setting. Polypronuclear zygotes used in this study were obtained from couples undergoing routine IVF procedures at the Erasmus MC in the period between June and September 2005. This study was approved by the Dutch Central Committee on Research involving Human Subjects (CCMO) and the local ethics review committee of the Erasmus university medical center. Human zygotes were produced by conventional in vitro fertilization (IVF) or after intracytoplasmic sperm injection (ICSI) 146, 147. After IVF, remaining cumulus cells and sperm cells were removed from the oocytes by gentle aspiration ~7 hrs after insemination and oocytes were moved to fresh drops of culture medium. All oocytes after both IVF and ICSI were checked hourly until 10 hrs past insemination for the appearance of pronuclei. To ensure that zygotes were fixed before the onset of S-phase, they were collected as soon as more then two

clearly discernible pronuclei were observed. Before fixation, zona pellucida were removed from zygotes by pronase treatment (0.5% in HEPES-buffered medium). Immobilization and fixation occurred as described above. After washing in PBS, fixed zygotes were either stored at 4ºC in PBS containing 10% normal goat serum and 0.05% NaN3 or frozen in culture medium containing 1.5 M DMSO.

Results

Presence of histone H3 in human sperm

Both the replacement and replication variants are detected in sperm by HPLC analysis [135]. To visualize histone H3 in sperm by immunofluorescence, we decondensed the cells by incubation with a mixture containing heparin and DTT. The dense structure of sperm chromatin does not allow antibody penetration without this treatment. Staining of decondensed sperm with the pan-H3 and H3.1/H3.2 antibodies showed a relatively homogeneous signal for both (see fig. 1).

Localisation of replication H3 variants in human paternal chromatin after heterologous ICSI

To find out whether human sperm derived histones are retained in paternal chromatin after decondensation we determined the presence of H3 replication variants in paternal chromatin in zygotic G1. Sperm from three fertile donors was used for injection in mouse oocytes. After injection, zygotes were incubated for different periods of time (75 to 370 min) prior to fixation to allow detection of H3.1/H3.2 at various stages of G1 [9]. At all stages we observed a prominent H3.1/H3.2 staining of maternal chromatin and a minor but clear staining of the paternal chromatin (see fig. 2a, b; n=60). Localisation of H3.1/H3.2 was found throughout the male chromatin, not concentrated in specific regions. Due to the increase of paternal pronuclear size after injection in time, signals became weaker after prolonged incubation times. The visualized H3.1/H3.2 fraction in paternal chromatin (fig. 2a-c) is an under representation of the total amount of H3 transmitted by the male gamete since the H3 replacement variant (H3.3) is also present in sperm [135] (fig 1).

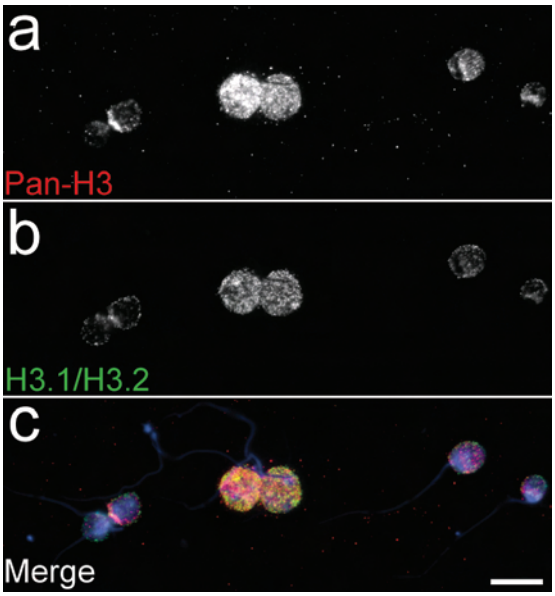

Figure 1 Presence of histone H3 variants in human sperm
Human sperm, treated with heparin to induce chromatin decondensation, stained with a pan-H3 antibody (**a**), which recognizes all histone H3 variants (H3.1, H3.2 and H3.3) or a H3.1/H3.2-specific antibody (**b**) revealed for both antibodies a diffuse, global staining. The merge (c) with DAPI, which labels DNA, shows the nuclear localisation of the histones. Bar represents 10 μm.

Localisation of replication H3 variants in paternal chromatin in human polypronuclear zygotes

To determine whether the H3 replication variants are also present in zygotic paternal human chromatin in a homologous setting, we localised H3.1/H3.2 in abnormally fertilized human oocytes, produced by IVF. From seven hours after insemination, appearance of the pronuclei was visually assessed every hour. Zygotes in which 3 or more pronuclei were observed were collected and fixed. Histone H3.1/H3.2 staining revealed an identical localisation as in the heterologous zygotes. Maternal chromatin clearly contained histone H3.1/H3.2, whereas the sperm-derived chromatin exhibited a less intense staining (see fig 2c; n=8). Zygotes after S-phase had a clear increase in pronuclear histone H3.1/H3.2 levels, as expected (see fig 2d; n=9).

Discussion

The relative abundance of nucleosomal chromatin and the presence of modified histones in human sperm [135] potentially allows a protein-based epigenetic program [32]. It has been suggested that genes that are contained in nucleosomal chromatin undergo earlier transcriptional activation as opposed to genes in protamine-based chromatin [138]. This implies a function for the dual nucleosome/protamine

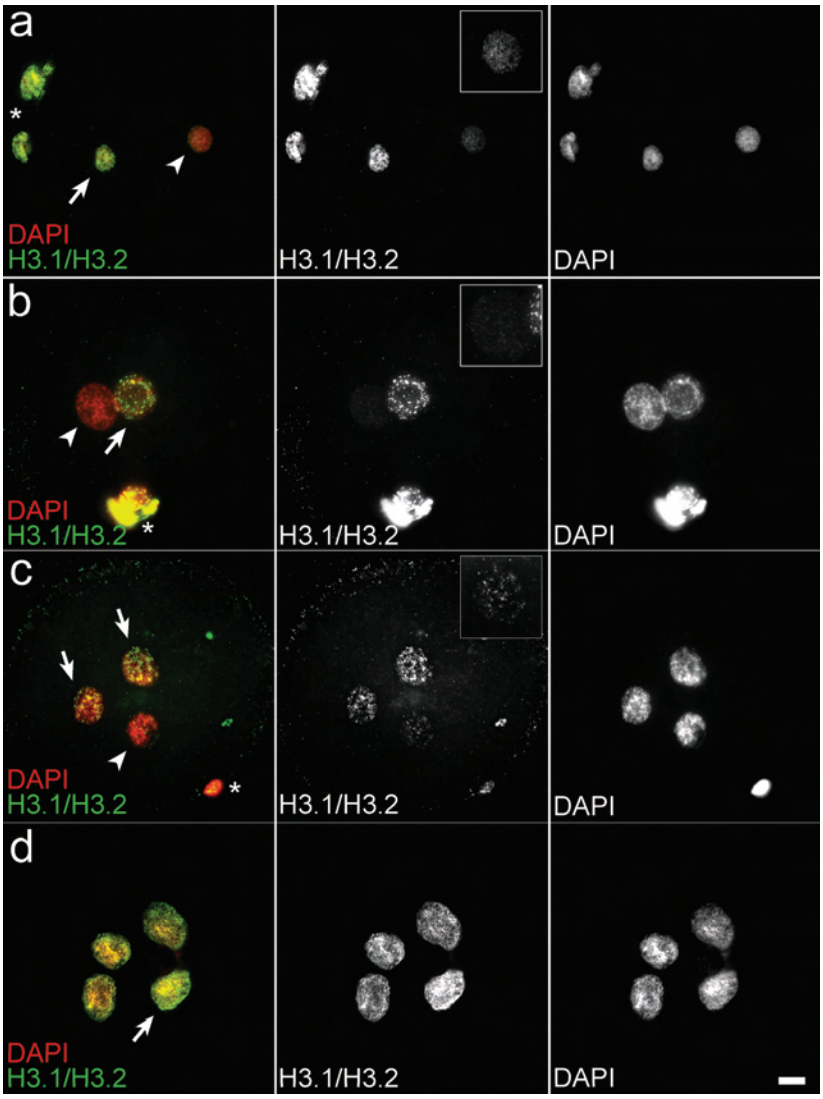

Figure 2 Presence of histone H3.1/H3.2 in paternal chromatin derived from human sperm in mouse and human oocytes

Zygotes obtained after heterologous ICSI (**a, b**) and human multipronuclear zygotes acquired after artificial fertilisation (**c, d**) stained for H3.1/H3.2 (middle column) and DAPI, which labels DNA (right column); merges are depicted in the left column.

Zygotes were obtained after heterologous ICSI and fixed respectively 60 minutes (**a**) and 150 minutes (**b**) after injection of human sperm. Arrow indicates maternal chromatin, arrowhead paternal chromatin and asterisk the polar bodies.

c. Human tripronuclear zygote fixed 7 hours after performing ICSI. Tripronuclear zygotes derived from ICSI are likely to be a consequence of a failure in second polar body extrusion. Similar to maternal mouse chromatin, these pronuclei exhibit clear H3.1/H3.2 staining (indicated by arrows). H3.1/H3.2 is also present in the paternal pronuclei (indicated by arrowhead) though the obtained signal is lower. Asterisk indicates polar body.
d. Human multipronuclear zygote fixed 22 hours after insemination with human sperm. Multipronuclear zygotes derived from IVF are likely formed by fusion of multiple sperm with an oocyte. The more intensely stained pronucleus (arrow) most likely represents the female nucleus since H3.1/H3.2 levels are higher in maternal chromatin [9]. Bar represents 10 μm.

chromatin structure in regulation of gene expression in the early embryo [114]. Furthermore, it has also been hypothesized that the cue which triggers inactivation of the paternally derived X chromosome (X_p) after gamete fusion is contained in the transmitted nucleosomal chromatin of the X_p [12]. A requirement for such paternal-derived epigenetic program to operate in the zygote is that sperm derived nucleosomes must be retained in paternal chromatin. After gamete fusion, sperm chromatin is subjected to intense remodelling and the protamines but possibly also the nucleosomes are removed from the DNA. Previously, we have shown that in mouse, modified nucleosomes present in sperm are transmitted to the zygote [148]. Here, we demonstrate that in human sperm, the H3 replication variants, contribute to paternal chromatin in the zygote (see Fig. 2). Since histone H3 forms the nucleosome complex with the other histone proteins, it is conceivable that also these other histones are retained in the paternal chromatin in the zygote. Recent work showed that H3.1/H3.2 containing nucleosomes are much more stable than H3.3 containing nucleosomes [149]. This difference might explain in part the association of H3.3 with actively transcribed genes and H3.1/H3.2 with silent regions [150]. Paternal sequences wrapped around H3.1/H3.2 containing nucleosomes could be poised to transcriptional inactivity and initiate self-propagation of this state at the service of structural chromosomal elements like centric heterochromatin (human sperm nuclei (Zalensky et al., 1993); bull sperm nuclei [98]; mouse sperm nuclei and zygote [148]; Arabidopsis zygote and endosperm nuclei [142]).

An estimated 15% of the genome in human sperm remains in a nucleosomal context [134-136]. The epigenetic potential by incorporation of these sperm derived nucleosomes into the paternal zygotic chromatin is obvious [32]. Future research, however, is needed to establish whether such programs exist.

The treatment of infertility via artificial reproduction enables men with hampered spermatogenesis to sire offspring. Preliminary studies have indicated a decrease in the protamine/nucleosome ratio when comparing sperm from infertile men to fertile men [151]. Higher histone content in sperm could have consequences for early developmental processes via enabling unscheduled downstream effects of sperm derived nucleosomal chromatin that contains variants and/or carries histone modifications.

Section 2.4

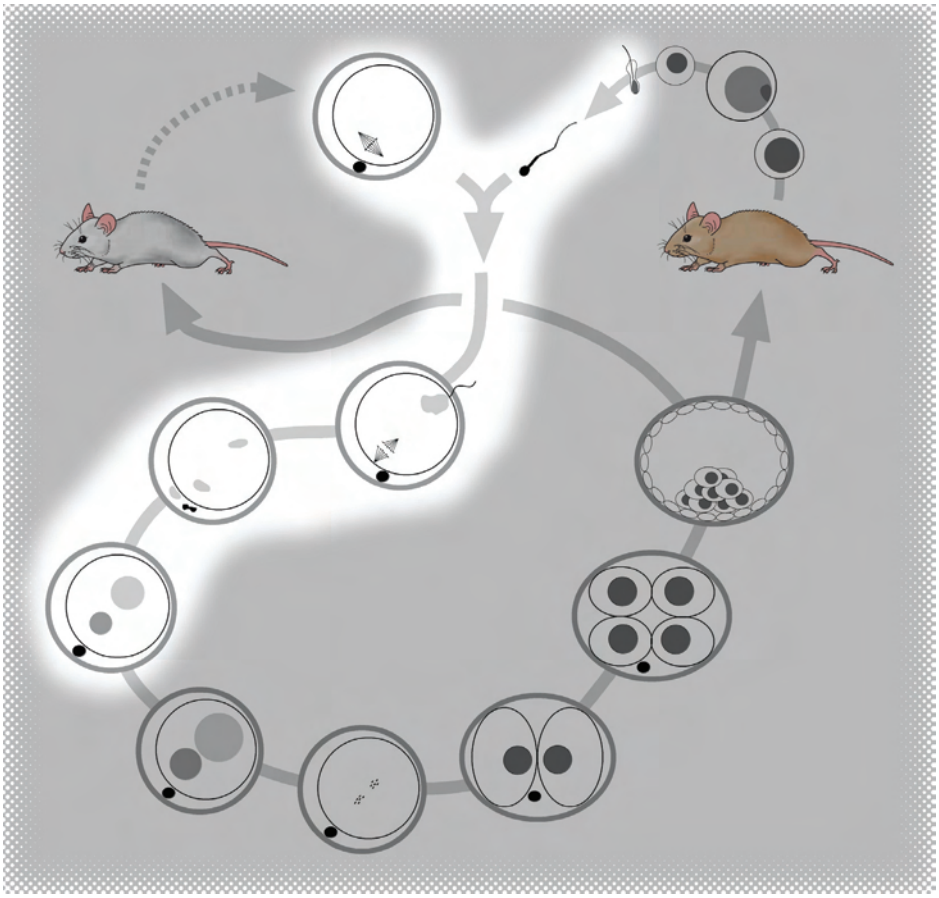

Mechanisms of Development 2005 September; 122(9):1008-22

Asymmetry in Histone H3 variants and lysine methylation between paternal and maternal chromatin of the early mouse zygote

Godfried W. van der Heijden[1,*], Jürgen W. Dieker[2,*], Alwin A.H.A. Derijck[1,*], Sylviane Muller[3], Jo H.M. Berden[2], Didi D.M. Braat[1], Johan van der Vlag[2], Peter de Boer[1,†]

[1]*Department of Obstetrics and Gynaecology, University Medical Centre St Radboud, PO Box 9101, 6500 HB Nijmegen, The Netherlands.*

[2] *Nephrology Research Laboratory, Nijmegen Center for Molecular Life Sciences and Division of Nephrology, University Medical Center, Geert Groteplein 26-28, 6500 HB, Nijmegen, The Netherlands*

[3]*Institut de Biologie Moléculaire et Cellulaire, CNRS, 15 rue Rene Descartes, 67000, Strasbourg, France.*

** These authors contributed equally*

Abstract

In mammalian fertilization, the paternal genome is delivered to the secondary oocyte by sperm with protamine compacted DNA, while the maternal genome is arrested in meiotic metaphase II. Thus, at the beginning of fertilization, the two gametic chromatin sets are strikingly different. We elaborate on this contrast by reporting asymmetry for histone H3 type in the pre-S-phase zygote when male chromatin is virtually devoid of histone H3.1/H3.2. Localisation of the histone H3.3/H4 assembly factor Hira with the paternal chromatin indicates the presence of histone H3.3. In conjunction with this, we performed a systematic immunofluorescence analysis of histone N-tail methylations at position H3K4, H3K9, H3K27 and H4K20 up to the young pronucleus stage and show that asymmetries reported on earlier are systematic for virtually all di- and trimethylations but not for mono-methylation of H3K4 and H4K20, the only marks studied present in the early male pronucleus. For H4K20 the expanding male chromatin is rapidly mono-methylated. This co-incides with the formation of maternally derived nucleosomes, a process which is observed as early as sperm chromatin decondensation occurs. Absence of tri-methylated H3K9, tri-methylated H4K20 and presence of loosely anchored HP1-β combined with the homogenous presence of mono-methylated H4K20 suggests the absence of a division of the paternal chromatin in eu- and heterochromatin. In summary the male, in contrast to female G1 chromatin, is uniform and contains predominantly histone H3.3 as histone H3 variant.

Introduction

In mammalian reproduction, the gametes of the two sexes have very different cell biological roles. After sperm entry, the cell cycle of the dormant metaphase II secondary oocyte is reactivated to proceed into telophase and subsequent female pronucleus (PN) formation, while at the same time the sperm nucleus is reshaped into the male PN (see for reviews [93, 94]).
The major function of the male sperm is to transfer genetic information to the future zygote. Therefore, the sperm chromatin is compacted at a degree of condensation 6-fold higher compared to a somatic cell nucleus [91]. This condensed state is reached through step-wise transformation of nucleosome-based chromatin into sperm-specific protamine-based chromatin during spermiogenesis. Protamine deposition takes place after spermatid elongation (see for time table [152]) whereas functions such as transcription and DNA repair slowdown at the onset of spermatid nuclear elongation [48, 153]. When the two gametes fuse, the sperm-specific chromatin is actively transformed into nucleosomal chromatin. The literature is not specific on the timing of the protamine-nucleosome transition and often contradictive [141, 154, 155].
Thus, the two gametic chromosome sets at the beginning of fertilization are strikingly different. It is this notion that might be at the basis of several biological, for instance epigenetic, differences observed between the parental nuclei in the zygote.

A series of recent reports describe the methylation states of several lysine residues in the N-termini of histone H3 and H4 [29, 79, 104, 108, 156-159]. Strikingly asymmetry for most positions studied was noted: tri-methylated H3K4; di- and tri-methylated H3K9, mono-, di- and tri-methylatedH3K27 and tri-methylated H4K20 are initially only present in the maternal chromatin of the 1-cell zygote. Only monomethylated H3K4, K9 and H3K27 was found to be symmetrical, being present in both PNs[160, 161]. Furthermore, differences between the parental nuclei at the transcriptional level have been observed. Although full zygotic genome activation takes place in the 2-cell embryo, leaky transcription is observed from early zygote S-phase on. Throughout the first cell cycle, transcription levels in the male PN are 4 to 5 times greater than in the female PN[125]. It is also known that the paternal PN exhibits higher levels of hyperacetylated his-

tone H4 compared to the female PN [101]. By elevating global acetylation levels of the zygote, transcription can also be observed in the maternal PN, indicating that transcriptional asymmetry is largely due to a more transcription favourable state of the male chromatin as influenced by its hyperacetylation [162].
At G1 of the zygotic cell cycle, DNA-methylation marks are actively removed from the paternal genome during the first 6 hours after gamete fusion [163, 164]. In contrast; this mark is passively diluted from the maternal DNA over subsequent cleavage divisions by the absence of maintenance methylation [165].

Another area where the two genomes are not each other's equivalent constitutes the reaction to DNA damage by DNA repair. In the early stages after gamete fusion, the vulnerability of the two genomes to irradiation as measured by the yields of chromosome abnormalities at first cleavage is strikingly different. The maternal complement exhibits levels two to three times higher than the paternal one [166].
To obtain a better conception of the chromatin differences between the sexes, that are particularly apparent at the morphological pre-PN level early after gamete fusion, we have chosen to study the protamine-nucleosome transition in mouse sperm after *in vitro* fertilization (IVF) in conjuncture with an epigenetic characterisation of the two parental genomes in the early zygote.
We determined chromatin remodelling up to 280 minutes post insemination *in vitro*, i.e. up to the PN stage, using antibodies that are specific for protamines, histones, dsDNA and nucleosomes, respectively. Subsequently, we have followed chromatin development in these early post-gamete fusion stages with histone H3 and H4 N-terminal tail methyl lysine modifications to evaluate one aspect of epigenetic differences between the two genomes. Our results reveal that after gamete fusion, nuclear morphology transition involves immediate chromatin remodelling, especially in the male complement. During this remodelling, paternal nucleosomes predominantly contain the histone H3.3 variant. As already known, epigenetic hallmarks are set differently between the male and female-derived genomes for di- and tri-methylation. However, we show that this is not necessarily the case for the mono-methylation state.

Methods

Gamete Collection and IVF

All media and culture dishes used for IVF were made one day in advance and kept at 37°C; 5% CO_2 in air to ensure maximum equilibration. Sperm was obtained from CBA/B6 F1 mice of 6-20 weeks old. Cauda epididymis were partially cut open in a 50 µl droplet HTF-HEPES (Cambrex; BE02-022F) 0.5% BSA (Sigma; A-4503) and were left for 5 min at 37°C to allow swimming-out. Hereafter the sperm suspension of 2 cauda was transferred to the bottom of a 4.5 ml Greiner bio-one PS-Tube with HTF (Cambrex; BE02-021F) 3% BSA and 10 µmol adenosine, a capacitation stimulator [194] (Sigma; A-5762). The sperm suspension was incubated at 37°C, 5% CO_2 in air for 1 hour. At 45 minutes a sample was taken to perform a sperm count. Female B6/CBA mice (4 to 12 weeks old) were housed with adjusted light hours set at 9.00 – 21.00. Superovulation was induced by injecting 7.5 U PMSG (Intervet, Boxmeer, The Netherlands) around 18.00 and 7.5 U HCG (Intervet) 48 hours later. Females were sacrificed the next morning at 9.00. Cumulus cell masses containing metaphase II oocytes were removed from the ampullae of oviducts and transferred per female to 50 µl HTF 0.5% BSA droplets covered with light mineral oil (Irvine Scientific; #9305). Sperm was added to these droplets to a final concentration of $1*10^6$ cells/ml.

Timing of zygote development

By paraformaldehyde (pfa) fixation (see fixation and immunofluorescence) and DAPI-staining at various time points post insemination (pi), it was determined that the majority of secondary oocytes was penetrated after 70 minutes. For dynamics of the protamine – nucleosome exchange and localisation of the histone chaperone Hira, zygotes were fixed at 4 time points pi: 70, 100, 150 and 280 min. Each time point yields zygotes in which the majority of the paternal nuclei represent a distinct morphology (see fig. 1). #34 double stainings were done with zygotes fixed at 150 minutes pi. For the lysine methylation stainings zygotes were fixed at 100 and 280 minutes pi. In addition Me(3)-H3K20 stainings were also carried out at 70 minutes pi. Between zygote variation with regard to progress of sperm head decondensation was observed at early time points (70 and 100 min pi), rendering pools of zygotes with different parental chromatin morphologies. This enabled us to obtain a clear picture of the sequence and timing of changes in parental chromatin. In general however, gamete fusion occurred relatively simultaneous and the timing of morphologies was similar to that of Adenot et. al. [95]. At later time points (150 and 280 min pi), hardly any variation in nuclear morphology remained, indicating

that the timing of gamete fusion between zygotes differs little but the process of sperm head decondensation is rapid. All zygote time points mentioned in this report are compensated for the 70-minute lag phase to give the minimal time periods for the stages described.

Antibodies

PL2-3, #34 and # 36 are monoclonal autoantibodies derived from either MRL/+ or MRL/lpr lupus (-prone) mice. PL2-3 is nucleosome-specific (M. Monestier; 1:12.000), # 36 is specific for dsDNA (1:800) [105 195], #34 is specific for histone H3.1 (this paper; 1:1500).
Upstate Biotechnology, Lake Placid, USA: AcH3 K18, (07-354; 1:500); AcH3 K23, (07-355; 1:500); PH3S28, (07-145; 1:1000)
Abcam ltd., Cambridge, UK: me1-H3K4, (8895; 1:500); me2-H3K4, (7766; 1:500); me3-H3K4, (8580; 1:3000); HP1-β, (P. Singh; 1:100); HP1-α, (P. Singh; 1:200); Protamines: HuP1, Hup2; (R. Balhorn; 1:1000); me1-H3K9, 1:250; Me(2)H3K9, 1:500; Me(3)H3K9, 1:500, me1-H3K27, 1:500, Me(2)H3K27, 1:500, Me(3)H3K27, 1:500; Me(1)H4K20, 1:500; Me(2)H4K20, 1:50; Me(3)H4K20, 1:500 (T. Jenuwein); Hira, (WC119, P. Adams; 1:100).
Secondary abs were used as following: Molecular Probes, Oregon, USA: A11001 fluor 488 goat anti-mouse IgG (H+L), A11012 fluor 594 goat anti-rabbit IgG (H+L), Sigma: F6258; anti-rat IgG, FITC conjugated. All were used in a 1:500 dilution.
All secondary abs were tested for non-specific binding, which was never observed.

Experimental procedures of #34 epitope mapping

The epitope recognized by antibody #34 was determined by screening, respectively, a 10-mer (kindly provided by Dr. C. Putterman,), a 12-mer (New England Biolabs, Beverly, USA) and a 15-mer (kindly provided by Dr. G. Smith, University of Missouri, Columbia, USA) random peptide phage display library with the purified antibody #34, as described previously [196].
The reactivity of #34 with several histone H3(18-37) peptides, containing either the H3.1 or H3.3 sequence and some modified residues (i.e. acetylated and/or phosphorylated at the indicated positions), and with a H3(23-34) peptide di-methylated at lysine 27 (Abcam, Camebridge, USA), was tested both in direct and inhibition ELISA. Briefly, in ELISA, Maxisorb® 96-well plates (Nunc, Roskilde, Denmark) were coated with 100 µl of peptide at 2 µM in 50 mM carbonate buffer pH 9.6 overnight at 4°C. The wells were washed with PBS/0.05% (v/v) Tween-20 (PBS-T) and blocked with 150 µl 1% BSA for 2 hours at room temperature. After

washing with PBS-T, 100 µl of monoclonal antibody was added in PBS-T and incubated for 2 hours at room temperature. After washing with PBS-T, 100 µl horseradish peroxidase-conjugated goat anti-mouse Ig(H+L) (Southern Biotechnology Associates, Birmingham, U.S.A.) diluted 1:7500 in TBS-T was added and incubated for 1 hour at room temperature. The plates were washed again with PBS-T and developed for 15 minutes using 100 µl 3,5,3',5'-tetramethylbenzidine (TMB) (SFRI Diagnostics, Saint Jean d'Ilac, France). The reaction was stopped by the addition of 100 µl 2 M H_2SO_4 and the optical density at 450 nm was measured in a microplate reader (Biorad, Veenendaal, The Netherlands). For inhibition studies, 0,5 µg/ml antibody #34 in PBS-T was pre-incubated in a 96-wells plate (Greiner) with a series of dilutions of a competitor peptide, and added to a Maxisorb® 96 plate coated with (unmodified) H3.1(18-37) peptide as described above.

Fixation and immunofluoresence

Before fixation of the zygotes the zona pellucida was removed with acidic tyrode (pH 2.5) containing 1% BSA. Thereafter cells were immobilised in a fibrin clot [106] (fibrinogen obtained from Calbiochem cat. nr. 341573; Thrombin obtained from Sigma, cat. nr. T-6634). IF was applied as described before [25]. HP1-β was washed away by incubating fibrin immobilised zygotes for 10 min in PBS 0.15% Triton-X-100 before fixation and IF.

BrdU incorperation

Zygotes were transferred 4 hours pi to culture medium containing 16 mM BrdU (Sigma; B-9285) and incubated until 7 or 8 hours pi. After immobilisation and fixation (see above) cells were incubated for 10 minutes at 37°C with the nuclease solution from the Amersham BrdU labelling kit (RPN202). Ab #34 and α-BrdU were differentially labelled with the Zenon direct labelling kit (Molecular Probes, Oregon, United States; Z-25102, Z-25107).

Collection of images

Images were collected with a Zeiss axioplan fluorescence microscope. Pictures were captured by a Zeiss AxioCam MR camara with Axiovision 3.1 software (Carl Zeiss). All images shown are derived from stacks with z-axis intervals of 0.2 µm. Stacks were deconveluted with Metamorph software version 6, using the nearest neighbour mode. Images shown are either stacks projected into a single image or a single slide of a stack. Photoshop was used to enhance levels if needed.

Results

Accessibility of epitopes for immunofluorescence

From penetration up to the formation of the male PN, there is a continuous morphological change of the sperm chromatin. We distinguish three distinct, successive nuclear shapes/states 1) type a nuclei, which are partially decondensed with a proximal part reminiscent of the initial sperm chromatin; 2) type b nuclei, which are fully decondensed and 3) type c nuclei, which are re-condensing (see fig. 1 and "timing of zygote development" in the M&M for an overview of the morphologies and their moment of appearance). We performed indirect immunofluorescence (IF) staining with a dsDNA-specific antibody (ab) #36 in combination with DAPI to determine whether the paternal chromatin was accessible for antibodies during the process of male PN formation. The staining by dsDNA ab #36 was nearly absent from condensed chromatin whereas decondensed chromatin was homogeneously stained (see fig. 2 A-F). An intense staining by #36 could be observed in the border region where the sperm chromatin transits into decondensed chromatin (see fig. 2 A-C). For the decondensed chromatin, a perfect co-localisation of #36 with DAPI was observed for each morphology (see fig. 2 D-F). Thus, antibody #36 (of IgG class) was not able to fully penetrate the sperm nuclei when still condensed. However, directly after decondensation the chromatin was fully accessible. Therefore conclusions presented here are solely based on observations made on decondensed sperm chromatin.

Loss of protamines

The removal of protamines is believed to be a 2-step process: after reduction of intra-protamine disulphide-bonds by glutathione, the actual protamines are removed [167 168]. To have a more precise description of the dynamics of this process, we applied indirect IF on early zygotes with an antibody mix recognizing both protamines 1 and 2. Suitability of these abs for IF was confirmed by obtaining a bright nuclear staining of artificially decondensed mouse sperm cells (data not shown). As expected and analogous to the results with the dsDNA ab, an antibody penetrability problem for condensed chromatin was encountered; a faint staining for protamines was observed before decondensation, while a more intense staining could be detected thereafter (see fig. 2A-F). Before the onset of de-

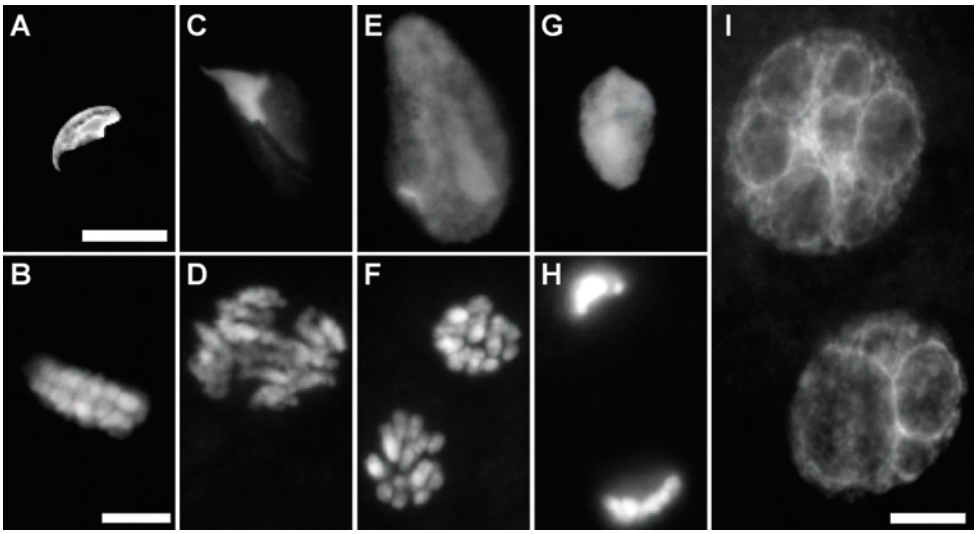

Figure 1 Dynamics and morphology of chromatin rearrangement in the early mouse zygote

Schematic overview of the dynamics and morphological changes of the male and female chromatin, before (**A-B**) and after (**C-I**) gamete fusion. All pictures are cut-outs from different zygotes (except I) stained with DAPI. Bar represents 10 μM. Each image shows a distinct phase up to PN formation. To obtain nuclei from each category, zygotes were fixed at specific time points after insemination (see Material & Methods). Before penetration of the sperm cell (**A**) the maternal chromosomes are aligned on the metaphase II spindle (**B**). After gamete fusion, activating factors of the sperm cell release the secondary oocyte from its arrest and the cell cycle progresses into anaphase II (**D**). At this time, decondensation of sperm chromatin has started (**C**) causing partial expansion. When both "original" sperm chromatin and the decondensed chromatin are present, we refer to type a nuclei. Expansion of sperm nuclei proceeds until the male nucleus is fully decondensed: type b nuclei (**E**). At that time, female meiosis is in early telophase II (**F**). This was observed 30 minutes after gamete fusion. Fifty minutes later the majority of the male nuclei started to recondense (**G**) followed by a second phase of decondensation, commencing in the early male PN stage (**I**, upper half; expanding male PN observed 3 hours past gamete fusion). After telophase II female chromosomes decondensed and simultaneously to the male complement transformed into a PN (**I**, lower half). These changes in paternal nuclei morphology have been described earlier [95].

condensation, extrusion of protamines in bulb-like spheres could be observed, which indicated that chromatin remodelling was already in progress before actual chromatin expansion (see fig. 2G-I). In decondensing chromatin no protamines could be detected that were part of the chromatin itself, the paternal chromatin was surrounded by protamine spheres (see fig. 2J-L). These protamine bodies were no longer observed 80 minutes after gamete fusion. We conclude that protamines were shed from the sperm DNA within thirty minutes after gamete fusion and had completely disappeared 50 minutes later.

Deposition of nucleosomes in the sperm DNA

Using PL2-3, an antibody specific for nucleosomes, we could visualize an increasing nucleosomal density upon the start of sperm nucleus decondensation. Signal was readily detected in the expanded chromatin of type a nuclei (see fig. 2M-O). Thirty minutes after gamete fusion, when the male nuclei had progressed into form b, the staining by PL2-3 was more intense and evenly spread throughout the nucleus (see fig. 2P-R).

Characterisation of an histone H3.1/H3.2 specific antibody

The epitope of antibody #34 was mapped by screening different random peptide phage display libraries. This resulted into the common motif: S-A-P-A-S/T, which corresponds to amino residues 28-32 of the N-terminal region of histone H3.1 (see S6 for a description of the techniques). In this region at position 31, the single N-terminal amino acid difference between H3.1 and H3.3 is located, i.e. a serine versus an alanine residue, respectively. We demonstrated that #34 was specific for H3.1 both in direct and inhibition ELISA (see S1), since we found absolutely no binding of #34 to the H3.3 peptide and no inhibition by the H3.3 peptide. We also tested in direct and inhibition ELISA the influence of some modifications of residues located in/close to the epitope of #34 (see S1) on the reactivity of #34. H3 peptides acetylated on lysine 18 and 23 and/or phosphorylated on serine 28 showed a decreased binding of #34 and an about 5-fold higher inhibitory effect compared to the unmodified H3.1 peptide, although less pronounced compared to the H3.3 peptide. We were not able to demonstrate direct binding of #34 to a H3.1 (23-34) peptide di-methylated at lysine 27, but this could be

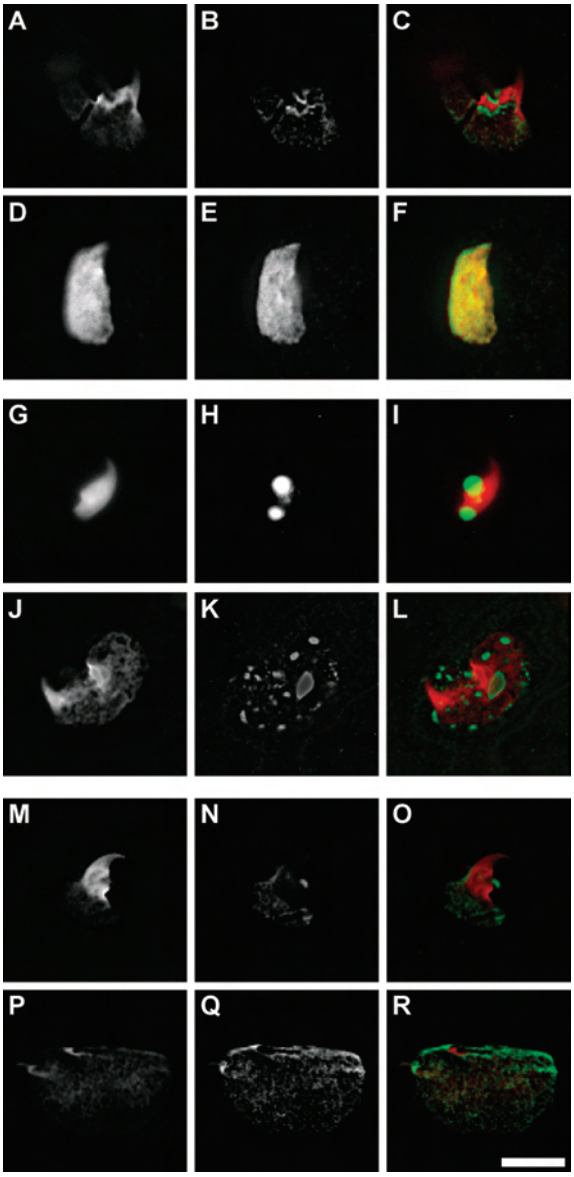

Figure 2 Accessibility of the decondensing sperm head, its loss of protamines and gain of nucleosomes
Images are cut-outs from whole zygote images. DAPI is pseudo coloured red and the abs green. Bar represents 10 μM.
A-F) Staining of the male nuclei by DAPI (A, D) and α-dsDNA (B, E), in sperm nuclei type a (A–C; n=12) and b/c (D–F; n=16).
G-L) Staining of the male nuclei by DAPI (G, J) and α-protamine 1 and 2 combined (H, K), in sperm nuclei type a (G-H; n=10) and a/b (J-L; n=24).
M-R) Staining of the male nuclei by DAPI (M, P) and α-nucleosomes (ab PL2-3) (N, Q). In sperm nuclei type a (M-O; n=15) and b (P-R; n=44).

explained by inefficient coating of short peptides. However, in inhibition ELISA the reactivity of #34 with H3.1 (18-37) was hardly influenced by Me(2)H3(23-34)K27 (see S1).

The paternal chromatin is virtually devoid of histone H3.1-2 during G1

We applied ab #34 on the pre-S phase zygote and did not detect staining in the paternal chromatin throughout PN formation in

contrast to maternal chromatin (see fig. 3), which suggests that the H3 replication variants are absent from the paternal chromatin.
However, because we could not test in ELISA the reactivity of #34 with all combinations of modifications located in or nearby the epitope of #34 (due to the limited availability of modified histone H3 peptides) and Ac-H3K18 as well as Ac-H3K23 are known to be present in the G1 PN (unpublished data; [102]) the possibility that the absence of staining by #34 was caused by an inhibiting effect of nearby H3.1 modifications in situ, still existed. We therefore investigated whether male nuclei type b, c had a low abundance of possibly interfering modifications.
Zygotes were fixed at 80 min post gamete fusion and double stained with #34 and antibodies specific for modifications in or nearby the epitope of #34 (i.e. Ac-H3K18, Ac-H3K23, Me(1, 2, 3)-H3K27 and P-H3S28). In type b, c nuclei, a faint staining by the antibody specific for Ac-H3K18 was observed, while none of the other modifications could be detected (see S2). At this time point #34 was usually absent from the paternal nuclei (see S2), although occasionally nuclei showed speckles. Around 80 minutes post gamete fusion the maternal complement progressed into late telophase II and did not reveal any Ac-H3K18, while levels of Ac-H3K23, Me(3)H3K27 and P-H3S28 were low or undetectable. In contrast, the antibodies specific for mono-, di-methylated H3K27 prominently stained the maternal complement (data not shown). Notably, staining by #34 was virtually absent from maternal metaphase II chromosomes, but during anaphase II the #34 signal appeared rapidly, while during telophase II, #34 brightly stained the maternal chromatin and that of the polar body (see fig 3). Opposite to the staining pattern by #34 of the maternal complement, the antibody specific for P-H3S28 strongly stained the maternal metaphase II chromosomes, but this staining quickly diminished after progression of meiosis II and disappeared completely during early telophase II, (see S2 and S3). It is only this H3.1 modification in the vicinity of the epitope of #34 whose disappearance showed a strong correlation with the appearance of staining by #34, which was in agreement with the ELISA data for #34 (see S1). All antibodies specific for the three methylation states of K27 on H3 did not block the epitope of #34 as revealed by double staining. This shows that these methyl groups do not, or to a lesser extent interfere with #34 binding compared to

the phosphoryl group on S28 of H3. The speckles of #34 staining occasionally observed in the male nuclei possibly result from DNA-synthesis coupled repair (when H3.1 is deposited) and/or from nucleosomes of paternal origin.
Taken together, the data of the ELISA and (double) stainings of the paternal/maternal chromatin by #34 and/or antibodies specific for H3 modifications showed that H3.1 is virtually absent from the paternal chromatin.

Presence of H3.3 specific histone chaperone Hira in paternal nuclei
Earlier we showed an increasing presence of nucleosomes in the pre-PN paternal chromatin. Combined with the notion that H3.1 was absent from this chromatin, the only candidate for fulfilling the histone H3 role in the paternal nucleosomes post gamete fusion is H3.3. The lack of a valid antibody specific for H3.3 forced us to use antibodies raised against the histone H3.3 chaperone Hira [169], recently shown to be specific for deposition of H3.3-H4 dimers onto the DNA [16]. Staining with a Hira specific ab revealed this protein to be present in the sperm chromatin from its initial phase of decondensation until early PN formation (see fig. 4 A-C). At 3.5 hours after gamete fusion however, the signal had diminished to undetectable levels in 52% of the paternal nuclei (n=46); indicating differences in the rate of paternal remodelling between zygotes. Hira was not detected in the maternal complement up to PN formation, after which it was present in a minority of the maternal PNs evaluated.
Apparently, DNA synthesis independent nucleosome deposition also occurs in the maternal complement in a subset of zygotes. The time window of presence of Hira in sperm chromatin specifies the dynamics of nucleosome deposition; apparently *de novo* histone deposition after gamete fusion starts at the very beginning of chromatin decondensation and is completed roughly 4 hours after gamete fusion.

Appearance of H3.1
Since deposition of the replication H3 variants is strictly coupled to DNA synthesis the epitope for ab #34 should appear in the paternal chromatin during S-phase. The onset of DNA replication in zygotes is well described in the literature and starts 7 hours after gamete fusion [99]. In our IVF system, the majority of zygotes start S-phase

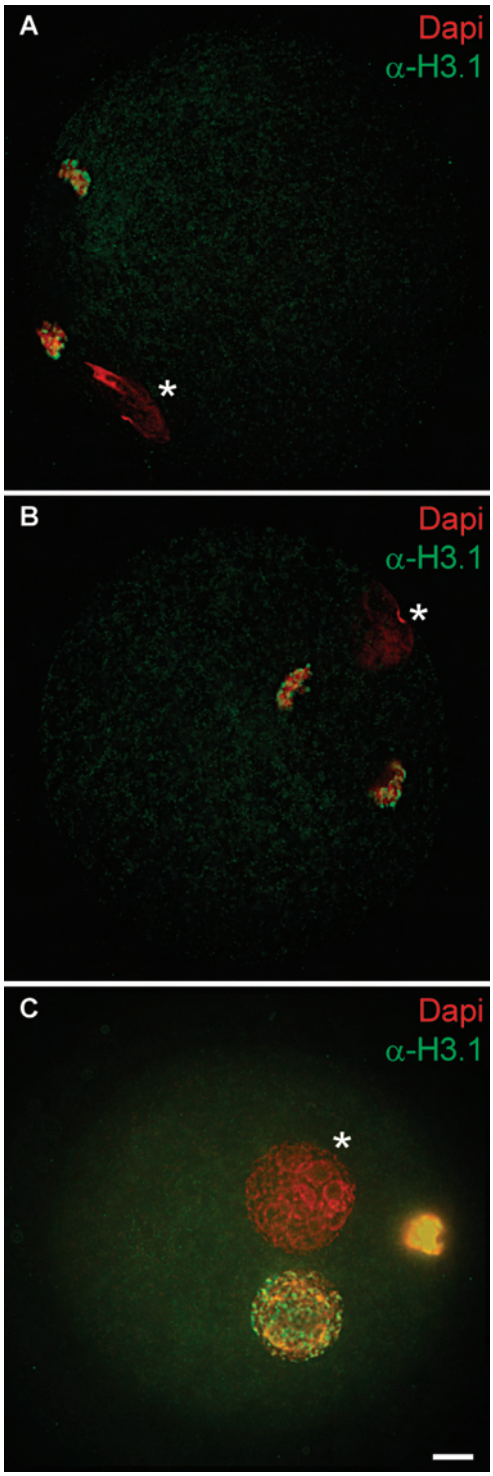

Figure 3 #34 co-localises with the maternal chromatin, not with the paternal

Whole zygote images stained with DAPI (pseudo coloured red) and #34 (pseudo coloured green). #34 does not stain type a nuclei (**3A**), type b nuclei (**4B**) nor the paternal PN (**3C**). Paternal chromatin is marked with an astrix. Bar represents 10 μM.

between 7 and 8 hours after insemination. Staining of zygotes that had progressed into S-phase showed a strong #34 signal in the parental chromatin sets (see fig 5C). To see if onset of DNA replication and appearance of #34 signal coincided, we cultured zygotes in the presence of BrdU and proceeded to detection of the incorporated nucleotide in combination with #34 staining, 7 and 8 hours after insemination. Zygotes showed either absence of both signals in the paternal PN (zygotes that had not yet progressed into S-phase) or presence of both signals (zygotes that had started DNA replication)

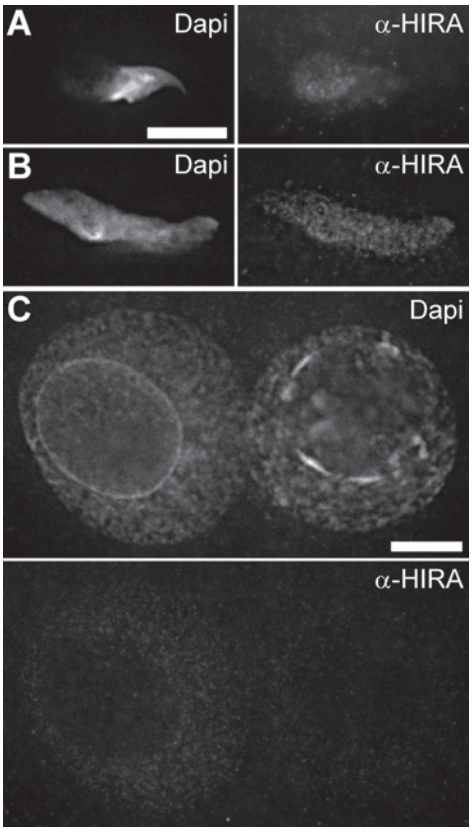

Figure 4 Presence of Hira in the decondensing sperm nuclei
A) Staining of the male nucleus type a by DAPI (left) and α-Hira (right) (n=9).
B) Staining of the male nucleus type b by DAPI (left) and α-Hira (right) (n=22).
C) Staining of the parental PNs by DAPI (upper panel) and α-Hira (lower panel) (n=46). The male PN is depicted left and the female PN right. Bar represents 10 μM.

(see fig. 5A, B). Paternal chromatin stained by BrdU or #34 only could not be detected, which again demonstrates the deposition of histone H3.1 to coincide with the start of DNA replication.

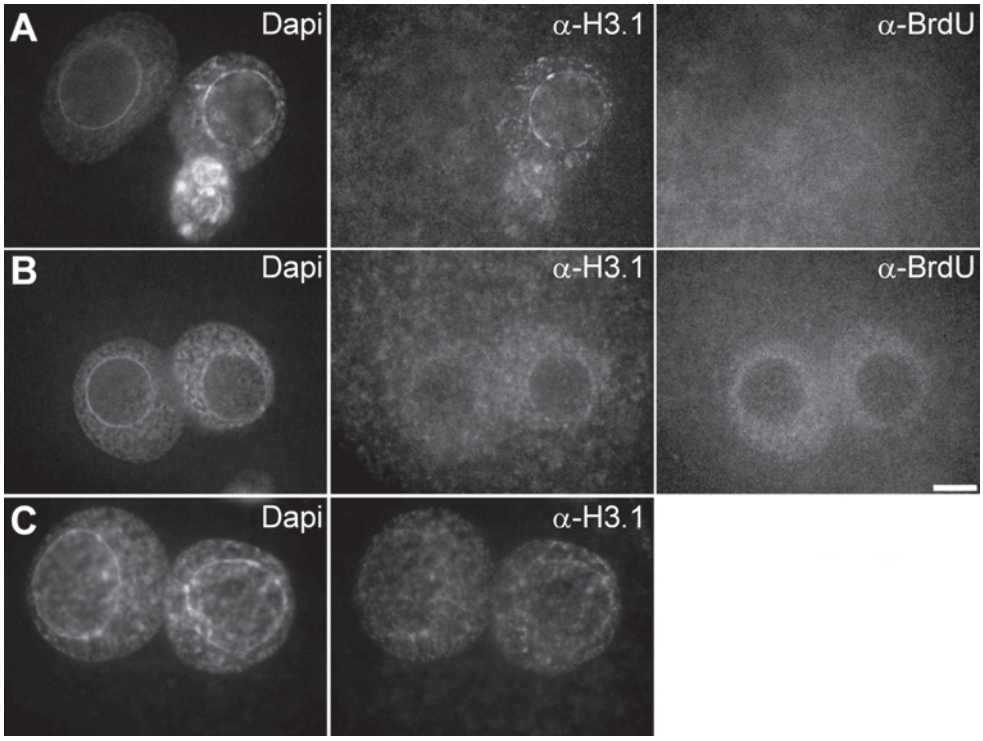

Figure 5 #34 appearance coincides with onset of DNA replication
Staining of zygote in early S-phase with DAPI and directly labelled α-BrdU and #34 (A, B) or #34 (C). Bar represents 10 μM.
A) Pre-S-phase PNs (n=32).
B) PNs at the onset of S-phase (n=32).
C) PNs that have progressed into S-phase (n=45).

Lysine methylation states of the parental chromatin in the early zygote

The presence and time of appearance of specific histone H3/H4 methylation before and after PN formation up to 210 minutes post-gamete fusion was visualised by using antibodies that are highly specific for mono-, di- and tri-methylated histone H3 (at positions K4, K9 and K27) and histone H4 (at position K20) [170]. All methylation states were present in the maternal metaphase II chromosomes up to PN formation except Me(2)H4K20 (see figs. 6A-D; S3; S5 for respectively PN stainings, metaphase II stainings and relative intensities in all stages and control cells). This mark was absent at all

stages, though present in cumulus cell nuclei used as a control (see S4). Me(1)H3K9 was usually present in the maternal PN but always at a low level (see fig. 6C); occasionally no signal was detected; again control cumulus cells always showed a prominent nuclear signal (see S4). During this period the male chromatin did not stain for: Me(1)-H3K9, -H3K27; Me(2)- H3K4, -H3K9, -H3K27, -H4K20 and Me(3)-H3K4, -H3K9, -H3K27, -H4K20 (see fig. 6a A-D). To test the possibility that these methyl marks are present in the original sperm chromatin but are removed during chromatin remodelling, as recently was assumed for Me(3)H4K20 [29], we stained type a and/or b nuclei. For none of the methyl marks absent in the male PN, IF signals were detected in the decondensed chromatin at these stages. As shown earlier, antibodies are not able to penetrate condensed sperm chromatin so we cannot draw any conclusions for this type of chromatin. Mono-methylation of H3K4 and H4K20 were the only marks present in both parental PNs. The appearance of these two modifications differed. Me(1)H4K20 was observed strikingly early after gamete fusion. In type a male nuclei Me(1)H4K20 could be detected in the periphery of the expanding chromatin and type b male nuclei were stained throughout the entire nucleus (see fig. 6E). Also in the early paternal PN a homogeneous signal was observed. This was different from the maternal PN where staining was less intense in heterochromatic regions, which reside around the precursor nucleolus (see fig. 6D). Me(1)H4K20 was absent from centromeric constitutive heterochromatin of maternal metaphase II chromosomes and DAPI bright heterochromatic regions in cumulus cell nuclei (see S3, S4) in concordance with an earlier report [171]. Me(1)H3K4 emerged in the male chromatin nearer to the time of PN formation. In the PN a speckled staining pattern was observed in both parental nuclei (see fig. 6A). Maternal metaphase II chromosomes showed a diffuse distribution of Me1-H3K4 and signal was absent in the heterochromatic regions of cumulus cell nuclei (see S3, S4).

Distribution of HP1α and β in the early zygote

Heterochromatin Protein 1 (HP1) is a crucial protein in the formation of heterochromatin domains through its ability to bind Me(3)H3K9 [172]. To see whether absence of this modification leads to a different location of HP1 in the male PN compared to the female

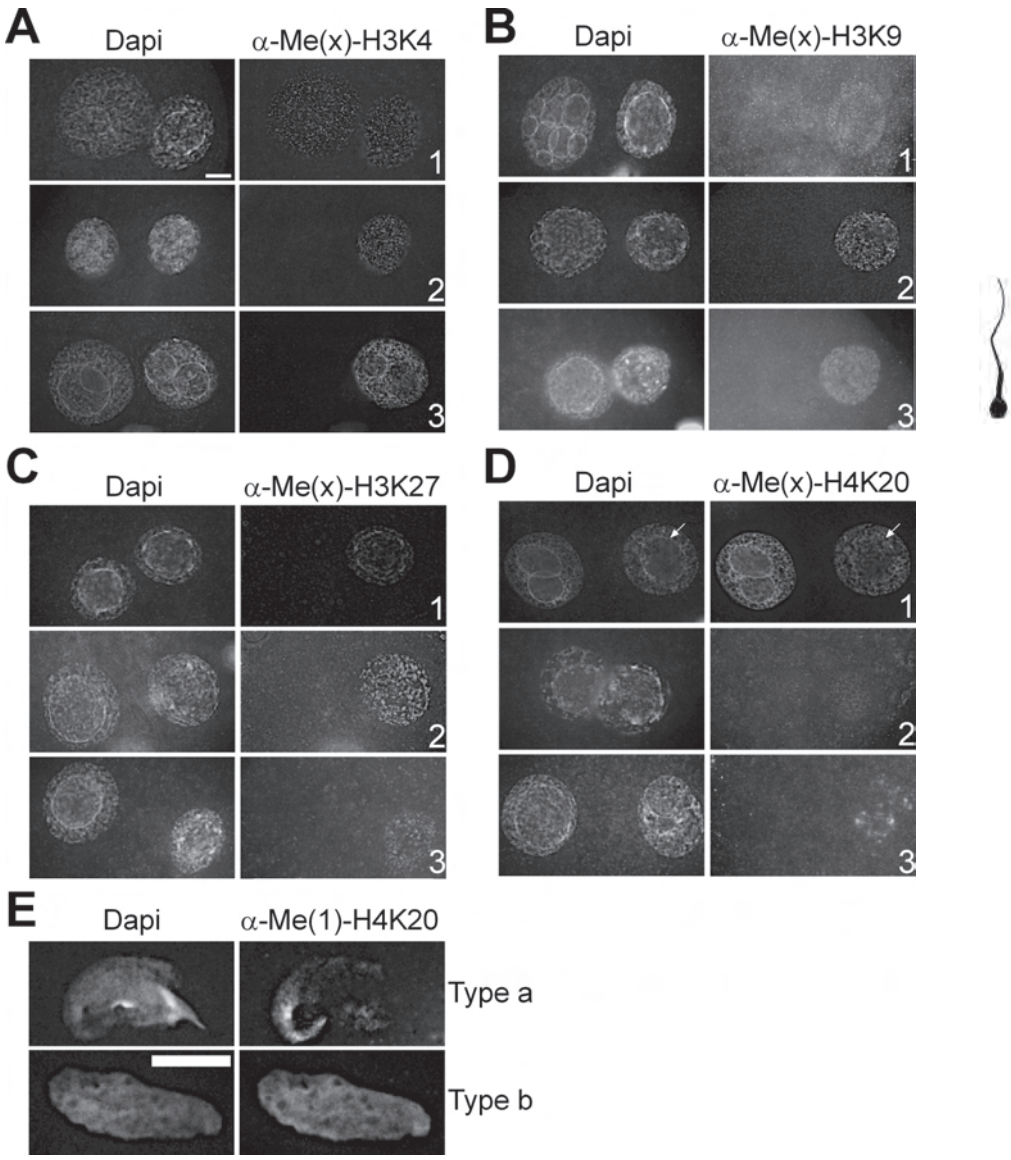

Figure 6 Localisation of mono-, di-, and tri-methylation of lysine K4, K9, K27 of histone H3 and histone H4 K20 in the early G1 zygote The male PN is always on the left side, the female on the right. Left column shows DAPI staining, right column staining with the ab. Bar represents 10 μM.

A. 1) α-Me(1)H3K4 (n=15); 2) α-Me(2)H3K4 (n=21) 3) α-Me(3)H3K4 (n=29)

B.1) α-Me(1)H3K9 (n=40); 2) α-Me(2)H3K9 (n=30); 3) α-Me(3)H3K9

(n=45)
C. 1) α-Me(1)H3K27 (n=13); 2) α-Me(2)H3K27 (n=17); 3) α-Me(3)H3K27 (n=17)
D. 1) α-Me(1)H4K20 (n=17); the arrow points at the heterochromatic region around the precursor-nucleolus of the female PN. 2) α-Me(2)H4K20 (n=10); 3) α-Me(3)H4K20 (n=15)
E. Localisation of Me(1)H4 K20 in the sperm nuclei type a and b
Staining of the male nucleus by DAPI (left) and α-Me(1)H4K20 (right) in sperm nuclei type a (n=9) and b (n=12). Bar represents 10 μM.

one, we stained with antibodies specific for the isoforms mostly associated with heterochromatin, HP1-α and HP1-β [173]. We did not detect HP1-α in the first cell cycle in both parental nuclei (see fig. 7A). HP1-β, on the other hand, was present in the maternal complement during anaphase II while absent from the male chromatin (see fig. 7B). Shortly after PN formation, HP1-β was observed in both PNs, as has been reported earlier [108]. Furthermore, a rim of HP1-β was seen around both nuclei that later disappeared (see fig. 7C). This may represent the entry of HP1-β into the nuclei. From this phase on a difference in localisation of HP1-β between the parental PNs is seen. In the maternal complement HP-1β co-localises with the bright DAPI stained heterochromatin while in the paternal PN, localisation is diffuse and does not co-localise specifically with any DNA domain (see fig 7D). To see if there is a difference between the anchoring of HP-1β to maternal and paternal chromatin we performed lysis experiments. In contrast to the female PN, levels of HP1-β decreased in the male PN upon treatment: although present, HP1-β is not tightly bound to the male chromatin (see fig. 7E).

Discussion

Removal of protamines and appearance of nucleosomes is an early process

Until now it has not definitively been shown at which phase of decondensation of the sperm nucleus, the actual removal of protamines takes place and maternal nucleosome deposition commences [174]. By immunofluorescence analysis with antibodies specific for protamines, dsDNA, histones and nucleosomes, we could correlate the

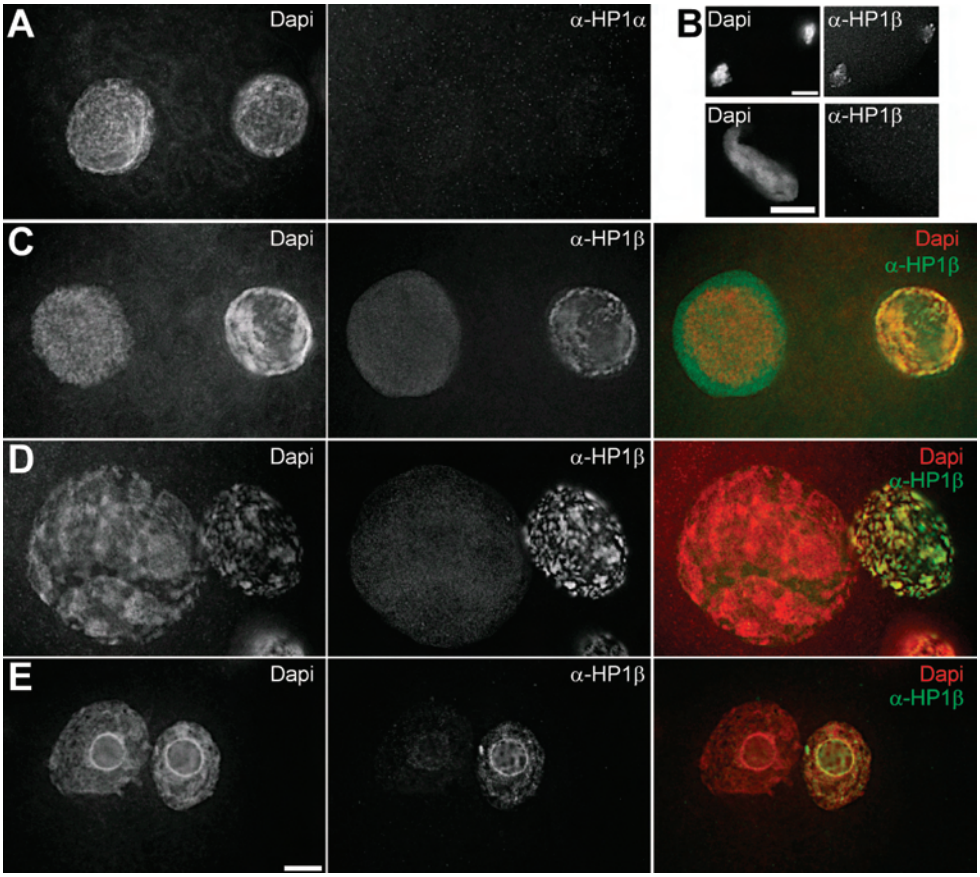

Figure 7 Appearance and localisation of HP1-α and β in the early zygote The male PN is depicted left and the female PN right. DAPI is pseudo coloured red, HP1-β green.

A) Staining of the parental PN with DAPI (left) and α-HP1-α (right) (n=9).

B) Staining of the male nuclei type b and maternal telophase with DAPI (left) and α-HP1-β (right) (n=40).

C) Staining of the early parental PN with DAPI (left) and α-HP1-β (right) (n=40).

D) Staining of the parental PN with DAPI (left) and α-HP1-β (right) (n=80).

E) Staining of the parental PN with DAPI (left) and α-HP1-β (right) after lysis (n=11). Bar represents 10 μM.

change of chromatin morphology with the presence or absence of protamines. Extrusion of protamines starts before decondensation and within 30 minutes post gamete fusion the male chromatin does not co-localise with the protamines any more (see fig. 2 G-L). A different observation has been made by Nonchev and Tsanev [141] who still were able to detect protamines 8 hours after sperm penetration in the paternal PN. We can only explain this apparent discrepancy by the use of different antibodies and techniques. We detected nucleosomes by staining with the nucleosome-specific antibody PL2-3 in the earliest stages of the expanding sperm nucleus, which could maybe in part be explained by the fact that an estimated 1% of mouse sperm DNA is bound to nucleosomes (personal communication R. Balhorn). A steep increase in nucleosome density was observed however, after the start of decondensation (see fig. 2M-R). Hira, a histone chaperone that deposits H3.3-H4 dimers onto DNA [16], co-localises with the expanding sperm chromatin in the zygote (see fig. 4A). Apparently, the onset of deposition of maternally derived nucleosomes takes place at the moment of paternal chromatin expansion. The only indication that DNA might be completely devoid of nucleosomes and protamines during expansion of the sperm chromatin was the brighter staining by the antibody specific for ds-DNA at the interphase of condensed and decondensed chromatin (see fig. 2A-C). This finding also indicates an absolute coincidence between decondensation and nucleosome formation.
We now have obtained a clear picture of paternal chromatin remodelling; protamines are removed from expanding chromatin, which is completed within 30 minutes after gamete fusion. During this period nucleosome formation starts, continuing over a period of roughly 4 hours in the zygote as deduced by absence of Hira in 52% of the paternal PNs at around that time point.

H3.3 is the predominant histone H3 variant in zygotic male chromatin before S-phase, H3.1 appears during DNA replication

The nucleosome core particle consists of two copies of Histone H2A, H2B, H3 and H4. For Histone H2A, H2B and H3 variants have been described [175]. Histone H3 has three functionally different subtypes: CenH3, which is strictly localised in the centromeres and highly diverged in sequence from the canonical H3 of which

two functional variants exists: the replication variants (H3.1 and H3.2), and the replacement variant (H3.3). The utilisation of the H3 replication variants, which differ from each other in only one amino acid, is strictly limited to DNA synthesis linked nucleosome assembly [176]. When nucleosomes are formed without occurrence of DNA synthesis, H3.3 is incorporated [177]. This specialisation of H3 subtypes is reflected in their chaperones. H3.1 (and H3.2) is deposited as a H3-H4 dimer by
Caf-1 while H3.3 is deposited, also as a H3-H4 dimer, by Hira [16].
The deposition of maternal nucleosomes onto paternal DNA directly after gamete fusion is not accompanied by DNA synthesis. By axioma these nucleosomes will contain H3.3 as histone H3 variant. Characteristic for mouse sperm chromatin is the near absence of nucleosomes. Therefore virtually all the paternal chromatin will be wrapped around newly deposited H3.3 containing maternal nucleosomes. We have characterized a monoclonal antibody (#34) whose epitope encompasses amino acid positions 28 to 32 of the N-terminus of H3. The single amino acid that differs between the N-terminus of the replication H3 variants, H3.1/H3.2, and the replication-independent variant, H3.3 is located within the epitope of #34 at position 31. It is this one amino acid difference that allows antibody #34 to discriminate between the two H3-types; recognizing only the replication variants (H3.1/H3.2) and not the DNA synthesis independent replacement variant (H3.3) (see S1). With this antibody we show that the H3 replication variants are virtually absent from the zygotic pre-S phase paternal chromatin, concordant with the specialised functions of the H3 subtypes. The antibody brightly staining the maternal chromatic counterpart is demonstration of its functionality (see fig. 3). We were not able to demonstrate the presence of H3.3 directly because of the lack of a valid antibody. However, we could show its presence indirectly by staining for the H3.3-specific chaperone Hira (see fig. 4). In conclusion, the absence of H3.1 combined with the presence of nucleosomal chromatin and Hira, strongly suggests that H3.3 is the predominant H3 variant present in the paternal chromatin during zygotic G1. The sheer absence of the H3 replication variants from the paternal chromatin allowed us to observe their first appearance which indeed coincided with the onset of S-phase as determined by BrdU incorporation (see fig. 5A, B).

Lysine methyl marks in the zygote

In recent years it has been shown that posttranslational modification of histones can act as regulators in a variety of biological processes. Attachment of methyl groups to designated lysine positions, preferably in H3 and H4, are highly stable modifications and thereby attain epigenetic properties [178, 179]. Lysine methyl marks function by creating a binding place for proteins that, in turn, exert their role, or alternatively block these binding places for other proteins [172, 180, 181]. Lysine residues can be mono-, di-, or tri-methylated [182]. The functional differences of the various methylation states begin to emerge only now. However, the tri-methylated state is often regarded as the being the most explicit one. The presence of histone N-termini methylations on the parental chromatin in the early zygote has been studied before but not in a systematic way [29, 79, 108, 156-161, 183]. Intriguingly there seem to be some discrepancies between observations on histone lysine methylation patterns in the zygote. Me(2)H3K9 has been reported to appear in both PNs 3-6 hours after gamete fusion[157], another report mentions this to occur after DNA replication [104] while other reports state that it is not present throughout the zygotic cell cycle in the paternal chromatin at all [160] or in some PNs, only barely detectable [158]. Our finding that Me(2)H3K9 is not present in the early paternal PN, however, seems to be in concordance with most reports. Regarding appearance of Me(3)H3K27 in the paternal PN, observations also differ. This mark has been reported to appear 3-6 hours after gamete fusion [157] while presence only after DNA replication (14 hours after gamete fusion) has also been communicated [104]. Our data regarding Me(1)H3K9 and Me(1)H3K27 is conflicting with Santos et. al., [104] who describe the appearance of these marks in the pre-PN paternal chromatin. We had troubles obtaining a sharp signal for Me(1)H3K9 though this does not seem to be due to our preparation technique since a clear nuclear signal was obtained when 4-cell embryos were stained (data not shown). Me(1)H3K27 we readily detected in the maternal chromatin (see fig. 6c) but we did not observe this mark in the paternal chromatin in the time window under study here. Whether all these differences are biologically significant remains an urgent question.

Parental Chromatic asymmetry and the Maternal to Zygote Transition

During pre-implantation development, the chromatin of the highly differentiated germ cells is transformed to accommodate a cleavage stage embryo with pluripotent blastomeres. This transformation is part of Maternal to Zygotic Transition (MZT), comprising degradation of maternal messengers, replacement of maternal transcripts by zygotic ones and the reprogramming of the parental genomes into the versatile embryonic genome [184].

It is at its onset that we, and during the MZT that others have observed asymmetries in the parental chromatin. In what way are these asymmetries observed linked to this process? Do they have a primary biological reason or are they just are mere consequence of sperm nuclear transformation? An answer to the first question regarding H3-type asymmetry seems apparent. The absence of H3.1 in the pre S-phase paternal nucleus fits well with recent reports, showing that H3.1 is only incorporated when nucleosome deposition is coupled to DNA synthesis, while H3.3 is deposited when nucleosome assembly is DNA synthesis independent [177]. The H3-type asymmetry therefore is likely to be a direct consequence of this H3-type specialisation. Although our finding is in concordance with this, it broadens the biological utilisation of H3.3. Deposition of H3.3 has until now been linked to transcriptionally active loci [177, 185-187]. Here we demonstrate that utilization of histone H3.3 is linked to DNA synthesis independent histone deposition, not involving gene activation; the zygotic chromatin is not transcriptionally active through G1 [125].

Throughout the animal kingdoms, sperm specific protamine-based chromatin is a common phenomenon [133]. The protamine-nucleosome transition will consequently result in a high paternal H3.3 content. The parental H3-type asymmetry observed here however, will not be an absolute on. Female germ cells enter meiotic prophase I arrest during foetal growth. Release follows from hormonal stimulation at reproductive age, subsequent to the period of oocyte growth during follicle development that demands transcription. Both the long time meiotic arrest, in which deposition of H3.1/H3.2 is likely to be minimal, and the transcriptional activity, when H3.3 is prone to be deposited at active chromatin, will probably elevate the H3.3 content of the maternal chromatin. From this we conclude that H3.3 is far more abundant in the early embryonic chromatin then previ-

ously may have been realised.

The general idea regarding nucleosome deposition during S-phase is that the newly synthesised DNA is assembled on parental and *de novo* synthesized nucleosomes. This implies that the level of original H3.3 in the paternal chromatin is diluted 2-fold every round of replication. With the paternal level of H3.3 containing nucleosomes close to 100%, this implies that in the G1 of the 2-cell zygote levels are reduced to ~50% and after the second S-phase to around 25% (if we ignore H3.3 deposition induced by transcriptional activation and possibly H3.1 deposition linked to DNA repair). It is during the second S-phase that a repressive state of chromatin for transcription is established [184]. Whether the drop of paternal H3.3 content to 25% in some way is linked to the reduced transcriptional activity observed in this S-phase remains to be investigated. The idea that H3.3 has an intrinsic transcription facilitating capacity has not yet been tested.

In mouse spermiogenesis, the nucleosome-protamine transition will diminish heritage of lysine methyl marks of paternal chromatin after gamete fusion. Initial asymmetry in the zygote is therefore a direct consequence of the almost absolute absence of nucleosomes in mouse sperm. The observed asymmetries are not all restricted to zygotic chromatin. In the 2-cell embryo, the paternal and maternal chromatin are still asymmetric for the heterochromatin associated marks Me(2,3)H3K9 and Me(3)H4K20 [29, 79, 158]. At the 4-cell stage chromatin is homogenously stained for Me(2,3)H3K9 and Me(3)H3K27, indicating that the corresponding Histone Methyl Transferases (HMTases) are active at that time [157, 158]. This has indeed been shown for the Me(2,3)H3K9 HMTases [158]. Thus, at least two histone lysine tri-methyl marks, perhaps more, appear in the paternal chromatin of the 4-cell embryo.
Absence of Me(3)H3K9 results into a-specific and more loosely bound HP1-β to the paternal chromatin (see fig. 7E). HP1 plays a central role in formation and maintenance of heterochromatin by binding Me(3)H3K9. Interestingly the three isoforms of HP1 (α, β, γ) all have different times of appearance: HP1-α was not detected up to the 4-cell stage, HP-1β was present in zygotic G1 and presence of HP1- γ has been observed in S/G2 phase of the zygote [108].

Possibly the instalment of modifications that induce chromatin compaction, like Me(3)H3K9, is prolonged until full reprogramming of the paternal genome is realised, as a way to prevent preliminary locking of chromatin domains into a more static form. During this reprogramming, several processes involving chromatin remodelling are likely to benefit from a more open chromatin structure of which we can mention three.

First, the deposition of maternal nucleosomes is probably occurring randomly onto the paternal DNA, placing regulatory sequences in a less favourable context. It has been suggested that the first round of DNA replication is used as an opportunity for the maternally derived transcription machinery to gain access to their target sequences [184] thereby explaining the stimulating effect of the zygotic S-phase on the level of transcription in the 2-cell stage [125]. The sliding of nucleosomes that will accompany this process will benefit from reduced chromatin condensation.

Second, the active removal of DNA methylation in the paternal chromatin is finalized six hours after gamete fusion [163]. The as yet unidentified machinery responsible for removing these marks is also likely to benefit from a lack of chromosome condensation, as hypothesized earlier by Cowell et al., [79].

And third, repair of DNA lesions, which is always accompanied with chromatin remodelling, will be swifter. The lower incidence of chromosomal abnormalities after ionising radiation at G1 in the paternal PN, when compared with the maternal PN might be a reflection thereof [166].

Thus, another motive for refraining from histone lysine methyl marks in paternal chromatin could be the embryo's need to erase the paternal DNA-methylation settings. As mentioned above, paternal DNA is actively de-methylated within 6 hours after gamete fusion [163]. In contrast, the maternal DNA does only undergo passive removal of this mark at S-phase caused by the absence of the maintenance DNA methyltransferase Dnmt1 [165]. Interplay between DNA methylation and histone lysine methyl marks has been described for Me(3)H3K9 in pericentric heterochromatic regions of mammalian cells where Me(3)H3K9 is able to direct DNA methylation [188]. If DNA methylation and lysine methyl marks interact, an erasure of paternal chromatin settings could be a prerequisite for proper embryo development. Prohibiting formation of these interacting lysine

methyl marks will then protect the future embryo from a precocious setting of paternal chromatin marks through an untimely interplay with DNA methylation, which is still present when the protamine-nucleosome transition has taken place [163].
Although the endpoint of demethylation of the paternal DNA has been described (6h post gamete fusion) [163]), the onset of this process is less clear. If demethylation of the paternal DNA commences after PN formation, the possibility exists that during the pre-PN stage, some of the epigenetic memory that is coded via DNA methylation, is transmitted through Me(1)H4K20, the only histone lysine methyl modification we found to be present from the beginning of sperm chromatin expansion on (see fig. 6E).
Deviating from the repressing tri-methyl lysine marks is Me(3)H3K4, which is associated with transcriptional activity [189]. The initially observed asymmetry for Me(3)H3K4 fully disappears 12 hours after gamete fusion when intensity levels are equal in the parental PNs [160]. Appearance of this mark might be linked to the transcriptional activation of the zygotic genome. The appearance of Me(1)H3K4 around the onset of PN formation appears to be a pre-requisite here for.

A role in sensing DNA damage for H4K20 methylation?
A recent finding in fission yeast indicates a role in DNA damage sensing for H4K20 methylation. In *Schizosaccharomyces Pombe* methylated H4K20 has been shown to form a binding site for the DNA damage cell cycle signalling protein Crb2 (a p53PB1 homologue) [190].
A role for MeH4K20 in DNA damage sensing has not been established in mammalian cells yet and it is therefore uncertain whether Me(1)H4K20, which we observe in the paternal chromatin from the onset of nucleosome formation on (see fig 6E), has a direct function in DNA damage sensing. Although not determined yet, the simultaneously appearance of Me(1)H4K20 with massive nucleosome assembly could imply that the HMTase responsible for this mark is part of the general nucleosome deposition machinery, increasing the likelihood of a biological function.
The differences observed in localisation of this mark between the parental nuclei can be explained by absence or inactivity of HMTase(s) that convert the mono methyl mark to di- or tri-methyl. This is most clear in the peri pre-cursor nucleolar region where the constitutive

heterochromatin is located. In the maternal PN, Me(1)H4K20 is absent in this region but Me(3)H4K20 is present while in the paternal PN only Me(1)H4K20 shows up at this location (see fig. 6D). This is another demonstration of the lack of distinction between euchromatin and heterochromatin in the male chomatin. Me(2)H4K20 was the only mark absent in both PNs (see fig. 6D). Elevated levels cause cytokinesis defects, as has been recently described [191]. The authors hypothesize that due to the stable nature of lysine methylation, a switch from mono- to di-methylation may result in a regulatory dead end [191]. Knowing that Me(3)-H4K20 is strictly localised in constitutive heterochromatin [29, 192] and Me(1)-H4K20 in euchromatin, Me(2)-H4K20 levels might be kept low to avoid an ambiguous choice between these two states in early development. The H4K20 HMTases that have been described is are mono-/di-methylases (prSet7, also referred to as Set8) [171, 193] and two tri-methylases (SuvH4-K20a and b) [192]. Our data indicate presence of another, specific H4K20 mono-methylase or a mechanism that narrows prSet7/Set8 activity to converting H4K20 into Me(1)H4K20.

Acknowledgements
Dr. A. Peters (FMI, Basel, Switzerland); Dr. T. Jenuwein (IMP, Vienna, Austria); Dr. H. Stunnenberg (Dept. of Molecular Biology, NCMLS, Nijmegen, The Netherlands); Dr. M. Monestier (Dept. of Microbiology and Immunology, Temple University School of Medicine, Philadelphia, U.S.A); Dr. P. Adams (FCCC, Philadelphia, USA); Dr. P. Singh (Nuclear Reprogramming Laboratory, The Roslin Institute, Midlothian, UK) and Dr. R. Balhorn (Electronic Engineering Technologies Division, Lawrence Livermore National Laboratory, Livermore, USA.) are gratefully acknowledged for the gift of their antibodies. This research was financed by the Dutch ministry of Health, Welfare and Sport.

Supplementary data section 2.4

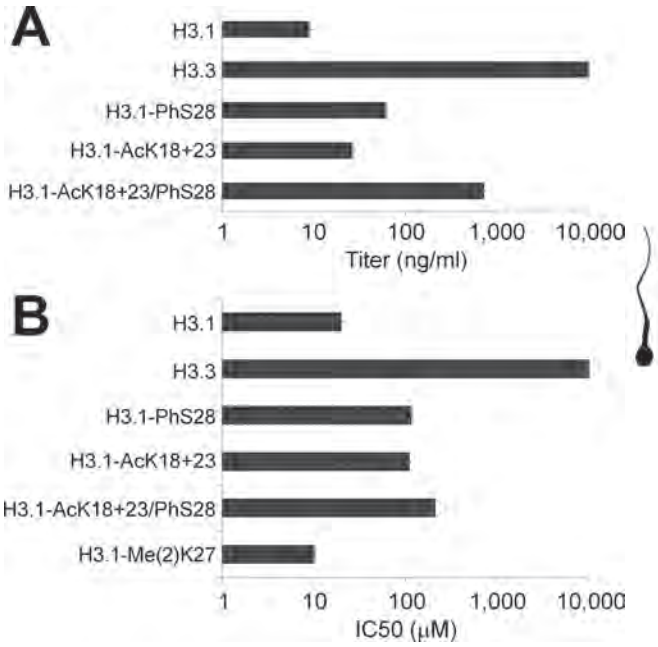

Figure S1 Reactivity of #34 with (modified) histone H3.1 and H3.3 peptides
A) Reactivity of #34 with directly coated peptides. The titer is calculated as the concentration of #34 giving an OD of 0.5 at 450 nm. **B**) Inhibition of the binding of #34 to unmodified H3.1(18-37) by (modified) H3.1 and H3.3 peptides. The inhibitory concentration of peptides that yields a 50% decrease of reactivity of #34 with H3(18-37) is given as IC50.

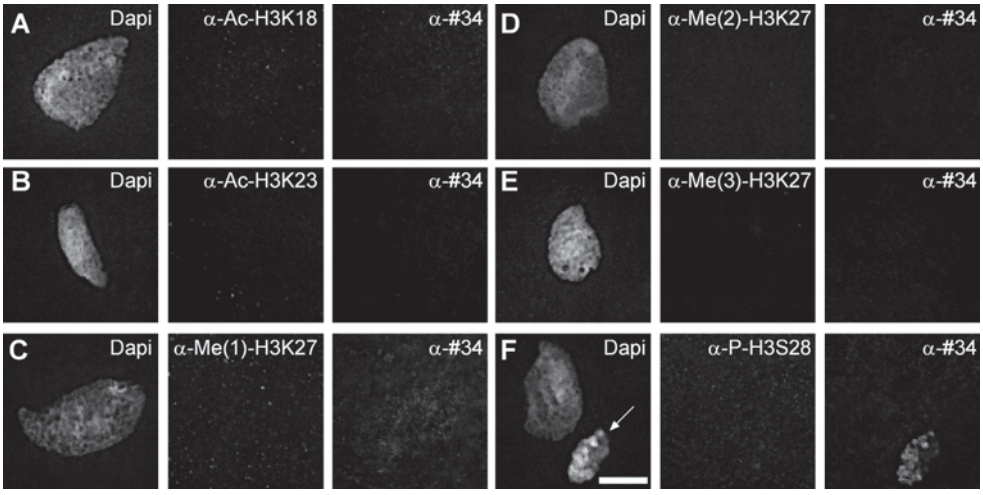

Figure S2 Absence of binding of #34 in the paternal pronucleus is not due to neighbouring tail modifications
Double stainings for modifications and #34 in type b/c male nuclei. Images are cut out from whole zygote images. Bar represents 10 μM.
A) DAPI, AcH3K18 and #34, (n=20); B) DAPI, AcH3K23 and #34, (n=12); C) DAPI, Me(1)H3K27 and #34, (n=12); D) DAPI, Me(2)H3K27 and #34, (n=6); E) DAPI, Me(3)H3K27 and #34, (n=20);

F) DAPI, PH3K28 and #34; (n=19). The arrow points at maternal complement in telophase II.

Figure S3 Stainings of metaphase II oocytes

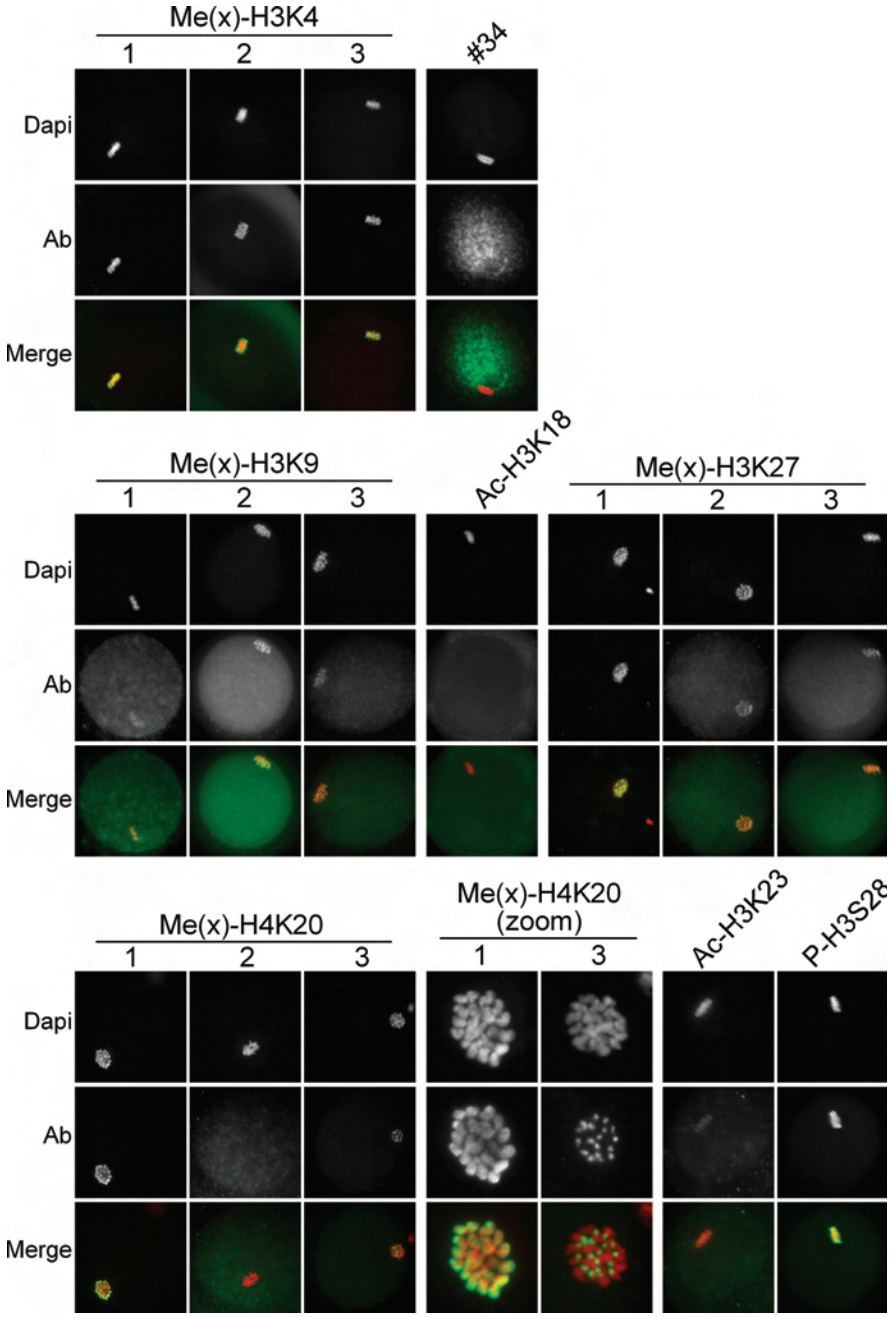

Figure S4 Stainings of cumulus cells

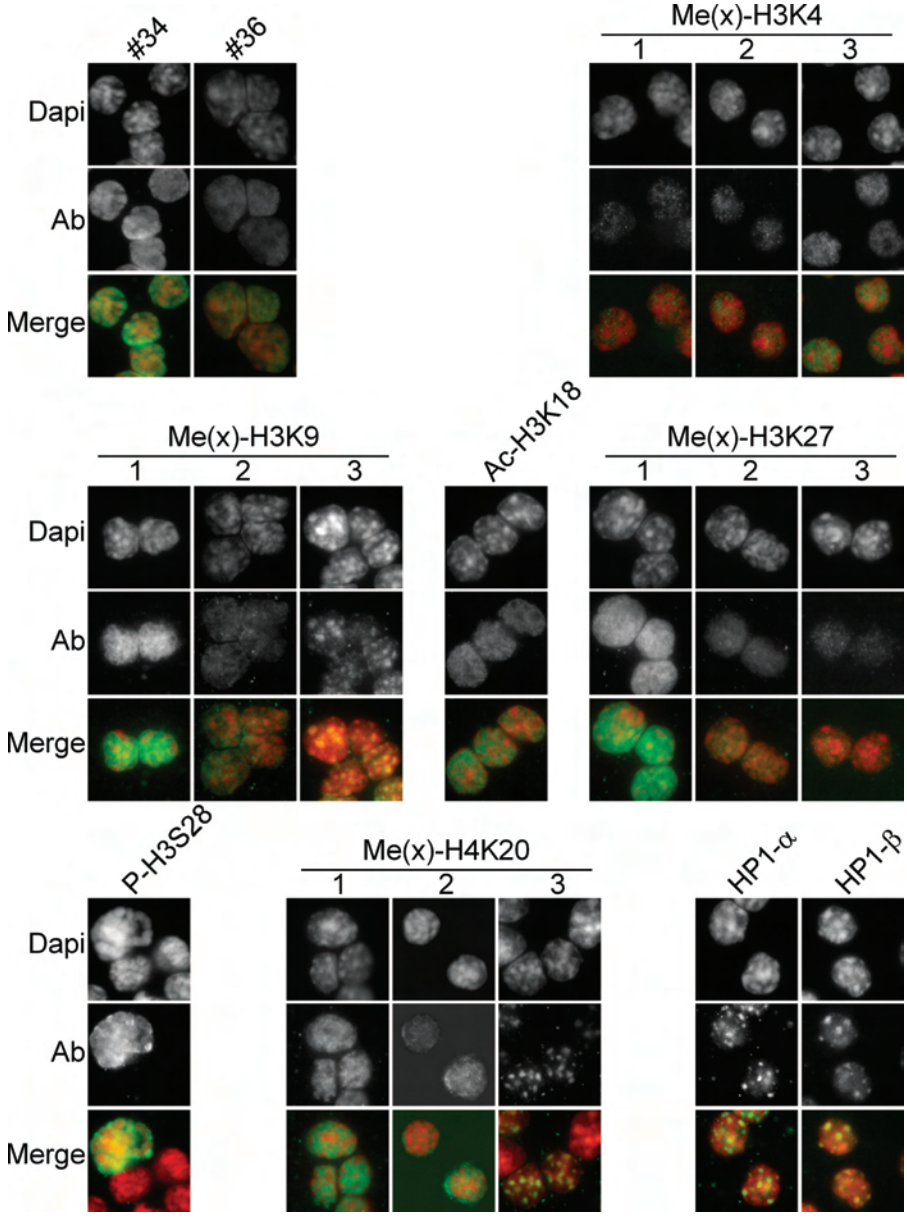

Table S5 Relative intensity of ab's at the different developmental stages and cumulus cells

Ab	#36	PL-2-3	#34	α-HIRA	α-HP1α	α-HP1β	α-H3K4 me1	α-H3K4 me2	α-H3K4 me3
Type a nuclei	++	++	-	++	-	-	-	-	-
Type b/c nuclei	+++	+++	-	++	-	-	-	-	-
Male Pronuclei	+++	+++	-	+	-	+++	++	-	-
Metaphase II	+++	+++	-	-	-	-	++	++	+++
Telophase II	+++	+++	+++	-	-	++	++	++	+++
Female PN	+++	+++	++	+/-	-	+++	++	++	+++
Follicle cells	+++	+++	+++	+	+++	+++	+	++	+++

Ab	α-H3K9 me1	α-H3K9 me2	α-H3K9 me3	α-H3K18 Ac	α-H3K23 Ac	α-H3K27 7me1	α-H3K27 me2	α-H3K27 me3	α-H3S28 ph	α-H4K20 me1	α-H4K20 me2	α-H4K20 me3
Type a nuclei	+/-	-	-	-	-	-	-	-	-	++	-	-
Type b/c nuclei	-	-	-	+	-	-	-	-	-	+++	-	-
Male Pronuclei	-	-	-	+++	++	-	-	-	+++*	+++	-	-
Metaphase II	+/-	+++	++	-	+	+++	++	+	+++	+++	-	+++
Telophase II	+/-	+++	++	-	+	+++	++	+	-	+++	-	+++
Female PN	+/-	+++	++	+++	++	++	+++	+	+++*	++	-	++
Follicle cells	+++	++	+++	+++	+++	+++	++	+	+++**	+++	+	+++

* With the H3S28ph ab, a strong staining in the pre-cursor nucleoli of both PNs was observed.
** Antibody only decorated mitotic chromosomes.

References

1. Handel,M.A. The XY body: a specialized meiotic chromatin domain. Exp. Cell Res. 296, 57-63 (2004).

2. Turner,J.M. et al. Silencing of unsynapsed meiotic chromosomes in the mouse. Nat. Genet. 37, 41-47 (2005).

3. Kierszenbaum,A.L. & Tres,L.L. Nucleolar and perichromosomal RNA synthesis during meiotic prophase in the mouse testis. J. Cell Biol. 60, 39-53 (1974).

4. Turner,J.M., Mahadevaiah,S. K., Ellis,P.J., Mitchell,M.J., & Burgoyne,P.S. Pachytene asynapsis drives meiotic sex chromosome inactivation and leads to substantial postmeiotic repression in spermatids. Dev. Cell 10, 521-529 (2006).

5. Baarends,W.M. et al. Silencing of unpaired chromatin and histone H2A ubiquitination in mammalian meiosis. Mol. Cell Biol. 25, 1041-1053 (2005).

6. Nightingale,K.P., O'neill,L. P., & Turner,B.M. Histone modifications: signalling receptors and potential elements of a heritable epigenetic code. Curr. Opin. Genet. Dev. 16, 125-136 (2006).

7. Kamakaka,R.T. & Biggins,S. Histone variants: deviants? Genes Dev. 19, 295-310 (2005).

8. Henikoff,S. & Ahmad,K. Assembly of variant histones into chromatin. Annu. Rev. Cell Dev. Biol. 21, 133-153 (2005).

9. van der Heijden,G.W. et al. Asymmetry in Histone H3 variants and lysine methylation between paternal and maternal chromatin of the early mouse zygote. Mech. Dev. 122, 1008-1022 (2005).

10. Loppin,B. et al. The histone H3.3 chaperone HIRA is essential for chromatin assembly in the male pronucleus. Nature 437, 1386-1390 (2005).

11. Khalil,A.M., Boyar,F.Z., & Driscoll,D.J. Dynamic histone modifications mark sex chromosome inactivation and reactivation during mammalian spermatogenesis. Proc. Natl. Acad. Sci. U. S. A 101, 16583-16587 (2004).

12. Namekawa,S.H. et al. Postmeiotic sex chromatin in the male germline of mice. Curr. Biol. 16, 660-667 (2006).

13. Greaves,I.K., Rangasamy,D., Devoy,M., Marshall Graves,J.A., & Tremethick,D.J. The X and Y chromosomes assemble into H2A.Z, containing facultative heterochromatin, follow-

ing meiosis. Mol. Cell Biol. 26, 5394-5405 (2006).

14. Kramers,K. et al. Specificity of monoclonal anti-nucleosome auto-antibodies derived from lupus mice. J. Autoimmun. 9, 723-729 (1996).

15. Dietrich A.J.J. & de Boer,P. A sequential analysis of the development of the synaptonemal complex in spermatocytes of the mouse by electron microscopy using hydroxyurea and agar filtration. Genetica 61, 119-129 (1983).

16. Tagami,H., Ray-Gallet,D., Almouzni,G., & Nakatani,Y. Histone H3.1 and H3.3 complexes mediate nucleosome assembly pathways dependent or independent of DNA synthesis. Cell 116, 51-61 (2004).

17. Hake,S.B. et al. Serine 31 phosphorylation of histone variant H3.3 is specific to regions bordering centromeres in metaphase chromosomes. Proc. Natl. Acad. Sci. U. S. A 102, 6344-6349 (2005).

18. Schulmeister,A., Schmid,M., & Thompson,E.M. Phosphorylation of the histone H3.3 variant in mitosis and meiosis of the urochordate Oikopleura dioica. Chromosome. Res. 15, 189-201 (2007).

19. Mahadevaiah,S.K. et al. Recombinational DNA double-strand breaks in mice precede synapsis. Nat. Genet. 27, 271-276 (2001).

20. Moens,P.B. Histones H1 and H4 of surface-spread meiotic chromosomes. Chromosoma 104, 169-174 (1995).

21. Oakberg,E.F. Duration of spermatogenesis in the mouse and timing of stages of the cycle in the seminiferous epithelium. Am. J. Anat. 99, 507-516 (1956).

22. de Boer,P., Searle,A.G., van der Hoeven,F.A., de Rooij,D.G., & Beechey,C.V. Male pachytene pairing in single and double translocation heterozygotes and spermatogenic impairment in the mouse. Chromosoma 93, 326-336 (1986).

23. Speed,R.M. Abnormal RNA synthesis in sex vesicles of tertiary trisomic male mice. Chromosoma 93, 267-270 (1986).

24. Turner,J.M. et al. BRCA1, histone H2AX phosphorylation, and male meiotic sex chromosome inactivation. Curr. Biol. 14, 2135-2142 (2004).

25. Baart,E.B., de Rooij,D. G., Keegan,K.S., & de Boer,P. Distribution of Atr protein in primary spermatocytes of a mouse chromosomal mutant: a comparison of preparation

techniques. Chromosoma 109, 139-147 (2000).

26. de Vries,F.A. et al. Mouse Sycp1 functions in synaptonemal complex assembly, meiotic recombination, and XY body formation. Genes Dev. 19, 1376-1389 (2005).

27. van Attikum,H. & Gasser,S.M. The histone code at DNA breaks: a guide to repair? Nat. Rev. Mol. Cell Biol. 6, 757-765 (2005).

28. Fernandez-Capetillo,O. et al. H2AX is required for chromatin remodeling and inactivation of sex chromosomes in male mouse meiosis. Dev. Cell 4, 497-508 (2003).

29. Kourmouli,N. et al. Heterochromatin and tri-methylated lysine 20 of histone H4 in animals. J. Cell Sci. 117, 2491-2501 (2004).

30. Peters,A.H., Plug,A.W., van Vugt,M.J., & de Boer,P. A drying-down technique for the spreading of mammalian meiocytes from the male and female germline. Chromosome. Res. 5, 66-68 (1997).

31. Ashley,T., Gaeth,A.P., Creemers,L.B., Hack,A.M., & de Rooij,D.G. Correlation of meiotic events in testis sections and microspreads of mouse spermatocytes relative to the mid-pachytene checkpoint. Chromosoma 113, 126-136 (2004).

32. Ooi,S.L. & Henikoff,S. Germline histone dynamics and epigenetics. Curr. Opin. Cell Biol. 19, 257-265 (2007).

33. Turner,J.M. Meiotic sex chromosome inactivation. Development(2007).

34. Kornberg,R.D. & Lorch,Y. Twenty-five years of the nucleosome, fundamental particle of the eukaryote chromosome. Cell 98, 285-294 (1999).

35. Luger,K., Mader,A.W., Richmond,R.K., Sargent,D. F., & Richmond,T.J. Crystal structure of the nucleosome core particle at 2.8 A resolution. Nature 389, 251-260 (1997).

36. Kouzarides,T. Chromatin modifications and their function. Cell 128, 693-705 (2007).

37. Solari,A.J. The behavior of the XY pair in mammals. Int. Rev. Cytol. 38, 273-317 (1974).

38. Romanienko,P.J. & Camerini-Otero,R.D. The mouse Spo11 gene is required for meiotic chromosome synapsis. Mol. Cell 6, 975-987 (2000).

39. Baudat,F., Manova,K., Yuen,J.P., Jasin,M., & Keeney,S. Chromosome synapsis defects and sexually dimorphic mei-

otic progression in mice lacking Spo11. Mol. Cell 6, 989-998 (2000).

40. Shinohara,A. & Shinohara,M. Roles of RecA homologues Rad51 and Dmc1 during meiotic recombination. Cytogenet. Genome Res. 107, 201-207 (2004).

41. Ashley,T. et al. Dynamic changes in Rad51 distribution on chromatin during meiosis in male and female vertebrates. Chromosoma 104, 19-28 (1995).

42. Plug,A.W. et al. Changes in protein composition of meiotic nodules during mammalian meiosis. J. Cell Sci. 111 (Pt 4), 413-423 (1998).

43. Marcon,E. & Moens,P.B. The evolution of meiosis: recruitment and modification of somatic DNA-repair proteins. Bioessays 27, 795-808 (2005).

44. Scully,R. et al. Dynamic changes of BRCA1 subnuclear location and phosphorylation state are initiated by DNA damage. Cell 90, 425-435 (1997).

45. Bellani,M.A., Romanienko,P.J., Cairatti,D.A., & Camerini-Otero,R.D. SPO11 is required for sex-body formation, and Spo11 heterozygosity rescues the prophase arrest of Atm-/- spermatocytes. J. Cell Sci. 118, 3233-3245 (2005).

46. Richler,C., Uliel,E., Rosenmann,A., & Wahrman,J. Chromosomally derived sterile mice have a 'fertile' active XY chromatin conformation but no XY body. Chromosoma 97, 465-474 (1989).

47. Hayashi,K., Yoshida,K., & Matsui,Y. A histone H3 methyltransferase controls epigenetic events required for meiotic prophase. Nature 438, 374-378 (2005).

48. Monesi,V. Synthetic activities during spermatogenesis in the mouse RNA and protein. Exp. Cell Res. 39, 197-224 (1965).

49. Dantzer,F. et al. Poly(ADP-ribose) polymerase-2 contributes to the fidelity of male meiosis I and spermiogenesis. Proc. Natl. Acad. Sci. U. S. A 103, 14854-14859 (2006).

50. Moens,P.B. et al. The association of ATR protein with mouse meiotic chromosome cores. Chromosoma 108, 95-102 (1999).

51. Perera,D. et al. TopBP1 and ATR colocalization at meiotic chromosomes: role of TopBP1/Cut5 in the meiotic recombination checkpoint. Mol. Biol. Cell 15, 1568-1579 (2004).

52. Reini,K. et al. TopBP1 localises to centrosomes in mi-

tosis and to chromosome cores in meiosis. Chromosoma 112, 323-330 (2004).

53. Goedecke,W., Eijpe,M., Offenberg,H.H., van,A.M., & Heyting,C. Mre11 and Ku70 interact in somatic cells, but are differentially expressed in early meiosis. Nat. Genet. 23, 194-198 (1999).

54. Eijpe,M., Offenberg,H., Goedecke,W., & Heyting,C. Localisation of RAD50 and MRE11 in spermatocyte nuclei of mouse and rat. Chromosoma 109, 123-132 (2000).

55. D'Amours,D. & Jackson,S. P. The Mre11 complex: at the crossroads of dna repair and checkpoint signalling. Nat. Rev. Mol. Cell Biol. 3, 317-327 (2002).

56. Barchi,M. et al. Surveillance of different recombination defects in mouse spermatocytes yields distinct responses despite elimination at an identical developmental stage. Mol. Cell Biol. 25, 7203-7215 (2005).

57. Gu,Y. et al. Growth retardation and leaky SCID phenotype of Ku70-deficient mice. Immunity. 7, 653-665 (1997).

58. Nussenzweig,A. et al. Requirement for Ku80 in growth and immunoglobulin V(D)J recombination. Nature 382, 551-555 (1996).

59. Lou,Z. et al. MDC1 maintains genomic stability by participating in the amplification of ATM-dependent DNA damage signals. Mol. Cell 21, 187-200 (2006).

60. Ahmed,E.A. et al. Differences in DNA double strand breaks repair in male germ cell types: Lessons learned from a differential expression of Mdc1 and 53BP1. DNA Repair (Amst)(2007).

61. Ward,I.M., Minn,K., van,D.J., & Chen,J. p53 Binding protein 53BP1 is required for DNA damage responses and tumor suppression in mice. Mol. Cell Biol. 23, 2556-2563 (2003).

62. van der,L.R. et al. Ubiquitin ligase Rad18Sc localizes to the XY body and to other chromosomal regions that are unpaired and transcriptionally silenced during male meiotic prophase. J. Cell Sci. 117, 5023-5033 (2004).

63. van der Heijden,G.W. et al. Chromosome-wide nucleosome replacement and H3.3 incorporation during mammalian meiotic sex chromosome inactivation. Nat. Genet. 39, 251-258 (2007).

64. Costa,Y. et al. Mouse MAELSTROM: the link be-

tween meiotic silencing of unsynapsed chromatin and microRNA pathway? Hum. Mol. Genet. 15, 2324-2334 (2006).

65. Turner,J.M., Burgoyne,P. S., & Singh,P.B. M31 and macroH2A1.2 colocalise at the pseudoautosomal region during mouse meiosis. J. Cell Sci. 114, 3367-3375 (2001).

66. Singh,P.B. The present status of mammalian HP1 function. 2003.
Ref Type: Unpublished Work

67. O'Carroll,D. et al. Isolation and characterization of Suv39h2, a second histone H3 methyltransferase gene that displays testis-specific expression. Mol. Cell Biol. 20, 9423-9433 (2000).

68. Changolkar,L.N. et al. Developmental Changes in Histone macroH2A1-Mediated Gene Regulation. Mol. Cell Biol. 27, 2758-2764 (2007).

69. Hoyer-Fender,S. et al. Localisation of histone macroH2A1.2 to the XY-body is not a response to the presence of asynapsed chromosome axes. J. Cell Sci. 117, 189-198 (2004).

70. Richler,C., Dhara,S.K., & Wahrman,J. Histone macroH2A1.2 is concentrated in the XY compartment of mammalian male meiotic nuclei. Cytogenet. Cell Genet. 89, 118-120 (2000).

71. Westerlaken ,J. Characterization of DMWD and its role in Myotonic Dystrophy (DM1). 2003.
Ref Type: Thesis/Dissertation

72. Miura,K. & Imaki,J. Phosphorylated extracellular signal-regulated kinase 1/2 is localized to the XY body of meiotic prophase spermatocytes. Biochem. Biophys. Res. Commun. 346, 1261-1266 (2006).

73. Rogers,R.S., Inselman,A., Handel,M.A., & Matunis,M.J. SUMO modified proteins localize to the XY body of pachytene spermatocytes. Chromosoma 113, 233-243 (2004).

74. Parraga,M. & del,M.J. XYbp, a novel RING-finger protein, is a component of the XY body of spermatocytes and centrosomes. Mech. Dev. 90, 95-101 (2000).

75. Yang,G., Zhang,Y.L., Buchold,G.M., Jetten,A.M., & O'Brien,D.A. Analysis of germ cell nuclear factor transcripts and protein expression during spermatogenesis. Biol. Reprod. 68, 1620-1630 (2003).

76. Kawamata,M. & Nishimori,K. Mice deficient in Dmrt7 show infertility with spermatogenic arrest at pach-

ytene stage. FEBS Lett. 580, 6442-6446 (2006).

77. Kim ,S. et al. A mammal-specific Doublesex homolog associates with male sex chromatin and is required for male meiosis. PLoS. Genet.(2007).

78. Vigodner,M. & Morris,P. L. Testicular expression of small ubiquitin-related modifier-1 (SUMO-1) supports multiple roles in spermatogenesis: silencing of sex chromosomes in spermatocytes, spermatid microtubule nucleation, and nuclear reshaping. Dev. Biol. 282, 480-492 (2005).

79. Cowell,I.G. et al. Heterochromatin, HP1 and methylation at lysine 9 of histone H3 in animals. Chromosoma 111, 22-36 (2002).

80. Klymenko,T. et al. A Polycomb group protein complex with sequence-specific DNA-binding and selective methyllysine-binding activities. Genes Dev. 20, 1110-1122 (2006).

81. Richler,C. et al. Splicing components are excluded from the transcriptionally inactive XY body in male meiotic nuclei. Mol. Biol. Cell 5, 1341-1352 (1994).

82. Turner,J.M. et al. Analysis of male meiotic "sex body" proteins during XY female meiosis provides new insights into their functions. Chromosoma 109, 426-432 (2000).

83. Takada,Y. et al. Mammalian Polycomb Scmh1 mediates exclusion of Polycomb complexes from the XY body in the pachytene spermatocytes. Development 134, 579-590 (2007).

84. Siep,M. et al. Basic helix-loop-helix transcription factor Tcfl5 interacts with the Calmegin gene promoter in mouse spermatogenesis. Nucleic Acids Res. 32, 6425-6436 (2004).

85. Hoeijmakers,J.H. Genome maintenance mechanisms for preventing cancer. Nature 411, 366-374 (2001).

86. Bekker-Jensen,S. et al. Spatial organization of the mammalian genome surveillance machinery in response to DNA strand breaks. J. Cell Biol. 173, 195-206 (2006).

87. Lorch,Y., Maier-Davis,B., & Kornberg,R.D. Chromatin remodeling by nucleosome disassembly in vitro. Proc. Natl. Acad. Sci. U. S. A 103, 3090-3093 (2006).

88. Stucki,M. & Jackson,S. P. gammaH2AX and MDC1: anchoring the DNA-damage-response machinery to broken chromosomes. DNA Repair

(Amst) 5, 534-543 (2006).

89. Hamer,G. et al. Function of DNA-protein kinase catalytic subunit during the early meiotic prophase without Ku70 and Ku86. Biol. Reprod. 68, 717-721 (2003).

90. Taccioli,G.E. et al. Targeted disruption of the catalytic subunit of the DNA-PK gene in mice confers severe combined immunodeficiency and radiosensitivity. Immunity. 9, 355-366 (1998).

91. Ward,W.S. & Coffey,D.S. DNA packaging and organization in mammalian spermatozoa: comparison with somatic cells. Biol. Reprod. 44, 569-574 (1991).

92. Haaf,T. & Ward,D.C. Higher order nuclear structure in mammalian sperm revealed by in situ hybridization and extended chromatin fibers. Exp. Cell Res. 219, 604-611 (1995).

93. Sutovsky,P. & Schatten,G. Paternal contributions to the mammalian zygote: fertilization after sperm-egg fusion. Int. Rev. Cytol. 195, 1-65 (2000).

94. Wright,S.J. Sperm nuclear activation during fertilization. Curr. Top. Dev. Biol. 46, 133-178 (1999).

95. Adenot,P.G., Szollosi,M. S., Geze,M., Renard,J.P., & Debey,P. Dynamics of paternal chromatin changes in live one-cell mouse embryo after natural fertilization. Mol. Reprod. Dev. 28, 23-34 (1991).

96. Dyban,A.P., De Sutter,P., & Verlinsky,Y. Okadaic acid induces premature chromosome condensation reflecting the cell cycle progression in one-cell stage mouse embryos. Mol. Reprod. Dev. 34, 402-415 (1993).

97. Zalenskaya,I.A., Bradbury,E.M., & Zalensky,A. O. Chromatin structure of telomere domain in human sperm. Biochem. Biophys. Res. Commun. 279, 213-218 (2000).

98. Palmer,D.K., O'Day,K., & Margolis,R.L. The centromere specific histone CENP-A is selectively retained in discrete foci in mammalian sperm nuclei. Chromosoma 100, 32-36 (1990).

99. Aoki,E. & Schultz,R.M. DNA replication in the 1-cell mouse embryo: stimulatory effect of histone acetylation. Zygote. 7, 165-172 (1999).

100. Peters,A.H. et al. Partitioning and plasticity of repressive histone methylation states in mammalian chromatin. Mol. Cell 12, 1577-1589 (2003).

101. Adenot,P.G., Mercier,Y., Renard,J.P., & Thompson,E.M.

Differential H4 acetylation of paternal and maternal chromatin precedes DNA replication and differential transcriptional activity in pronuclei of 1-cell mouse embryos. Development 124, 4615-4625 (1997).

102. Stein,P., Worrad,D.M., Belyaev,N.D., Turner,B.M., & Schultz,R.M. Stage-dependent redistributions of acetylated histones in nuclei of the early preimplantation mouse embryo. Mol. Reprod. Dev. 47, 421-429 (1997).

103. Kim,J.M., Liu,H., Tazaki,M., Nagata,M., & Aoki,F. Changes in histone acetylation during mouse oocyte meiosis. J. Cell Biol. 162, 37-46 (2003).

104. Santos,F., Peters,A.H., Otte,A.P., Reik,W., & Dean,W. Dynamic chromatin modifications characterise the first cell cycle in mouse embryos. Dev. Biol. 280, 225-236 (2005).

105. Losman,M.J., Fasy,T.M., Novick,K.E., & Monestier,M. Monoclonal autoantibodies to subnucleosomes from a MRL/Mp(-)+/+ mouse. Oligoclonality of the antibody response and recognition of a determinant composed of histones H2A, H2B, and DNA. J. Immunol. 148, 1561-1569 (1992).

106. Hunt,P., LeMaire,R., Embury,P., Sheean,L., & Mroz,K. Analysis of chromosome behavior in intact mammalian oocytes: monitoring the segregation of a univalent chromosome during female meiosis. Hum. Mol. Genet. 4, 2007-2012 (1995).

107. Russell,L.D., Ettlin,R. A., Hikim,A.P.S., & Clegg,E. D. Histopathological Evaluation of the Testis(Cache River Press, Clearwater, FL, 1990).

108. Arney,K.L., Bao,S., Bannister,A.J., Kouzarides,T., & Surani,M.A. Histone methylation defines epigenetic asymmetry in the mouse zygote. Int. J. Dev. Biol. 46, 317-320 (2002).

109. Sobel,R.E., Cook,R.G., Perry,C.A., Annunziato,A.T., & Allis,C.D. Conservation of deposition-related acetylation sites in newly synthesized histones H3 and H4. Proc. Natl. Acad. Sci. U. S. A 92, 1237-1241 (1995).

110. Hazzouri,M. et al. Regulated hyperacetylation of core histones during mouse spermatogenesis: involvement of histone deacetylases. Eur. J. Cell Biol. 79, 950-960 (2000).

111. Singh,P.B. & Georgatos,S. D. HP1: facts, open questions, and speculation. J. Struct. Biol.

140, 10-16 (2002).

112. Hoyer-Fender,S., Singh,P. B., & Motzkus,D. The murine heterochromatin protein M31 is associated with the chromocenter in round spermatids and Is a component of mature spermatozoa. Exp. Cell Res. 254, 72-79 (2000).

113. Pittoggi,C. et al. A fraction of mouse sperm chromatin is organized in nucleosomal hypersensitive domains enriched in retroposon DNA. J. Cell Sci. 112 (Pt 20), 3537-3548 (1999).

114. Rousseaux,S. et al. Establishment of male-specific epigenetic information. Gene 345, 139-153 (2005).

115. Sterner,D.E. & Berger,S. L. Acetylation of histones and transcription-related factors. Microbiol. Mol. Biol. Rev. 64, 435-459 (2000).

116. Oliva,R., Bazett-Jones,D., Mezquita,C., & Dixon,G.H. Factors affecting nucleosome disassembly by protamines in vitro. Histone hyperacetylation and chromatin structure, time dependence, and the size of the sperm nuclear proteins. J. Biol. Chem. 262, 17016-17025 (1987).

117. Pivot-Pajot,C. et al. Acetylation-dependent chromatin reorganization by BRDT, a testis-specific bromodomain-containing protein. Mol. Cell Biol. 23, 5354-5365 (2003).

118. Widlund,H.R. et al. Identification and characterization of genomic nucleosome-positioning sequences. J. Mol. Biol. 267, 807-817 (1997).

119. Peters,A.H. et al. Loss of the Suv39h histone methyltransferases impairs mammalian heterochromatin and genome stability. Cell 107, 323-337 (2001).

120. de Lange,T. Protection of mammalian telomeres. Oncogene 21, 532-540 (2002).

121. Yang,X.J. Lysine acetylation and the bromodomain: a new partnership for signaling. Bioessays 26, 1076-1087 (2004).

122. Liu,L., Blasco,M., Trimarchi,J., & Keefe,D. An essential role for functional telomeres in mouse germ cells during fertilization and early development. Dev. Biol. 249, 74-84 (2002).

123. Kishigami,S. et al. Epigenetic abnormalities of the mouse paternal zygotic genome associated with microinsemination of round spermatids. Dev. Biol. 289, 195-205 (2006).

124. Berger,S.L. Histone modifications in transcriptional regulation. Curr. Opin. Genet.

Dev. 12, 142-148 (2002).

125. Aoki,F., Worrad,D.M., & Schultz,R.M. Regulation of transcriptional activity during the first and second cell cycles in the preimplantation mouse embryo. Dev. Biol. 181, 296-307 (1997).

126. Waterborg,J.H. Dynamics of histone acetylation in vivo. A function for acetylation turnover? Biochem. Cell Biol. 80, 363-378 (2002).

127. de la Barre,A.E., Angelov,D., Molla,A., & Dimitrov,S. The N-terminus of histone H2B, but not that of histone H3 or its phosphorylation, is essential for chromosome condensation. EMBO J. 20, 6383-6393 (2001).

128. Prigent,C. & Dimitrov,S. Phosphorylation of serine 10 in histone H3, what for? J. Cell Sci. 116, 3677-3685 (2003).

129. Verlhac,M.H., Kubiak,J. Z., Clarke,H.J., & Maro,B. Microtubule and chromatin behavior follow MAP kinase activity but not MPF activity during meiosis in mouse oocytes. Development 120, 1017-1025 (1994).

130. Kemp,M.G., Ghosh,M., Liu,G., & Leffak,M. The histone deacetylase inhibitor trichostatin A alters the pattern of DNA replication origin activity in human cells. Nucleic Acids Res. 33, 325-336 (2005).

131. Bird,A. DNA methylation patterns and epigenetic memory. Genes Dev. 16, 6-21 (2002).

132. McNairn,A.J. & Gilbert,D.M. Epigenomic replication: linking epigenetics to DNA replication. Bioessays 25, 647-656 (2003).

133. Lewis,J.D., Song,Y., de Jong,M.E., Bagha,S.M., & Ausio,J. A walk though vertebrate and invertebrate protamines. Chromosoma 111, 473-482 (2003).

134. Bench,G.S., Friz,A.M., Corzett,M.H., Morse,D.H., & Balhorn,R. DNA and total protamine masses in individual sperm from fertile mammalian subjects. Cytometry 23, 263-271 (1996).

135. Gatewood,J.M., Cook,G. R., Balhorn,R., Schmid,C.W., & Bradbury,E.M. Isolation of four core histones from human sperm chromatin representing a minor subset of somatic histones. J. Biol. Chem. 265, 20662-20666 (1990).

136. Tanphaichitr,N., Sobhon,P., Taluppeth,N., & Chalermisarachai,P. Basic nuclear proteins in testicular cells and ejaculated spermatozoa in

man. Exp. Cell Res. 117, 347-356 (1978).

137. Zalensky,A.O., Breneman,J.W., Zalenskaya,I.A., Brinkley,B.R., & Bradbury,E. M. Organization of centromeres in the decondensed nuclei of mature human sperm. Chromosoma 102, 509-518 (1993).

138. Gardiner-Garden,M., Ballesteros,M., Gordon,M., & Tam,P.P. Histone- and protamine-DNA association: conservation of different patterns within the beta-globin domain in human sperm. Mol. Cell Biol. 18, 3350-3356 (1998).

139. Wykes,S.M. & Krawetz,S. A. The structural organization of sperm chromatin. J. Biol. Chem. 278, 29471-29477 (2003).

140. Gatewood,J.M., Cook,G. R., Balhorn,R., Bradbury,E.M., & Schmid,C.W. Sequence-specific packaging of DNA in human sperm chromatin. Science 236, 962-964 (1987).

141. Nonchev,S. & Tsanev,R. Protamine-histone replacement and DNA replication in the male mouse pronucleus. Mol. Reprod. Dev. 25, 72-76 (1990).

142. Ingouff,M., Hamamura,Y., Gourgues,M., Higashiyama,T., & Berger,F. Distinct Dynamics of HISTONE3 Variants between the Two Fertilization Products in Plants. Curr. Biol. 17, 1032-1037 (2007).

143. Capmany,G., Taylor,A., Braude,P.R., & Bolton,V.N. The timing of pronuclear formation, DNA synthesis and cleavage in the human 1-cell embryo. Mol. Hum. Reprod. 2, 299-306 (1996).

144. Baart,E.B. et al. Reduced oocyte activation and first cleavage rate after ICSI with spermatozoa from a sterile mouse chromosome mutant. Hum. Reprod. 19, 1140-1147 (2004).

145. Kimura,Y. & Yanagimachi,R. Intracytoplasmic sperm injection in the mouse. Biol. Reprod. 52, 709-720 (1995).

146. Huisman,G.J., Fauser,B. C., Eijkemans,M.J., & Pieters,M. H. Implantation rates after in vitro fertilization and transfer of a maximum of two embryos that have undergone three to five days of culture. Fertil. Steril. 73, 117-122 (2000).

147. Hohmann,F.P., Macklon,N.S., & Fauser,B.C. A randomized comparison of two ovarian stimulation protocols with gonadotropin-releasing hormone (GnRH) antagonist cotreatment for in vitro fertilization commencing recombinant follicle-stimulating hor-

mone on cycle day 2 or 5 with the standard long GnRH agonist protocol. J. Clin. Endocrinol. Metab 88, 166-173 (2003).

148. van der Heijden,G.W. et al. Transmission of modified nucleosomes from the mouse male germline to the zygote and subsequent remodeling of paternal chromatin. Dev. Biol. 298, 458-469 (2006).

149. Jin,C. & Felsenfeld,G. Nucleosome stability mediated by histone variants H3.3 and H2A.Z. Genes Dev. 21, 1519-1529 (2007).

150. Hake,S.B. & Allis,C.D. Histone H3 variants and their potential role in indexing mammalian genomes: the "H3 barcode hypothesis". Proc. Natl. Acad. Sci. U. S. A 103, 6428-6435 (2006).

151. Zhang,X., Gabriel,M.S., & Zini,A. Sperm nuclear histone to protamine ratio in fertile and infertile men: evidence of heterogeneous subpopulations of spermatozoa in the ejaculate. J. Androl 27, 414-420 (2006).

152. Baarends,W.M. et al. Histone ubiquitination and chromatin remodeling in mouse spermatogenesis. Dev. Biol. 207, 322-333 (1999).

153. Sega,G.A., Sotomayor,R. E., & Owens,J.G. A study of unscheduled DNA synthesis induced by X-rays in the germ cells of male mice. Mutat. Res. 49, 239-257 (1978).

154. Rodman,T.C., Pruslin,F. H., Hoffmann,H.P., & Allfrey,V. G. Turnover of basic chromosomal proteins in fertilized eggs: a cytoimmunochemical study of events in vivo. J. Cell Biol. 90, 351-361 (1981).

155. Kopecny,V. & Pavlok,A. Autoradiographic study of mouse spermatozoan arginine-rich nuclear protein in fertilization. J. Exp. Zool. 191, 85-96 (1975).

156. Roest,H.P. et al. The ubiquitin-conjugating DNA repair enzyme HR6A is a maternal factor essential for early embryonic development in mice. Mol. Cell Biol. 24, 5485-5495 (2004).

157. Erhardt,S. et al. Consequences of the depletion of zygotic and embryonic enhancer of zeste 2 during preimplantation mouse development. Development 130, 4235-4248 (2003).

158. Liu,H., Kim,J.M., & Aoki,F. Regulation of histone H3 lysine 9 methylation in oocytes and early pre-implantation embryos. Development 131, 2269-2280 (2004).

159. Sarmento,O.F. et al. Dynamic alterations of specific his-

tone modifications during early murine development. J. Cell Sci. 117, 4449-4459 (2004).

160. Lepikhov,K. & Walter,J. Differential dynamics of histone H3 methylation at positions K4 and K9 in the mouse zygote. BMC. Dev. Biol. 4, 12 (2004).

161. Hewitson,L. et al. Unique checkpoints during the first cell cycle of fertilization after intracytoplasmic sperm injection in rhesus monkeys. Nat. Med. 5, 431-433 (1999).

162. Wiekowski,M., Miranda,M., & DePamphilis,M. L. Requirements for promoter activity in mouse oocytes and embryos distinguish paternal pronuclei from maternal and zygotic nuclei. Dev. Biol. 159, 366-378 (1993).

163. Santos,F., Hendrich,B., Reik,W., & Dean,W. Dynamic reprogramming of DNA methylation in the early mouse embryo. Dev. Biol. 241, 172-182 (2002).

164. Oswald,J. et al. Active demethylation of the paternal genome in the mouse zygote. Curr. Biol. 10, 475-478 (2000).

165. Carlson,L.L., Page,A.W., & Bestor,T.H. Properties and localization of DNA methyltransferase in preimplantation mouse embryos: implications for genomic imprinting. Genes Dev. 6, 2536-2541 (1992).

166. Matsuda,Y., Seki,N., Utsugi-Takeuchi,T., & Tobari,I. Changes in X-ray sensitivity of mouse eggs from fertilization to the early pronuclear stage, and their repair capacity. Int. J. Radiat. Biol. 55, 233-256 (1989).

167. Sutovsky,P. & Schatten,G. Depletion of glutathione during bovine oocyte maturation reversibly blocks the decondensation of the male pronucleus and pronuclear apposition during fertilization. Biol. Reprod. 56, 1503-1512 (1997).

168. Perreault,S.D., Barbee,R. R., & Slott,V.L. Importance of glutathione in the acquisition and maintenance of sperm nuclear decondensing activity in maturing hamster oocytes. Dev. Biol. 125, 181-186 (1988).

169. Hall,C. et al. HIRA, the human homologue of yeast Hir1p and Hir2p, is a novel cyclin-cdk2 substrate whose expression blocks S-phase progression. Mol. Cell Biol. 21, 1854-1865 (2001).

170. Perez-Burgos,L. et al. Generation and characterization of methyl-lysine histone antibodies. Methods Enzymol. 376, 234-254 (2004).

171. Fang,J. et al. Purification

and functional characterization of SET8, a nucleosomal histone H4-lysine 20-specific methyltransferase. Curr. Biol. 12, 1086-1099 (2002).

172. Lachner,M., O'Carroll,D., Rea,S., Mechtler,K., & Jenuwein,T. Methylation of histone H3 lysine 9 creates a binding site for HP1 proteins. Nature 410, 116-120 (2001).

173. Li,Y., Kirschmann,D.A., & Wallrath,L.L. Does heterochromatin protein 1 always follow code? Proc. Natl. Acad. Sci. U. S. A 99 Suppl 4, 16462-16469 (2002).

174. McLay,D.W. & Clarke,H.J. Remodelling the paternal chromatin at fertilization in mammals. Reproduction 125, 625-633 (2003).

175. Henikoff,S., Furuyama,T., & Ahmad,K. Histone variants, nucleosome assembly and epigenetic inheritance. Trends Genet. 20, 320-326 (2004).

176. Ahmad,K. & Henikoff,S. Histone H3 variants specify modes of chromatin assembly. Proc. Natl. Acad. Sci. U. S. A 99 Suppl 4, 16477-16484 (2002).

177. Ahmad,K. & Henikoff,S. The histone variant H3.3 marks active chromatin by replication-independent nucleosome assembly. Mol. Cell 9, 1191-1200 (2002).

178. Lachner,M. & Jenuwein,T. The many faces of histone lysine methylation. Curr. Opin. Cell Biol. 14, 286-298 (2002).

179. Sims,R.J., III, Nishioka,K., & Reinberg,D. Histone lysine methylation: a signature for chromatin function. Trends Genet. 19, 629-639 (2003).

180. Plath,K. et al. Role of histone H3 lysine 27 methylation in X inactivation. Science 300, 131-135 (2003).

181. Santos-Rosa,H. et al. Methylation of histone H3 K4 mediates association of the Isw1p ATPase with chromatin. Mol. Cell 12, 1325-1332 (2003).

182. Fischle,W., Wang,Y., & Allis,C.D. Histone and chromatin cross-talk. Curr. Opin. Cell Biol. 15, 172-183 (2003).

183. El Maarri,O. et al. Maternal methylation imprints on human chromosome 15 are established during or after fertilization. Nat. Genet. 27, 341-344 (2001).

184. Schultz,R.M. The molecular foundations of the maternal to zygotic transition in the preimplantation embryo. Hum. Reprod. Update. 8, 323-331 (2002).

185. Janicki,S.M. et al. From silencing to gene expression: real-time analysis in single cells. Cell 116, 683-698 (2004).

186. Schwartz,B.E. & Ahmad,K. Transcriptional activation triggers deposition and removal of the histone variant H3.3. Genes Dev. 19, 804-814 (2005).

187. Chow,C.M. et al. Variant histone H3.3 marks promoters of transcriptionally active genes during mammalian cell division. EMBO Rep. 6, 354-360 (2005).

188. Lehnertz,B. et al. Suv39h-mediated histone H3 lysine 9 methylation directs DNA methylation to major satellite repeats at pericentric heterochromatin. Curr. Biol. 13, 1192-1200 (2003).

189. Santos-Rosa,H. et al. Active genes are tri-methylated at K4 of histone H3. Nature 419, 407-411 (2002).

190. Sanders,S.L. et al. Methylation of histone H4 lysine 20 controls recruitment of Crb2 to sites of DNA damage. Cell 119, 603-614 (2004).

191. Julien,E. & Herr,W. A Switch in Mitotic Histone H4 Lysine 20 Methylation Status Is Linked to M Phase Defects upon Loss of HCF-1. Mol. Cell 14, 713-725 (2004).

192. Schotta,G. et al. A silencing pathway to induce H3-K9 and H4-K20 trimethylation at constitutive heterochromatin. Genes Dev. 18, 1251-1262 (2004).

193. Nishioka,K. et al. PR-Set7 is a nucleosome-specific methyltransferase that modifies lysine 20 of histone H4 and is associated with silent chromatin. Mol. Cell 9, 1201-1213 (2002).

194. Fraser,L.R. In vitro capacitation and fertilization. Methods Enzymol. 225, 239-253 (1993).

195. Smeenk,R.J., Brinkman,K., van den Brink,H. G., & Westgeest,A.A. Reaction patterns of monoclonal antibodies to DNA. J. Immunol. 140, 3786-3792 (1988).

196. Valadon,P., Nussbaum,G., Boyd,L.F., Margulies,D.H., & Scharff,M.D. Peptide libraries define the fine specificity of anti-polysaccharide antibodies to Cryptococcus neoformans. J. Mol. Biol. 261, 11-22 (1996).

Section 3

Maternal effects on DNA repair

Section 3.1

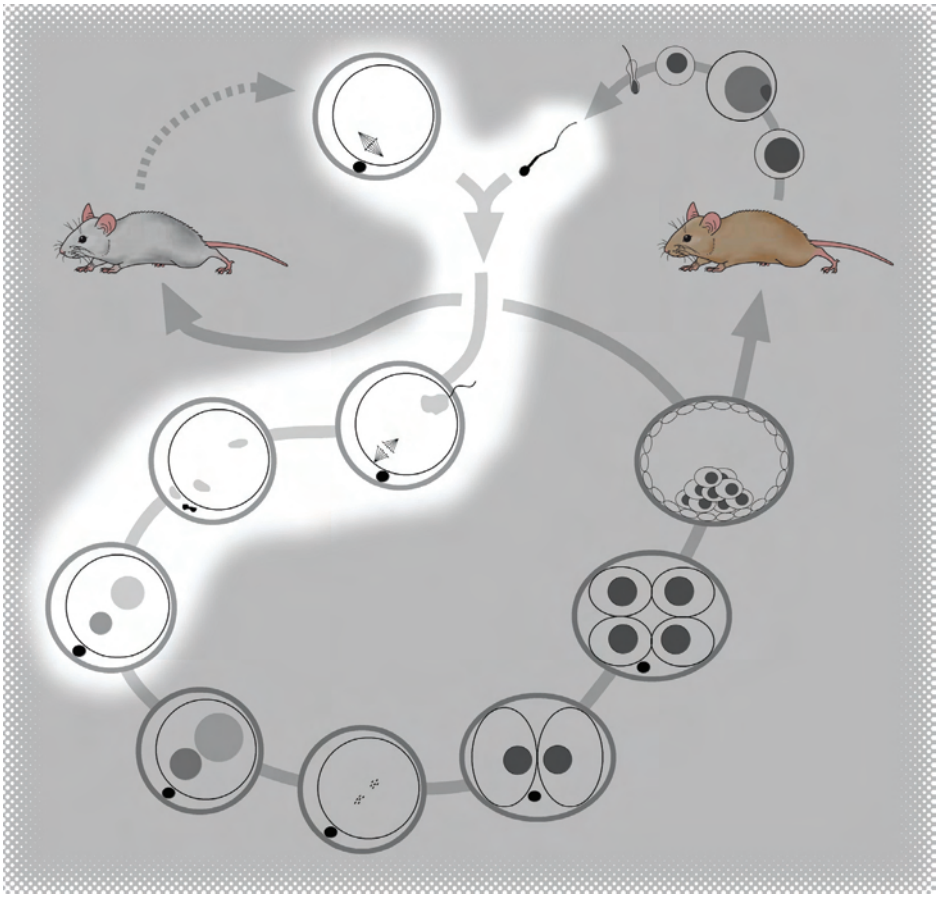

DNA Repair (Amst) 2006 August; 5(8):959-71

γH2AX signalling during sperm chromatin remodelling in the mouse zygote

Alwin AHA Derijck[# 1], Godfried W van der Heijden[# 1], Maud Giele[1], Marielle E.P. Philippens[2], Casandra CAW van Bavel[1], Peter de Boer[1]

[#] *Both authors contributed equally*

1 Department of Obstetrics and Gynaecology, Radboud University Nijmegen Medical Centre, PO Box 9101, 6500 HB Nijmegen, The Netherlands

2 Department of Radiation Oncology, Radboud University Nijmegen Medical Centre, PO Box 9101, 6500 HB Nijmegen, The Netherlands

Abstract

In the mouse, the paternal post-meiotic chromatin is assumed to be devoid of DNA-repair after nuclear elongation and protamine-induced compaction. Hence, DNA lesions induced thereafter will have to be restored upon gamete fusion in the zygote. Misrepair of such lesions often results in chromosome type aberrations at the first cleavage division, suggesting that the repair event takes place prior to S-phase. During this stage of the zygotic cell cycle, the paternal chromatin transits from a protamine- to a nucleosome-based state. We addressed the question whether the canonical signalling pathway to DNA double strand breaks (DSBs), the phosphorylated form of histone H2AX (γH2AX) is active during chromatin restructuring of the male genetic complement in the zygote.

Here, we describe the detailed characterization of γH2AX signalling in the early stages of zygotic development up to the appearance of the pronuclei.

We have found the γH2AX signalling pathway to be already active during sperm chromatin remodelling after gamete fusion in a dose dependent manner, reflecting the amount of DSBs present in the sperm nucleus after in vivo male irradiation. Using DNA damaging compounds to induce lesions in the early zygote, differences in DSB sensitivity and γH2AX processing between paternal and maternal chromatin were found, suggesting differences in DNA repair capacity between the parental chromatin sets.

Introduction

Throughout the course of evolution, organisms have acquired DNA repair to cope with the fact that the genetic material is not chemically inert. The DNA in any cell can be altered in many ways, from mere base changes possibly leading to changes in the genetic code, to highly deleterious breaks in the double helix. The sources of these varied forms of damage can either be exogenous, i.e. irradiation and chemicals, or endogenous, i.e. reactive metabolites and DNA replication errors [1] (and references herein). Hence, there are a plethora of proteins, i.e. protein modifications, which aid in the processing of these alterations. These molecules can be grouped into either "sensor", "transducer" or "effector" molecules for every repair pathway that has been described so far [2].

A well-studied signalling response is the one reacting to a DNA double strand break (DSB). Within minutes, the cell reacts to a DSB by phosphorylating the histone H2A variant, H2AX, at serine 139 (serine 129 in *S.cerevisiae*) in the nucleosomes surrounding the DSB over a megabase domain. This phosphorylated form is referred to as γH2AX [3, 4]. The reaction is catalyzed by the phosphoinositide 3-kinase related kinases (PIKKs), ATM, ATR and DNA-PK$_{cs}$ and shows a tight correlation with the amount of DSB present in the DNA [3, 5-7]. The number of DSBs produced by the decay of ^{125}I incorporated into nuclear DNA further strengthens the notion that each γH2AX focus represents an individual DSB [8]. γH2AX subsequently attracts other factors involved in the repair of the break [9]. The comparison of DSB repair by pulse field gel electrophoresis (PFGE) and γH2AX foci dynamics has shown that the disappearance of γH2AX foci coincides with the actual repair [10, 11]. This supports the generally accepted idea that the formation of and loss of γH2AX foci are indicative of recognition and repair of DNA DSBs [12] (and references herein).

In sexual reproduction, the origin of every new multicellular life starts with the fusion of a male and female gamete. In contrast to somatic cells, the zygote mainly generates non-translated transcripts [13, 14]. In the mouse, transcription becomes fully functional during "zygotic gene activation" (ZGA) in the G2 phase of 2-cell stage embryo [15] (and references herein) [16] and even later in the human [17] and farm animals [18, 19]. Hence, the mRNAs and proteins stored in the maternal gamete, the oocyte, will have to provide the zygote with

the necessary molecules to perform all its basic cellular functions till ZGA. DNA repair pathways are active during this early pre-ZGA stage of life [20, 21] and transcripts for repair genes are more abundant then in later preimplantation stages [22]. In addition to the altered cellular physiology as compared to somatic cells, the zygote has several cell cycle and chromatin related properties that are fundamentally different from somatic cells. After gamete fusion, parallel to the resumption of the female 2nd meiotic division, an extensive remodelling of the paternal chromatin takes place (reviewed in [23, 24]).

Prior to gamete fusion, during spermiogenesis, the post-meiotic spermatid nucleus undergoes a rigorous alteration of its chromatin, stepwise removing most of the nucleosomes from the DNA and replacing them with protamines which enable the high degree of compaction found in the sperm nucleus [25]. After entry in the oocyte, reversal to nucleosome-based chromatin is a necessity to enable progression into a pronucleus that can enter S-phase in conjunction with the maternal pronucleus [26].

The spermatid nucleus is devoid of DNA repair upon the start of protamine-induced compaction at stage 12 of spermatogenesis [27, 28], some 2 weeks before ejaculation. Hence, DNA lesions present in the paternal nucleus at this period, will have to be repaired after entry into the oocyte, by factors stored herein. Repair of male DNA lesions takes place by the oocyte [21, 29] and misrepair often results in chromosome type aberrations at first cleavage suggesting the repair event to take place prior to S-phase [30, 31].

After gamete fusion, when the oocyte completes the second meiotic division, the sperm nucleus quickly sheds its protamines and rapidly acquires a nucleosome based state [32]. This is morphologically reflected by a consecutive decondensation and recondensation of the male nucleus [33]. This difference in origin of the parental chromatin results in a different histone composition (predominantly histone H3.3 in the pre-S phase paternal pronucleus) [26, 32] and post translational histone modification asymmetry (PTM) [26, 32, 34-40]. These dissimilarities confer specific chromatin configurations and might be related to the differences in response to DNA damage induction in the male and female complement of the zygote [31].

The repair of DNA damage present in the parental genomes is crucial for embryonic development [41]. A role for γH2AX signalling in the zygote for both male and female chromatin could be expected

shortly after fertilisation, as a consequence of male chromatin remodelling. Here we describe γH2AX signalling in the early zygote up to pronucleus formation. We found that shortly after gamete fusion γH2AX signalling is active and reacts to various DNA damaging agents. In addition, we show a difference in sensitivity to DNA damaging compounds for the paternal and maternal chromatin followed by sex specific repair kinetics.

Materials and Methods

Sperm Irradiation

DNA-damaged sperm was generated by whole body irradiation of male CBA/B6 F1 mice up to 3 days prior to sperm isolation for in vitro fertilisation using (external beam radiation) 6-MV photons of an Elekta linear accelerator (Crawley, UK) with a dose-rate of 0.5 Gy/min in doses of up to 4 Gy. The administered dose was verified using TLD (thermo luminescent dosimetry) measurements.

Gamete Collection and IVF

Gametes were obtained for in vitro fertilisation as described before [32]. Briefly, mice were housed with adjusted light hours set at 9.00-21.00. Sperm was obtained from the caudae epididymis of 6-20 weeks old CBA/B6 F1 mice and exposed to capacitation medium (HTF, Cambrex, BE02-021F), 3%(w/v) BSA (Sigma, A-4503), 10 μM adenosine (Sigma, A-5762; a capacitation stimulator [42]). Capacitation was performed at 37°C, 5% CO_2 in air for 1-1.5 hours.

Superovulation was induced in B6/CBA F1 mice (4 to 12 weeks old) by injecting 7.5 U PMSG (Intervet, Boxmeer, The Netherlands) between 18.00-19.00 and 7.5 U HCG (Intervet) 48 hours later. Secondary oocytes plus adhering cumulus cells were placed in 50 μl droplets of IVF medium (HTF, 0.5% (w/v) BSA) covered with light mineral oil (Irvine Scientific, #9305) equilibrated with sterile PBS. Sperm was added to these droplets in a final concentration of ~ $1.5*10^6$ cells/ml.

Timing of zygote development

By paraformaldehyde (pfa) fixation (see below under fixation and immunofluorescence) and DAPI-staining at various time points post insemination (pi), it was determined that the majority of secondary oocytes was penetrated around 70 min pi [32]. For the visualisation of γH2AX signalling during male chromatin remodelling, zygotes were fixed at various time

points, yielding zygotes at different stages of development with distinct morphologies for the paternal nuclei as described before [32, 33]: 90 min pi (early decondensing male chromatin), 105 min pi (progressed decondensing male chromatin), 150 min pi (recondensing male chromatin) and 280 min pi (pronuclei). At all time points, some variation in nuclear morphology remained. The differences in timing of gamete fusion between zygotes in vitro are small. However, the process of sperm head decondensation is rapid. All zygote time points mentioned in this report (except for the Materials and Methods section, which only gives actual time pi) are compensated for the 70-minute lag phase to give the approximate time periods after gamete fusion for the described stages.

DNA damaging agents

Etoposide (VP-16) (Sigma, E-1383) and Bleomycin (Pharmachemie BV, Haarlem, Netherlands, 6012159) were dissolved in DMSO and PBS respectively. Stock concentrations of 10mM Etoposide and 7.5 U/ml Bleomycin were stored at –80 and –20 °C. Pilot experiments using Etoposide were based on the finding that this drug induces massive chromosomal aberrations in the male nucleus when administered during and after chromatin remodelling [43]. Therefore, zygotes were placed in the indicated 1 μM Etoposide in IVF medium at 90 or 120 minutes pi and cultured up to the recondensing male nucleus stage (150 minutes pi, 60 and 30 min exposure respectively). Zygotes were either fixed at 150 min pi or washed in fresh IVF medium and cultured till the pronucleus stage (fixation at 280 min pi).

To phenocopy the γH2AX foci patterns found in zygotes from irradiated sperm (3-4 Gy) a pulse-like drug exposure was given during the sperm decondensation phase (120 min pi). Zygotes were placed in droplets of IVF medium containing either 0.25 μM Etoposide or 750 μU/ml Bleomycin for 5 min. After drug treatment the zygotes were washed 5 times in droplets of IVF medium and returned to a centre well dish containing 1 ml of IVF medium. Zygotes were cultured up to the sperm recondensation phase (155 min pi) or pronuclear stage (285 min pi).

Antibodies

The γH2AX mouse monoclonal (Upstate #05-636, clone JBW301, 1:10,000) was used throughout, the γH2AX rabbit polyclonal (Upstate #07-164, 1:1,000) to verify several findings.

Rabbit anti-H3K9me2, 1:500 (Dr T. Jenuwein) [44] was used to discriminate between paternal and maternal pronuclei, solely staining the maternal pronucleus [32].

Rabbit anti-H3S10ph (Upstate #06-570, 1:1,000) served to follow sperm

nucleus development [45].
Secondary abs were applied as following: Molecular Probes, Oregon, USA: A11001 fluor 488 goat anti-mouse IgG (H+L), A11012 fluor 594 goat anti-rabbit IgG (H+L), both in a 1:500 dilution.
All secondary abs were tested for non-specific binding, which was never observed.

Fixation, immunofluorescence (IF) and foci quantification

Before fixation of the zygotes the zona pellucida was removed by acidic tyrode (pH 2.5) containing 1% (w/v) BSA. Thereafter cells were immobilised in a fibrin clot [46] (fibrinogen obtained from Calbiochem, #341573; Thrombin from Sigma, # T-6634). IF was applied as described before [47]. γH2AX foci were counted by one observer (AAHAD). The paternal chromatin and maternal chromatin were analysed separately. At the recondensing sperm stage (150 min pi), pre-pronuclear maternal chromatin was quantified only when an unambiguous spatial distinction with the chromatin of the second polar body could be made.

Collection of images

Images were collected with a Zeiss axioplan fluorescence microscope. Pictures were captured by a Zeiss AxioCam MR camera with Axiovision 3.1 software (Carl Zeiss). All images shown are either a single plane derived from stacks with z-axis intervals of 0.4 μm or deconvoluted projections created with Metamorph software version 6, using the nearest neighbour mode.

Statistics

Non-parametrical statistical analysis was performed using Prism (Graphpad) and SPSS (Appache software foundation) software. Details are indicated in the figure legends.

Results

Irradiation induced DNA double strand breaks in sperm from the cauda epididymis elicit a H2AX phosphorylation response during sperm chromatin remodelling

Before the onset of fertilisation, the mammalian secondary oocyte is arrested at meiotic metaphase II. Metaphase II chromatin is highly decorated with a fine punctuated γH2AX signal (Figure 1A, using the two independent antibodies). After gamete fusion, the zygote finishes the second meiotic division. During the progression of anaphase II, the maternal chromosomes start to loose their γH2AX staining (Figure 1B and C) and this signal has diminished within 30 minutes after fusion. Hereafter, no DNA damage related signal was found in the pre-pronuclear female derived chromatin. The second polar body often contained large γH2AX foci (data not shown).

In the zygote, H3S10ph shows a gradual increase during the de/recondensation phase of sperm chromatin, brightly decorating the recondensed sperm chromatin (Figure 1H). The female chromatin shows a gradual decrease of this PTM during the metaphase II to telophase II transition. The transitory state of this mark is apparent at the pronucleus stage, when both PNs hardly contain H3S10ph [45]. Hence, we have used this PTM, in conjunction with DAPI morphology, as an indicator for the progression of male nuclear remodelling. During the remodelling of the paternal chromatin, a diffuse γH2AX staining becomes apparent in the decondensing sperm nucleus, whether the sperm has been irradiated or not. Qualitative observations on γH2AX foci dynamics were made using 3 Gy irradiated sperm. Irradiated and non-irradiated male nuclei did not show qualitative differences in γH2AX signals. At sites where histone H3 is phosphorylated at serine 10 (H3S10ph) compactions of γH2AX signal become apparent (Figure 1D, E). During the continuation of decondensation, a fuzzy focus like γH2AX staining pattern starts to build up within the diffuse γH2AX "background" (Figure 1F and G). Approximately 80 minutes after gamete fusion, the male chromatin is in its recondensation phase and shows very bright γH2AX foci in a faint γH2AX background staining. H3S10ph fully decorates the recondensing male nucleus (Figure 1H). At this stage, clear differences in γH2AX focus morphology could be observed. Small specks of signal (Figure 1H, arrow) were distinguished from amorphous foci clearly larger then these specks but varying in size,

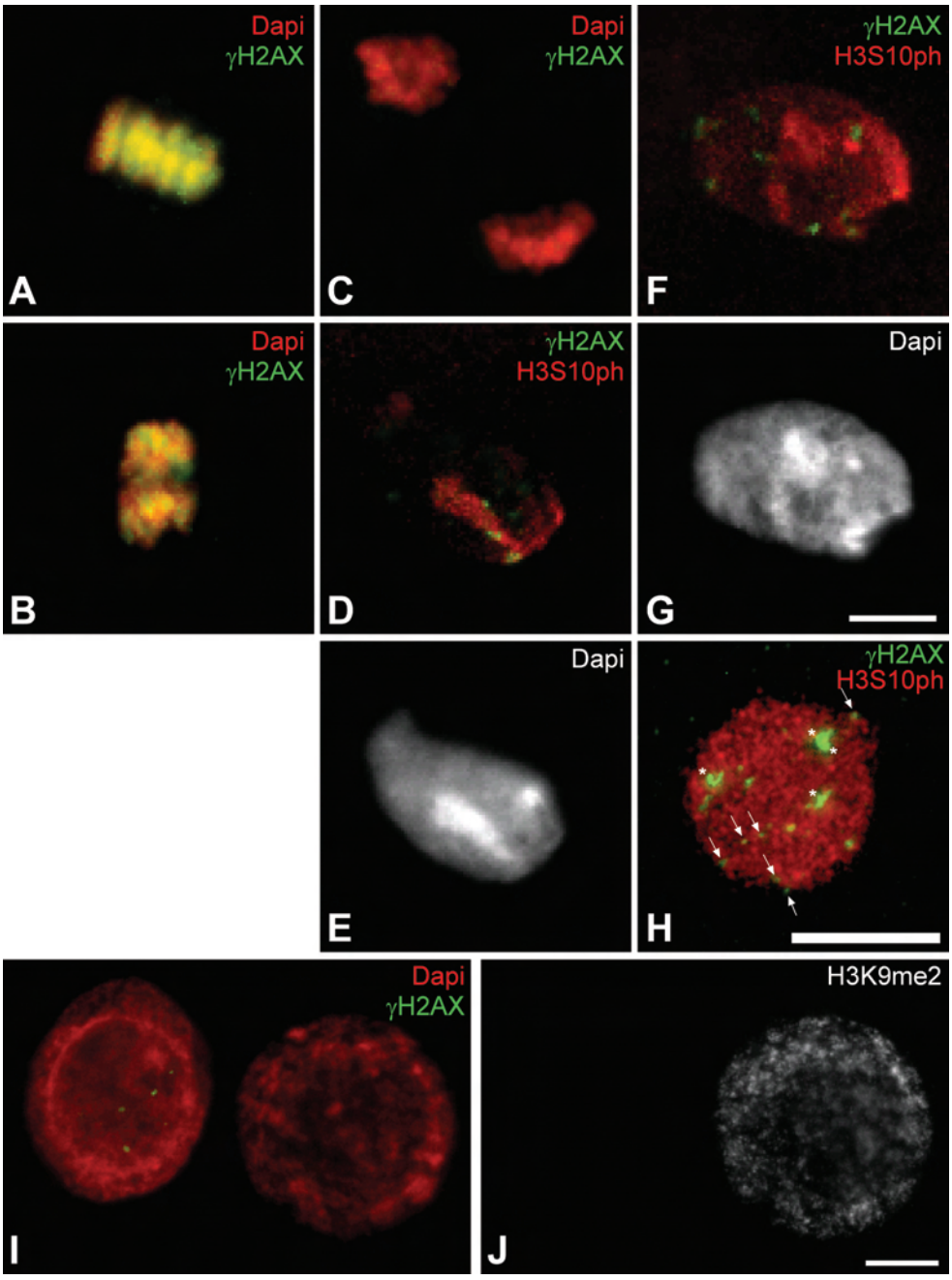
Dapi
γH2AX
A
Dapi
γH2AX
C
γH2AX
H3S10ph
F
Dapi
γH2AX
B
γH2AX
H3S10ph
D
Dapi
G
Dapi
E
γH2AX
H3S10ph
H
Dapi
γH2AX
I
H3K9me2
J

Figure 1 Signalling of DNA double strand breaks in mouse secondary oocytes and early zygotes Pseudocoloured images of cut outs of oocytes fused with 3 Gy irradiated sperm. **(A)** γH2AX staining of the meiotic chromosomes arrested at metaphase II (n=115). **(B)** Onset of maternal anaphase II (n=5); **(C)** progressing anaphase II (corresponding male chromatin in D, E, approximately 20 minutes after penetration) (n=14). **(D)** γH2AX staining of the decondensing male chromatin at an early state of remodelling co-stained with phosphorylated histone H3 at serine 10 (H3S10ph), **(E)** corresponding DAPI stain. **(G)** Progressed decondensation of the male chromatin (approximately 35 minutes after fusion) (DAPI, n=19), **(F)** stained for γH2AX and H3S10ph. **(H)** Recondensed male chromatin showing bright γH2AX foci ~80 minutes after sperm penetration (n=38). Variation in focus morphology: examples of small γH2AX foci are indicated with an arrow, large γH2AX foci are indicated with an asterisk. (Additional examples in Supplementary Figure 2) **(I)** The pronuclear stage, approximately 3.5 hours after fusion, (DAPI/γH2AX, n=38), **(J)** corresponding maternal specific H3K9me2 staining. Bars indicate 10 μm, first bar (A, B, C, D, E, F and G), second bar (H) and third bar (I and J).

collectively called large foci (Figure 1H, asterisk). The formation of γH2AX foci could be prevented by incubating the zygotes in 100 μM Wortmannin, a PI-3 kinase inhibitor, in culture medium (data not shown). After chromatin remodelling of the male nucleus, the zygote starts to form the paternal and maternal pronuclei. Approximately 210 min after gamete fusion, when the pronuclei had formed, predominantly small γH2AX foci were observed in the paternal one. The female pronucleus never showed signs of γH2AX staining (Figure 1I and 1J).

Irradiation induced γH2AX foci show a dose related response in male chromatin

In somatic nuclei the amount of γH2AX foci formed is tightly correlated with the amount of DSBs introduced [3]. In order to investigate whether this proportionate reaction exists in zygotes, oocytes were inseminated with sperm isolated from the cauda epididymis of (non-) irradiated mice, followed by analysis for γH2AX foci at the recondensing sperm and pronuclei stages. At the recondensing

Table 1 Statistics of irradiation induced γH2AX foci shown in figure 2

Dose (Gy)	Recondensing male chromatin				Male pronucleus				$\frac{\overline{X}_{rec} - \overline{X}_{PN}}{\overline{X}_{rec}}$
	Large		Small		Large		Small		
	Mean	SE	Mean	SE	Mean	SE	Mean	SE	
0	0.9** (22)	0.25	2.7	0.42	0.4 (18)	0.20	4.3$	0.55	0.57
1	1.2## (57)	0.17	2.7	0.29					
3	4.0*#Δ (38)	0.44	3.1	0.45	0.8 (38)	0.21	5.5&	0.58	0.80
4	7.3 *#Δ (14)	0.79	2.4	0.50	0.6 (28)	0.17	8.1$&	0.75	0.92

At each dose of irradiation of epididymal sperm, the mean numbers of large and small foci are given for two early zygote stages. SE= Standard Error. Number of zygotes between parenthesis. Matched symbols indicate significant differences by non-parametric statistical analysis. The relative reduction of large γH2AX foci, comparing the PN and recondensing male chromatin stage, are indicated in the last column.

* Indicates significant differences (P<0.001) between 0 and X Gy determined by Kruskal-Wallis and Dunn's posttest.

# Indicates significant differences (P<0.001) between 1 and X Gy determined by Kruskal-Wallis and Dunn's posttest.

Δ Indicates significant differences (P<0.05) determined by Mann Whitney test.

$ Indicates significant differences (P<0.01) between 0 and X Gy determined by Kruskal-Wallis and Dunn's posttest.

& Indicates significant differences (P<0.05) between 3 and X Gy determined by Kruskal-Wallis and Dunn's posttest.

male chromatin stage (~80 min after fusion, Figure 1H) the large foci showed a clear dose response relation (Figure 2 and Table 1). Although, a high degree of variability was observed, a significant increase in the number of large γH2AX foci in response to sperm irradiation was found (Table 1). The high degree of variability was also observed for small foci, while no increase due to irradiation was noticed. No correlation was found between the number of small and large foci per male nucleus. Strikingly, both small and large γH2AX foci were present in recondensing male nuclei from non-irradiated mice, with 50% of non-irradiated male nuclei containing at least 1 large γH2AX focus. This fraction rises with increasing doses

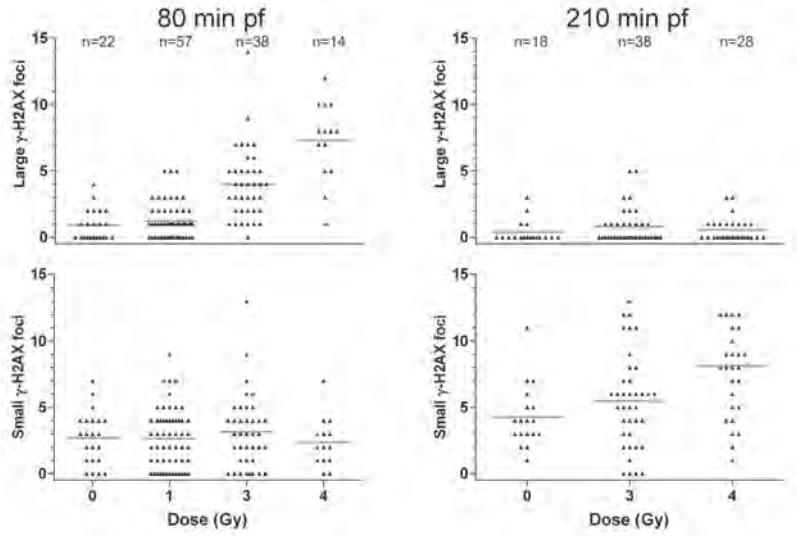

Figure 2 Dose response of γH2AX foci in male chromatin at two stages of early zygotic developmental to irradiated sperm The two panels show the quantitative data at the recondensing male chromatin stage (80 min post fusion) (visually represented in Figure 1H) and pronucleus stage (210 min post fusion) (visually represented Figure 1I). Both large and small foci are indicated in their respective plots. Each triangle indicates a single zygote, with n given at the top of each column. The horizontal grey lines indicate the mean number of foci in each sample. Averages and standard errors can be found in table 1.

of irradiation (1 Gy, 68%; 3 Gy, 97%; 4 Gy, 100%).
Chromatin of PN-stage zygotes, derived from either non-irradiated or irradiated sperm, showed a reduction in the number of large γH2AX foci compared to the recondensing male chromatin stage (Figure 2 and Table 1). However, irradiation of sperm did elevate the level of small γH2AX foci at the PN stage. The fraction of PN-stage zygotes that did contain large γH2AX foci was slightly elevated after sperm irradiation, being 22% in PN from non-irradiated sperm and 39% (3 and 4 Gy) in PN from irradiated sperm. However, the average numbers of foci did not vary significantly between these groups (Table 1).
By comparing the number of large γH2AX foci at the recondensing male chromatin stage with the corresponding amount at the PN stage, the relative reduction of foci for each irradiation dose was cal-

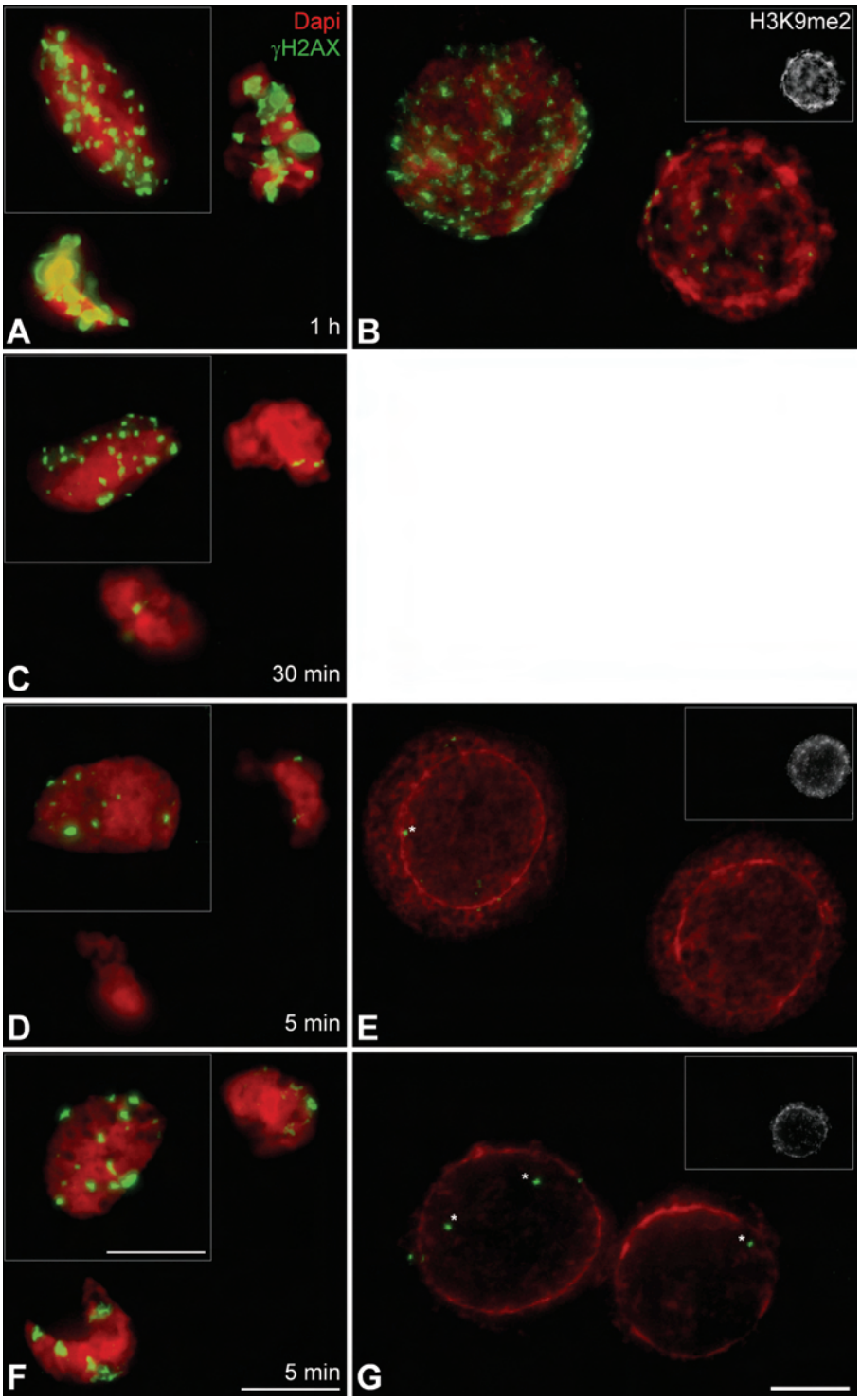
Dapi
γH2AX
A
1 h
B
H3K9me2
C
30 min
D
5 min
E
F
5 min
G

Figure 3 Etoposide and Bleomycin induced γH2AX signalling in zygote development during sperm chromatin remodelling. A, C, D and F show the progressing maternal ana/telophase and corresponding male chromatin in the inset. B, E and F show the paternal (left) and maternal (right) PN (staining for the maternal specific H3K9me2 in the inset). In all colour figures DAPI is pseudocoloured in red and γH2AX in green. **(A)** During early male chromatin decondensation (20 min post penetration) zygotes were exposed to 1 μM Etoposide for one hour and analysed (80 min after penetration; n= 21). **(B)** Zygotes that had received this treatment were recovered up to the PN stage (210 minutes after penetration; n=17). **(C)** The effect of a shorter exposure (30 min) to 1 μM Etoposide, starting 50 minutes after fusion (n=14). Zygotes which received a pulse-based administration of either **(D)** 0.25 μM Etoposide or **(F)** 750 μU/ml Bleomycin, during male chromatin remodelling (50 min after fusion), were analysed at the recondensing male chromatin phase (80 min post fusion) (n=28 and n=41 respectively) or PN stage (**E**; n=21 and **G**; n=37 respectively). * Indicates the presence of large γH2AX foci in one or both PNs. Bar indicates 10 μm, bars are matched to each respective group; recondensed male chromatin insets, maternal ana/telophase II groups and PN stage zygotes.

culated (Table 1). This gives an estimate of the efficiency by which the zygote removes irradiation induced large γH2AX foci from its chromatin, hence, an approximation of the repair efficiency.

DNA damage induction during sperm decondensation evokes a prominent γH2AX response

To analyze whether the mouse zygote is able to sense exogenously induced DNA damage during the male chromatin remodelling phase, cells were treated with the Topoisomerase II inhibitor, Etoposide (VP-16), during the decondensation phase. Etoposide is a likely candidate to induce a significant amount of foci since it has been shown to induce massive chromosome aberrations in one cell androgenones [43] and Topoisomerase II plays an active role during male chromatin remodelling in the zygote [48, 49].

Initially, zygotes were continuously incubated with 1 μM of Etoposide from 20 min after gamete fusion up to the sperm recondensation phase (~80 min after fusion) resulting in a 60 min incubation

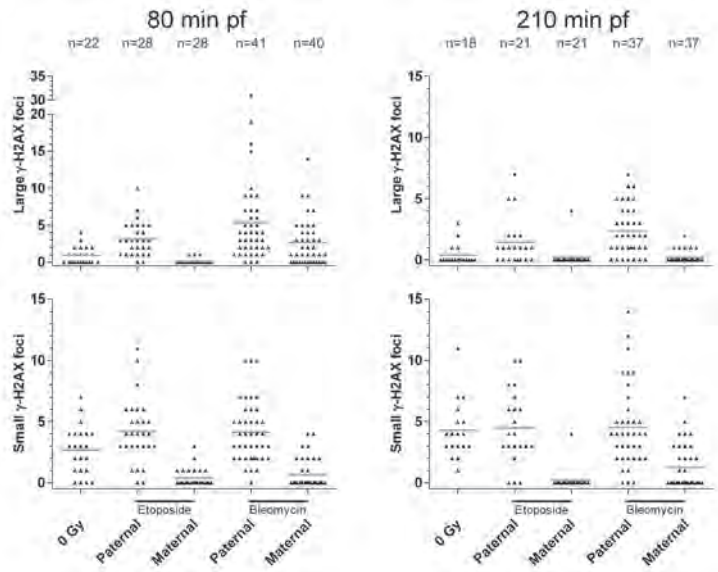

Figure 4 γH2AX foci in zygotic chromatin in response to DNA damaging agents during male chromatin remodelling measured at two developmental stages Two panels show the quantitative data on foci development at the recondensing male chromatin stage (80 min post fusion; visually represented in Figure 3D and 3F) and PN stage (210 min post fusion; visually represented in Figure 3E and 3G) after 5-minute exposure of zygotes to drugs during sperm remodelling (50 min after fusion). Both the paternal and maternal response to the treatment is given compared to control sperm from Figure 2 (0 Gy). Large and small foci are indicated in their respective plots. Each triangle indicates a single zygote, with n given at the top of each column. The horizontal grey lines indicate the mean number of foci.

(Figure 3A). In contrast to the faint γH2AX signal normally found in progressing anaphase (Figure 1C) a dominant domain-like staining of γH2AX was observed in the maternal chromatin of most zygotes (20/21). The recondensing male chromatin also showed an induction level far beyond that of 3 or 4 Gy irradiated sperm (Figure 3A, inset). After exposure to 1 μM Etoposide for 30 min, starting at late male chromatin decondensation (approximately 50 minutes after gamete fusion), a different pattern was found in zygotes at the male chromatin recondensation phase, ~80 min post fusion. This later initiated incubation resulted in a severe reduction in the amount

Table 2 Statistics of drug induced γH2AX foci shown in figure 4

Treatment	P/M	Recondensing male chromatin stage				Pronuclei stage				$\frac{\bar{X}_{rec} - \bar{X}_{PN}}{\bar{X}_{rec}}$
		Large		Small		Large		Small		
		Mean	SE	Mean	SE	Mean	SE	Mean	SE	
0 Gy	P	0.9** (22)	0.25	2.7	0.42	0.4# (18)	0.20	4.3	0.55	0.57
Etoposide (0.25 μM)	P	3.1* (28)	0.43	4.2	0.50	1.4 (21)	0.42	4.5	0.65	0.55
	M	0.1& (28)	0.06	0.4	0.14	0.2 (21)	0.19	0.2$	0.19	n.a.
Bleomycin (750 μU/ml)	P	5.3* (41)	0.93	4.1	0.39	2.4# (37)	0.33	4.5	0.55	0.55
	M	2.7& (40)	0.50	0.7	0.19	0.2 (37)	0.08	1.2$	0.30	0.93

For each drug the mean number of large and small foci for both the paternal (P) and maternal (M) complement are given at their respective developmental stages. Control sperm (0 Gy) data from table 1 is also given. SE= standard error. Number of zygotes between parenthesis. The relative reduction of large γH2AX foci, comparing the PN and recondensing male chromatin stage, is indicated in the last column. This could not be calculated for the maternal complement after Etoposide treatment due to the low damage induction. Symbols: significant differences by non-parametric statistical analysis.

* Indicates significant differences ($P<0.01$) between the given treatment and 0 Gy at recondensing sperm stage determined by Kruskal-Wallis and Dunn's posttest.

# Indicates significant differences ($P<0.01$) between the given treatment and 0 Gy at the PN stage determined by Kruskal-Wallis and Dunn's posttest.

& Indicates significant differences ($P<0.01$) between maternal chromatin at given stage and treatment determined by Mann-Whitney test.

$ Indicates significant differences ($P<0.05$) between maternal chromatin at given stage and treatment determined by Mann-Whitney test.

of γH2AX signal formed at maternal ana/telophase (Figure 3C). The recondensing male chromatin also showed a reduction (Figure 3C, inset) but no quantitative data were collected. Zygotes with a history of a 60 min exposure to 1 μM Etoposide during their male chromatin remodelling stage (Figure 3A) were still showing a significant amount of γH2AX signal in both the maternal and paternal pronucleus with the latter staining stronger (Figure 3B). In addition, the paternal pronuclear morphology was distorted, showing an unstructured chromatin mass (compare Figure 3B with 3E).

To further analyse the kinetics of exogenously induced γH2AX foci in the early zygote, a 5 min pulse of Etoposide was given during male chromatin decondensation (50 min after gamete fusion), to be compared with a pulse of Bleomycin, a radiomimetic inducer of single and double strand DNA breaks ([50] and references herein). γH2AX foci formed in zygotes treated with either compound were quantitatively analysed, at the recondensing male chromatin and PN stages (80 min and 210 min after gamete fusion respectively) (Figure 4 and Table 2).
Both compounds induced γH2AX foci formation in the male nucleus above background levels. (Figure 3D and 3F, inset). Maternal chromatin of resting metaphase II oocytes was liable to damage induction using both compounds (Supplementary Figure 1). However, maternal chromatin in zygotes was significantly affected by Bleomycin only in these pulse-based treatments (Figure 3D and 3F), indicating a difference in sensitivity between paternal and maternal chromatin for these two clastogenic compounds. In contrast to PN-stage zygotes derived from irradiated sperm (Figure 1I), drug treated zygotes showed a higher abundance of large γH2AX foci in their pronuclear chromatin (Figure 3E and 3G). Both the paternal and maternal chromatin showed a reduction of the amount of large γH2AX foci in PN-stage zygotes, relative to the recondensing male chromatin stage, 80 min after gamete fusion (Figure 4 and Table 2). After Bleomycin treatment, the maternal chromatin showed a much higher relative reduction of large γH2AX foci then the paternal chromatin (Figure 4 and Table 2).

Discussion

Different aspects of γH2AX signalling

The analysis of γH2AX signalling in unfertilised oocytes and early zygotes yielded several distinct patterns. The metaphase II chromosomes of the arrested oocyte are brightly stained for γH2AX in a fine punctuate manner (Figure 1A). The physiology of the secondary oocyte resembles somatic cells in mitosis. Recently, a mitotically linked γH2AX signal not related to DSBs has been described in cell lines of several species, including mouse and human [51, 52]. These studies have shown that this mitotic γH2AX signal, mainly depen-

dent on ATM, is rapidly lost from the chromatin during progressing anaphase, returning to background levels at telophase. After sperm had fused with the oocyte, the maternal chromatin showed a similar loss of signal during the second meiotic division (Figure 1B and 1C). Mitotic H2AX phosphorylation in somatic cells apparently is mechanistically conserved in the female gametes of mice.

In addition, we have found that during initial male chromatin remodelling (~20 min post fusion), the onset of γH2AX signalling emerges as concluded by the observation of faint γH2AX domains. These converge into more prominent γH2AX regions, finally leading to the distinction of two classes of γH2AX foci in a faint γH2AX background, typical for the nucleosome based paternal chromatin 80 min after gamete fusion (Figures 1D, 1F, 1H). Focus formation was abolished upon PI-3 kinase inhibition, indicative for PIKK involvement. The protamines within the male chromatin are fully substituted by nucleosomes 30 min after gamete fusion [32]. It is around this time that the DSB related large γH2AX foci start to become visually apparent (Figure 1F), albeit less well defined compared to the morphology found 80 min after gamete fusion (Figure 1H). Therefore, it is plausible that γH2AX signalling starts as soon as the chromatin template is a valid PIKK substrate, already during the protamine to nucleosome transition. The actual manifestation of γH2AX foci, as known in somatic nuclei, is only observed upon a further maturation of the paternal chromatin fibre.

A dose response type analysis of γH2AX signal formation after irradiation of sperm showed that the two focus types found in recondensed male chromatin have a different etiology. Whereas the small γH2AX foci showed no response to the administered dose, the large γH2AX foci showed a clear elevation with dose (Figure 2 and Table 1).

In addition to the mitotic γH2AX signal described above, other forms of γH2AX signalling not directly linked to a DSB have been described, for instance in the sex body (X and Y chromosome) during male meiosis [53]. The addition of chloroquine, a DNA intercalator that induces alterations in the twists of internucleosomal linker DNA, activates ATM in a non-DSB related manner as shown by IF staining [54]. Therefore, changes in higher-order-chromatin organisation can potentially influence γH2AX signalling. Chromatin remodelling of the sperm nucleus after incorporation in the oocyte is

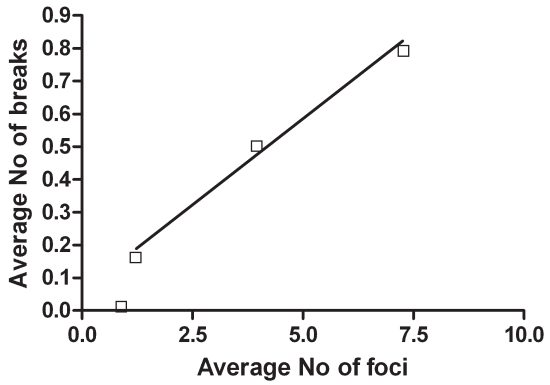

Figure 5 Comparison of large γH2AX foci at recondensing male chromatin stage with No of breaks at first cleavage division as calculated from literature data on the radio induction of chromosome abnormalities[31] Plotted are the average number of γH2AX foci at each dose of irradiation with their corresponding number of breaks at first cleavage division calculated from fragments (1 break) and dicentrics (2 breaks) Dose of sperm irradiation; 0, 1, 3 and 4 Gy.

one of the most extensive chromatin remodelling events found in biology. Hence, the nature of small γH2AX foci remains elusive and a link with sperm chromatin remodelling is plausible.

Large γH2AX foci induction and repair kinetics

Amorphous large γH2AX foci were found in the recondensing male chromatin, the number of which showed a correlation with the irradiation dose of the sperm in vivo (Figure 2). The degree of variance found in the number at each dose does not reflect an uncertainty in the counting of foci but is indicative for the stochastic nature of induction by radiation, as has been shown in somatic nuclei [55]. For somatic cells an average of 30-35 γH2AX foci per Gy irradiation has been determined in G1 stage nuclei [7, 10, 11, 55-57]. FACS analysis has shown that the ploidy of the nucleus quantitatively influences number [56]. Therefore, a total number of 15-18 γH2AX foci per Gy irradiation are expected for a haploid postmeiotic nucleus. Nothing is known about γH2AX foci kinetics in zygotes so far, but even when assuming a 30 to 40 percent reduction within the first 30 minutes after foci formation, as is observed in somatic cells [10], 9-13 foci per Gy irradiation are expected in the male nucleus at the recondensing

stage, ~80 min after fusion. Our data indicate a considerable lower number (Table 1).

This somatic-early zygotic difference can be due to several factors. The level of oxygenation in vitro and in vivo influences the amount of DNA breaks produced by irradiation, thereby rendering cells in the hypoxic testis radioresistant [58, 59]. However, the epididymis is not considered to be hypo-oxygenated [60].

We have shown that the addition of DNA damaging compounds during male chromatin remodelling post gamete fusion induces large γH2AX foci in numbers higher than after in vivo irradiation of sperm, depending on dose and exposure time (Figure 3 and 4). This demonstrates that early zygotes are capable of "marking" a large number of DSBs by γH2AX signalling. Results from in vitro irradiated zygotes of the same age support this observation (data not shown). Therefore, the substantially lower amount of large γH2AX foci per Gy after in vivo irradiation is most likely due to the radioresistant properties of the sperm nucleus [61]. Conclusively, the amount of large γH2AX foci formed after in vivo irradiation of sperm in the recondensing male nucleus cannot be predicted from in vitro somatic cell experiments and clearly is much lower. However, a certain fraction of breaks could be quickly restored during early remodelling of the male chromatin, which is Topoisomerase II dependent, and could thereby escape detection via the γH2AX pathway.

When comparing the number of breaks (calculated form the average number of chromosome type aberrations [31]) with the average number of large γH2AX foci found in recondensing male chromatin, a linear relation was found (Figure 5, $r^2>0.99$), strengthening the causality of these two radiation effect parameters.

The number of DSBs in nuclei of non-irradiated non-cycling somatic cells is about 0.05 [55]. Correcting for a haploid DNA content this would give 0.025 DSBs per nucleus as the background level. Non-irradiated sperm showed an average DSB level of 0.9 DSBs per male nucleus (Table 1), with 50% of the nuclei containing at least 1 γH2AX focus. This suggests an induction by a factor of at least 36 in remodelling male chromatin. During spermiogenesis, numerous DNA strand breaks can be detected at chromatin remodelling during nuclear elongation [62]. These transient DSBs are Topoisomerase II-induced and -religated [63]. Topoisomerase II also plays a role during sperm decondensation in the zygote [48]. Therefore the relatively

high background of large γH2AX foci is likely due to the chromatin remodelling of the sperm nucleus [43]. In agreement with this supposition, the Topoisomerase II inhibitor Etoposide is a strong inducer of γH2AX foci at chromatin remodelling. Under normal conditions, only a fraction of these breaks will lead to a γH2AX signal and are restored at high efficiency, since non-irradiated sperm does not give rise to a high number of chromosome aberrations [30, 31] (also indicated by the 0 Gy point in Figure 5).

At the early pronucleus stage, the number of large γH2AX foci was reduced relative to numbers in the recondensing male chromatin. 97-100% of 3-4 Gy irradiated sperm showed large γH2AX positive nuclei during chromatin remodelling, which was reduced to 39% in the early pronucleus. The relative reduction in number of foci at the PN stage was 0.8 and 0.9 for 3 and 4 Gy irradiated sperm respectively (Table 1). In somatic nuclei, the reduction of γH2AX foci after irradiation, hence repair of radiation induced DSBs, shows two distinct phases. A fast reduction to approximately 20% residual damage within the first 2 hours after induction and a slow reduction of the residual 10% damage starting approximately 4 hours after induction [10]. These phases have also been connected to distinct biochemical sub-pathways of repair and are linked to the complexity of the DSB [11]. We analysed the PN stage 3.5 hours after gamete fusion. Taking into account sperm chromatin remodelling and the onset of γH2AX signalling, the DSBs we observed 2-3 hours after initial detection most likely are residual DSBs resilient to quick repair. So, a match with the fast repair kinetics as found in somatic nuclei is suggested.

The nature of a DSB is reflected in the kinetics of its repair. γH2AX foci of "easy breaks" disappear faster then those of "difficult breaks" that need end processing [11]. Etoposide creates simple protein-bridged DSBs, which upon Etoposide removal form frank DSBs that require repair by NHEJ [64]. The radiomimetic agent Bleomycin generates both staggered and blunt end breaks [50, 65]. The numbers of large γH2AX foci induced in decondensed male chromatin (Figure 4) after pulse-treatment with these compounds were on average, 3.1 (Etoposide) and 5.3 (Bleomycin) per male nucleus (Table 2). Both treatments resulted into residual large γH2AX foci in the male PN with a relative reduction of 0.55, indicating that 45% of large γH2AX foci were still found in the male pronuclei of these zygotes.

When comparing α-particles, that make complex breaks, with Etoposide, similar foci kinetics were found within the first 2 hours after exposure of somatic cells [11], both giving a relative reduction of 0.5-0.6 (calculated from [11]). Therefore, the similarity in foci reduction kinetics found for Etoposide and Bleomycin induced breaks appears to be in accordance with the somatic data of Riballo et al [11].

γH2AX DSB signalling within the zygote occurs in a dynamic system with differences between parental chromatin

Apart from the mitotic γH2AX signal, no spontaneous H2AX phosphorylation has been found in the pre-pronuclear maternal chromatin of the zygote. However, using DNA damaging compounds, DSB signalling via γH2AX has been shown in the female chromatin as well (Figure 3). Several differences in response to DNA damaging agents between paternal and maternal chromatin of the zygote have been noted.

There was a clear difference in sensitivity for the compounds used. When treating zygotes during male chromatin recondensation (female chromatin in telophase II) with Etoposide, either during a 30 min exposure (Figure 3C) or a pulse (Figure 3D and 4), a lower number of large γH2AX foci was found in the maternal chromatin (pulse: an average of 3.1 vs. 0.1 foci, Table 2). A similar tendency was found for a Bleomycin pulse (an average of 5.3 vs. 2.7 foci, Table 2).

Etoposide influenced the maternal chromatin only at a higher concentration and a longer exposure time, starting at oocyte activation (Figure 3A). Treatment with Etoposide after anaphase II showed a reduction in sensitivity. A lower sensitivity of the female chromatin for Etoposide after the onset of anaphase I, established by the analysis of chromosome aberrations in Chinese hamster oocytes, has been described before [66]. Also Etoposide sensitivity as a measure for Topoisomerase II activity is cell cycle specific, declining towards the end of M-phase [67]. The decline in sensitivity when meiosis proceeds therefore reflects the reduction of Topoisomerase II activity. The difference in damage induction by Bleomycin for paternal and maternal chromatin is likely attributable to differences in chromatin structure [32].

Zygotes incubated for 1 hour in Etoposide, starting at oocyte activation, showed extensive damage in both paternal and maternal chro-

matin (Figure 3A). Approximately 2 hours later, at the early pronucleus stage, the paternal PN had diminished its γH2AX foci to a lesser extent then the maternal PN (Figure 3B). A Bleomycin pulse induced an average of 5.3 γH2AX foci in paternal and 2.7 –foci in maternal chromatin. The relative reduction at the PN stage was 0.55 for paternal and 0.93 for maternal chromatin (Table 2). This would also indicate a higher repair capacity for the maternal chromatin compared to the paternal chromatin. However, when early zygotes were irradiated in vitro, a higher frequency of chromosome aberrations was found for the maternal complement [31].

Conclusively, we have described the presence of the conserved DNA double stranded break signalling pathway via γH2AX in the mouse zygote. The signalling pathway is already active during male chromatin remodelling in the early stages of fertilisation and reacts dose dependent to DSBs present in the sperm. Both the kinetics of these breaks and of chemically induced DSBs, early after gamete fusion, suggest a quick repair component that is comparable to a G1 somatic cell system. When induction takes place after gamete fusion, female chromatin seems much more repair proficient than male chromatin. The background level of γH2AX foci during male chromatin remodelling in the zygote is strongly increased when compared with a somatic cell system. However, these most likely Topoisomerase II related breaks do not lead to the genesis of chromosome abnormalities at the first cleavage division.

Acknowledgements

We would like to acknowledge, Dr T. Jenuwein (IMP, Vienna, Austria); Dr H. Stunnenberg (Dept. of Molecular Biology, NCMLS, Nijmegen, The Netherlands) for the gift of their antibodies and L. van Bolderen (Dept. of Radiotherapy, Radboud University Nijmegen Medical Centre, The Netherlands) for his help with animal irradiation. Further, we would like to thank Prof. Dr. A.J. van der Kogel (Dept. of Radiation Oncology, Radboud University Nijmegen Medical Centre, The Netherlands) for his helpful discussions. The Dutch ministry of Health, Welfare and Sport, financed this research.

Supplementary data Section 3.1

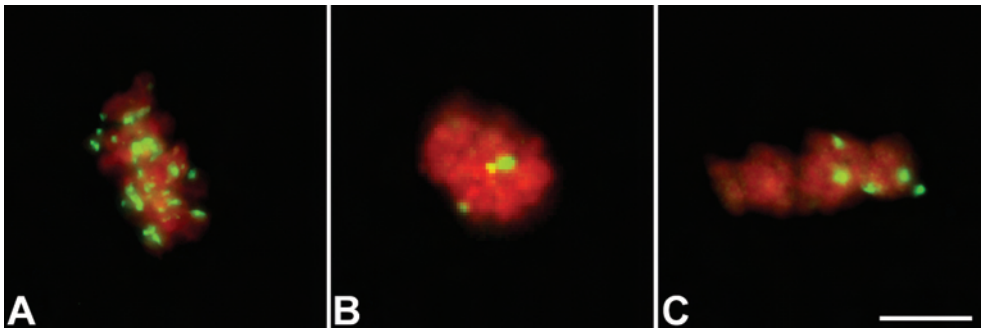

Supplementary Figure 1 Drug treated metaphase II oocytes Cut-outs of metaphase II chromosomes stained with γH2AX (green) and DAPI (red). **(A)** 1 hour 1 μM Etoposide treatment. **(B)** 5 min pulse 0.25 μM Etoposide **(C)** 5 min pulse 750 μU/ml Bleomycin

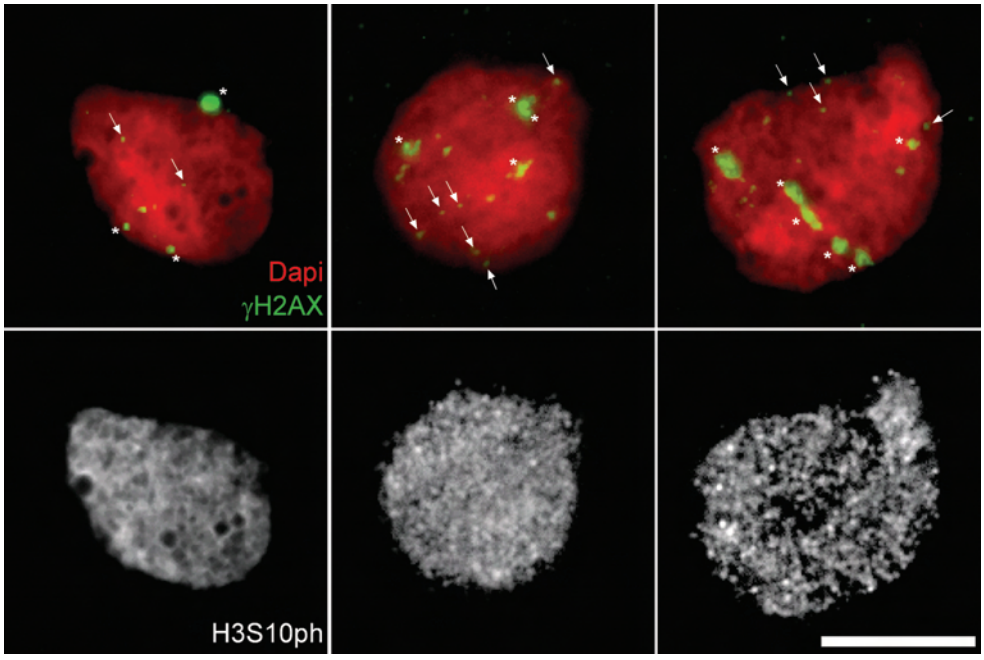

Supplementary Figure 2 Additional images of cut outs of recondensed male chromatin (~80 min post fusion) derived from 3 Gy irradiated sperm. Examples of small γH2AX foci are indicated with an arrow, large γH2AX foci are indicated with an asterisk.

Section 3.2

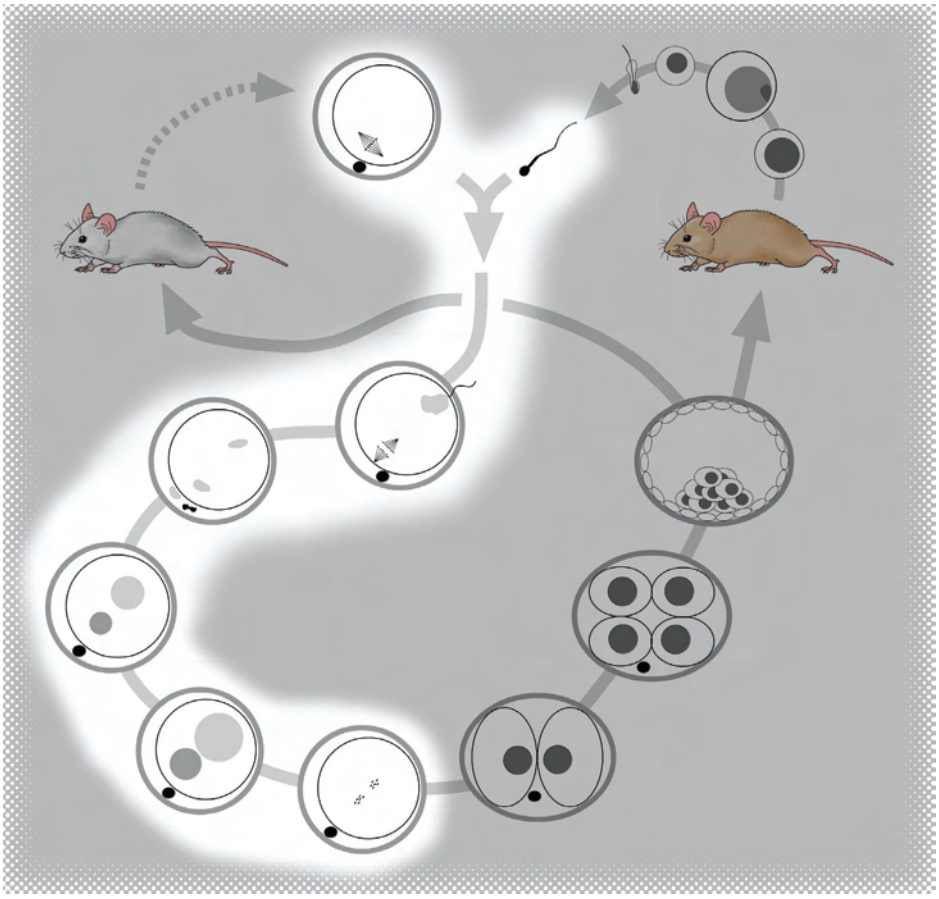

Submitted

DNA double strand break repair in parental chromatin of mouse zygotes

Alwin AHA Derijck[# 1], Godfried W van der Heijden[# 1], Maud Giele[1], Marielle E.P. Philippens[2], Peter de Boer[1]

[#] *Both authors contributed equally*

1 Department of Obstetrics and Gynaecology, Radboud University Nijmegen Medical Centre, PO Box 9101, 6500 HB Nijmegen, The Netherlands

2 Department of Radiation Oncology, Radboud University Nijmegen Medical Centre, PO Box 9101, 6500 HB Nijmegen, The Netherlands

Abstract

In somatic cells, repair of DNA double strand breaks (DSBs) is executed by non homologous end joining (NHEJ) and homologous recombination (HR). Whereas differentiated somatic cells often resolve DSBs by NHEJ, embryonic stem cells use HR as the preferred method for repair. For the understanding of de novo mutation induction in the germline, mechanistic insight on DNA repair during the first mammalian cell cycle, the zygote, is mandatory. This stage of development depends on proteins and mRNAs provided by the oocyte. Using genetic dissection in oocytes, we show NHEJ and HR to be both functional during the zygotic cell cycle. NHEJ is already active during replacement of sperm protamines by nucleosomes. The kinetics of G1 repair is influenced by DNA-PK_{cs} hypomorphic activity. HR and NHEJ are both operative in S-phase, HR being more active in the male pronucleus. DNA-PK_{cs} deficiency upregulates HR activity. Both after sperm remodeling and at first mitosis, spontaneous levels of γH2AX foci (marker for DSBs) are high. Findings are discussed against the background of the high frequency and male origin of reciprocal translocations in man.

Introduction

Both cell functioning and the environment pose threats to the integrity of the genetic information of the cell. A nucleus can be confronted with a variety of potentially genotoxic damages to which an intricate set of DNA repair mechanisms has evolved [1]. A DNA double strand break (DSB) is the most toxic lesion and is mainly repaired by either non homologous end joining (NHEJ) or homologous recombination (HR) [68, 69].
These pathways are not of equal importance during the cell cycle. NHEJ is operational during the whole cell cycle, while HR functions during late S/G2 [57] ensuing the typical radioresistance found during S-phase [70]. DSBs produced by replication stalling are preferably repaired by HR [57, 68, 71].
Additionally, the cell type and developmental stage influence the balance between DSB repair pathways, making HR relatively more important in pluripotent embryonic stem cells and embryonic stages [72]. During adulthood the contribution of HR to the repair of ionizing radiation (IR) induced DSBs is detected when both NHEJ and HR are abrogated [72-74].
Analysis of mutant cell lines is often combined with fluorescence microscopy of the DSB marker γH2AX [3, 10, 11, 55, 57] and of factors involved in repair and cell cycle regulation. Such proteins show specific nuclear localization patterns after damage induction [75] as they relocalize into ionizing radiation induced foci (IRIF) that are implicated in DSB repair. The IRIF forming molecule Rad51, a protein involved in HR, is essential for cellular viability [76, 77]. Rad51 IRIF are mainly associate with a ssDNA microcompartment [75, 78].

During mammalian spermiogenesis DNA repair comes to a halt 2 weeks prior to ejaculation at chromatin remodeling during nuclear elongation, when nucleosomes are replaced by protamins in a stepwise manner [25, 27, 28]. As a consequence, sperm DNA damage is repaired in the zygote after fusion with the oocyte [21, 30, 31].
The zygote has several unique features influencing DNA repair such as: i) lack of transcription coupled translation, hereby relying on mRNAs and proteins stored in the oocyte [15, 16] ii) Topoisomerase II mediated remodeling of sperm derived chromatin resulting in transient DSBs [33, 48, 79] iii) start of the cell cycle after gamete fusion, lacking known checkpoints [80, 81] iv) male and female chromatin

is physically separated and epigenetically dissimilar [32, 35]. Finally, in the genesis of chromosome aberrations (CA), the zygote shows a bias for chromosome type over chromatid type abnormalities [30, 31, 82]. This is illustrated by UV irradiation, solely inducing chromatid type abnormalities in somatic cells [83], whereas chromosome and chromatid type abnormalities were found in the zygote after treatment of sperm [82]. Sperm mutagenised by the alkylating agents MMS and EMS, result in only chromosome type aberrations, strengthening this notion [82]. Chromosome type aberrations point towards NHEJ as the favored repair pathway, a highly active mechanism in zygotes of several model organisms (including mouse) as determined by microinjected DNA fragments [84-86].

As assisted reproductive techniques (ART) are becoming habitual in human reproduction, research on zygotic DNA repair has gained a new perspective. Sperm from sub-fertile males has an increased likelihood to contain DNA damage and poses an increased risk for the induction of de novo CA and maybe other mutations as well [87, 88].

Here we utilize mouse oocytes defective in either NHEJ or HR for the analysis of cell survival, chromosome aberrations, and immunofluorescent signals of γH2AX and Rad51, Brca1 repair proteins to determine the balance between the two DSB repair pathways during the zygotic cell cycle. Special attention is given to the behavior of paternal versus maternal chromatin and to the transmission of γH2AX foci to the 2-cell stage. NHEJ and HR are both active and cell biological features of the zygote uniquely influence DNA repair, determining the fate of damaged sperm DNA in combination with suboptimal oocytes, with implications for the genetic outcome of ART.

Materials and Methods

Mice

Male CBA/B6 F1 (Charles River) mice served as sperm donors. Oocytes came from the following mouse hybrids and strains: B6/CBA F1 (Charles River), C.B17 (Taconic), scid (Charles River), B6.129 and *mRad54*$^{-/-}$*mRad54B*$^{-/-}$. The latter two were bred from heterozygous founder mice kindly provided by Dr R. Kanaar (Department of Cell Biology and Genetics, Erasmus MC, Rotterdam, The Netherlands) [93]. Mice were housed

with adjusted light hours set at 9.00-21.00.

PCR primers genotyping B6.129 and *mRad54*$^{-/-}$*mRad54B*$^{-/-}$ mice
Primers for *mRad54* Wt and KO alleles ; F1-Rad54 (5'-TGGGACATGTAAGATCGTTGG-3'), R1-Rad54 (5'-CAAGTTCCAGGCCATCTAGG-3'), 54KO2 (5'-TTTGCTTCCTCTTGCAAACCA-3'). Primers for *mRad54B* Wt and KO alleles; 54B(F1) (5'-TATGATATCGATTGGAACCCAGCTA-3'),54B-n-(R1)(5'-CACAACTGTCATCCCCAGTG-3'), 54KO2 (5'-TTTGCTTCCTCTTGCAAACCA-3').

Gamete Collection and IVF
Gametes were obtained for in vitro fertilization as described before [79]. Zygotes were cultured in IVF medium [HTF, 0.5% (w/v) BSA] covered with light mineral oil (Irvine Scientific, #9305). Zygotes were transferred to Yamada medium [119] at 5 hours post fusion. For arresting zygotes at first cleavage, Vinblastine-sulphate (Sigma, V-1377) was added to Yamada medium at 0.020 μg/ml. Harvest followed at 20 hours post fusion.

Timing of zygote development
We previously determined [32] that the majority of secondary oocytes was penetrated around 70 min post insemination (pi). The described stages are timed post fusion (pf), hence compensated for this lag phase [79].

Carnoy fixation of chromosome complements and karyotype analysis
Chromosome preparations were made from single zygotes by a variant of the Tarkowski air-dry technique [120] that minimized breakage of chromosome complements. Centric heterochromatin was differentiated by C-banding [121] followed by DAPI staining to distinguish between dicentric chromosomes and acentric fragments. The Y chromosome, the often longer male chromosomes and the supposition that sperm irradiation only induces CA in male derived chromosomes [30] was used in discriminating the two chromosome complements.

PFA based fixation of zygotes
Whole mount preparations for immunofluorescence were made as describe before [79]
For paraformaldehyde fixation of sedimented nuclei and chromosome complements ("PFA spread", Figure 4) the zona pellucida was removed with pronase [HTF-HEPES (Cambrex, BE02-022 F), 0.5% BSA 1% Pronase (NBS Biologicals, 9036-06-0)] and zygotes were placed on a slide

covered by a film of fixative (1% PFA; 0.1 mM DTT; 0.1% Triton-X100, pH 9.2 in milliQ) in a humid container for 30 min. Thereafter slides were air dried, washed twice in 0.08% Photoflow (Kodak), air dried once more and stored at -20°C.

Sperm and zygote DNA damaging treatments

DNA-damaged sperm was generated by whole body irradiation of male CBA/B6 F1 mice 1 day prior to sperm isolation for in vitro fertilization. Zygote irradiation was performed using a custom made mobile thermostated CO_2 incubator. After irradiation, zygotes were returned to a regular incubator. External beam radiation was used, 6-MV photons of an Elekta linear accelerator (Crawley, UK), with a dose-rate of 0.5 Gy/min in doses of up to 3 Gy. The administered dose was verified using TLD (thermo luminescent dosimetry) measurements. Timing of zygote irradiation (pf) is indicated in the figures.

Mitomycin C (Sigma, M-0503) and 4-Nitroquinoline 1-oxide (4NQO) (Sigma, N-8141) were dissolved in culture medium at specified concentration. Zygotes were treated for 1 hour, starting at 3.5 hours pf, washed and placed in a new culture dish.

Antibodies

Mouse anti-γH2AX, 1:10,000 (Upstate #05-636, clone JBW301); rabbit anti-H3S10ph, 1:1,000 (Upstate #06-570); rabbit anti-H3K9me2, 1:500 (Dr T. Jenuwein); rabbit anti-H4K20me3, 1:500 (Dr T. Jenuwein); rabbit anti-hRAD51, 1:1,200 (Dr R. Kanaar); rabbit anti-Brca1(exon 11), 1:250 (Dr CX Deng).

Secondary abs were applied as following: Molecular Probes, Oregon, USA: A11001 fluor 488 goat anti-mouse IgG (H+L), A11012 fluor 594 goat anti-rabbit IgG (H+L), both in a 1:500 dilution.

Immunofluorescence (IF) and foci quantification

Immunofluorescent staining was performed as previously described [79] on whole mount and pfa spread preparations. At the end of chromatin remodeling (80 min pf), as judged by staining with phosphorylated histone H3S10 (H3S10ph), γH2AX foci are present in remodeled nucleosomal male chromatin in two varieties: small, not DSB related and large DSB related. The latter were shown to correlate with sperm IR and treatment of early zygotes with DNA damaging compounds [79]. The male pronucleus (PN) (210 and 285 min pf), is distinguished from the female PN by DAPI morphology and female PN specific histone H3 lysine 9 dimethylation (H3K9me2) [79]. Pericentric heterochromatin stained for histone H4 lysine 20 trimethylation (H4K20me3) specifically labels female chromo-

somes [38]. Quantification of foci was performed on coded samples by one observer.

Collection of images

Images were collected with a Zeiss axioplan fluorescence microscope. Pictures were captured by a Zeiss AxioCam MR camera with Axiovision 3.1 software (Carl Zeiss). All images shown are either a single plane derived from stacks with z-axis intervals of 0.4 μm or deconvoluted projections created with Metamorph software version 6, using the nearest neighbor mode. Photoshop (Adobe) was used for correcting background when necessary.

Statistics

Statistical analysis was performed using Prism (Graphpad) and R 2.3.1 (The R foundation for statistical computing, http://www.r-project.org/) software. Details are indicated in the figure legends.

Results

A maternal effect on misrepair and non-repair of sperm DSBs at the first cleavage division

Historically, the outcome of DSB DNA repair is measured by chromosome analysis. Zygotic DSB repair can therefore be analyzed at the first mitotic cleavage division. To address the relative contributions of the NHEJ and HR pathways in the repair of sperm DSBs, genetic dissection was applied by use of scid and *mRad54*$^{-/-}$*mRad54B*$^{-/-}$ (henceforth *mRad54/54B*$^{-/-}$) oocytes. C.B17 has a similar genetic background as scid and serves as the appropriate control for the scid DNA-PK$_{cs}$ hypomorphic phenotype [89]. The role of HR was addressed by comparison of the HR deficient double mutant *mRad54/54B*$^{-/-}$ with its respective control B6.129. Both mouse stocks were bred from the same founder population.

According to expectation [31], 3 Gy irradiation of cauda epididymal sperm readily induced chromosome-type and a small minority of chromatid-type CA in the paternal chromosome complement at first mitotic division (Sup Figure 1). Zygotes of NHEJ proficient strains show similar radiosensitivities (Table I). Scid zygotes are more frequently affected by a paternal CA (factor 2 – 2.4). The CA frequency is up by a factor 3.5 relative to C.B17. Maternal deficiency for Rad54/54B had little effect on the outcome of repair of sperm DSBs. However, a significant shift towards chromatid type abnormalities was found when compared to scid derived zygotes (Ratio 0.11 Vs 0.45, Table I). These data demonstrate a role for ooplasmic DNA-PK$_{cs}$, hence the NHEJ pathway, in the repair of sperm derived DSBs.

The number of γH2AX positive chromatin domains at sperm chromatin remodeling is affected by the oocyte

After sperm entry in the oocyte, paternal chromatin starts its transit to a nucleosome based state and forms a pronucleus (PN) that enters zygotic S-phase 5-6 hours post fusion (pf) (Figure 1A). DSBs, marked by γH2AX, are frequently found in remodeled paternal chromatin and are more numerous after sperm irradiation [79]. To determine the influences of genetic background and NHEJ on the manifestation of DSBs at chromatin remodeling, cauda epididymal sperm from one genetic background (CBA/B6 F1) was used to fertilize oocytes form 4 different mouse strains. In all strains analyzed,

Table I Chromosome abnormalities at first mitotic cleavage in the male chromosome complement after 3 Gy sperm irradiation

	C.B17	scid	B6.129	*mRad54/54B*$^{-/-}$
% of zygotes with male CA	29.3 (17/58)	69.0[a] (40/58)	31.3 (15/48)	35.9 (38/106)
Fragment freq. (#/n)	0.24 (14/58)	0.88 (51/58)	0.23 (11/48)	0.27 (29/106)
Dicentric freq. (#/n)	0.14 (8/58)	0.48 (28/58)	0.08 (4/48)	0.12 (13/106)
Chromatid gap + fragment freq. (#/n)	0.05 (3/58)	0.16 (9/58)	0.04 (2/48)	0.09 (10/106)
Quadriradial freq. (#/n)	0 (0/58)	0 (0/58)	0.06 (3/48)	0.09 (9/106)
Ratio Chromatid type/Chromosome type	0.14 (3/22)	0.11 (9/79)	0.33 (5/15)	0.45[b] (19/42)

Number of zygotes and aberrations between parentheses.
Statistical analysis Chi square
a $p<0.01$ with all other strains
b $p<0.01$ with scid ratio

γH2AX foci were found in remodeled paternal chromatin, ~80 min pf (Figure 1B/C and Table II). Maternal chromatin showed no DSB related γH2AX foci, as has been reported previously [79]. The average number of γH2AX foci found in remodeled paternal chromatin from control sperm ranged from 0.9 – 3.8 depending on oocyte genotype (Figure 1D and Table II). Oocytes from repair proficient strains (B6/CBA and B6.129) showed similar numbers of γH2AX foci in remodeled paternal chromatin. C.B17 contains a hypomorphic allele for the NHEJ key enzyme DNA-PK$_{cs}$ not found in most commonly used mouse strains (i.e. C57BL/6, DBA) [90]. Functionally, this DNA-PK$_{cs}$ variant acts as a wild-type allele, in contrast to the severely compromised scid DNA-PK$_{cs}$ allele [89]. Both C.B17 and scid, showed an elevated number of DSB related γH2AX foci at sperm chromatin remodeling (Figure 1D and Table II).
Irradiation of cauda epididymal sperm introduces DSBs that are detected by the oocyte [79]. In oocytes from all 4 genotypes a significant increase of γH2AX foci in remodeled paternal chromatin was observed (3 Gy, Figure 1D and Table II). The level of induced foci was highest in scid oocytes with C.B17 reaching an intermediate number (Fig 1D and Table II)

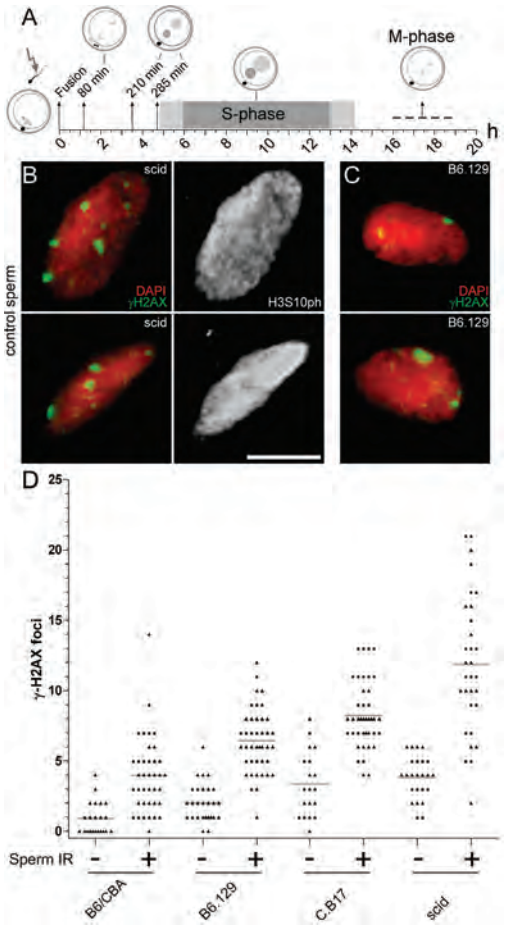

Figure 1 Number of DNA double strand breaks arising during sperm chromatin remodeling is influenced by ooplasm **(A)** Schematic overview zygotic cell cycle. S- and M-phase are indicated (light gray area indicates variation in inter zygotic S-phase timing). Lightning symbol stands for ionizing radiation (IR) used to introduce DSBs in cauda epididymal sperm. **(B)** γH2AX foci (in fully remodeled sperm chromatin (H3S10ph) 80 min pf of CBA/B6 control sperm with scid oocyte. **(C)** γH2AX foci 80 min pf of CBA/B6 control sperm with B6.129 oocyte. **(D)** Quantitative data on γH2AX foci in sperm chromatin 80 min pf. Oocytes from the indicated genetic background were fused with either control or 3 Gy irradiated CBA/B6 sperm. Triangles represents the amount of γH2AX foci in remodeled male chromatin from a single zygote. Horizontal bar indicates mean. Details are listed in Table I. Scale bar: 10 μm. B6/CBA data was taken from [79].

Processing of γH2AX foci during zygotic G1 shows two classes of DSB repair kinetics

In a somatic G1 nucleus repair of DSBs induced by irradiation or chemical treatment can be followed by measuring the number of γH2AX foci at different intervals after DSB induction [10, 11, 55, 57]. Chromatin in a somatic G1 nucleus is rather static compared to the highly dynamic chromatin of pre-S phase zygotes. Both parental chromatin sets mature into a PN capable of entering S-phase. In the B6/CBA hybrid background, processing of γH2AX foci in paternal chromatin derived from (non-)irradiated sperm showed γH2AX kinetics comparable to a somatic G1 nucleus [79]. To address

Table II DSBs measured by γH2AX in remodeled male chromatin 80 min pf of various oocyte genotypes

Oocyte strain	Control sperm		3 Gy IR sperm		Induced – Control
	Mean	S.E.	Mean	S.E.	
B6/CBA	0.9[b,c] (22)	0.25	4.0[a] (38)	0.44	3.1
B6.129	2.0[b] (29)	0.25	6.4[a,d] (42)	0.35	4.4
C.B17	3.4 (19)	0.53	8.2[a,d] (42)	0.37	4.8
Scid	3.8 (25)	0.30	12.0[a,d,e] (31)	0.89	8.2

B6/CBA data was taken from [79].
S.E.= standard error. Number of zygotes between parentheses.
Statistical analysis by Kruskal-Wallis and Dunn's post-test (KWD)
a) $p<0.01$ with respective non-treated control
b) $p<0.01$ with non-treated scid
c) $p<0.01$ with non-treated C.B17
Statistical analysis by ANOVA
d) $p<0.01$ with 3 Gy IR treated B6/CBA
e) $p<0.01$ with 3 Gy IR treated B6.129 and C.B17
Only $p<0.01$ is indicated.

whether differences in CA frequency at first mitotic cleavage (Table I) could be explained by altered G1 repair kinetics, γH2AX foci in early (~210 min pf) and late (~285 min pf) G1 PN were determined. B6/CBA oocytes fertilized with non-irradiated sperm showed a low incidence of DSB related γH2AX foci throughout G1 (male PN, Figure 2C and Table III). The increased frequency of γH2AX foci in remodeled paternal chromatin after fusion with C.B17 and scid oocytes persisted into the early G1 male PN stages (Figure 2A/C and Table III). In addition, at late G1, a significant increase in the number of γH2AX foci was observed in scid zygotes (Figure 2C and Table III). After fusion with 3 Gy irradiated sperm, both B6/CBA and B6.129 showed a reduction in γH2AX foci during G1 (Figure 2B/D and Table III). Although the reduction in number of γH2AX foci is initially faster in the B6/CBA oocytes, both B6/CBA and B6.129 had similar levels of γH2AX foci in late G1 (Figure 2D and Table III). The DNA-PK_{cs} hypomorphic C.B17 and NHEJ deficient scid oocytes showed a reduction in early G1 followed by a significant rise at late G1 (Figure 2D and Table III).
Thus, we were able to distinguish two types of zygotes. One type (B6/CBA and B6.129) was able to reduce γH2AX foci in number by late G1 (~285 min pf). The other type (C.B17 and scid), initially reduced numbers but showed an increase to an equal or higher level

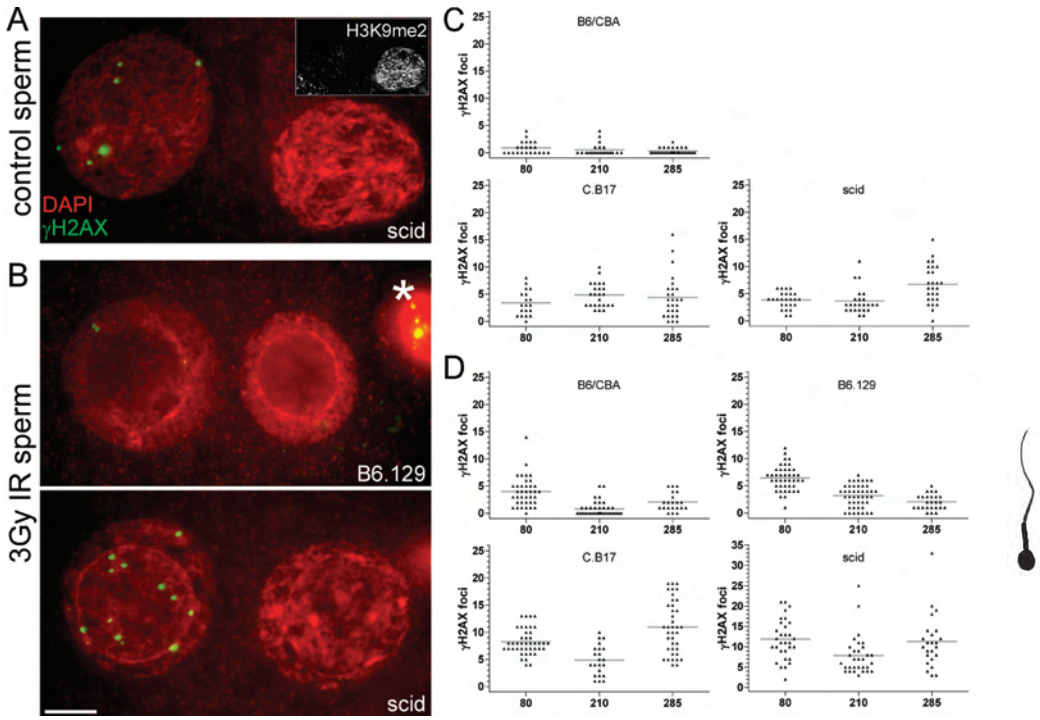

Figure 2 Dynamics of γH2AX foci during zygotic G1 (A) γH2AX foci persist in male chromatin of zygotes derived from scid oocytes at 285 min pf. Male and female PN can be distinguished by DAPI morphology and H3K9me2. Male PN depicted on the left side. **(B)** DNA-PK$_{cs}$ proficient B6.129 zygotes have only few γH2AX foci left at 285 min pf in male PN derived from 3 Gy irradiated sperm. DNA-PK$_{cs}$ deficient scid zygotes have an increased amount of residual γH2AX foci in male PN at 285 min pf. *= second polar body **(C)** Amount of γH2AX foci in male chromatin at 80, 210 and 285 min pf in zygotes derived from control CBA/B6 sperm fused to indicated oocyte strain. **(D)** Same γH2AX kinetics plot for 3 Gy irradiated CBA/B6 sperm. Triangles represents the amount of γH2AX foci in male chromatin from a single zygote. Horizontal bar indicates mean. Details are listed in Table III. Scale bar: 10 μm. 80 and 210 min pf B6/CBA data was taken from [79].

Table III γH2AX foci in paternal pronuclei at G1

Oocyte strain	Control sperm				3 Gy IR sperm			
	210 min pf		285 min pf		210 min pf		285 min pf	
	Mean	S.E.	Mean	S.E.	Mean	S.E.	Mean	S.E.
B6/CBA	0.5 (23)	0.23	0.3 (32)	0.09	0.8[b] (38)	0.21	2.1 (21)	0.36
B6.129					3.2[b] (45)	0.31	2.0[c] (25)	0.28
C.B17	4.8 (24)	0.46	4.4 (27)	0.76	4.9[b] (22)	0.59	11.0[d,e,f] (39)	0.77
Scid	3.6 (24)	0.49	6.7[a] (27)	0.67	7.9[b] (31)	0.86	11.3[d,e,f] (24)	1.33

B6/CBA 210 min pf data was taken from [79]
Number of zygotes between parenthesis
Statistical analysis by ANOVA
a) $p<0.01$ with 210 min pf scid and control sperm
b) $p<0.01$ with 80 min pf (Table 1)
c) $p<0.05$ with 210 min pf
d) $p<0.05$ with 210 min pf
e) $p<0.001$ with B6/CBA and B6.129 at 285 min pf
f) $p<0.001$ with respective control sperm at 285 min pf

when S-phase approached.

The homologous recombination mediating protein Rad51 localizes to male and female chromatin during zygotic S-phase

To determine HR activity during the zygotic cell cycle, localization of one of the key HR proteins, Rad51, was analyzed in control zygotes. In late G1, ample cytoplasmic but little pronuclear Rad51 staining was found (Figure 3A). The male PN starts S-phase prior to the female PN [91]. After the onset of S-phase, bright focal γH2AX staining was visible, coinciding with transfer of Rad51 to the male PN (Figure 3B). When S-phase had progressed, a punctate Rad51 signal was found in both PNs (Figure 3C). The female PN exits S-phase first, showing diminished γH2AX staining. No difference in overall Rad51 staining was found at this stage (Figure 3D). Upon chromosome condensation Rad51 starts to leave the PNs (Figure 3E) and at M-phase was no longer visible, whereas mitotic chromosomes displayed an overall non-focal γH2AX staining (Figure 3F). Zygotes treated with 2 Gy IR during S-phase (8.3 hours pf) were analyzed 1.5 hours post treatment, to investigate whether a functional HR response is present in zygotes. Both Rad51 and Brca1 IRIF were found and showed colocalization with a subset of γH2AX

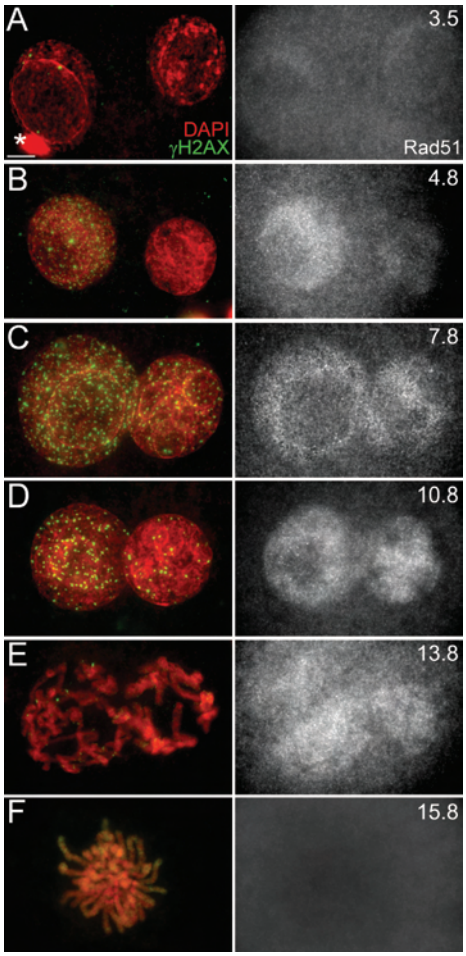

Figure 3 Cell cycle dynamics of γH2AX and the HR protein Rad51 Male PN depicted on the left side. Zygotes are derived from control CBA/B6 sperm fertilizing B6/CBA oocytes. **(A)** 3.5 hours pf. *= non-fertilizing sperm nucleus. **(B)** 4.8 hours pf. **(C)** 7.8 hours pf. **(D)** 10.8 hours pf. **(E)** 13.8 hours pf. **(F)** 15.8 hours pf. Scale bar: 10 μm.

foci, indicative for an active HR response (Sup Figure 2 A/B).

Pronuclear stalling and residual γH2AX foci at first mitotic cleavage as tools to follow DNA repair

Zygotes from B6.126, *mRad54/54B*$^{-/-}$, C.B17 and scid oocytes were treated with either 4NQO or IR and allowed to progress to first mitotic cleavage that was inhibited by Vinblastine (Figure 4A). At 20 hrs pf, PFA spreads, that are suitable for subsequent immunofluorescent staining were made. In these preparations, CA often are unambiguously present (Figure 4D/G/I/J/K) but are not safely quantified (in contrast to acetic acid/methanol spread mitotic chromosomes, Sup Figure 1). Staining of γH2AX depicted a fine punctate chromosome-wide signal on both parental chromosomes as has been reported earlier [51]. Costaining the histone modification H4K20me3 that at this stage is a female heterochromatin marker [38], that allows unambiguous distinction between male and female derived chromosomes (Figure 4B/C). In these preparations, DSB related DNA processing was visible by γH2AX foci (Figure 4 /D/F/G/H). Zygotes that were delayed or blocked in their development showed PNs with high amounts

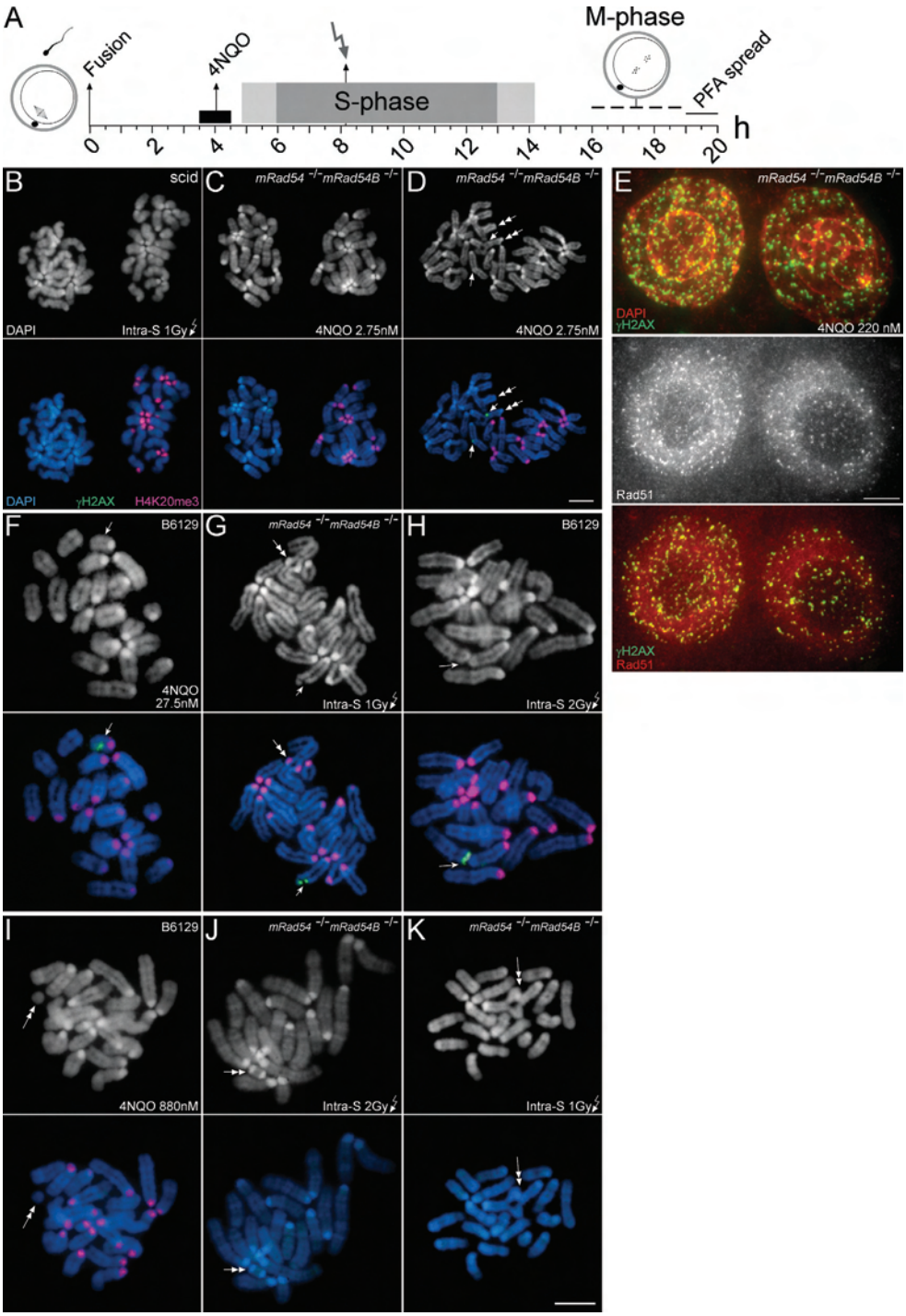
A
Fusion
4NQO
S-phase
M-phase
PFA spread
0
2
4
6
8
10
12
14
16
18
20
h
B
scid
DAPI
Intra-S 1Gy
DAPI
γH2AX
H4K20me3
C
mRad54 -/-mRad54B -/-
4NQO 2.75nM
D
mRad54 -/-mRad54B -/-
4NQO 2.75nM
E
mRad54 -/-mRad54B -/-
DAPI
γH2AX
4NQO 220 nM
Rad51
γH2AX
Rad51
F
B6129
4NQO
27.5nM
G
mRad54 -/-mRad54B -/-
Intra-S 1Gy
H
B6129
Intra-S 2Gy
I
B6129
4NQO 880nM
J
mRad54 -/-mRad54B -/-
Intra-S 2Gy
K
mRad54 -/-mRad54B -/-
Intra-S 1Gy

Figure 4 S-phase DNA damage results in residual γH2AX and stalled PN at first mitotic cleavage (A) Schematic overview zygotic cell cycle with two types of DNA insult: 1 hour 4NQO (or mitomycin C) prior to S-phase and IR during S-phase. "PFA spread" indicates harvest technique (see M and M). (B-K) Zygotes were derived from control CBA/B6 sperm. Oocyte genotypes and treatments are indicated. (B-E) Paternal chromosomes/PN depicted on left side. Maternal pericentric heterochromatin is positive for H4K20me3. Single arrows indicate γH2AX foci, double arrows indicate a CA. **(B-C)** Examples of spreads showing no residual γH2AX foci. **(D)** Example of spread with residual γH2AX foci. **(E)** Stalled PN stained for γH2AX and Rad51. **(F)** Chromatid type γH2AX focus without CA. **(G)** Chromatid type γH2AX focus with chromatid gap. **(H)** Chromosome type γH2AX focus. (I-K) CA's were mainly devoid of γH2AX staining, **(I)** fragment, **(J)** dicentric, **(K)** chromatid quadriradial. Scale bars: 10 μm.

of γH2AX, Rad51 and Brca1 foci (Figure 4E and data not shown). At mitosis, bright γH2AX foci usually were positioned in a single chromatid (Figure 4 D/F). Occasionally, these chromatid foci were found adjacent to a chromatid gap (Figure 4G). At a much lower frequency, isochromatid γH2AX foci that are at seemingly homologous locations on single chromosomes, depict chromosome-type lesions (Figure 4H). Usually the chromosome abnormalities found in these preparations were not associated with γH2AX foci (Figure 4 D/G/I/J/K).

Figure 5 gives the mitotic γH2AX foci data, including the effect of sperm irradiation as an extra comparison. Mitotic index data are presented as well. Statistical differences are given in Table IV. The background frequency of γH2AX foci at first mitotic cleavage was higher in B6.129 and *mRad54/54B*$^{-/-}$ zygotes compared to C.B17 and scid zygotes.

C.B17 and scid zygotes derived from 3 Gy irradiated sperm showed a reduction in mitotic index (Figure 5A and Table IV). Mitotic chromosomes of male descent were characterized by an increased frequency of chromatid type γH2AX foci, especially for C.B17 (Figure 5B). B6.129 and *mRad54/54B*$^{-/-}$ oocytes fertilized with 3 Gy irradiated sperm neither showed a reduction in mitotic index, nor an effect on the frequency of persisting γH2AX foci (Table IV and Figure 5B).

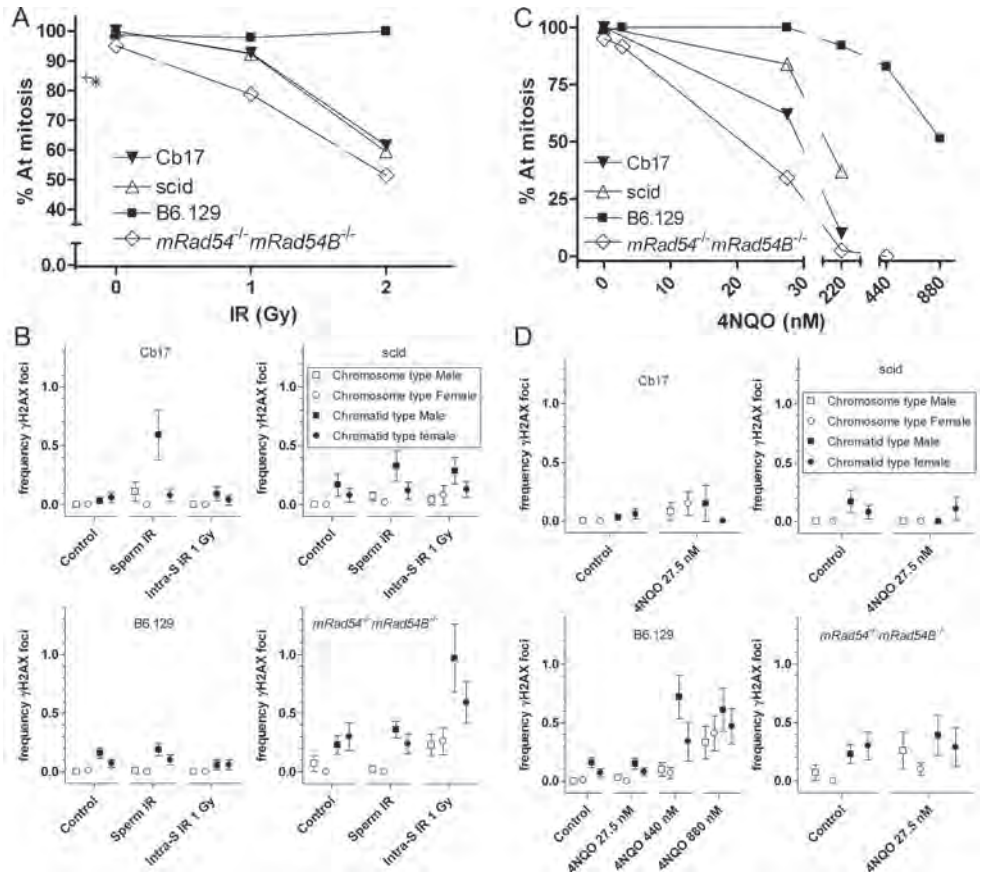

Figure 5 Maternal effects on zygotic DNA repair initiated by pre-S-phase and S-phase DNA damage (A) Survival curves expressing the percentage of zygotes at first mitotic cleavage after IR during S-phase. + and * indicate mitotic index of zygotes derived from 3 Gy IR treated sperm fused with C.B17 and scid oocytes respectively. **(B)** Plots of the frequencies of chromosome and chromatid type γH2AX foci at first mitotic cleavage in male and female derived chromosomes after IR of sperm (3 Gy) or S-phase (1 Gy), oocyte genotype indicated. **(C)** Similar curves for 4NQO. **(D)** Similar to B for 4NQO. Standard error is plotted. Details are listed in Table IV and Sup Table I.

Table IV Mitotic indexes of zygotes after sperm/S-phase irradiation and 4NQO pre-S-phase treatment

	C.B17	Scid	B6.129	*mRad54/54B*$^{-/-}$
Control	100 (38/38)	100 (24/24)	98.7 (75/76)	95.1 (39/41)
Sperm IR				
3 Gy	84.4[a] (27/32)	83.0[a] (44/53)	100 (71/71)	100 (46/46)
Intra-S IR				
1 Gy	92.6 (25/27)	92.3 (24/26)	97.8 (45/46)	78.7[b] (48/61)
2 Gy	61.5 (59/96)	59.4 (38/64)	100[c] (33/33)	51.5 (51/99)
4NQO treatment in nM				
2.75	-	-	100 (15/15)	91.7 (22/24)
27.5	61.9 (13/21)	84.0 (21/25)	100[*] (60/60)	34.4[d,c] (33/96)
220	10.0[f] (2/20)	37.0 (10/27)	92.0[*] (23/25)	2.6[d] (2/78)
440	-	-	82.9[*] (29/35)	0 (0/21)
880	-	-	51.4 (18/35)	-
MMC treatment in µM [ug/ml]				
1 [0.33]	97.2 (35/36)	-	100 (8/8)	94.1 (16/17)

Number of zygotes between parentheses.

Statistical analysis Chi square

a) $p<0.01$ with B6.219 and *mRad54/54B*$^{-/-}$

b) $p<0.01$ with B6.129

c) $p<0.01$ with all other strains

d) $p<0.01$ with scid

e) $p<0.05$ with C.B17

f) C.B17 and scid at 220 nM 4NQO, $p=0.078$

After 1 Gy irradiation of zygotes during mid-S phase (~8.3 hours pf, Figure 4A) a significant reduction in mitotic index was found for *mRad54/54B*$^{-/-}$ zygotes compared to B6.129. No significant reduction was found for either C.B17 or scid zygotes (Figure 5A, Table IV). A dose of 2 Gy reduced the mitotic index of C.B17, scid and *mRad54/54B*$^{-/-}$ zygotes alike. (Figure 5A, Table IV). In B6.129 zygotes this effect was not found. Persisting focal DNA damage at first mitotic cleavage was analyzed for 1 Gy irradiated zygotes as a high mitotic index reduces the possibility of selection for non-damaged cells. After 1 Gy, both C.B17 and B6.129 zygotes showed no effect (Figure 5B). For scid zygotes, a minor effect was observed, mainly for chromatid type foci in male derived chromosomes. The HR deficient *mRad54/54B*$^{-/-}$ zygotes showed a distinct increase in frequency of both chromosome and chromatid type γH2AX foci, especially in paternal but also in maternal chromosomes (Figure 5B).

HR deficient zygotes are highly sensitive to 4-nitroquinoline 1-oxide (4NQO)

To further determine the importance of HR for zygote development, two genotoxic compounds were used. The first one, mitomycin C (MMC) [92], introduces interstrand cross-links that are mainly repaired by HR [93] (Figure 4A). At a dose that induced 55 – 65 % cell death in ES cells of this genotype [93], MMC treated *mRad54/54B*$^{-/-}$ zygotes did not show any sensitivity as measured by mitotic index at first cleavage division (Table IV).

Topoisomerase I mediates DNA replication by reducing torsion of the double helix. Topoisomerase I linked single strand DNA breaks are short lived catalytic intermediates commonly referred to as TopoI cleavage complexes (TopIcc). DNA damage, like ssDNA breaks, base adducts and UV photoproducts, can stabilize TopIcc and generate DSBs at replication forks ([94] and references herein). HR plays an important role in repair of replication fork associated DSBs [71]. DNA damage generated by 4NQO partially mimics UV induced damage and both agents stabilize TopIcc [95, 96].

B6.129 derived zygotes are capable of coping with 4NQO type damage only showing a reduced mitotic index in the higher nM range (440-880 nM) (Figure 5C and Table IV). At these concentrations a distinct induction of chromatid type (440 and 880 nM) and chromosome type (880 nM) γH2AX foci was observed in paternally and maternally derived chromosomes (Figure 5D). At dose levels of 27.5 and 220 nM, *mRad54/54B*$^{-/-}$, C.B17 and scid derived zygotes showed a reduction in mitotic index. HR deficient zygotes were most severely affected with hardly any zygotes progressing to first mitotic division (Figure 5C and Table IV). Both dose levels produced the same trend in sensitivity as determined by mitotic index at first cleavage: *mRad54/54B*$^{-/-}$ > C.B17 > scid > B6.129. (confirmed by trend in proportions test) (Figure 5C and Table IV). 4NQO is able to induce chromosome- and chromatid-type γH2AX foci at first mitotic cleavage as found in B6.129 cells after high nM treatment (Figure 5D). At 27.5 nM a small effect on the frequency of foci at first mitotic division was found for C.B17 and *mRad54/54B*$^{-/-}$, the latter showing a greater induction of especially chromosome type foci (Figure 5D).

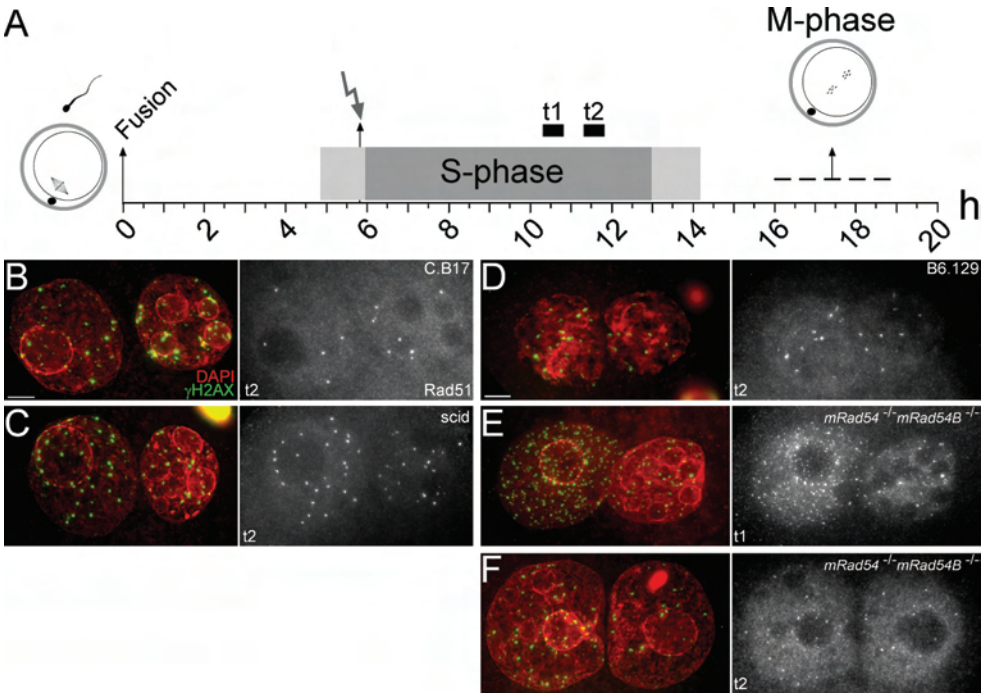

Figure 6 Irradiation of zygotes at the onset of S-phase results in residual Rad51 foci at late S (A) Schematic overview zygotic cell cycle with 2 Gy irradiation and t1 and t2 fixation times. **(B-F)** Rad51 foci level in zygotes derived from indicated genotype showing effect of HR and time of harvest. Male PN on left side. Scale bar: 10 μm.

Persistence of Rad51 foci after irradiation at the onset of S-phase

In the previous sections, we observed zygotic S-phase to play an important role in the repair of newly formed DNA damage in the zygote. Effects for both NHEJ and HR were found.

To address the balance between NHEJ and HR, zygotes derived from oocytes of both repair deficient genotypes and their controls were irradiated with 2 Gy at early S-phase (~5.8 hours pf) and Rad51 foci were counted at the end of S-phase (t1: ~10.3-10.8, t2: 11.3-11.8 hours pf) (Figure 6A). C.B17, scid and B6.129 showed no statistical difference in Rad51 foci between time points and data were pooled. When comparing residual Rad51 foci in C.B17 (Figure 6B) with scid (Figure 6C) a significant increase was found for both paternal and maternal PN of the latter (Figure 7 and Table V). B6.129 zygotes

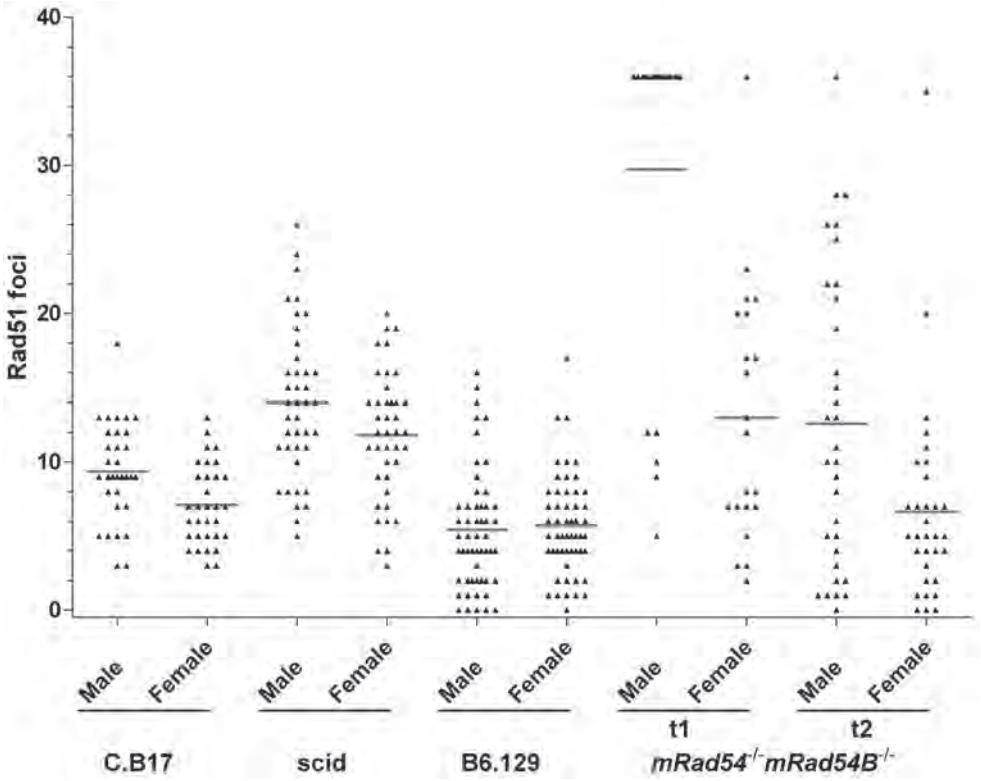

Figure 7 Residual Rad51 foci after 2 Gy irradiation at the onset of S-phase Triangles represent the number of Rad51 foci in a single PN from male or female origin. Horizontal bar indicates mean. Details listed in Table V.

showed a lower level of Rad51 foci and no difference between male and female PN (Figure 6D, Figure 7, Figure 8 and Table V). Zygotes derived from *mRad54/54B*$^{-/-}$ oocytes showed a clear difference between the two time points. At t1, the male PN contained a very high number of Rad51 foci (Figure 6E, Figure 7 and Table V) but also in the female PN, the amount of Rad51 foci was elevated. One hour later, in the female PN, Rad51 levels had returned to the control value. In the male PN, Rad51 levels remained elevated (Figure 6F, Figure 7 and Table V).

The ratio of Rad51 foci between male en female PN gives an indication of the difference in repair capacity of both pronuclei. Because the average M/F ratio was above 1 in all strains (Figure 8 and Table VI) we determined the number of zygotes with an amount of Rad51

Table V Residual Rad51 foci 5 – 6 hr after 2 Gy IR at onset of S-phase

Oocyte strain	Male		Female		Total	
	Mean	S.E.	Mean	S.E.	Mean	S.E.
C.B17	9.4 (32)	0.59	7.1 (32)	0.48	16.8 (35)	0.66
scid	14.0[a] (40)	0.81	11.8[a] (40)	0.68	25.6[b] (43)	1.18
B6.129	5.4[c] (55)	0.54	5.7[d] (55)	0.48	12.0[c] (65)	1.00
mRad54/54B$^{-/-}$ t1	>30[e,f] (21)	n/a	13.0[g] (21)	1.87	>40[e,f] (23)	n/a
mRad54/54B$^{-/-}$ t2	12.8[h] (32)	1.90	6.6 (32)	1.20	19.8[i] (40)	2.04

Statistical analysis by ANOVA
a) p<0.001) with C.B17
b) p<0.05) with C.B17
c) p<0.01) with C.B17 and scid
d) p<0.001) with scid
Statistical analysis by KWD
e) p<0.001 with B6.129
f) High number of foci, prevented accurate counting. Cut-off at 35 foci was chosen and used for statistics.
g) p<0.05 with B6.129
h) p<0.05 with B6.129
i) p<0.05) with B6.129

foci in the male PN equal or higher than in the female one (Table VI). The repair proficient B6.129 derived zygotes showed an equal distribution of residual Rad51 foci between male and female PN (Table VI). C.B17 had a slight increase in the number of zygotes with a higher residual number of male Rad51 foci (Table VI). This effect increased in the order scid, *mRad54/54B*$^{-/-}$. The analysis shows that a repair deficient ooplasm more severely affects the male PN then the female PN.

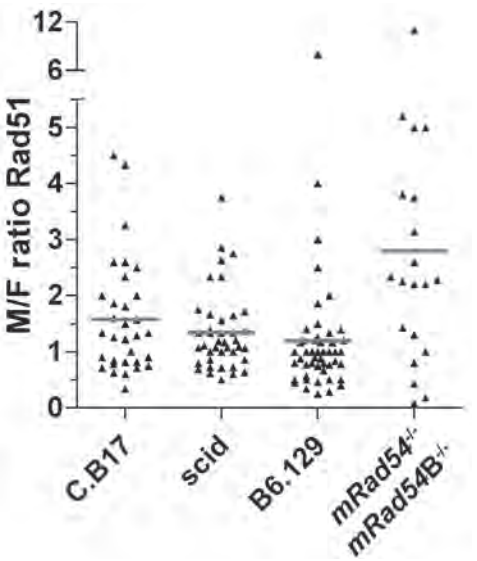

Figure 8 Ratio between male and female residual Rad51 foci after 2 Gy irradiation at the onset of S-phase Triangles represent the ratio between male and female Rad51 foci in a single zygote. Horizontal bar indicates mean. Details listed in Table VI.

Table VI Male-Female ratio analysis of residual Rad51 foci 5 – 6 hr after 2 Gy IR at onset of S-phase

	Average ratio	SD	Ratio lower then 1	Ratio equal to or higher then 1	Ratio equal to 1
C.B17	1.6 (32)	0.18	37.5% (12/32)	62.5% (20/32)	9.4% (3/32)
Scid	1.3 (40)	0.11	27.5% (11/40)	72.5% (29/40)[c,e]	2.5% (1/40)
B6.129	1.2 (51)	0.16	49.0% (27/55)	51.0% (28/55)	20% (11/55)
mRad54/54B$^{-/-}$ t2[a]	3.7[b] (25)	1.11	18.7 (6/32)	81.3 (26/32)[d,f]	3.1% (1/32)

Number of zygotes indicated between parentheses.

a) Only t2 was used for ratio analysis due to the uncountable number of Rad51 foci in male PN at t1.

b) $p<0.05$ with scid and $p<0.001$ B6.129 by KWD

c) $p=0.056$ with B6.129 by Chi square

d) $p<0.01$ with B6.129 by Chi square

e) Deviant from 1:1 ratio $p=0.066$ by Chi square

f) Deviant from 1:1 ratio $p<0.05$ by Chi square

Discussion

Sperm derived DSBs are mainly restored by NHEJ

The analysis of zygote chromosomes derived from 3 Gy irradiated sperm shows an increase in chromosome type aberrations after fertilization of scid oocytes. The scid maternal effect was found both at the level of the affected percentage of zygotes (2.4 fold) and the frequency of aberrations (3.5 fold) (Table I). The NHEJ proficient strains, C.B17, B6.129 and *mRad54/54B*$^{-/-}$ showed similar rates of chromosome type abnormalities. Therefore, DNA-PK$_{cs}$ stored in the oocyte plays an important role in the repair of sperm DSBs after the onset of fertilization. When comparing γH2AX foci in remodeled male chromatin with those in the early male PN, zygotes with a maternal wildtype DNA.PK$_{cs}$ allele showed a relative reduction of 0.5-0.8. Both C.B17 and scid derived zygotes showed impaired kinetics, with a reduction of 0.3-0.4. The G1 foci kinetics in wildtype and DNA-PK$_{cs}$ deficient zygotes resembles that of somatic G1 cell counterparts [10, 11, 55, 57] (see Sup Table II). C.B17 is exceptional in that it is different from scid in somatic cells [89] but not so much in zygotes. C.B17 contains a hypomorphic variant of the DNA-PK$_{cs}$ gene, *Prkdc* [90]. This hypomorphic allele does not severely affect DSB repair [89, 97]. Therefore the similarity in γH2AX foci kinetics suggests that repair during chromatin remodeling and early PN development is sensitive for variation in DNA-PK$_{cs}$ activity. However, the hypomorphic allele has no long term effect on genetic stability as shown by chromosome analysis of C.B17 derived zygotes (Table I). Zygotes derived from either C.B17 or scid oocytes fused with 3 Gy irradiated sperm show a reduction in mitotic index (Figure 5A and Table IV) and an increase in residual γH2AX foci at first mitotic cleavage (Figure 5B and Sup Table I). The kinetics of γH2AX foci in zygotic G1 combined with mitotic index reduction and residual γH2AX foci at first mitotic cleavage suggest that DNA-PK$_{cs}$ mediated repair of sperm derived DNA damage continues during S-phase.

The ooplasm effects the fidelity of sperm chromatin remodeling and interacts with sperm DNA damage

A dose response relation between IR treatment of cauda epididymal sperm and γH2AX foci at chromatin remodeling post gamete fusion has been described before [79]. Here we show that the source of the ooplasm influences the level of γH2AX foci found after chro-

matin remodeling (Table II). IR treatment [55] and fertilization [98] are stochastic events. 3 Gy IR treatment of sperm from different males of the same CBA/B6 hybrid would therefore theoretically result in a comparable increase in the number of γH2AX foci found at sperm chromatin remodeling in repeated fertilization experiments. In scid oocytes the difference between control and induced numbers of γH2AX foci is high compared to the other strains (Table II). This suggests that in the absence of DNA-$PK_{cs,}$ IR induced DNA damage in sperm interferes with chromatin remodeling. A role for DNA-PK_{cs} in safeguarding DNA integrity during the topological changes necessary to facilitate the protamine to histone transition is implied. Conclusively, there is a maternal effect on the level of DSBs as measured by γH2AX focus formation at the end of male chromatin remodeling.

Spontaneous DSBs during G1 PN development

Radiosensitivity of zygotes increases to the pronuclear stage with highest sensitivity in G1 PN. [99, 100]. For instance, BALB/c zygotes irradiated at this stage have peak sensitivity for first cleavage failure [99]. We observed an increase in male γH2AX foci at the G1 – S transition in zygotes from scid oocytes and non-irradiated sperm (Figure 2C and Table III). Repair proficient zygotes derived from 3 Gy irradiated sperm show a reduction in γH2AX foci from 80 min pf to early G1 with comparable kinetics to IR treated G1 somatic cells [10, 11, 55, 57 and Sup Table II]. However, in C.B17 and scid zygotes at late G1 a rise was observed (Figure 2D and Table III). This would argue for the intrinsic formation of DSBs during maturation of the male PN. This propensity of the male PN during late G1 to form DSBs might be related to the radiosensitivity described for this stage of development. The male PN undergoes active DNA demethylation prior to DNA replication, resulting in asymmetrical 5-MeC staining in late G1 zygotes [101]. In *Xenopus* oocytes, active DNA demethylation is catalyzed by the Nucleotide Excision Repair (NER) endonuclease XPG in conjunction with Gadd45a [102]. The NER pathway is present in mouse oocytes [20] and induces a non-focal diffuse γH2AX signaling [103]. This opens the possibility that the induction of γH2AX foci during G1 is related to DNA demethylation involving single strand DNA breaks and mainly manifests in a DNA-PK_{cs} hypomorphic background. Unfortunately, the S-phase

related γH2AX signal conceals the fate of residual G1 γH2AX foci (Figure 3B/C) in validating the previously suggested use of γH2AX for repair measurements during S-phase of somatic nuclei [57]. Systematic DSBs from sperm origin can be tolerated by the male PN until the collapse of chromatin at the onset of replication [104].

S-phase coincides with pronuclear γH2AX and Rad51 staining

The first cell cycle of life like somatic cell cycles shows an S-phase specific γH2AX and Rad51 pattern but with a temporal difference between male and female chromatin [105-107]. The onset of S-phase is earlier in the male PN [91] and coincides with γH2AX and Rad51 staining (Figure 3B). During the progression of S-phase, bright γH2AX and Rad51 foci become conspicuous (Figure 3C). The end of S-phase is reached first in the female pronucleus [91], which was reflected by disappearance of γH2AX signals.

Unrepaired DNA damage likely persists to next stages of preimplantation development

IR induced DSBs in condensed chromosomes are marked by γH2AX in unfertilized oocytes and somatic cells [79, 108]. Such γH2AX foci have been found on chromosomal fragments and in intact metaphase chromosomes [108]. In addition, γH2AX foci have been observed on metaphase chromosomes at fragile sites after replication stress [109]. Here we found mitotic γH2AX foci, that were in majority of the chromatid type on usually intact chromosomes. This indicates the processing of replication mediated DSBs at this stage. Somatic cells irradiated in S/G2 have been shown to progress through mitosis, with γH2AX foci located at ends of chromosome fragments [57]. Hence, in the zygote, these foci will likely persist to the 2-cell stage, with chances for de novo mutation.

NHEJ and HR function in response to DSBs after IR and replication stalling

Radioresistance during S-phase is attributed to HR repair [70] and, like somatic cells, zygotes show a decrease in radiosensitivity during S-phase [99, 100]. The radioresistant nature of zygotes during S-phase was clearly demonstrated in B6.129, showing no reduction in mitotic index after 2 Gy (Figure 5A and Table IV). At this stage, both Rad51

and Brca1 show clear IRIF that partially colocalize with γH2AX, indicative for active repair of DSBs by HR after IR treatment during S-phase (Sup Figure 2). Further evidence for a functional role of HR in S-phase radioresistance is provided by a reduced mitotic index of *mRad54/54B*$^{-/-}$ zygotes after 1 and 2 Gy IR (Figure 5A and Table IV). Analysis of Rad51 foci at the end of S-phase, induced by 2 Gy IR at its onset, confirmed that both NHEJ and HR play a role in DSB repair as the number of Rad51 foci is influenced by deficiencies in both repair pathways (Figure 7 and Table V). When we attribute the stronger increase in Rad51 foci for scid relative to C.B17 to a greater activity of HR (that supposedly is better induced with lower NHEJ performance), the reported compensating interplay between NHEJ and HR [57, 110, 111] also exist in zygotes. The contribution of NHEJ after IR in mid-S-phase maybe lower, as a clear reduction of mitotic index was not found at 1 Gy IR (Figure 5A and Table IV). An increase in the frequency of γH2AX foci at first mitotic cleavage is especially clear in irradiated *mRad54/54B*$^{-/-}$ zygotes (Figure 5B). The lack of sensitivity of *mRad54/54B*$^{-/-}$ zygotes for mitomycin C (Table IV) was unexpected and needs further investigation. Conclusively, both NHEJ and HR protect the zygotic genome of IR damage at S-phase and strengthen the results found by injection of DNA substrates that have underscored the importance of HR for the zygote [86].

DNA damage generated by 4NQO partially mimics UV induced damage and results in chromatid type CA [83]. DSBs at replication forks are produced [94, 96]. Cells defective for RecQ helicases (like Werner and Bloom syndrome proteins), enzymes facilitating replisome progression and re-initiation of replication after replication-fork demise [112], are sensitive for 4NQO [113-115]. This sensitivity manifests in reduced survival after prolonged exposure to 260-300 nM [114, 115] or 1 hour at 525 nM 4NQO [113]. Here we find that DSB repair compromised zygotes are very sensitive to 4NQO (Figure 5C/D and Table IV). The repair proficient B6.129 zygote showed a reduced mitotic index at 440 nM 4NQO followed by the presence of residual γH2AX foci at mitotic cleavage (Figure 5C/D and Table IV). HR deficient zygotes were unable to cope with 4NQO dose levels above 27.5 nM, indicative for the crucial role of HR in the repair of these lesions (Figure 5A and Table IV). Quadriradials are typical for

RecQ defective cells [116]. HR deficient zygotes already displayed this CA at a dose of 2.75 nM (approximately 20% of the male chromosome complements affected, data not shown). Up to 5 quadriradials could be observed per male haploid set. By segregation at mitosis, these quadriradials can resolve as a reciprocal translocations in one daughter blastomere. In contrast to B6.129 zygotes, both DNA. PK_{cs} hypomorphic C.B17 and NHEJ deficient scid are sensitive to 4NQO, C.B17 more than scid (Figure 5C/D and Table IV). Thus, better survival for scid compared to C.B17 (Figure 5C) suggests improved induction of HR, as was already found after irradiation (Figure 7 and Table V). Possibly, a combination of partial impairment of NHEJ and insufficient compensatory HR activity in C.B17 governs the enhanced sensitivity for 4NQO compared to scid. Indications for an interplay between NHEJ and HR in the zygote translating into the probability of expanded simple tandem repeat mutations later in life were found by us before [117].
Conclusively, the data show that zygotic S-phase is extremely sensitive for replication fork demise and highly relies on HR to resolve such damage.

Male and female DNA damage related differences and S-phase in the genesis of de novo chromosome translocations

A number of observations made in this study point at a difference between male and female chromosome complements in attracting DNA damage at the onset of life:
a) Extending on our earlier observations [79], we compared γH2AX foci at male chromatin remodeling with the number of residual breaks (calculated from fragments (1 break) and dicentrics (2 breaks)) at first cleavage division (Figure 9). A very tight association was observed.
b) Whether derived from non-irradiated or 3 Gy irradiated sperm, γH2AX foci during G1 were only found in the male PN. Residual γH2AX foci at first mitotic cleavage originating from S-phase irradiation and pre-S-phase 4NQO treatment were also more often found in paternal chromosomes (Figure 5B/D).
c) In repair deficient zygotes, radiation induced residual Rad51 foci at late S-phase were generally higher in the male PN (Figure 8 and Table VI). A skewed M/F ratio can be explained by the existence of a subset of oocytes that has difficulties in handling male DNA

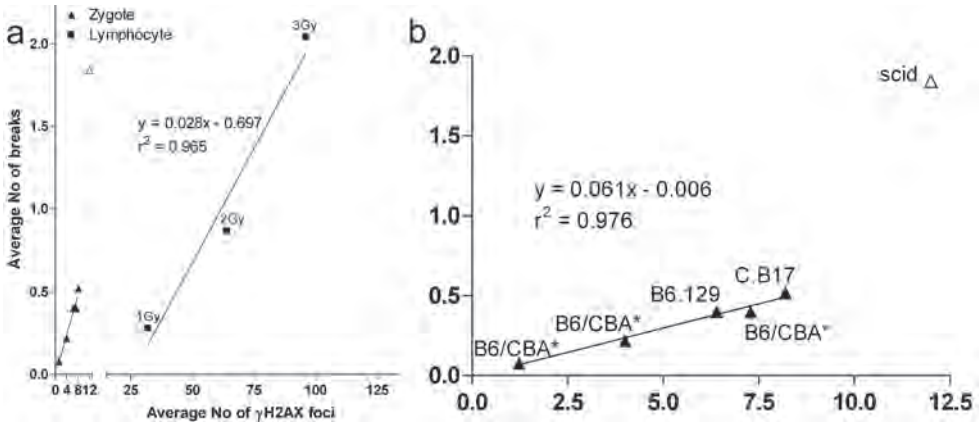

Figure 9 Comparison of γH2AX foci with number of breaks at mitosis Number of breaks were calculated from fragments (one break) and dicentrics (two breaks). **(A)** γH2AX foci in recondensing male chromatin (zygote) and G1 somatic nuclei (generally accepted induction 1Gy = 32 foci) were plotted against No of breaks at first cleavage division (zygote) or mitosis (mouse lymphocytes). Mouse lymphocyte data taken from [122]. Linear regression was performed on both data sets. Regression coefficients suggest that a γH2AX focus in recondensing male chromatin is approximately two times more likely to result in a lasting chromosome type abnormality compared to mouse lymphocytes **(B)** Blowup of zygotic dataset. (*) B6/CBA γH2AX foci data was taken from [79], No of breaks were taken from [30]. Linear regression indicates that γH2AX foci in recondensing male chromatin have predictive value for the amount of lasting chromosome type abnormalities at first cleavage division.

damage at this stage of the cell cycle.
d) Quadriradial induction at an ultra-low 4NQO dose in male pronuclei of HR compromised zygotes indicates that reciprocal translocations can efficiently be induced by replication stalling, shedding a different light on the translocation induction found in certain forms of ART [87]. At first cleavage, chromatid exchanges potentially segregate into a reciprocal translocation in one of two blastomeres. An 4-10 times increase (depending on the assumed spontaneous de novo rate of appearance) of reciprocal translocation carriers was observed when a large cohort of ICSI pregnancies was followed by amniocentesis [87]. Support for their emergence at S-phase is provided by the variance in length of the first cell cycle, with longer cycles related to

a lower chance of pregnancy [118], that is observed in IVF clinics the world over.

The data presented and discussed here promote insight into the relation between the fist cell cycle and mutation induction via the characteristics of DSB repair at the onset of mouse development, highlighting the role of stalled replication fork management in especially the male pronucleus.

Acknowledgements

We first would like to thank Dr R. Kanaar (Erasmus MC, Rotterdam, The Netherlands) for founder mRad54$^{-/-}$ and *mRad54B*$^{-/-}$ ko mice and the Rad51 antibody.
We would like to acknowledge, Dr T. Jenuwein (IMP, Vienna, Austria), Dr H. Stunnenberg (NCMLS, The Netherlands) and Dr C.X. Deng (National Institutes of Health, Bethesda, USA) for the gift of antibodies; L. van Bolderen (Radboud University Nijmegen MC, The Netherlands) for animal and zygote irradiation; T. Arnoldussen, J. Evers and G. Toenders (Radboud University Nijmegen MC, The Netherlands) for developing the custom incubator for zygote irradiation; P. Borst (Wageningen University, The Netherlands) and E. Commandeur (Tilburg University, The Netherlands) for help with statistics. Dr J. Essers (Erasmus MC, Rotterdam, The Netherlands) and Dr A.H.F.M. Peters (FMI, Basel, Switzerland) are thanked for helpful comments on the manuscript. The Dutch ministry of Health, Welfare and Sport and the EU financed this research.

Supplementary Data Section 3.2

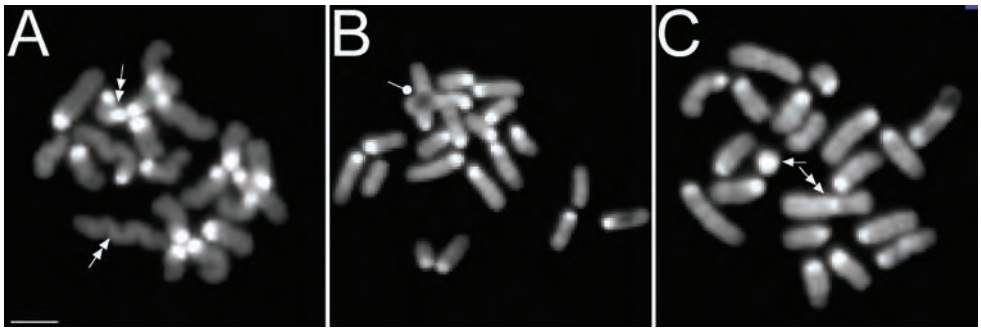

Sup Figure 1 Paternal chromosomal aberrations derived from 3 Gy irradiated sperm at first mitotic cleavage (A) Dicentric and acentric fragment (double arrow) in scid derived zygote. **(B)** Chromatid exchange (quadriradial, ball on stick) in *mRad54/54B*$^{-/-}$ derived zygote. **(C)** Dicentric and fragment in *mRad54/54B*$^{-/-}$ derived zygote.

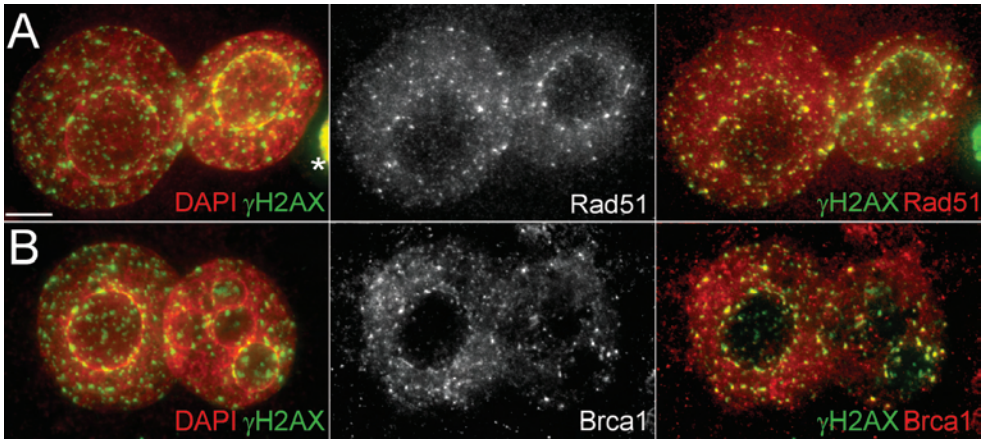

Sup Figure 2 Repair proteins 1.5 hours after 2 Gy irradiation during S-phase Zygotes derived from control CBA/B6 sperm fertilizing B6.129 oocytes were irradiated at 8.3 hours pf. Co-stain for (A) Rad51 (B) Brca1. *= second polar body. Scale bars: 10 μm.

Sup Table I Frequency of residual γH2AX foci at first mitotic cleavage

		Chromosome foci					***Chromatid foci***					
		% damaged nuclei			Frequency		% damaged nuclei			Frequency		
		None	Male	Female	Male	Female	None	Male	Female	Male	Female	n
Control												
C.B17		100	0	0	0	0	90.9	3.0	6.1	0.03	0.06	33
Scid		100	0	0	0	0	83.3	12.5	8.3	0.17	0.08	24
B6.129		98.7	0	1.3	0	0.01	78.7	16.0	5.3	0.16	0.07	75
mRad54$^{-/-}$ *mRad54B*$^{-/-}$		96.7	3.3	0	0.07	0	66.7	23.3	23.3	0.23	0.30	30
3 Gy Sperm IR												
C.B17		92.3	7.7	0	0.11	0	57.7	38.5^{b}	7.7	0.59^{a}	0.08	26
Scid		92.7	4.9	2.4	0.07	0.02	82.9	17.1	7.3	0.33	0.12	41
B6.129		98.5	1.5	0	0.01	0	74.6	17.9	9.0	0.19	0.10	67
mRad54$^{-/-}$ *mRad54B*$^{-/-}$		97.8	2.2	0	0.02	0	55.6	35.6	20.0	0.36	0.24	45
Intra-S IR (Gy)												
C.B17	1	100	0	0	0	0	91.3	8.7	4.3	0.09	0.04	23
Scid	1	91.7	4.2	4.2	0.04	0.08	66.7	25.0	12.5	0.29	0.13	24
B6.129	1	100	0	0	0	0	87.9	6.1	6.1	0.06	0.06	33
mRad54$^{-/-}$ *mRad54B*$^{-/-}$	1	76.9	15.4	15.4	0.23	0.26^{a}	38.5	48.7^{c}	30.8	0.97^{a}	0.59	39
4NQO treatment (nM)												
C.B17	27.5	76.9	7.7	15.4	0.08	0.15^{a}	92.3	7.7	0	0.15	0.00	13
Scid	27.5	100	0	0	0	0	94.7	0	5.3	0.00	0.11	19
B6.129	27.5	96.7	3.3	0	0.05	0	76.7	15.0	8.3	0.15	0.08	60
	440	89.7	10.3^{b}	6.9	0.10	0.07	51.7	41.4^{b}	17.2	0.72^{a}	0.34	29
	880	52.9	23.5^{b}	35.5^{b}	0.33^{a}	0.41^{a}	41.2	41.2^{b}	41.2^{b}	0.61^{a}	0.47^{a}	17
mRad54$^{-/-}$ *mRad54B*$^{-/-}$	27.5	83.9	9.7	9.7	0.26	0.10	64.5	25.8	16.1	0.39	0.29	31

Percentage of chromosome complements containing at least one γH2AX focus of indicated type is listed. The frequency (plotted in Figure 6B/D) and total number of zygotes (n) is indicated.

a) $p<0.05$ with control by KWD

b) $p<0.05$ with control by Chi square

c) $p=0.057$ with control Chi square

Supplementary Table II. Relative reduction of foci during G1

		Reduction at 210 min pf	Reduction at 285 min pf
		2.2 hours post remodeling	3.4 hours post remodeling
Oocyte strain	**IR dose sperm (Gy)**		
B6.CBA	3	0.80	0.48
B6.129	3	0.50	0.69
C.B17	3	0.40	-0.34
Scid	3	0.34	0.06
Time post IR treatment	**IR dose (Gy)**	**2 hours**	**4 hours**
Cell line			
AA8 (Wt)	1	0.80[a]	0.80[a]
MRC-5 (Wt)	2	0.70[b], 0.64[c], 0.60[d]	0.83[c], 0.74[d]
HSF2 (Wt)	2	0.62[d]	0.82[d]
V3 (DNA-PK_{cs}-defective)	1	0.16[a]	0.43[a]
180BR (DNA-ligase IV deficient)	2	0.28[b], 0.35[c]	0.35[c]
AT1BR (ATM-deficient)	2	0.70[c] (foci formation delayed)	0.74[c]
irs1SF ($XRCC3^{-/-}$)	1	Comparable to AA8[a]	Comparable to AA8[a]

Relative reducion:
For zygotes
(Number of foci at chromatin remodeling – Number of foci at indicated t)/(Number of foci at chromatin remodeling)

For cell lines
(Number of foci after IR treatment – Number of foci at indicated t)/ (Number of foci after IR treatment)

Data taken from
a) Ref 57
b) Ref 55
c) Ref 10
d) Ref 11

Section 3.3

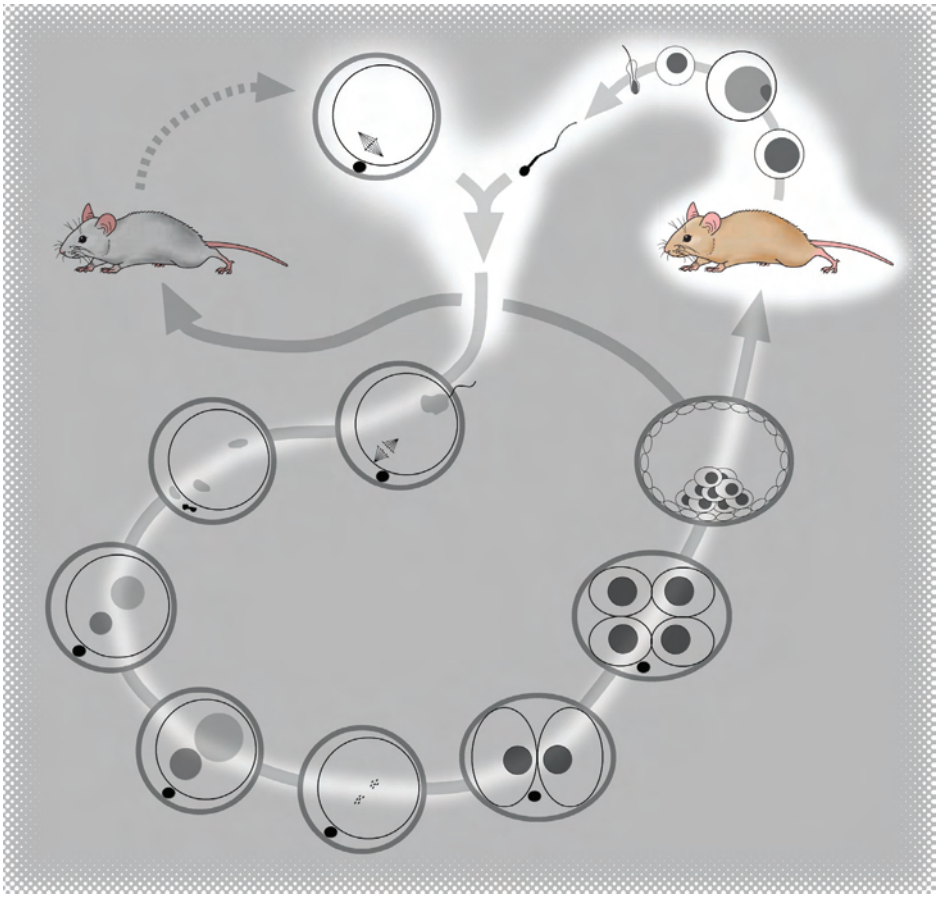

Oncogene 2007 July; 26(32):4720-4

Maternal effects of the scid mutation on radiation-induced transgenerational instability in mice

T Hatch[1 #], AAHA Derijck[2 #], PD Black[1], GW van der Heijden[2], P de Boer[2] and YE Dubrova[1]

 # Both authors contributed equally

1 Department of Genetics, University of Leicester, Leicester LE1 7RH, United Kingdom

2 Department of Obstetrics and Gynaecology, Radboud University Nijmegen Medical Centre P.O. Box 9101, 6500 HB Nijmegen, The Netherlands

Abstract

The results of a number of recent studies show that mutation rates in the offspring of irradiated parents are substantially elevated, however the effect of parental genotype on transgenerational instability remains poorly understood. Here we have analysed the mutation frequency at an expanded simple tandem repeat (ESTR) locus in the germline and bone marrow of the first generation male offspring of control and irradiated male mice. The frequency of ESTR mutation was studied in the offspring of two reciprocal matings ♂scid x ♀BALB/c and ♂BALB/c x ♀scid, which were compared with that in BALB/c mice. In the offspring of the BALB/c x BALB/c and ♂scid x ♀BALB/c matings, which were conceived after paternal sperm irradiation, the frequency of ESTR mutation was significantly elevated in both tissues. In contrast, ESTR mutation frequency was only slightly elevated in the offspring of ♂BALB/c x ♀scid mating conceived after paternal irradiation. The results of this study suggest that the oocytes of scid females are unable to fully support the repair of double-strand breaks induced in paternal sperm which may in turn result in the elimination of cells/embryos containing high levels of DNA damage, thus partially preventing the manifestation of genomic instability.

To analyse transgenerational changes in mutation rate, tissue samples were taken from the non-exposed 7-week-old male offspring of control and irradiated (2 Gy of acute X-rays) BALB/c and severe combined immunodeficient (scid) males. The frequency of mutations at an expanded simple tandem (ESTR) locus, *Ms6-hm*, was analysed in the offspring of two reciprocal matings ♂scid x ♀BALB/c and ♂BALB/c x ♀scid which were compared with those of BALB/c mice (Table 1). To ensure that all offspring included in this study were derived from irradiated sperm from the caudal epididymis and vas deferens, the exposed males were mated within 5 days after irradiation with non-exposed females [123]. Homozygous scid mice used in this study are on the C.B17 genetic background. The C.B17 strain was derived from a multiple backcross of (BALB/c x C57BL/Ca) x BALB/c and its characteristics are essentially those of BALB/c [124]. The progenitor allele size at the *Ms6-hm* locus in scid, C.B17 and BALB/c mice included in this study were all approximately 3 kb. Importantly, the same allelic variants of the genes encoding the proteins $p16^{INK4a}$ [125] and DNA-dependant protein kinase catalytic-subunit, $DNA\text{-}PK_{cs}$ [126] are found in both strains [127, 128]. Given that the $p16^{INK4a}$ protein plays a vital role in cell-cycle control and $DNA\text{-}PK_{cs}$ is involved in the non homologous end-joining (NHEJ) pathway of DNA double-strand break (DSB) repair, it therefore appears that the presence of these allelic variants in both strains may have a similar effect on the genome stability. Indeed, our previous data show a remarkable similarity in ESTR mutation rates in the germline of non-exposed BALB/c and C.B17 males [128].

Using a single-molecule (SM-PCR) approach [129, 130], the frequency of ESTR mutation at the *Ms6-hm* locus was evaluated in bone marrow (BM) and sperm DNA samples taken from 18 offspring (3 animals per experimental group). We first compared the frequency of ESTR mutation in the offspring of non-irradiated parents. Given that the frequency of mutation in the offspring of the reciprocal matings (♂scid x ♀BALB/c and ♂BALB/c x ♀scid) did not significantly differ (sperm, 0.096 ± 0.018 and 0.094 ± 0.018; $t=0.09$; $P=0.9283$; BM, 0.072 ± 0.014 and 0.057 ± 0.013; $t=0.75$; $P=0.4335$), these data were therefore combined for further analysis (Table 1). Overall, a significant 1.8-fold increase in the mean frequency of ESTR mutation was found in the sperm of F_1 hybrid animals compared to that in the BALB/c strain ($t=2.35$; $P=0.0190$); a similar 1.5-fold increase was

Table 1 ESTR mutation frequencies in controls and the offspring of irradiated males

	Control		F_1 of irradiated males		Ratio‡	t §	Prob.§
	No mutations*	Mutation frequency†	No mutations*	Mutation frequency†			
♂BALB/c x ♀BALB/c							
Sperm	21 (393)	0.053±0.012	34 (336)	0.101±0.018	1.89	2.16	0.0311
BM	20 (456)	0.044±0.010	38 (402)	0.094±0.016	2.15	2.62	0.0089
♂*scid* x ♀BALB/c							
Sperm	60 (643)¶	0.095±0.013	92 (616)	0.149±0.018	1.57	2.49	0.0129
BM	52 (802)¶	0.065±0.010	51 (435)	0.117±0.018	1.81	2.59	0.0097
♂BALB/c x ♀*scid*							
Sperm	60 (643)¶	0.095±0.013	41 (350)	0.117±0.020	1.24	0.95	0.3423
BM	52 (802)¶	0.065±0.010	51 (569)	0.090±0.014	1.38	1.50	0.1338

* Number of amplifiable molecules is given in brackets.

† ± standard error.

‡ Ratio to the frequency in the offspring of non-exposed males from the same mating.

§ Student's test and probability for difference between the offspring of irradiated males and controls.

¶ Aggregated data for the offspring of non-exposed mating ♂scid x ♀BALB/c and ♂BALB/c x ♀scid (see text for details).

also detected in BM (t=1.88; P=0.0603). scid mice carrying a nonsense mutation in the DNA-PK_{cs} are deficient in the repair of DSBs by the non-homologous end joining (NHEJ) pathway [131, 132]. Given that the activity of DNA-PK_{cs} in BALB/c mice is also substantially compromised [90], the effects of a nonsense scid mutation can therefore manifest in BALB/c x scid F_1 hybrid animals, thus resulting in elevated spontaneous mutation rate.

We next analysed transgenerational changes in the first generation (F_1) offspring of irradiated wild-type BALB/c mice. For both tissues, a statistically significant ~2-fold increase in the mean muta-

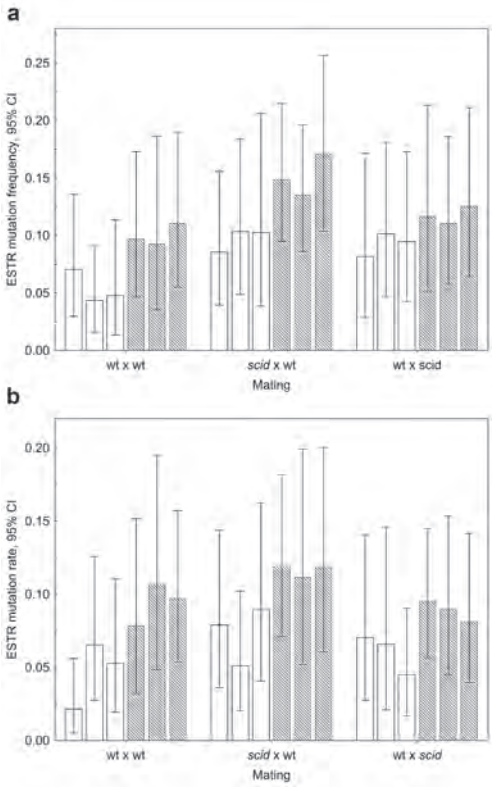

Figure 1 Frequency of ESTR mutations in controls males (open bars) and the first-generation offspring of irradiated males (hatched bars) Each bar represents the frequency of mutations measured in an individual male. **(A)** Frequency of ESTR mutations in sperm. **(B)** Frequency of ESTR mutations in the bone marrow tissue. The standard errors (s.e.) are shown on all graphs. DNA samples were prepared as previously described [130]. Approximately 5 μg of each DNA sample was digested with 20 U MseI (New England Biolabs). The frequency of ESTR mutation was be evaluated using a single-molecule PCR (SM-PCR) approach [129, 130]. DNA was amplified on an MJ DNA engine PTC 220 in 10 μl reactions using 0.6 μM flanking primers, 1 U enzyme mix (Expanded High Fidelity PCR system, Roche), 1 M Betaine and 200 μM dNTPs. After denaturing at 96ºC for 3 min, PCRs were cycled at 96ºC for 20 sec, 58ºC for 30 sec, and 68ºC for 3 min for 30 cycles, ending with 10-min incubation at 68ºC. PCR products were resolved on a 40 cm long agarose gel and detected by Southern blot hybridisation [144]. To increase the robustness of the estimates of individual ESTR mutation frequencies, on average 139 amplifiable molecules were analyzed for each tissue for each male mouse. The frequencies of ESTR mutation and standard errors were estimated using modified approach proposed by Chakraborty [145].

tion frequency was found in the offspring of irradiated males. Most importantly, the frequency of ESTR mutation was elevated in the germline and somatic tissue of all the offspring of irradiated males (Figure 1).

In our previous studies ESTR mutation rates were analysed in the offspring conceived 3 and 6 weeks after paternal exposure irradiation [127, 130, 133]. Given that these stages of the mouse spermatogenesis are transcriptionally active, their exposure to radiation could result in an accumulation of certain classes of RNA in the paternal germ cells which, being transmitted to the fertilised egg, may affect gene expression and stability in the developing embryo. If transgenerational instability is attributed to the zygotic transfer of RNA [134], then the offspring conceived just few days after paternal irradiation, from transcriptionally inert sperm cells [135], should be genetically stable. However, a similar magnitude of transgenerational increases in ESTR mutation frequency was found in the F_1 offspring of exposed BALB/c males conceived from either transcriptionally active or inactive stages of spermatogenesis (Figure 2).

Given that the efficiency of DNA repair in sperm cell is greatly diminished [136] and the fertilising ability of irradiated sperm is not substantially compromised [98], the majority of pre-mutational radiation-induced lesions are transmitted to the fertilised egg where they are repaired within a few hours [79, 137]. As a result, radiation-induced damage to sperm DNA triggers a cascade of events in the zygote, including profound changes in the expression of DNA repair genes [81, 138] and alterations in DNA methylation and histone acetylation [139]. The presence of such dramatic changes at fertilisation could also result in delayed effects, which may influence the stability of the developing embryo.

To evaluate the effect of the scid mutation, the frequency of ESTR mutation was compared in the offspring of two reciprocal crosses, where irradiated BALB/c and scid males were mated to non-exposed scid and BALB/c females, respectively. In the offspring of ♂scid x ♀BALB/c mating, the frequency of ESTR mutation was significantly elevated in both tissues (Table 1). The magnitude of this increase was very similar to that observed in the offspring of irradiated ♂BALB/c x ♀BALB/c. In contrast, ESTR mutation frequency was only slightly elevated in the offspring of reciprocal cross. We therefore conclude that in the maternal scid background the manifestation of radiation-induced transgenerational instability is partially suppressed.

Given that the maternally-derived NHEJ pathway is fully active in zygote [86], in the offspring of ♂BALB/c x ♀scid mating it should

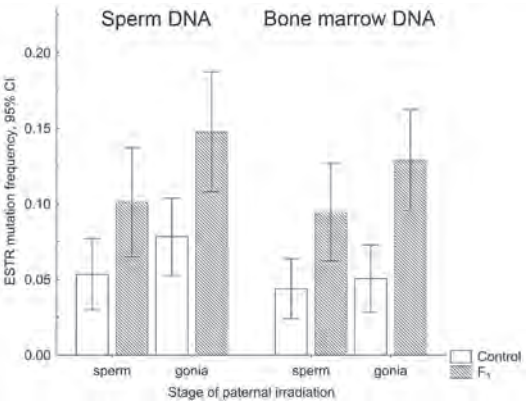

Figure 2 Frequency of ESTR mutations in the F_1 offspring of BALB/c males conceived 5 days (sperm) and 6 weeks (spermatogonia) after acute exposure to X-rays. Data for the spermatogonia irradiation are taken from Barber et al. (2006)[130].

be severely compromised during the early stages of their development. The inability of the scid oocytes to fully support the repair of radiation-induced DSBs in sperm may therefore lead to the elimination of embryos containing high level of DNA damage. Previously reported lack of mutation induction in irradiated scid mice can also be explained by the high cell killing effects of irradiation on their germline [128].

As the mouse embryo undergoes early zygotic activation of transcription during the 2-cell stage where over 800 genes, including the gene encoding DNA-PK$_{cs}$, are re-expressed [22], the level of NHEJ in the offspring of ♂BALB/c x ♀scid mating should be restored very early by transcription of the paternal BALB/c allele. The alleged elimination of some highly unstable embryonic cells should therefore occur at the very early stages of development, perhaps before the 4-cell stage, where the ability to repair DSBs by NHEJ still remains under the scid maternal control.

The suppression of mutation induction and radiation-induced genomic instability in homozygous scid cells can be explained by the DNA-PK-independent activation of p53 and p21, resulting in a high level of apoptosis and cell-cycle arrest in the irradiated DNA-PK$_{cs}$ deficient cells [140]. The inter-strain variation in the responses to ionising radiation, including the manifestation of radiation-induced genomic instability, has previously been explained by differences in the intensity of apoptosis [141]. According to the results of this study, cells from the radiation-resistant C57BL/6 mice undergo rapid apoptosis after irradiation, which could in turn suppress radiation-induced genomic instability in this strain.

Our recent data show that radiation-induced DSBs in the sperm head

are repaired in the wild-type zygote during pre S-phase [79], where they should be almost exclusively repaired by the NHEJ pathway [57]. Given that unrepaired DSBs are highly mutagenic and result in chromosome type aberrations in early zygote [137], their early repair in the offspring of ♂BALB/c x ♀scid mating should be compensated, most likely by homologous recombination [110]. Given the high fidelity of HR and its well-established role in the repair of DSBs during replication, the activation of this pathway may suppress mutation process at ESTR loci, the mechanisms of which are most probably attributed to replication slippage [128, 129]. However, as the period of time when in the offspring of ♂BALB/c x ♀scid mating remains under the scid maternal control is very brief, it appears unlikely that such a short burst of HR activity may substantially affect ESTR stability, unless the long-term epigenetic up-regulation of HR in these animals is suspected.

In conclusion, the data presented here show that radiation-induced transgenerational instability in the offspring of ♂BALB/c x ♀scid mating is suppressed and therefore suggest a long lasting effect of maternal genotype and DNA repair proficiency on ESTR mutation rate in the germline and somatic tissues. Together with the results of our previous study showing strain-specific differences in the extent of transgenerational instability in mice [127], these data highlight the importance of genetic factors in the manifestation of this phenomenon. Moreover, they provide further insights on the mechanisms underlying the phenomenon of maternal effect for DNA repair in mammals. The results of early studies show that the inter-strain differences in the efficiency of DNA repair in oocyte can significantly affect the yield of dominant-lethal mutations induced in male germ cells [21, 142]. According to these data, the frequency of mutations detected in the offspring of exposed male mice depends on the ability of maternal strain to repair DNA lesions induced in sperm. However, these maternal effects were detected in the wild-type strains of mice where the efficiency of DNA repair is not substantially compromised. In contrast, the scid mutation almost completely abolishes the activity of DNA-PK_{cs}, thus dramatically affecting the early responses to DNA damage in zygote. Presumably on this maternal background, a considerable fraction of DNA lesions induced in sperm cannot be properly repaired, resulting in the elimination of

most unstable cells/embryos. As in the surviving embryos, the manifestation of transgenerational instability is suppressed after paternal sperm irradiation, maternal effects of the scid mutation may thus be regarded as protective. Finally, given the wide range of inherited variation in DNA repair capacity in humans [143], there is potential that the same phenomenon may also exist in humans.

Acknowledgments

We thank Bianca Lemmers and Iris Lamers of the Central Animal Facility of Radboud University for expert animal care. This work was supported by a grant from the European Commission (YED and PDB). YED work was also supported in part by grants from the Wellcome Trust, the Department of Energy and the Medical Research Council.

References

1. Hoeijmakers, J.H. Genome maintenance mechanisms for preventing cancer. *Nature* **411**, 366-374 (2001).

2. Zhou, B.B. & Elledge, S.J. The DNA damage response: putting checkpoints in perspective. *Nature* **408**, 433-439 (2000).

3. Rogakou, E.P., Pilch, D.R., Orr, A.H., Ivanova, V.S., & Bonner, W.M. DNA double-stranded breaks induce histone H2AX phosphorylation on serine 139. *J. Biol. Chem.* **273**, 5858-5868 (1998).

4. Rogakou, E.P., Boon, C., Redon, C., & Bonner, W.M. Megabase chromatin domains involved in DNA double-strand breaks in vivo. *J. Cell Biol.* **146**, 905-916 (1999).

5. Burma, S., Chen, B.P., Murphy, M., Kurimasa, A., & Chen, D.J. ATM phosphorylates histone H2AX in response to DNA double-strand breaks. *J. Biol. Chem.* **276**, 42462-42467 (2001).

6. Ward, I.M. & Chen, J. Histone H2AX is phosphorylated in an ATR-dependent manner in response to replicational stress. *J. Biol. Chem.* **276**, 47759-47762 (2001).

7. Stiff, T. *et al.* ATM and DNA-PK function redundantly to phosphorylate H2AX after exposure to ionizing radiation. *Cancer Res.* **64**, 2390-2396 (2004).

8. Sedelnikova, O.A., Rogakou, E.P., Panyutin, I.G., & Bonner, W.M. Quantitative detection of (125)IdU-induced DNA double-strand breaks with gamma-H2AX antibody. *Radiat. Res.* **158**, 486-492 (2002).

9. Paull, T.T. *et al.* A critical role for histone H2AX in recruitment of repair factors to nuclear foci after DNA damage. *Curr. Biol.* **10**, 886-895 (2000).

10. Kuhne, M. *et al.* A double-strand break repair defect in ATM-deficient cells contributes to radiosensitivity. *Cancer Res.* **64**, 500-508 (2004).

11. Riballo, E. *et al.* A pathway of double-strand break rejoining dependent upon ATM, Artemis, and proteins locating to gamma-H2AX foci. *Mol. Cell* **16**, 715-724 (2004).

12. Redon, C. *et al.* Histone H2A variants H2AX and H2AZ. *Curr. Opin. Genet. Dev.* **12**, 162-169 (2002).

13. Matsumoto, K. *et al.* Onset of paternal gene activation in early mouse embryos fertilized with transgenic mouse sperm. *Mol. Reprod. Dev.* **39**, 136-140 (1994).

14. Nothias, J.Y., Miranda, M., &

DePamphilis, M.L. Uncoupling of transcription and translation during zygotic gene activation in the mouse. *EMBO J.* **15**, 5715-5725 (1996).

15. Schultz, R.M. The molecular foundations of the maternal to zygotic transition in the preimplantation embryo. *Hum. Reprod. Update.* **8**, 323-331 (2002).

16. Hamatani, T., Carter, M.G., Sharov, A.A., & Ko, M.S. Dynamics of global gene expression changes during mouse preimplantation development. *Dev. Cell* **6**, 117-131 (2004).

17. Braude, P., Bolton, V., & Moore, S. Human gene expression first occurs between the four- and eight-cell stages of preimplantation development. *Nature* **332**, 459-461 (1988).

18. Camous, S., Kopecny, V., & Flechon, J.E. Autoradiographic detection of the earliest stage of [3H]-uridine incorporation into the cow embryo. *Biol. Cell* **58**, 195-200 (1986).

19. Calarco, P.G. & McLaren, A. Ultrastructural observations of preimplantation stages of the sheep. *J. Embryol. Exp. Morphol.* **36**, 609-622 (1976).

20. Brandriff, B. & Pedersen, R.A. Repair of the ultraviolet-irradiated male genome in fertilized mouse eggs. *Science* **211**, 1431-1433 (1981).

21. Generoso, W.M., Cain, K.T., Krishna, M., & Huff, S.W. Genetic lesions induced by chemicals in spermatozoa and spermatids of mice are repaired in the egg. *Proc. Natl. Acad. Sci. U. S. A* **76**, 435-437 (1979).

22. Zeng, F., Baldwin, D.A., & Schultz, R.M. Transcript profiling during preimplantation mouse development. *Dev. Biol.* **272**, 483-496 (2004).

23. Wright, S.J. Sperm nuclear activation during fertilization. *Curr. Top. Dev. Biol.* **46**, 133-178 (1999).

24. Sutovsky, P. & Schatten, G. Paternal contributions to the mammalian zygote: fertilization after sperm-egg fusion. *Int. Rev. Cytol.* **195**, 1-65 (2000).

25. Ward, W.S. & Coffey, D.S. DNA packaging and organization in mammalian spermatozoa: comparison with somatic cells. *Biol. Reprod.* **44**, 569-574 (1991).

26. Loppin, B. *et al.* The histone H3.3 chaperone HIRA is essential for chromatin assembly in the male pronucleus. *Nature* **437**, 1386-1390 (2005).

27. Sega, G.A., Sotomayor, R.E., & Owens, J.G. A study of unscheduled DNA synthesis induced by X-rays in the germ cells of male mice. *Mutat. Res.* **49**, 239-257 (1978).

28. Kofman-Alfaro, S. & Chandley, A.C. Radiation-initiated DNA synthesis in spermatogenic cells of the mouse. *Exp. Cell Res.* **69**, 33-44 (1971).

29. Perry, A.C. Hijacking oocyte DNA repair machinery in transgenesis? *Mol. Reprod. Dev.* **56**, 319-324 (2000).

30. Matsuda, Y., Yamada, T., & Tobari, I. Studies on chromosome aberrations in the eggs of mice fertilized in vitro after irradiation. I. Chromosome aberrations induced in sperm after X-irradiation. *Mutat. Res.* **148**, 113-117 (1985).

31. Matsuda, Y., Seki, N., Utsugi-Takeuchi, T., & Tobari, I. Changes in X-ray sensitivity of mouse eggs from fertilization to the early pronuclear stage, and their repair capacity. *Int. J. Radiat. Biol.* **55**, 233-256 (1989).

32. van der Heijden, G.W. *et al.* Asymmetry in Histone H3 variants and lysine methylation between paternal and maternal chromatin of the early mouse zygote. *Mech. Dev.* **122**, 1008-1022 (2005).

33. Adenot, P.G., Szollosi, M.S., Geze, M., Renard, J.P., & Debey, P. Dynamics of paternal chromatin changes in live one-cell mouse embryo after natural fertilization. *Mol. Reprod. Dev.* **28**, 23-34 (1991).

34. Cowell, I.G. *et al.* Heterochromatin, HP1 and methylation at lysine 9 of histone H3 in animals. *Chromosoma* **111**, 22-36 (2002).

35. Arney, K.L., Bao, S., Bannister, A.J., Kouzarides, T., & Surani, M.A. Histone methylation defines epigenetic asymmetry in the mouse zygote. *Int. J. Dev. Biol.* **46**, 317-320 (2002).

36. Roest, H.P. *et al.* The ubiquitin-conjugating DNA repair enzyme HR6A is a maternal factor essential for early embryonic development in mice. *Mol. Cell Biol.* **24**, 5485-5495 (2004).

37. Liu, H., Kim, J.M., & Aoki, F. Regulation of histone H3 lysine 9 methylation in oocytes and early pre-implantation embryos. *Development* **131**, 2269-2280 (2004).

38. Kourmouli, N. *et al.* Heterochromatin and tri-methylated lysine 20 of histone H4 in animals. *J. Cell Sci.* **117**, 2491-2501 (2004).

39. Sarmento, O.F. *et al.* Dynamic alterations of specific histone modifications during early murine development. *J. Cell Sci.* **117**, 4449-4459 (2004).

40. Santos, F., Peters, A.H., Otte, A.P., Reik, W., & Dean, W. Dynamic chromatin modifications characterise the first cell cycle in mouse embryos. *Dev. Biol.* **280**, 225-236 (2005).

41. Marchetti, F., Bishop, J.B., Cosentino, L., Moore, D., &

Wyrobek, A.J. Paternally transmitted chromosomal aberrations in mouse zygotes determine their embryonic fate. *Biol. Reprod.* **70**, 616-624 (2004).

42. Fraser, L.R. In vitro capacitation and fertilization. *Methods Enzymol.* **225**, 239-253 (1993).

43. Tateno, H. & Kamiguchi, Y. Chromosome analysis of mouse one-cell androgenones derived from a sperm nucleus exposed to topoisomerase II inhibitors at pre- and post-fertilization stages. *Mutat. Res.* **556**, 117-126 (2004).

44. Perez-Burgos, L. *et al.* Generation and characterization of methyl-lysine histone antibodies. *Methods Enzymol.* **376**, 234-254 (2004).

45. van der Heijden, G.W. *et al.* Transmission of modified nucleosomes from the mouse male germline to the zygote and subsequent remodeling of paternal chromatin. *Dev. Biol.* **298**, 458-469 (2006).

46. Hunt, P., LeMaire, R., Embury, P., Sheean, L., & Mroz, K. Analysis of chromosome behavior in intact mammalian oocytes: monitoring the segregation of a univalent chromosome during female meiosis. *Hum. Mol. Genet.* **4**, 2007-2012 (1995).

47. Baart, E.B., de Rooij, D.G., Keegan, K.S., & de Boer, P. Distribution of Atr protein in primary spermatocytes of a mouse chromosomal mutant: a comparison of preparation techniques. *Chromosoma* **109**, 139-147 (2000).

48. Bizzaro, D., Manicardi, G., Bianchi, P.G., & Sakkas, D. Sperm decondensation during fertilisation in the mouse: presence of DNase I hypersensitive sites in situ and a putative role for topoisomerase II. *Zygote.* **8**, 197-202 (2000).

49. St Pierre, J., Wright, D.J., Rowe, T.C., & Wright, S.J. DNA topoisomerase II distribution in mouse preimplantation embryos. *Mol. Reprod. Dev.* **61**, 335-346 (2002).

50. Chen, J. & Stubbe, J. Bleomycins: towards better therapeutics. *Nat. Rev. Cancer* **5**, 102-112 (2005).

51. McManus, K.J. & Hendzel, M.J. ATM-dependent DNA Damage-independent Mitotic Phosphorylation of H2AX in Normally Growing Mammalian Cells. *Mol. Biol. Cell* **16**, 5013-5025 (2005).

52. Ichijima, Y. *et al.* Phosphorylation of histone H2AX at M phase in human cells without DNA damage response. *Biochem. Biophys. Res. Commun.* **336**, 807-812 (2005).

53. Mahadevaiah, S.K. *et al.* Recombinational DNA double-strand breaks in mice precede synapsis. *Nat. Genet.* **27**, 271-276 (2001).

54. Bakkenist, C.J. & Kastan, M.B. DNA damage activates ATM

through intermolecular autophosphorylation and dimer dissociation. *Nature* **421**, 499-506 (2003).

55. Rothkamm, K. & Lobrich, M. Evidence for a lack of DNA double-strand break repair in human cells exposed to very low x-ray doses. *Proc. Natl. Acad. Sci. U. S. A* **100**, 5057-5062 (2003).

56. MacPhail, S.H. *et al.* Expression of phosphorylated histone H2AX in cultured cell lines following exposure to X-rays. *Int. J. Radiat. Biol.* **79**, 351-358 (2003).

57. Rothkamm, K., Kruger, I., Thompson, L.H., & Lobrich, M. Pathways of DNA double-strand break repair during the mammalian cell cycle. *Mol. Cell Biol.* **23**, 5706-5715 (2003).

58. Joshi, D.S., Yick, J., Murray, D., & Meistrich, M.L. Stage-dependent variation in the radiosensitivity of DNA in developing male germ cells. *Radiat. Res.* **121**, 274-281 (1990).

59. Zheng, H. & Olive, P.L. Influence of oxygen on radiation-induced DNA damage in testicular cells of C3H mice. *Int. J. Radiat. Biol.* **71**, 275-282 (1997).

60. Free, M.J., Schluntz, G.A., & Jaffe, R.A. Respiratory gas tensions in tissues and fluids of the male rat reproductive tract. *Biol. Reprod.* **14**, 481-488 (1976).

61. van Loon, A.A. *et al.* Induction and repair of DNA single-strand breaks and DNA base damage at different cellular stages of spermatogenesis of the hamster upon in vitro exposure to ionizing radiation. *Mutat. Res.* **294**, 139-148 (1993).

62. McPherson, S.M. & Longo, F.J. Nicking of rat spermatid and spermatozoa DNA: possible involvement of DNA topoisomerase II. *Dev. Biol.* **158**, 122-130 (1993).

63. Laberge, R.M. & Boissonneault, G. On the nature and origin of DNA strand breaks in elongating spermatids. *Biol. Reprod.* **73**, 289-296 (2005).

64. Caldecott, K., Banks, G., & Jeggo, P. DNA double-strand break repair pathways and cellular tolerance to inhibitors of topoisomerase II. *Cancer Res.* **50**, 5778-5783 (1990).

65. Povirk, L.F. DNA damage and mutagenesis by radiomimetic DNA-cleaving agents: bleomycin, neocarzinostatin and other enediynes. *Mutat. Res.* **355**, 71-89 (1996).

66. Tateno, H. & Kamiguchi, Y. Meiotic stage-dependent induction of chromosome aberrations in Chinese hamster primary oocytes exposed to topoisomerase II inhibitor etoposide. *Mutat. Res.* **476**, 139-148 (2001).

67. Burden, D.A., Goldsmith, L.J., & Sullivan, D.M. Cell-cycle-dependent phosphorylation and activity of Chinese-hamster ovary topoisomerase II. *Biochem. J.* **293 (Pt 1)**, 297-304 (1993).

68. Sonoda, E., Hochegger, H., Saberi, A., Taniguchi, Y., & Takeda, S. Differential usage of non-homologous end-joining and homologous recombination in double strand break repair. *DNA Repair (Amst)* **5**, 1021-1029 (2006).

69. Agarwal, S., Tafel, A.A., & Kanaar, R. DNA double-strand break repair and chromosome translocations. *DNA Repair (Amst)* **5**, 1075-1081 (2006).

70. Tamulevicius, P., Wang, M., & Iliakis, G. Homology-directed repair is required for the development of radioresistance during S phase: interplay between double-strand break repair and checkpoint response. *Radiat. Res.* **167**, 1-11 (2007).

71. Arnaudeau, C., Lundin, C., & Helleday, T. DNA double-strand breaks associated with replication forks are predominantly repaired by homologous recombination involving an exchange mechanism in mammalian cells. *J. Mol. Biol.* **307**, 1235-1245 (2001).

72. Essers, J. *et al.* Homologous and non-homologous recombination differentially affect DNA damage repair in mice. *EMBO J.* **19**, 1703-1710 (2000).

73. Takata, M. *et al.* Homologous recombination and non-homologous end-joining pathways of DNA double-strand break repair have overlapping roles in the maintenance of chromosomal integrity in vertebrate cells. *EMBO J.* **17**, 5497-5508 (1998).

74. Couedel, C. *et al.* Collaboration of homologous recombination and nonhomologous end-joining factors for the survival and integrity of mice and cells. *Genes Dev.* **18**, 1293-1304 (2004).

75. Bekker-Jensen, S. *et al.* Spatial organization of the mammalian genome surveillance machinery in response to DNA strand breaks. *J. Cell Biol.* **173**, 195-206 (2006).

76. Lim, D.S. & Hasty, P. A mutation in mouse rad51 results in an early embryonic lethal that is suppressed by a mutation in p53. *Mol. Cell Biol.* **16**, 7133-7143 (1996).

77. Sonoda, E. *et al.* Rad51-deficient vertebrate cells accumulate chromosomal breaks prior to cell death. *EMBO J.* **17**, 598-608 (1998).

78. Haaf, T., Golub, E.I., Reddy, G., Radding, C.M., & Ward, D.C. Nuclear foci of mammalian Rad51 recombination protein in somatic cells after DNA damage and its localization in synaptonemal com-

plexes. *Proc. Natl. Acad. Sci. U. S. A* **92**, 2298-2302 (1995).

79. Derijck, A.A. *et al.* gamma-H2AX signalling during sperm chromatin remodelling in the mouse zygote. *DNA Repair (Amst)* **5**, 959-971 (2006).

80. Harrison, R.H., Kuo, H.C., Scriven, P.N., Handyside, A.H., & Ogilvie, C.M. Lack of cell cycle checkpoints in human cleavage stage embryos revealed by a clonal pattern of chromosomal mosaicism analysed by sequential multicolour FISH. *Zygote.* **8**, 217-224 (2000).

81. Shimura, T. *et al.* p53-dependent S-phase damage checkpoint and pronuclear cross talk in mouse zygotes with X-irradiated sperm. *Mol. Cell Biol.* **22**, 2220-2228 (2002).

82. Matsuda, Y. & Tobari, I. Chromosomal analysis in mouse eggs fertilized in vitro with sperm exposed to ultraviolet light (UV) and methyl and ethyl methanesulfonate (MMS and EMS). *Mutat. Res.* **198**, 131-144 (1988).

83. Takahashi, E.I., Tobari, I., Shiomi, T., & Sato, K. Chromosomal hypersensitivity in mutant M10 and Q31 mouse cells exposed to ultraviolet radiation (UV) and 4-nitroquinoline-1-oxide (4NQO). *Mutat. Res.* **109**, 207-217 (1983).

84. Hagmann, M. *et al.* Dramatic changes in the ratio of homologous recombination to nonhomologous DNA-end joining in oocytes and early embryos of Xenopus laevis. *Biol. Chem. Hoppe Seyler* **377**, 239-250 (1996).

85. Hagmann, M. *et al.* Homologous recombination and DNA-end joining reactions in zygotes and early embryos of zebrafish (Danio rerio) and Drosophila melanogaster. *Biol. Chem.* **379**, 673-681 (1998).

86. Fiorenza, M.T., Bevilacqua, A., Bevilacqua, S., & Mangia, F. Growing dictyate oocytes, but not early preimplantation embryos, of the mouse display high levels of DNA homologous recombination by single-strand annealing and lack DNA nonhomologous end joining. *Dev. Biol.* **233**, 214-224 (2001).

87. Bonduelle, M. *et al.* Prenatal testing in ICSI pregnancies: incidence of chromosomal anomalies in 1586 karyotypes and relation to sperm parameters. *Hum. Reprod.* **17**, 2600-2614 (2002).

88. Zini, A. & Libman, J. Sperm DNA damage: importance in the era of assisted reproduction. *Curr. Opin. Urol.* **16**, 428-434 (2006).

89. Rothkamm, K., Kuhne, M., Jeggo, P.A., & Lobrich, M. Radiation-induced genomic rearrangements formed by nonhomologous end-joining of DNA double-strand

breaks. *Cancer Res.* **61**, 3886-3893 (2001).

90. Okayasu, R. *et al.* A deficiency in DNA repair and DNA-PKcs expression in the radiosensitive BALB/c mouse. *Cancer Res.* **60**, 4342-4345 (2000).

91. Ferreira, J. & Carmo-Fonseca, M. Genome replication in early mouse embryos follows a defined temporal and spatial order. *J. Cell Sci.* **110 (Pt 7)**, 889-897 (1997).

92. Tomasz, M. *et al.* Isolation and structure of a covalent cross-link adduct between mitomycin C and DNA. *Science* **235**, 1204-1208 (1987).

93. Wesoly, J. *et al.* Differential contributions of mammalian Rad54 paralogs to recombination, DNA damage repair, and meiosis. *Mol. Cell Biol.* **26**, 976-989 (2006).

94. Strumberg, D. *et al.* Conversion of topoisomerase I cleavage complexes on the leading strand of ribosomal DNA into 5'-phosphorylated DNA double-strand breaks by replication runoff. *Mol. Cell Biol.* **20**, 3977-3987 (2000).

95. Subramanian, D., Rosenstein, B.S., & Muller, M.T. Ultraviolet-induced DNA damage stimulates topoisomerase I-DNA complex formation in vivo: possible relationship with DNA repair. *Cancer Res.* **58**, 976-984 (1998).

96. Miao, Z.H. *et al.* 4-nitroquinoline-1-oxide induces the formation of cellular topoisomerase I-DNA cleavage complexes. *Cancer Res.* **66**, 6540-6545 (2006).

97. Chang, C., Biedermann, K.A., Mezzina, M., & Brown, J.M. Characterization of the DNA double strand break repair defect in scid mice. *Cancer Res.* **53**, 1244-1248 (1993).

98. Ahmadi, A. & Ng, S.C. Fertilizing ability of DNA-damaged spermatozoa. *J. Exp. Zool.* **284**, 696-704 (1999).

99. Jacquet, P., Kervyn, G., & De Clercq, G. Studies in vitro on mouse-egg radiosensitivity from fertilization up to the first cleavage. *Mutat. Res.* **110**, 351-365 (1983).

100. Yamada, T., Yukawa, O., Matsuda, Y., & Ohkawa, A. Changes in radiosensitivity of the in vitro fertilized mouse ova during zygotic stage from fertilization to first cleavage. *J. Radiat. Res. (Tokyo)* **23**, 450-456 (1982).

101. Santos, F., Hendrich, B., Reik, W., & Dean, W. Dynamic reprogramming of DNA methylation in the early mouse embryo. *Dev. Biol.* **241**, 172-182 (2002).

102. Barreto, G. *et al.* Gadd45a promotes epigenetic gene activation by repair-mediated DNA demethylation. *Nature* **445**, 671-675 (2007).

103. Marti, T.M., Hefner, E., Feeney, L., Natale, V., & Cleaver, J.E. H2AX phosphorylation within the G1 phase after UV irradiation depends on nucleotide excision repair and not DNA double-strand breaks. *Proc. Natl. Acad. Sci. U. S. A* **103**, 9891-9896 (2006).

104. Yamauchi, Y., Shaman, J.A., Boaz, S.M., & Ward, W.S. Paternal Pronuclear DNA Degradation Is Functionally Linked to DNA Replication in Mouse Oocytes. *Biol. Reprod.*(2007).

105. Tashiro, S. *et al.* S phase specific formation of the human Rad51 protein nuclear foci in lymphocytes. *Oncogene* **12**, 2165-2170 (1996).

106. MacPhail, S.H., Banath, J.P., Yu, Y., Chu, E., & Olive, P.L. Cell cycle-dependent expression of phosphorylated histone H2AX: reduced expression in unirradiated but not X-irradiated G1-phase cells. *Radiat. Res.* **159**, 759-767 (2003).

107. Huang, X., Tanaka, T., Kurose, A., Traganos, F., & Darzynkiewicz, Z. Constitutive histone H2AX phosphorylation on Ser-139 in cells untreated by genotoxic agents is cell-cycle phase specific and attenuated by scavenging reactive oxygen species. *Int. J. Oncol.* **29**, 495-501 (2006).

108. Suzuki, M., Suzuki, K., Kodama, S., & Watanabe, M. Phosphorylated histone H2AX foci persist on rejoined mitotic chromosomes in normal human diploid cells exposed to ionizing radiation. *Radiat. Res.* **165**, 269-276 (2006).

109. Schwartz, M. *et al.* Homologous recombination and nonhomologous end-joining repair pathways regulate fragile site stability. *Genes Dev.* **19**, 2715-2726 (2005).

110. Allen, C., Kurimasa, A., Brenneman, M.A., Chen, D.J., & Nickoloff, J.A. DNA-dependent protein kinase suppresses double-strand break-induced and spontaneous homologous recombination. *Proc. Natl. Acad. Sci. U. S. A* **99**, 3758-3763 (2002).

111. Fukushima, T. *et al.* Genetic analysis of the DNA-dependent protein kinase reveals an inhibitory role of Ku in late S-G2 phase DNA double-strand break repair. *J. Biol. Chem.* **276**, 44413-44418 (2001).

112. Hickson, I.D. RecQ helicases: caretakers of the genome. *Nat. Rev. Cancer* **3**, 169-178 (2003).

113. Ogburn, C.E. *et al.* An apoptosis-inducing genotoxin differentiates heterozygotic carriers for Werner helicase mutations from wild-type and homozygous mutants. *Hum. Genet.* **101**, 121-125 (1997).

114. Wang, L. *et al.* Cellular Werner

phenotypes in mice expressing a putative dominant-negative human WRN gene. *Genetics* **154**, 357-362 (2000).

115. Poot, M., Gollahon, K.A., Emond, M.J., Silber, J.R., & Rabinovitch, P.S. Werner syndrome diploid fibroblasts are sensitive to 4-nitroquinoline-N-oxide and 8-methoxypsoralen: implications for the disease phenotype. *FASEB J.* **16**, 757-758 (2002).

116. Werner-Favre, C. *et al.* Cytogenetic study in a mentally retarded child with Bloom syndrome and acute lymphoblastic leukemia. *Am. J. Med. Genet.* **18**, 215-221 (1984).

117. Hatch, T. *et al.* Maternal effects of the scid mutation on radiation-induced transgenerational instability in mice. *Oncogene*(2007).

118. Fenwick, J., Platteau, P., Murdoch, A.P., & Herbert, M. Time from insemination to first cleavage predicts developmental competence of human preimplantation embryos in vitro. *Hum. Reprod.* **17**, 407-412 (2002).

119. Yamada, T., Yukawa, O., Asami, K., & Nakazawa, T. Effect of chronic HTO beta or 60Co gamma radiation on preimplantation mouse development in vitro. *Radiat. Res.* **92**, 359-369 (1982).

120. Tarkowski AK An airdrying method for chromosome preparation from mouse eggs. *Cytogenetics* **5**, 394-400 (1966).

121. Salamanca, F. & Armendares, S. C bands in human metaphase chromosomes treated by barium hydroxide. *Ann. Genet.* **17**, 135-136 (1974).

122. de Boer, P., van Buul, P.P., Van, B.R., van der Hoeven, F.A., & Natarajan, T. Chromosomal radiosensitivity and karyotype in mice using cultured peripheral blood lymphocytes, and comparison with this system in man. *Mutat. Res.* **42**, 379-394 (1977).

123. Searle, A.G. & Beechey, C.V. Sperm-count, egg-fertilization and dominant lethality after X-irradiation of mice. *Mutat. Res.* **22**, 63-72 (1974).

124. Festing M. Origin and characteristics of Inbred strains of mice in *Genetic Variants and Strains of the Laboratory Mouse* (eds. Lyon M.F., Rastan S. & Brown S.D.M.) 1537-1576 (Oxford University Press, 1996).

125. Zhang, S., Ramsay, E.S., & Mock, B.A. Cdkn2a, the cyclin-dependent kinase inhibitor encoding p16INK4a and p19ARF, is a candidate for the plasmacytoma susceptibility locus, Pctr1. *Proc. Natl. Acad. Sci. U. S. A* **95**, 2429-2434 (1998).

126. Yu, Y. *et al.* Elevated breast cancer risk in irradiated BALB/c mice associates with unique func-

tional polymorphism of the Prkdc (DNA-dependent protein kinase catalytic subunit) gene. *Cancer Res.* **61**, 1820-1824 (2001).

127. Barber, R., Plumb, M.A., Boulton, E., Roux, I., & Dubrova, Y.E. Elevated mutation rates in the germ line of first- and second-generation offspring of irradiated male mice. *Proc. Natl. Acad. Sci. U. S. A* **99**, 6877-6882 (2002).

128. Barber, R.C. *et al.* Germline mutation rates at tandem repeat loci in DNA-repair deficient mice. *Mutat. Res.* **554**, 287-295 (2004).

129. Yauk, C.L., Dubrova, Y.E., Grant, G.R., & Jeffreys, A.J. A novel single molecule analysis of spontaneous and radiation-induced mutation at a mouse tandem repeat locus. *Mutat. Res.* **500**, 147-156 (2002).

130. Barber, R.C. *et al.* Radiation-induced transgenerational alterations in genome stability and DNA damage. *Oncogene* **25**, 7336-7342 (2006).

131. Biedermann, K.A., Sun, J.R., Giaccia, A.J., Tosto, L.M., & Brown, J.M. scid mutation in mice confers hypersensitivity to ionizing radiation and a deficiency in DNA double-strand break repair. *Proc. Natl. Acad. Sci. U. S. A* **88**, 1394-1397 (1991).

132. Blunt, T. *et al.* Identification of a nonsense mutation in the carboxyl-terminal region of DNA-dependent protein kinase catalytic subunit in the scid mouse. *Proc. Natl. Acad. Sci. U. S. A* **93**, 10285-10290 (1996).

133. Dubrova, Y.E., Plumb, M., Gutierrez, B., Boulton, E., & Jeffreys, A.J. Transgenerational mutation by radiation. *Nature* **405**, 37 (2000).

134. Rassoulzadegan, M. *et al.* RNA-mediated non-mendelian inheritance of an epigenetic change in the mouse. *Nature* **441**, 469-474 (2006).

135. Rousseaux, S. *et al.* Establishment of male-specific epigenetic information. *Gene* **345**, 139-153 (2005).

136. Olsen, A.K., Lindeman, B., Wiger, R., Duale, N., & Brunborg, G. How do male germ cells handle DNA damage? *Toxicol. Appl. Pharmacol.* **207**, 521-531 (2005).

137. Matsuda, Y. & Tobari, I. Repair capacity of fertilized mouse eggs for X-ray damage induced in sperm and mature oocytes. *Mutat. Res.* **210**, 35-47 (1989).

138. Harrouk, W., Codrington, A., Vinson, R., Robaire, B., & Hales, B.F. Paternal exposure to cyclophosphamide induces DNA damage and alters the expression of DNA repair genes in the rat preimplantation embryo. *Mutat. Res.* **461**, 229-241 (2000).

Section 4

Fundamental biological answers on clinical questions

Section 4.1

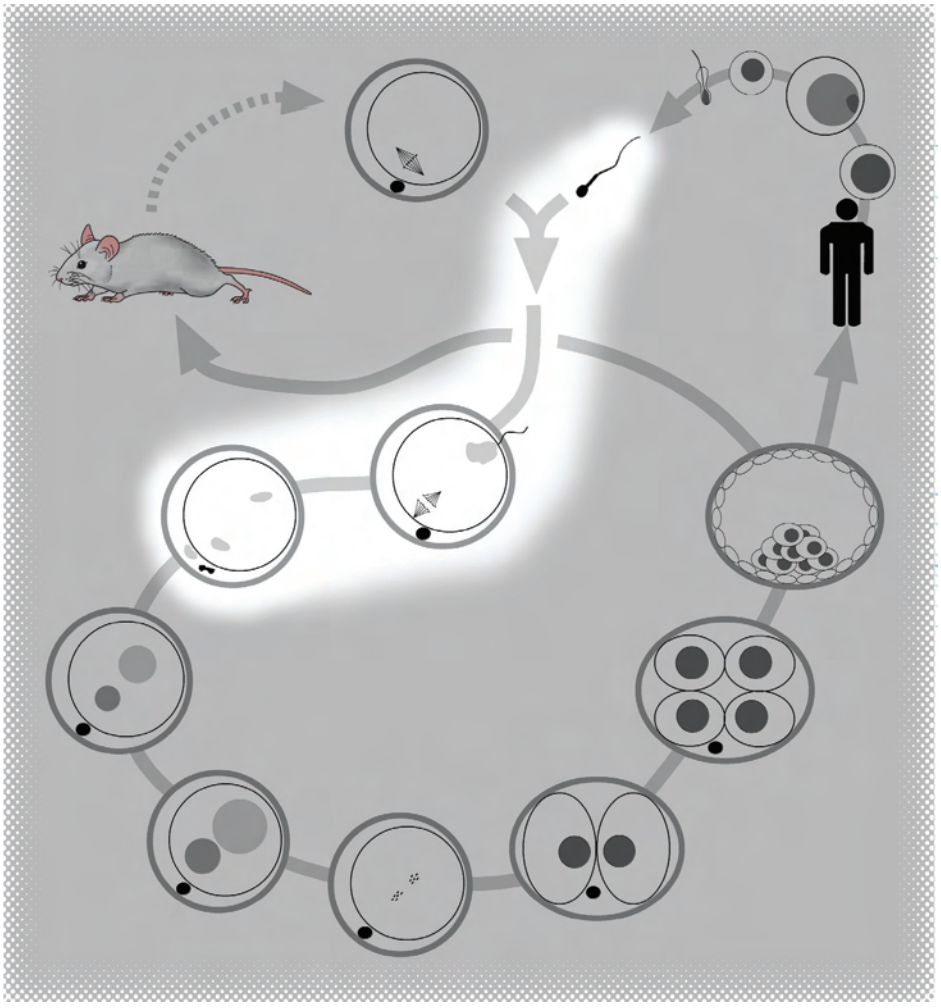

Human Reproduction 2007 June

Motile human normozoospermic and oligozoospermic semen samples show a difference in double strand DNA break incidence

Alwin AHA Derijck[#1], Godfried W van der Heijden[#1], Liliana Ramos[1], Maud Giele[1], Jan AM Kremer[1], Peter de Boer[1]

[#] *Both authors contributed equally*

1 Department of Obstetrics and Gynaecology, Radboud University Nijmegen Medical Centre, PO Box 9101, 6500 HB Nijmegen, The Netherlands

Abstract

Background Among ICSI children de novo structural chromosome aberrations of male descend are increased. Misrepair of double strand DNA breaks (DSBs) is a prerequisite for such aberrations to occur. To date, no absolute assessment of the number of DSBs in human sperm nuclei after gamete fusion has been described.

Methods Using man-mouse heterologous ICSI and γH2AX immunofluorescent staining, capable of detecting a single DSB, the number of lesions in ICSI selected sperm from normozoospermic men (n = 2) and oligozoospermic patients (n = 3) was quantified. A comparison with a sub-fertile male mouse model (n = 5) has been made. In addition, the fate of morphologically normal ejaculated immotile sperm after ICSI was examined.

Results A significant increase in the fraction of sperm cells bearing DSBs was found in oligozoospermic semen compared with that from normozoospermic men ($P < 0.01$). The majority of morphologically normal immotile human sperm showed excess γH2AX staining and nuclear disintegration. However, some had a non-deviant DSB pattern.

Conclusions The increased fraction of DSB positive sperm in both human and mouse oligozoospermic semen is adding to the surmise that semen from oligozoospermic patients has a reduced chromatin quality, causally related to reduced preimplantation embryo development. The use of ejaculated immotile sperm for *in vitro* reproduction is debatable due to sperm DNA degradation.

Introduction

With the introduction of assisted reproduction techniques (ART), infertility no longer poses an absolute hurdle for couples to parent a child. In biological terms, ICSI is a less physiological form of ART, as this technique circumvents biological selection. As sperm selection is a poorly defined concept [1] and ICSI is the sole option for many cases of male factor infertility, this poses a degree of concern. Sperm from such men usually meet several or all of the World Health Organization (WHO) criteria for oligo-astheno-teratozoospermia (OAT). One major concern pertains to an increased risk of de novo mutation at both the level of the gene and chromosome. An increased risk of de novo mutation at the chromosomal level has been indicated. In sperm of OAT males, the normally low incidence of numerical chromosomal abnormalities is about doubled implying meiotic defects [2], possibly illustrated by lower recombination rates [3], giving rise to an increased number of aneuploid offspring [4].
The aetiology of structural chromosome aberrations, that are also more frequent among ICSI descendants [4], remains unclear. For a long time, this class of mutation has been known to be largely of male descent [5]. Misrepair of double-strand DNA breaks (DSBs) is a prerequisite for structural chromosome aberrations to occur [6]. Indeed, radiation-induced DSBs in mouse and human sperm lead to chromosome abnormalities, detectable in the paternal chromosomes at the first cleavage division [7, 8].

DSBs are a characteristic of living cells in that they do occur spontaneously in the cell cycle during DNA replication and are instrumental in the generation of antibody diversity [9] and meiotic recombination If left unrepaired, DSBs would inhibit the cell cycle or alternatively would lead to gross structural alteration of the chromosome complement, most likely by a high frequency of deletions. Therefore a DSB is considered to be a most serious DNA lesion. Hence, special DNA repair pathways, notably homologous recombination repair (HR) and non-homologous end joining (NHEJ) evolved in the course of evolution to take care of such damage [see for review [10]]. Structural chromosome abnormalities such as dicentric chromosomes, reciprocal translocations and acentric fragments are conceptualized as failures of both NHEJ and HR, for which the word misrepair is coined.

DSBs are also used to rearrange chromatin, a most prominent example being the elongation of round spermatids when the enzyme Topoisomerase II [11] both creates and religates these lesions. This breakage activity is implicated in the loss of the nucleosomal chromatin structure on the way to transition protein and protamine occupation of DNA in sperm.
Sperm present a special group of nuclei with respect to DNA damage as nuclei are very compact. Yet, several methods have yielded indications for the presence of DNA damage at a larger scale than in somatic cell systems that rely on active DNA repair, that is not available to the sperm nucleus [12, 13].
For the past decades, the DNA integrity of the sperm nucleus has been measured by numerous techniques: i.e. NT (in situ nick translation), TUNEL (terminal deoxynucleotidyl transferase dUTP end labelling), SCE (single cell electrophoresis or Comet assay in alkaline and "neutral" variants), sperm chromatin dispersion test and SCSA (sperm chromatin structure assay) [14, 15]. Apart form the neutral comet assay [16], these methods do not specifically sense DSBs. Moreover, the neutral comet assay does not generate absolute numbers of breaks.

For the cytogenetic analysis of human sperm after heterologous insemination, hamster [17] and mouse [18] secondary oocytes have been used in the past. Heterologous ICSI of mouse oocytes is a proven method for the assessment of oocyte activating power and chromosomal constitution of human sperm, mimicking the ICSI-involved sperm selection procedure [18, 19]. Frequencies of 1.3% and 6.9% for, respectively, numerical and structural chromosome aberrations, have been found in morphologically normal semen using these methods [18]. However, from the data on structural chromosome abnormalities, the absolute number of breaks per sperm nucleus cannot be deduced, due to an absence of knowledge regarding the reliability of repair mechanisms, i.e. the amount of misrepair of HR and NHEJ, in the zygote [20]. Because of the fact that DNA repair is not error free, knowledge about the absolute number of DSBs in sperm is required.

As every living cell has to cope with DNA damage, highly sensitive signalling and repair mechanisms have evolved [9]. The surveil-

lance and repair machinery that protects the cell from DSBs uses enzymes that recognize the DSB and phosphorylate proteins surrounding the break, notably Histone H2AX, denoted as γH2AX (Rogakou et al., 1998).
This reaction, appearing within minutes after the insult in most cellular systems, is pivotal to genome stability and conserved from yeast to human [21, 22]. As a prerequisite for the present investigation, we have investigated whether γH2AX signalling was operative in the early mouse zygote, which was the case for both paternal and maternal chromatin [23].

Upon gamete fusion followed by activation of the secondary oocyte, the second meiotic division is completed. Simultaneously, a speedy transition from sperm nucleus to male pronucleus occurs, [24] during which paternal chromatin undergoes remodelling from a protamine-rich sperm chromatin configuration, to the histone-based nucleosomal configuration. γH2AX can be detected after the onset of chromatin remodelling .
During temporary recondensation of the unfolded sperm nucleus, histone H3 is increasingly phosphoryated at serine 10. With uniform staining for this epitope, γH2AX foci are distinctly present and large foci representing DSBs can be positively identified [23].
Here we quantify DSBs present in human sperm after chromatin remodelling using the mouse heterologous ICSI and γH2AX staining (HIGH) assay. Sperm from normozoospermic men and oligozoospermic patients, selected by WHO criteria, was analysed. A comparison with a sub-fertile male mouse model has been made. For the first time, absolute numbers of sperm DSBs could be determined.

Sperm motility is a crucial factor that influences the outcome of ICSI. Both pregnancy rate and embryo quality are reduced after ICSI with immotile sperm [25]. DNA damage assays have been shown to give lower readings in sperm selected for motility, both after swim up [16] and manual selection [26]. By theory and in practice, immotile sperm is composed of a viable and non-viable fraction with a large variation between samples. Hence, the use of ejaculated immotile sperm for ICSI is still under debate. Therefore, we also examined ejaculated immotile but morphologically normal sperm by the HIGH assay under the assumption that this dichotomy could be clarified from

zygote chromatin behaviour, which was the case.

Methods

Reagents

For oocyte storage, injection and culture, minimum essential alpha medium was used (Cat no. 22571, GIBCO Life Tech, Gaithersburg, MD), supplemented per 500 ml with 2.5 g HEPES, 684 mg 50% sodium lactate solution, 55 mg sodium pyruvate, 65 mg penicillin G (1596 U/mg) and 6% fetal calf serum (BioWhittaker Europe, Verviers, Belgium).

Semen donors

Semen samples from three OAT men [by WHO criteria [27]] attending our fertility clinic for diagnosis were cryopreserved for this study. Cryopreserved semen samples of two normozoospermic men of proven fertility served as controls. The percentage of severely DNA-damaged sperm of each sample was assessed by TUNEL assay [26] after thawing. All patients gave written informed consent before inclusion in this study.

Preparation of cryopreserved human sperm

Sperm samples were diluted 1:1 (drop wise) with test yolk buffer (Irvine Scientific, Santa Ana, CA, USA) and equilibrated for 10 min at room temperature. The sperm/cryoprotectant mixture was aspirated in 0.5 ml straws (CBS, France), sealed, placed in a cooling chamber and rapidly frozen in liquid nitrogen vapour for 10 min [4, 28, 29]. Straws were stored in liquid nitrogen. Thawing, occurred for 10 min at room temperature, followed by dilution of cryoprotectant with 1 ml human tubal fluid (HTF)-HEPES. Suspension was centrifuged for 5 min at 500 g and the pellet was gently resuspended in HTF-HEPES. This was repeated once and the samples were kept at room temperature until ICSI.

Preparation of mouse sperm

Male mice, heterozygous for two semi-identical reciprocal translocations *T(1;13)70H* and *T(1;13)1Wa* (abbreviated *T/T'*) usually are sterile by OAT [30]. Sterility is caused by reduced chromosome synapsis at first meiotic prophase for translocation chromosomes. This mouse model is maintained on a Swiss random bred background. Zygotes derived by ICSI with cauda epididymal sperm show a severely reduced cleavage rate and developmental delay/arrest during the zygotic S-/G2-phases [31]. Sperm of five OAT mice [8-10 weeks, testes 50-70 mg, [31]] was obtained by disper-

sion of the contents of the two cauda epididymidi in 200 µl HTF-Hepes 3% bovine serum albumin (Sigma, A-4503). Samples were kept at room temperature.

Preparation of mouse oocytes

B6D2 F1 females (4-10 weeks) (Charles River, Sulzfeld, Germany) were used as oocyte donors and kept at a 9.00 am - 9.00 pm light schedule. Superovulation was induced by i.p. injection of 7.5 IU pregnant mare's serum gonadotrophin (PMSG) (Intervet, Boxmeer, The Netherlands) around 9 pm, followed by 7.5 IU HCG (Intervet, Boxmeer, The Netherlands) 48 h later. Oocytes were freed from the oviducts 13 h after HCG, and stored without cumulus cells at 37 °C for up to 5 h.

Heterologous and homologous ICSI

Microinjection was performed as described [32] with some adaptations. The injection medium was kept at 24 °C. Both human and mouse sperm were selected for normal morphology and motility at 400x magnification. Morphologically normal immotile sperm of OAT men were used as well. The sperm tail of mouse sperm was removed using the piezo driven injection needle. After injection, oocytes were kept on the microscope stage for 5 min, were then gradually warmed to 37 °C and placed in culture medium at 37 °C, 5% CO2 in air.

Fixation and staining of zygotes

For immunofluorescent detection of γH2AX chromatin domains and status of paternal chromatin remodelling (by anti-H3S10ph) zygotes were processed two hours after ICSI as described [24]. The following antibodies were used: γH2AX mouse monoclonal (Upstate #05-636, clone JBW301, 1:10,000) and rabbit anti-H3S10ph (Upstate #06-570, 1:1,000). Secondary antibodies were: Molecular Probes, Oregon, USA: A11001 fluor 488 goat anti-mouse IgG (H+L), A11012 fluor 594 goat anti-rabbit IgG (H+L), both in a 1:500 dilution. DNA was stained with 4',6-diamidino-2-phenylindole (DAPI) in phoshate-buffered saline (0.33 mg/l) and fading was counteracted with Vectashield (Vector Laboratories).

Analysis

Microscopic observations were made from coded samples by one observer (A.A.H.A.D.). Oocyte activation status was assessed, as was the degree of decondensation and chromatin remodelling of the sperm nucleus. Large DSB related γH2AX foci of fully remodelled paternal nuclei (judged by histone H3 serine10 phosphorylation and DAPI morphology)

were counted. Unlike small foci, large foci can be induced by sperm irradiation and treatment of the early zygote with proven inducers of DSBs [23].

Non-parametrical statistical analysis was performed using Prism (Graphpad) and SPSS (Appache software foundation) software.

Results

Semen quality and heterologous ICSI efficiency

Semen samples were categorised using the hallmark parameters of fertility; concentration, motility and morphology. The TUNEL staining provides a further reference to semen quality. A TUNEL score >14% is indicative for poor DNA integrity and correlates with reduced fertility [26, 33]. As expected, the DNA integrity of OAT sperm was reduced (higher TUNEL scores, Table 1).

Heterologous ICSI was performed on 274 mouse oocytes, resulting in 225 analysable zygotes (82.1% survival). Zygotes were classified in three classes: a) normal zygotes with maternal chromosomes in anaphase II – telophase II and fully remodelled sperm (Figure 1A); b) activated secondary oocytes without sperm decondensation; c) sperm nucleus expansion without oocyte activation. Between patient samples, no significant differences were observed for class distributions (Table 2). However, morphologically normal immotile sperm (pooled from OAT semen, all patients) showed a significant shift in ICSI characteristics, with almost half of the sperm lacking oocyte activating capacity (Table 2).

Table 1. Clinical parameters of semen samples with corresponding TUNEL score

Donor	Semen sample parameters			% TUNEL
	Total Concentration (10^6 sperm/ejaculate)	% Motile	% Normal morphology	
Normo 1	102	65	15	14
Normo 2	300	60	29	8
OAT 1	36	10	1	35
OAT 2	13.2	30	2	66
OAT 3	6.3	15	2	70

DSB analysis of human sperm using γH2AX

All normal developing zygotes were analysed for γH2AX signalling. The mouse oocyte remodels the human sperm nucleus to a nucleosomal chromatin structure [mouse [24, 34]]. The DNA damage signalling mechanism of the oocyte marks DSBs via γH2AX which show as large foci in paternal chromatin (Figure 1A). These can be counted provided the remodelling process has advanced far enough, which is indicated by uniform H3S10ph staining [23] (Figure 1A). Background

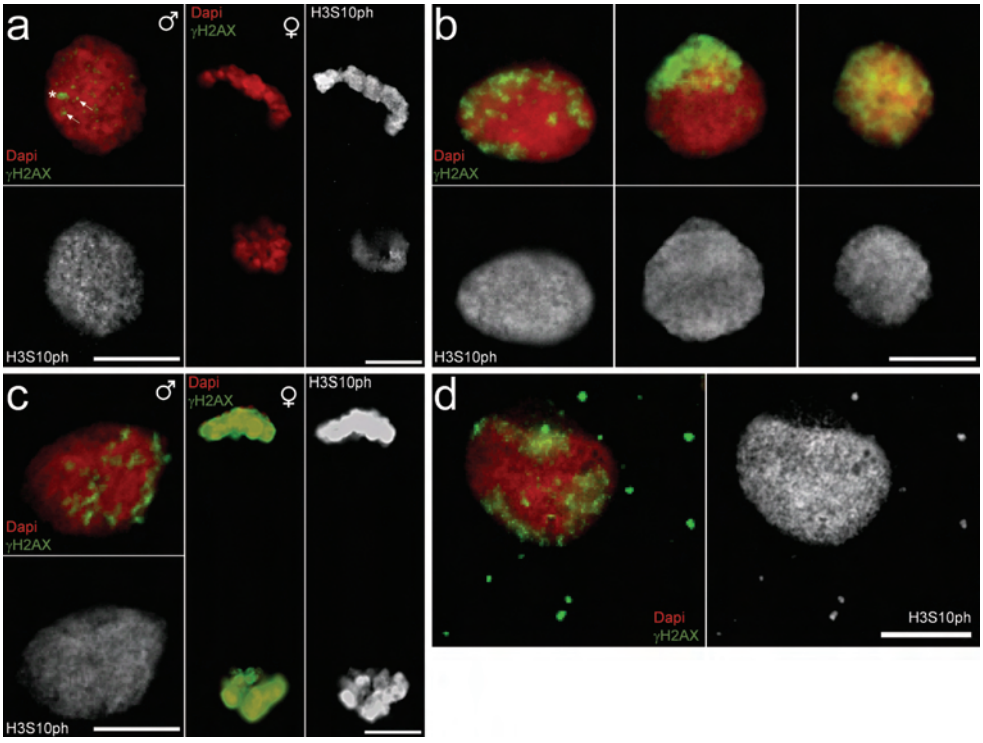

Figure 1 gH2AX patterns in zygotes derived from human sperm in heterologous ICSI

(**A**) Remodelled paternal chromatin showing DSB related gH2AX focus (asterisk) and examples of non-DSB related gH2AX foci (arrows) (male symbol). Homogenous histone H3S10ph is indicative of fully remodelled male chromatin. The corresponding mouse maternal ana-/telophase II is also depicted (female symbol). (**B**) Examples of aberrant paternal gH2AX staining found after injection of immotile, morphologically normal sperm. (**C**) Aberrant staining of paternal chromatin after ICSI with immotile sperm (male symbol) evokes gH2AX signalling on

the mouse maternal ana-/telophase II chromatin (female symbol). (**D**) In addition to the aberrant staining patterns shown in 1B/C, sperm lacking oocyte activating power could fragment after chromatin remodelling. Double labelling with H3S10ph verifies the paternal origin of the gH2AX fragments.

Table 2. Zygote development with human semen and oligospermic mouse semen

Semen	# Cells	Abnormal development		Normal development
		% Activation without sperm decondensation (#)	% No activation with sperm decondensation (#)	% Activation with sperm decondensation (#)
Normo 1	52	21.2 (11)	0.0 (0)	78.8 (41)
Normo 2	35	22.9 (8)	0.0 (0)	77.1 (27)
OAT 1	54	16.7 (9)	1.9 (1)	81.5 (44)
OAT 2	38	18.4 (7)	0.0 (0)	81.6 (31)
OAT 3	25	12.0 (3)	4.0 (1)	84.0 (21)
Pool non-motile	21	0.0 (0) [&]	42.9 (9) [&]	57.1 (12) [&]
Oligo mouse	46	2.2 (1)	4.3 (2)	93.5 (43)

The percentages of abnormal and normal development are given
[&]: Statistically different ($p<0.05$) from all other groups using Pearson chi-Square (not including mouse sperm)

staining and small γH2AX foci, intrinsic to the sperm remodelling stage are not DSB related [23]. Occasionally a non-focal pattern often covering the larger part of the nucleus, is observed (Figure 1B and 1C). This type of γH2AX staining was mostly found in morphologically normal immotile sperm (see below).

When the ranges and averages of DSB related γH2AX foci from all five men were compared, no significant differences could be detected (Figure 2A).

Zygotes were divided into three groups on the basis of paternal γH2AX staining (Table 3): without DSB foci (negative), with foci and with an aberrant γH2AX pattern. The fraction of sperm with DSB-related foci is increased in OAT men, as shown in the graphical representation (Figure 2B).

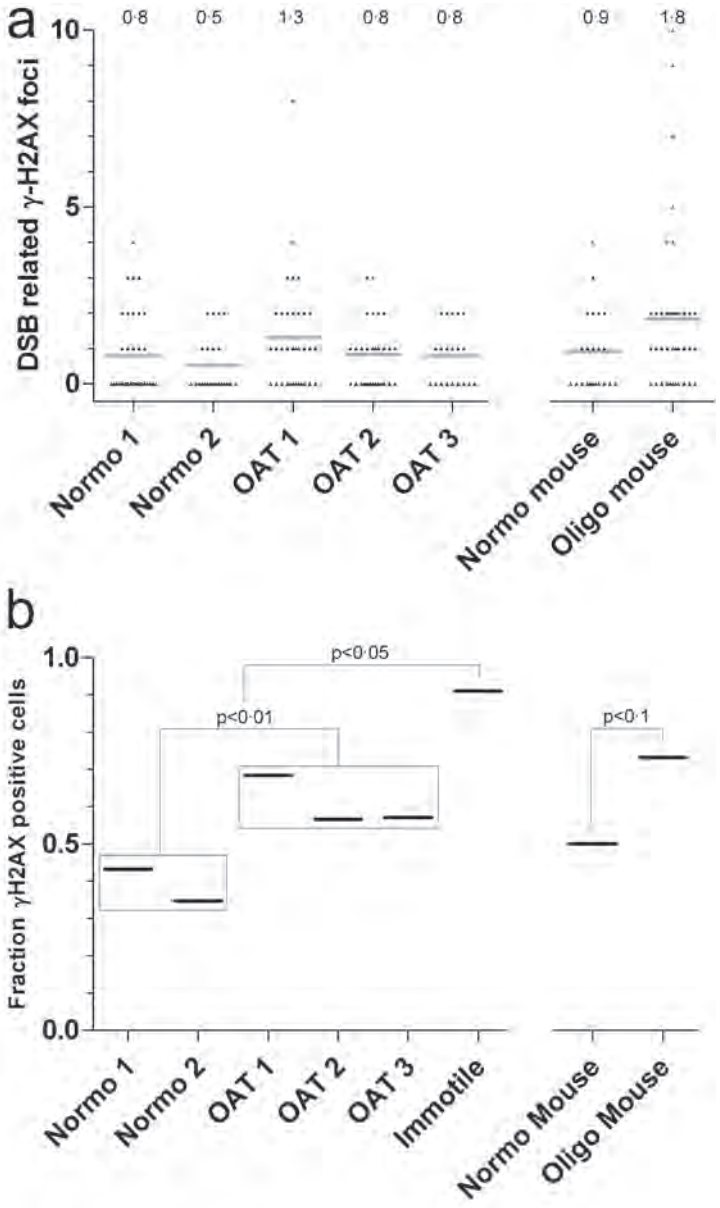

Figure 2 gH2AX analysis of paternal chromatin in normal developing zygotes (**A**) Distributions and averages of DSB related gH2AX foci found in remodelled paternal chromatin after heterologous- (normospermic and OAT donors; left) and homologous ICSI (mouse; right). The value of the average is given above each column. (**B**) Fraction of cells containing at least 1 DSB related gH2AX focus, including aberrant staining patterns (Table 3). Significant differences by Pearson Chi

square are indicated. No statistical differences within boxed groups. The normozoospermic mouse (normo) data were taken from[22].

Table 3. γH2AX analysis of human semen in heterologous ICSI

Semen	# Analyzed sperm nuclei	% Negative sperm (#)	% Aberrant staining (#)	% Sperm with DSB foci (#)
Normo 1	37	56.8 (21)	5.4 (2)	37.8 (14)
Normo 2	23	65.2 (15)	0.0 (0)	34.8 (8)
OAT 1	38	31.6 (12)	5.3 (2)	63.2 (24)
OAT 2	30	43.3 (13)	0.0 (0)	56.7 (17)
OAT 3	21	42.9 (9)	4.8 (1)	52.4 (11)
Pool non-motile (oocyte activated)	12*	9.1 (1)	71.4 (7)	27.3 (3)
Pool non-motile (oocyte not activated)	9	0.0 (0)	77.8 (7)	22.2 (2)

Negative nuclei are defined as remodelled and not containing DSB related γH2AX foci. Aberrant staining shows as a non-focal pattern that often covers the larger part of the nucleus. *1 zygote had progressed to early pronuclear stage, not suitable for γH2AX analysis

Chromatin from morphologically normal ejaculated immotile sperm displays an increased incidence of aberrant γH2AX staining

Ejaculated immotile sperm are prone to lack oocyte activating activity (Table 2). In addition, both immotile sperm which do activate oocytes and those which do not, show a significant increase in aberrant γH2AX staining patterns (Table 3 and Figure 2B). Larger positive nuclear domains up to heavily stained paternal chromatin prevail (Figure 1B and 1C). Of the sperm nuclei lacking oocyte activating capacity, 4 out of 9 showed chromatin disintegration within the oocyte cytoplasm, as indicated by chromatin fragments double stained for γH2AX and H3S10ph (Figure 1D). Although ICSI with immotile sperm resulted in 81% (17/21) abnormal zygotes, 28.6% (6/21) was able to produce normal remodelled paternal chromatin (2 non-activating and 4 activating sperm). The level of DSB related

Table 4. Comparison γH2AX reaction of parental chromatin in relation to oocyte activation

	No Activation		Activation		Grouped	
P \ M	Normal(M)	Abnormal(M)	Normal(M)	Abnormal(M)	Normal(M)	Abnormal(M)
Normal(P)	2	0	5	0	7	0
Abnormal(P)	2	5	2	5	4	10

Paternal (P) development was categorized as normal (with or without foci, Figure 1A) or with abnormal non-focal staining (Figure 1B and 1C). Bright staining of maternal (M) chromatin, either in the arrested metaphase II chromosomes, or at ana-/telophase II (Figure 1C) was scored

foci of these nuclei, showed no significant difference with motile sperm (average 1.8).

Maternal chromatin reacts to abnormal paternal chromatin from immotile sperm

The maternal chromatin arrested at meiotic metaphase II shows a clear punctuate non-DSB related γH2AX staining, similar to that found in normal mitosis [35]. After resumption of meiosis II this meiotic γH2AX diminishes rapidly (Figure 1A and [23]). However, zygotes containing aberrantly γH2AX stained paternal chromatin from immotile sperm (Figure 1B and 1C) often showed an abnormal intense labelling of the maternal anaphase II (Figure 1C). Table IV shows the status of parental chromatin of all oocytes/zygotes from injected immotile sperm. Abnormal γH2AX intensities/patterns often correlated between parental chromatin complements.

ICSI with epididymal sperm of a sterile mouse model

Morphologically normal motile sperm of *T/T*' mice was used for ICSI. A total of 46 analysable zygotes was obtained (90.2% survival). Zygote development is given in Table 2. DSB related γH2AX foci were counted in normal zygotes and compared with sperm from normozoospermic males (Table V and Figure 2). The average amount of DSBs was doubled in OAT mouse sperm. However, no statistical significant difference was obtained (Figure 2A). A significant increase of the fraction of γH2AX positive remodelled nuclei was also observed in OAT mouse sperm (Figure 2B).

Table 5. Comparison of γH2AX analysis between normospermic (IVF) and oligospermic (ICSI) mouse sperm

Semen	# Analyzed sperm heads	% Negative sperm (#)	% Aberrant staining (#)	%Sperm with DSB foci (#)
Normo mouse	22	50.0 (11)	0.0 (0)	50.0 (11)
Oligo mouse	41	26.8 (11)	2.4 (1)	70.7 (29)

CBA.B6.F1 sperm tested by IVF with B6.CBA F1 oocytes have been used as controls (**Section 2.1**). Negative nuclei do not contain DSB related γH2AX foci

Discussion

In situ DSB detection in sperm via γH2AX at chromatin remodelling post gamete fusion

The chromatin composition of sperm nuclei differs from somatic nuclei by the presence of protamines. Although human sperm chromatin remodelling during spermiogenesis is incomplete when compared with mouse (residual nucleosomes: mouse ~1%, human ~15%) [36], no γH2AX signal can be detected in *in vitro* decondensed sperm of both species (L. Ramos personal communication). The analysis of H2AX phosphorylation in human sperm after heterologous ICSI, indicates that human sperm is comparable to mouse sperm (Figure 1) [23].

It was already known that mouse oocytes can efficiently remodel human sperm chromatin to a somatic state, capable of chromosome condensation during first mitosis [18]. Both studies demonstrate the suitability of the heterologous zygote system for the study of human sperm chromatin and chromosomes.

Sperm quality measurements compared

Sperm quality assessments based on the basic WHO sperm parameters are often supported by DNA integrity measurements like TUNEL, SCE and SCSA [33]. The fraction of presumably apoptotic (i.e. TUNEL positive) sperm within an ejaculate correlates well between assays and is ~11% in normozoospermics [33, 37], see also Table I. Selection of individual morphologically normal progressively motile sperm reduces the TUNEL-positive fraction to <1% [26] in line with

the general notion that more heavily DNA-compromised sperm nuclei are found in the immotile fraction [16].
The HIGH assay measures the absolute amount of DSBs [23] after sperm selection by ICSI criteria and sperm chromatin remodelling in the oocyte. The DSB-"positive" fraction in the HIGH assay was 36% (fertile donor average) and 57% (OAT average), showing discriminative power for motile sperm [in contrast to TUNEL [26]] and demonstrating the improved sensitivity of the HIGH assay. Hence, both at the level of the total sperm population (DNA integrity assays) and in stringent "ICSI"-selected sperm (HIGH assay) a difference between normozoospermic and infertile semen was found, adding to the evidence that sperm chromatin and DNA integrity is altered in male infertility syndromes. It is reassuring that for these small samples the average absolute number of DSBs in semen from normozoospermic donors was not significantly different from that of OAT patients. We have to stress h owever, that the OAT donors used, were not at the extreme end of the spectrum. Assuming the incidence of DSBs to be applicable to ICSI candidates in general, the increase of de novo structural chromosome abnormalities after ICSI, by at least 4-fold [4], can not be attributed to an elevated number of DSBs in OAT semen per se (Figure 2) and could therefore arise early in embryonic development (zygote and cleavage stage) or during spermatogenesis. Indeed, inspection of synaptonemal complexes in pachytene spermatocytes of infertile men has yielded indications for quadrivalents representing reciprocal translocations [38].

The minor increase of DSBs in OAT sperm could relate to a hampered preimplantation development

Zygotes derived from cauda epididymal sperm of *T/T*' OAT mice showed a reduced cleavage rate (33% versus 87-96%) due to developmental delay and arrest during zygotic S- or G2-phase [31]. In sperm of these mice, the measured number of DSBs was similar to 1.5-2 Gy sperm irradiation [23]. Irradiation-induced damage, that leads to chromosome abnormalities at first cleavage division including reciprocal translocations, does not block the progression of the zygotic cell cycle [7]. Therefore, the marginal increase of DSBs in conjunction with the developmental block at S/G2 phase found after insemination with *T/T*' OAT sperm [31] indicates that the HIGH assay does not measure the total burden of aberrant chromatin. Cauda epididy-

mal sperm from *Tnp1*-/-,*Tnp2*+/- mice that have an abnormal chromatin compaction due to a defect in the nucleosome to protamine transition, produced lower implantation rates and yields of live born offspring [39].Therefore, depending on the aetiology of these OAT mouse models, an early or late onset phenotype of preimplantation development has been described.

In human reproduction, a link between a paternal factor and poor embryo quality [40] resulting in reduced pregnancy rates, has been observed [41]. Poor sperm quality as judged by the conventional DNA integrity assays is often found to be linked to reduced cleavage/blastocyst rates [42-46], reduced in vivo fertility and ART outcome [45, 47-51] [for reviews, see [52, 53]]. Early onset paternal effects on zygote development [54] and early cleavage [52] have also been described. Thus, also for the human, the increased fraction of sperm with DSBs (Figure 2B) could indicate a pathology related to aberrant chromatin, i.e. expressed during preimplantation development. However, this burden does not originate from the absolute number of DSBs that were either present in the sperm before penetration or were induced at chromatin remodelling before pronucleus formation [23, 55]

Immotile sperm and DNA fragmentation

Protamine dominated sperm chromatin is generally regarded as highly stable. In contrast, chromatin from immotile human sperm often disintegrated after heterologous ICSI . In line with our results, Rybouchkin and co-workers (1997) found a strong correlation between zygote arrest and the proportion of non-viable sperm among the immotile ones, also using man-mouse heterologous ICSI [56]. γH2AX staining revealed male nucleus disintegration during the chromatin remodelling phase before pronucleus formation (Figure 1). Recently, mammalian sperm including human sperm was found to contain endonucleases which become activated after membrane permeabilization in the presence of divalent cations [57]. DNA degradation by these endonucleases was noticed already after 15 min and eventually digested the DNA to 50 kb loop domain fragments [57], suggestive of an apoptosis-like pathway, represented by the fraction of TUNEL-positive spermatozoa [58]. The γH2AX pattern of 70% of nuclei from immotile sperm is indicative for high DNA damage (Figure 1B-D) . We have to stress that nuclear fragmentation after gamete fusion (Figure 1D) was not found after ICSI with motile

sperm that indeed are TUNEL negative [26]. In 71% (10/14) of the cases, highly damaged non-motile sperm triggered a signalling response in the maternal chromatin, as deduced from the increase in H2AX phosphorylation (Table 4 and Figure 1C). Normally, the condensed maternal second meiotic chromosomes loose γH2AX upon oocyte activation (Figure 1A). A functional role for the oocyte chromatin in supporting preimplantation development of zygotes with damaged paternal chromatin has been shown in the mouse [39]. The nature of this maternal role remains elusive and needs further investigation. The maternal reaction found by us, supports the existence of a role of maternal chromatin in determining paternal chromatin integrity in the zygote.
In ~20% of immotile ejaculated sperm injections (4/21, Table 3) we found a normal γH2AX pattern in paternal and maternal chromatin. This assessment may well be in line with clinical results obtained with immotile ejaculated sperm, notwithstanding the multifactorial background of this condition.

Conclusively, by use of man-mouse heterologous ICSI combined with the examination of the most pronounced chromatin marker for DSBs (γH2AX) we have for the first time obtained an objective assessment for the absolute number of these most serious DNA lesions in sperm. The incidence of DSBs was comparable in mouse and man (Figure 2). For both species, an indication was found for a decrease of the fraction of DSB-free sperm in OAT. This observation could be one aspect of data in the current literature, that hypothesize a paternal chromatin-linked factor to negatively influence preimplantation embryonic development. In addition, this approach has unequivocally demonstrated the nuclear disintegration of the larger part of morphologically normal ejaculated immotile human sperm and supports further deliberation on the use of such sperm in assisted reproduction.
In this project we for practical reasons made an exclusive use of cryopreserved samples, which in case of an interaction between resistance to cryopreservation and donor status (i.e. fertile or subfertile) could influence the interpretation of our data. On the other hand, survival after cryopreservation could lead to a general improvement of DNA integrity as measured by a modified alkaline Comet assay (Donnelly et al., 2001) no mention being made of any

relation between sperm quantity and direction of change with this assay.
The HIGH assay could also be an asset in the analysis of DNA integrity of testicular sperm in non-obstructive azoospermia and of immature testicular spermatids, in both cases capable of addressing possible relations with altered sperm chromatin remodelling. Due to the delicacy of mouse ICSI and time-consuming analysis, the HIGH assay will not be a suitable system for clinical sperm DNA integrity testing. From a biological point of view however, this system provides a highly sensitive single-sperm analysis, to study principal questions on sperm DNA integrity and the oocyte response in man and mouse.

Acknowledgements

The Dutch ministry of Health, Welfare and Sport financed this research.

Section 4.2

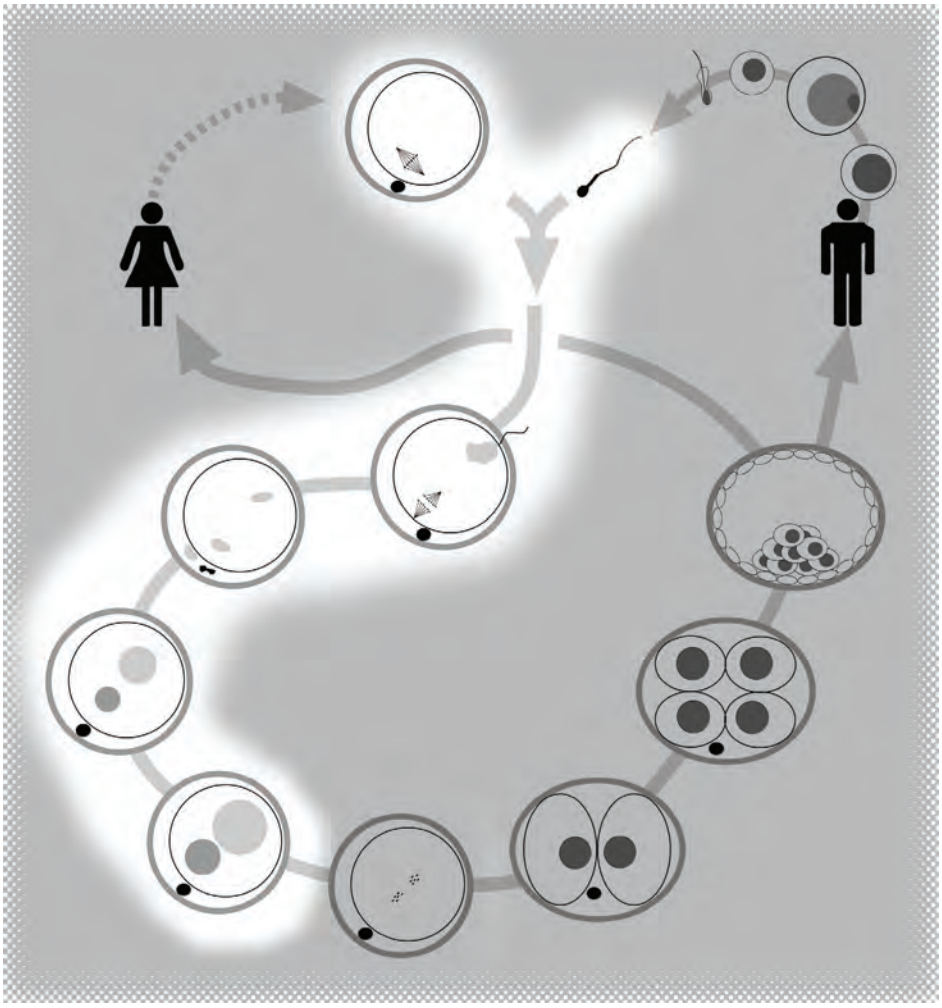

Submitted

Parental origin of chromatin in human monopronuclear zygotes revealed by asymmetric histone methylation patterns, differs between IVF and ICSI

Godfried W. van der Heijden [a,#], Ilse M. van den Berg [b,#], Esther B. Baart [b], Alwin A.H.A. Derijck [a], Elena Martini [b], Peter de Boer [a]

[a] *Department of Obstetrics and Gynaecology, Radboud University Nijmegen Medical Centre, P.O. Box 9101, 6500 HB Nijmegen, The Netherlands*

[b] *Division of Reproductive Medicine, Department of Obstetrics and Gynaecology, Erasmus MC, University Medical Center, Gravendijkwal 230, 3015CE Rotterdam, The Netherlands*

[#] *Both authors contributed equally*

Abstract

In mouse zygotes, many post translational histone modifications are asymmetrically present in male and female pronuclei. We investigated whether this principle could be used to determine the genetic composition of monopronuclear zygotes in conventional IVF and ICSI. First we determined whether the principle of male female asymmetry is conserved from mouse to human by staining polypronuclear zygotes with antibodies against a subset of histone N-tail post-translational modifications. To analyze human monopronuclear zygotes, a modification was selected that is solely present in the maternal chromatin. A total of 17 IVF-derived monopronuclear zygotes all showed a non-uniform staining pattern, which is proof of a bi-parental origin and is assumed to result in a diploid conception. In contrast, ICSI-derived monopronuclear zygotes (n=20) could be divided into three groups based on their staining pattern: 1) of maternal origin (n=12), 2) of paternal origin (n=5) or 3) consisting of two chromatin domains as in IVF (n=5). Our data show that monopronuclear zygotes originating from IVF arise through fusion of parental chromatin after sperm penetration. In contrast, monopronuclear zygotes derived from ICSI in most cases contain uni-parental chromatin. The fact that chromatin was of paternal origin in one-quarter of ICSI zygotes indicates an additional mechanism for haploid embryo generation. Implications for embryo transfer are discussed.

Introduction

Fertilization entails both cytoplasmic and chromatin fusion of two highly specialized gamete types. Cytoplasmic fusion occurs at sperm penetration. Nuclear fusion follows after syngamy of the two pronuclei when nuclear envelopes dissolve and at the first cleavage division, one mitotic spindle is constructed [59]. In *in vitro* fertilization (IVF), a zygote with two distinct pronuclei is considered to be the result of normal fertilization and is usually encountered. Two types of abnormal fertilization are known to occur after both conventional IVF and intra cytoplasmic sperm injection (ICSI): monopronuclear and polypronuclear zygotes. Both types of zygotes are able to undergo cleavage divisions and can result in embryos of good morphological quality.

After insemination, 2-6% of the oocytes will display only a single pronucleus after conventional IVF [60] and 5-27% after ICSI [61, 62]. Traditionally and inspired by research into the artificial activation of mouse secondary oocytes [63], monopronuclear zygotes are thought to lead to haploid parthenogenetic embryonic development [64]. However, previous studies investigating the chromosomal status of embryos resulting from monopronuclear zygotes by fluorescence in situ hybridization (FISH), have shown a diploid chromosome constitution in 49-62% of IVF-derived and 10-30% of ICSI-derived embryos [65, 66]. Diploid embryos may be generated from uni-parental monopronuclear zygotes and subsequent diploidization [63, 67] or by early fusion of paternal and maternal chromatin [68]. Due to imprinting requirements only the latter ones may result in offspring whereas mono-parental diploid embryos of paternal descend can yield complete hydatidiform mole (CHM) pregnancies [69]. Monopronuclear zygotes have been reported to lead to progeny in the human [60, 70, 71] which indicates these to originate from a fusion of male and female chromatin.

Although chromosomal FISH analysis can differentiate between haploidy and diploidy, it cannot absolutely distinguish between diploid bi-parental and diploid mono-parental female embryos. Therefore, to know if monopronuclear zygotes may be precociously fertilized by the untimely fusion of paternal and maternal chromatin, and according to the definition of fertilization are suitable for embryo transfer, it is necessary to determine the origin of the chromatin present in a monopronuclear zygote.

Histones are proteins that together with DNA form the nucleosome, the basic repeat unit of chromatin. The nucleosome protein complex consists of four different histones (H2A, H2B, H3 and H4), each of them present twice [72]. Around this complex approximately 150 base pairs DNA are wrapped. The histones can be modified at specific amino acids by covalent attachment of small molecules (e.g. acetyl, phosphoryl, methyl) or peptides (e.g. ubiquitin, sumo) [73, 74]. These post translational modifications are especially numerous at the N-tails of H3 and H4, that extend form the nucleosomal globular domain. Depending on their biological context these modifications influence for instance chromatin compaction, hence gene transcription and DNA repair [73, 75]. It has been shown that in the mouse zygote, several H3, H4 lysine methylation marks are absent in the paternal pronucleus but present in the maternal one, a phenomenon denoted as pronuclear asymmetry [24, 76-80].
In mouse zygotes, we observed that the asymmetrical setting of lysine methylation is maintained when parental chromatin is precociously fused, leading to a monopronuclear zygote. If the asymmetric setting of parental marks is conserved in the human, it could be used to determine the origin of the chromatin present in monopronuclear zygotes. We therefore collected tripronuclear zygotes and determined the presence of methylated lysine residues at positions 4, 9 and 27 of the N-terminal tail of histone H3 by probing with antibodies specific for these modifications. A clear asymmetry was observed for trimethylated histone H3 lysine 9 (H3K9me3) and lysine 27 (H3K27me3). We subsequently stained monopronuclear zygotes derived from ICSI or IVF with α-H3K9me3 antibodies, which allowed unambiguous identification of the parental origin. This enabled us to distinguish maternal from paternal chromatin and determine the chromatin composition of monopronuclear zygotes on day one after conventional IVF or intracytoplasmic sperm injection.

Materials en methods

Collection of mono- and multipronucleated zygotes

Ovarian stimulation, oocyte retrieval and IVF procedures were performed as described previously [81, 82]. The study was approved by the Dutch Central Committee on Research Involving Human Subjects (CCMO) and the local ethics review committee of the Erasmus MC hospital. Written

consent was obtained from the couples in order to confirm that the zygotes could be used for research purposes. The stage of fertilization was checked 16-20 hours post insemination or sperm injection. Only zygotes that had less or more than two pronuclei were used. Mouse zygotes were collected in parallel to previous projects [23, 24].

Fixation and immunofluorescence staining

Prior to fixation the zona pellucida was removed with 0,05% pronase in calcium/magnesium free medium (G-PGD, Vitrolife Sweden).
Thereafter, cells were immobilized in a fibrin clot [83]. Fibrinogen was obtained from Calbiochem (cat. nr. 341573) and thrombin was obtained from Sigma (cat. nr. T-6634). Cells were fixed in 2% paraformaldehyde (PFA), 0.15% Triton-X-100 for 30 min. Immunofluorescence (IF) was applied as described before [84].

Antibodies

The following antibodies were used: HP1-β (raised in rat, P. Singh; 1:100), Polyclonal rabbit antibodies against H3K9me3; H3K27me3 and H4K20me3 were diluted 1:250, (T.Jenuwein). Rabbit polyclonal antibody for H3K4me3 and H3K9me3 were purchased from Abcam (ab8580, 1:1500 and ab1186, 1:250 respectively).
Secondary antibodies used were goat anti-rabbit IgG (H+L) conjugated with Alexa Fluor 594 (Molecular Probes, Oregon, USA) and anti-rat IgG, FITC-conjugated (Sigma F6258). All were used in a 1:500 dilution. Negative controls were performed by omitting the first antibody, but non-specific binding was never observed.

Collection of images

Images were collected with a Zeiss Axioplan fluorescence microscope. Pictures were captured by a Zeiss AxioCam MR camera with Axiovision 3.1 software (Carl Zeiss). Shown images are either stacks projected into a single image or a single slide of a stack. Whenever necessary, images where deconvoluted with Metamorph software version 6.

Results

During previous studies in which we determined patterns of post translational histone modifications and response to double strand DNA breaks in the early mouse zygote, we occasionally observed monopronuclear zygotes [23, 24]. These were either the result of par-

thenogenic activation of the secondary oocyte or of fusion of the parental chromatin domains. This conclusion was based on the fact that the partition of chromatin into histone methylation positive and negative domains was maintained (Fig 1). Depending on the modification, the asymmetry existed throughout the first cell cycle (Fig. 1h). Experiments done in four different mouse strains showed an average incidence ranging from 2.2 to 6.1 % for three of these strains but 11.6 % for the C.B17 strain (Table 1). Apparently there is a strain-specific factor that influences susceptibility for early fusion of the parental chromatin in the mouse.

To determine whether origin-specific chromatin differences are also observed in human zygotes, we studied the distribution of trimethyl-

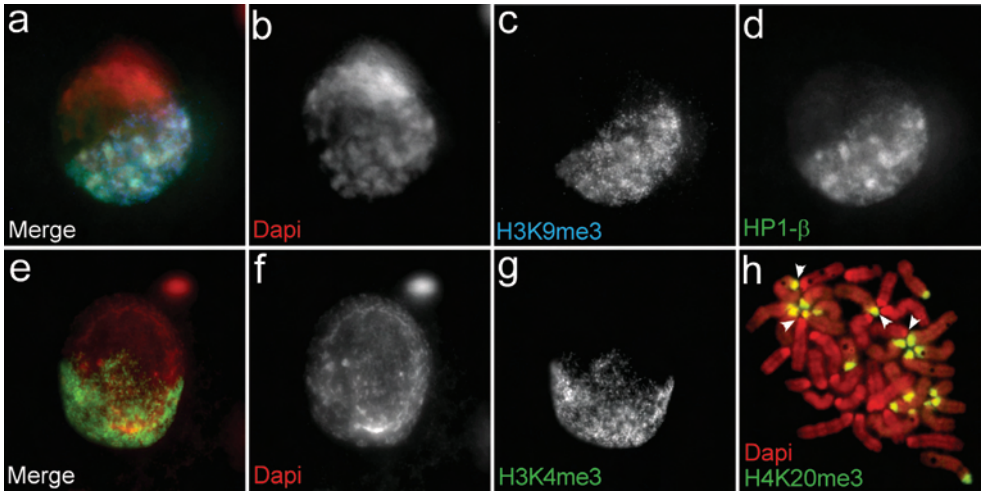

Figure 1 Diploid mouse monopronuclear zygotes

Examples of pre S-phase (**a-g**) and mitotic (**h**) monopronuclear zygotes **a-d**) zygote stained for H3K9me3 (blue) and the H3K9me2,3 binding protein HP1-b(Lachner, O'Carroll et al., 2001) (green), Dapi labels DNA (red).

e-g) zygote stained for H3K4me3 (green), Dapi labels DNA (red).

h) zygote stained for H4K20me3 (green), Dapi labelled DNA (red). Histone H4K20me3 marks 20 maternal chromosomes at the constitutive heterochromatin. It has been reported that chromosomes in the mouse zygote are interconnected via their a-satellite sequences (Dozortsev, Coleman et al., 2000). This causes some chromosomes to be positioned in a head to head position. Arrowheads indicate head-to-head position of maternal and paternal chromosomes.

ated histone H3 at lysine 4, 9 and 27 in polypronuclear post S-phase human zygotes derived from IVF and ICSI. We observed a clear staining of both parental chromatin domains for H3K4me3 (Fig. 2b, n=10) whereas trimethylated H3K9 and H3K27 were asymmetrically set (Fig. 2c, n=13; Fig. 2d, n=14). In IVF derived zygotes that originated from polyspermia, we consistently found one positive pronucleus (Fig. 2c,d). In the few polypronuclear zygotes obtained via ICSI, which arise as a consequence of failure of extrusion of the 2nd polar body, two positive pronuclei were found (Fig. 2e). This

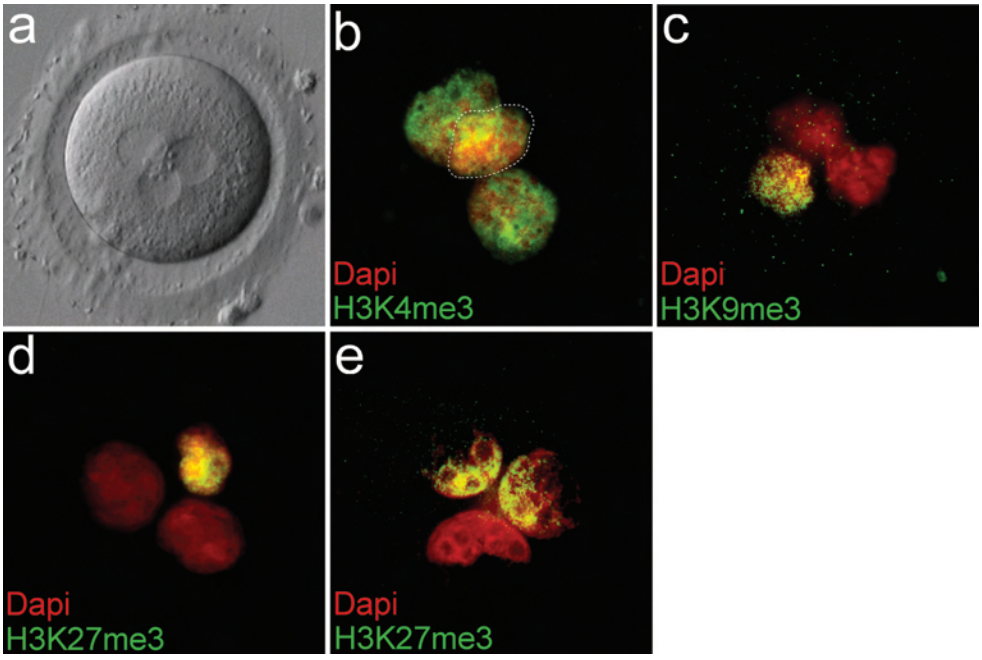

Figure 2 Distribution of H3K4me3, H3K9me3 and H3K27me3 in human tripronuclear zygotes

a) A light microscopic image of a tripronuclear zygote prior to removal of zona pellucida and fixation.

b) Symmetrical distribution of trimethylated histone H3 lysine 4. Dotted line indicates position of the maternal PN, which can be distinguished from the paternal PN by size.

c) Asymmetrical localization of histone H3K9me3. A tripronuclear zygote obtained after conventional insemination and therefore likely the result of polyspermia. This histone modification is absent from the two larger paternal pronuclei.

d-e) Absence of histone H3K27me3 from paternal chromatin. In tripronuclear zygotes obtained after insemination, H3K27me3 was present in the smaller maternal PN (d). A rare case of a tripronuclear zygote after ICSI (**e**). In these zygotes failure of second polar body extrusion is responsible for the extra PN. Therefore two PNs show this maternal mark.

Table 1. Frequency of monopronuclear zygotes in different mouse strains

Strain	Mono PN frequency (x/n)	No IVF experiments
B6.CBA hybrid	2.5 (2/79)	6
B6.129 synthetic	2.2 (1/46)	4
C.B17	11.6 (13/112)	6
Scid	6.1 (4/66)	7
Total without C.B17	3.7 (7/191)	
Total	6.6 (20/303)	

Data selected from H3K9me2 and H4K20me3 stained zygotes obtained in **Section 3.1** and **3.2**.

strongly suggested that, as in mouse and fly, the sperm derived chromatin lacks certain histone lysine methylations [24, 76, 85].

We decided to study the constitution of human monopronuclear zygotes by staining with an antibody against H3K9me3. A total number of 17 monopronuclear zygotes as determined by routine light microscopy (Fig 3a) were collected 18-20 hours after the start of a conventional IVF procedure. In all cases we observed one positive and one negative domain after staining. Among the apposed chromatin domains we now could distinguish two morphological types: 12 zygotes displayed a clear fusion of the chromatin masses similar to observations in mouse monopronuclear zygotes (Fig 3b). In five zygotes, however, the two chromatin domains were not fused but in very close proximity of each other as if within the nucleus, a stricter compartmentalisation had occurred (Fig. 3c). This difference in appearance might be due to chromatin compaction which occurs during zygotic G2 and is more advanced for maternal chromatin. In both cases, one of these domains showed overall staining for the histone modification whereas the other domain was largely negative: although distinct foci could occasionally be observed. A clear distinction in chromatin compaction between the two domains was also noticed (Fig. 3c). The maternal H3K9me3 positive domain was always of a smaller size than the paternal counterpart.

A total number of 20 monopronuclear zygotes derived from ICSI were collected. We observed three staining patterns in these pronuclei: 1) two asymmetrically stained, fused chromatin domains (n= 3). 2) a chromatin domain without staining (n= 5; chromatin present in polar bodies stained positive, indicating successful IF). 3) a

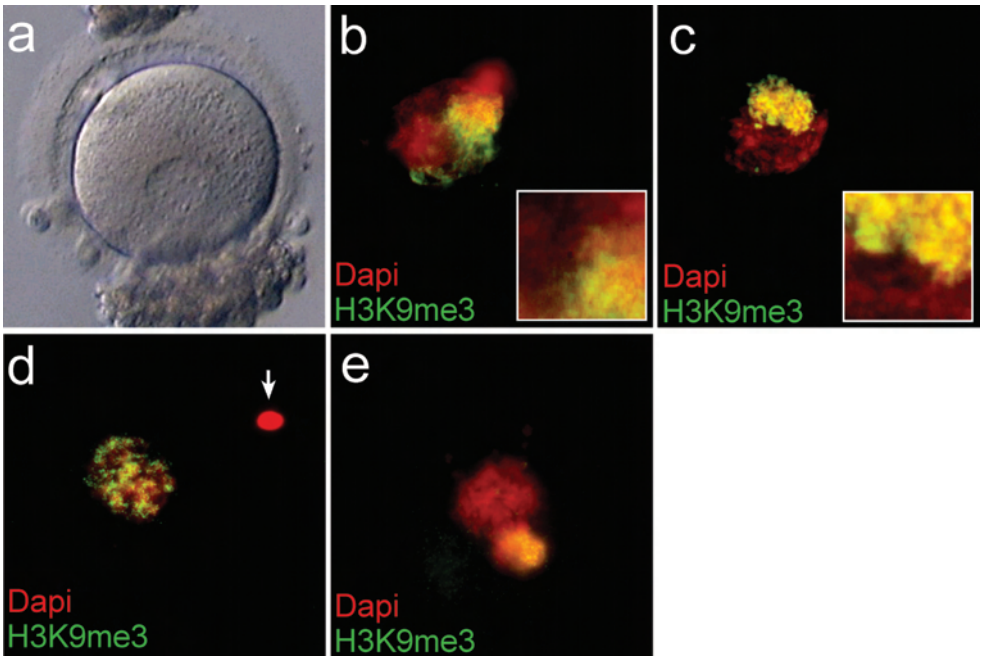

Figure 3 Distribution of H3K9me3 in human monopronuclear zygotes

a) A monopronuclear zygote prior to removal of zona pellucida and fixation. **b**) A monopronuclear zygote with a clear fusion of the chromatin domains alike the mouse monopronuclear zygotes in Fig 1. Two out of focus sperm heads are overlying the zygote. Higher magnification shows a diffuse region in between parental chromatin domains. **c**) The monopronuclear zygote depicted in 3a after staining. Two not overlapping chromatin domains in close proximity are observed. Higher magnification shows a clear separation of the parental domains. **d**) A monopronuclear zygote obtained after ICSI in which the oocyte is activated by the sperm (indicated by arrow) but no further nuclear decondensation of the sperm has occurred. **e**) A monopronuclear zygote obtained after ICSI which contains paternally derived chromatin only. The positive domain in proximity of the PN is a polar body.

stained chromatin domain and a condensed sperm head (n= 12).

Discussion

The asymmetrical setting of histone lysine methylation for paternal and maternal chromatin in the zygote is observed in a range of species [24, 76, 85]. Our results demonstrate this to extend to the human as well. Our observations for H3K4me3 and H3K9me3 are identical to the mouse post S-phase zygote [79, 80]. The presence of trimethylated H3K4 in the paternal human PN is intriguing (Fig 2b). This mark is firmly associated with transcriptional active chromatin [73, 74]. In mouse zygotes, it appears in the paternal pronucleus during S-phase and could be linked to the (minor) transcriptional activation of the zygotic genome at this stage [79, 86]. In the human early embryo, genetic activation of the embryo occurs between the four- and eight-cell stages, suggesting that the presence of H3K4me3 in zygotic paternal chromatin is not related to transcriptional activation [87]. Trimethylation of paternal histone H3 lysine 27, an important regulatory mark for down regulation of transcription and heterochromatin formation in embryogenesis, occurs during DNA replication in the mouse zygote [80]. In this study human tripronuclear zygotes were collected 16-20 hours after insemination. Most likely, the majority, if not all, of these zygotes were progressing into S-phase or had reached G2. The absence of H3K27me3 in these zygotes might indicate species-specific dynamics of H3K27 methylation, hence heterochromatin formation at first cleavage.

All monopronuclear zygotes obtained by conventional IVF in this study appeared to be bi-parental. In the human, the sperm nucleus can enter the oocyte at any location whereas in mouse the region overlying the metaphase II spindle is inaccessible for sperm [88]. However, this does not seem to prevent pronuclear fusion in the mouse (Table 1). The proximity of the parental chromatin domains early after gamete fusion has an effect on the chance of fusion. This is illustrated by the finding that in the mouse, injection of the sperm close to the maternal complement resulted in 22% monopronuclear zygotes [89]. These authors provide evidence for aggregation of chromatin masses before pronucleus formation. In the human, evidence for pronucleus fusion as the way to the monopronuclear state, has

only been obtained after injection of round spermatids [90]. Bi-parental monopronuclear human zygotes most likely are the result of sperm entry close to the metaphase II spindle, suggesting this to be a distinct possibility at natural conception, too. The bi-parental monopronuclear zygotes obtained after ICSI are likely to have the same origin. Although clinical practise aims to puncture the oolemma and deposit the sperm without disturbing the metaphase II spindle, one cannot rule out the possibility that the sperm is close to the maternal complement after injection. Especially since the first polar body has proven to be a unreliable marker for the location of the metaphase plate [91].

The majority of the ICSI-derived monopronuclear zygotes (85%) contained an abnormal genomic composition. This high rate of haploid zygotes after ICSI confirms previously published studies [65,92]. A total of 12 zygotes (60%) contained a maternal pronucleus with a condensed sperm head. It has been reported that among low numbers of sperm, the main reason to revert to ICSI, there are nuclei with a decreased ability to undergo decondensation while still able to induce oocyte activation [93, 94].

To our surprise, we found almost one-third of the 1PNs after ICSI to consist of paternal chromatin only. Staessen et al. (1997) reported 15% of embryos resulting from monopronuclear zygotes after ICSI to be haploid with only a Y chromosome [66]. Assuming an equal ratio of X- and Y-bearing spermatozoa, we found the same proportion of 1PN embryos with only a paternal contribution. This demonstrates clearly that complete extrusion of the female chromatin is a frequently occurring mechanism of 1PN formation. There are a few case reports [95, 96] that imply a relation between monopronuclear embryos and a risk of a complete hydatidiform mole (CHM) pregnancy. These could be male haploid zygotes carrying an X chromosome that undergo diploidisation at first cleavage [69].

There have been reports of live births after the transfer of human embryos which had only one pronucleus [60, 70, 71]. Apparently, the setting of the parent specific chromatin marks can be correctly executed within one nuclear membrane. The fact that we did not observe a mingling of histone post translational states within a monopronuclear zygote confirms this.

In the mouse, the implantation success rate of monopronuclear zy-

gotes is around 19% (15/79) [89] whereas in humans one study reported a percentage of 8% (3/38) [60]. Although one should be cautious of over interpretation of the relatively small numbers in these studies, human monopronuclear zygotes could have a decreased developmental potential. The mouse study on bi-parental monopronuclear zygotes indicated that negative effects of a pronuclear fusion in the zygote are limited. No changes in *in vitro* blastocyst development were observed. Also, most offspring derived from mouse monopronuclear zygotes were healthy and fertile [89].

Pertinent for clinical practice is the question of a disturbing interaction between paternal and maternal chromatin within one nuclear envelope. For mouse zygotes it has been shown that some proteins, in this case implicated in chromosome condensation, are specifically targeted to the female PN [97]. The fusion of the parental PN could potentially disrupt such parent specific mechanisms in the zygote. However, an indication for origin specific chromatin condensation in G2 was also obtained for the human monopronuclear zygotes (Fig 3c). In chromosome spreads of monopronulear mouse zygotes, trimethylated histone H4 lysine 20 was absent from paternal chromosomes as is the case in normal fertilization (Fig 1h; [78]). Centric heterochromatin domains are intimately apposed around the nucleolus precursor body at interphase [98]. This indicates that for this modification, fusion of the PNs does not lead to an apparent change in localisation of parent of origin specific chromatin marks. The difference in background of male and female zygotic chromatin maybe large enough to ensure their identities, even when present within one nuclear envelope.

Although this study has demonstrated that monopronuclear zygotes originated after conventional IVF are indeed fertilized, more research into their epigenetic status is needed to determine whether these embryos are suitable for transfer.

Acknowledgements

Dr. T. Jenuwein (IMP, Vienna, Austria), Dr. H. Stunnenberg (Dept. of Molecular Biology, NCMLS, Nijmegen, The Netherlands) and Dr. P. Singh (Research Centre Borstel, Germany) are gratefully acknowledged for the gift of their antibodies. This research was financed by the Dutch ministry of Health, Welfare and Sport.

References

1. Cohen,J. & McNaughton,D.C. Spermatozoa: the probable selection of a small population by the genital tract of the female rabbit. *J. Reprod. Fertil.* **39**, 297-310 (1974).

2. Marchetti,F. & Wyrobek,A.J. Mechanisms and consequences of paternally-transmitted chromosomal abnormalities. *Birth Defects Res. C. Embryo. Today* **75**, 112-129 (2005).

3. Gonsalves,J. *et al.* Defective recombination in infertile men. *Hum. Mol. Genet.* **13**, 2875-2883 (2004).

4. Bonduelle,M. *et al.* Prenatal testing in ICSI pregnancies: incidence of chromosomal anomalies in 1586 karyotypes and relation to sperm parameters. *Hum. Reprod.* **17**, 2600-2614 (2002).

5. Olson,S.B. & Magenis,R.E. Preferential paternal origin of de novo structural chromosome rearrangements in *The Cytogenetics of Mammalian Autosomal Rearrangements* 583-599 (Alan R. Liss, Inc., 1988).

6. Richardson,C. & Jasin,M. Frequent chromosomal translocations induced by DNA double-strand breaks. *Nature* **405**, 697-700 (2000).

7. Matsuda,Y., Yamada,T., & Tobari,I. Studies on chromosome aberrations in the eggs of mice fertilized in vitro after irradiation. I. Chromosome aberrations induced in sperm after X-irradiation. *Mutat. Res.* **148**, 113-117 (1985).

8. Kamiguchi,Y. & Tateno,H. Radiation- and chemical-induced structural chromosome aberrations in human spermatozoa. *Mutat. Res.* **504**, 183-191 (2002).

9. Hoeijmakers,J.H. Genome maintenance mechanisms for preventing cancer. *Nature* **411**, 366-374 (2001).

10. Wyman,C. & Kanaar,R. DNA double-strand break repair: all's well that ends well. *Annu. Rev. Genet.* **40**, 363-383 (2006).

11. Laberge,R.M. & Boissonneault,G. On the nature and origin of DNA strand breaks in elongating spermatids. *Biol. Reprod.* **73**, 289-296 (2005).

12. Kofman-Alfaro,S. & Chandley,A.C. Radiation-initiated DNA synthesis in spermatogenic cells of the mouse. *Exp. Cell Res.* **69**, 33-44 (1971).

13. Sega,G.A., Sotomayor,R.E., & Owens,J.G. A study of unscheduled DNA synthesis induced by X-rays in the germ cells of male mice. *Mutat. Res.* **49**, 239-257 (1978).

14. Fernandez,J.L. *et al.* Simple determination of human sperm DNA fragmentation with an im-

proved sperm chromatin dispersion test. *Fertil. Steril.* **84**, 833-842 (2005).

15. Evenson,D.P. & Wixon,R. Clinical aspects of sperm DNA fragmentation detection and male infertility. *Theriogenology* **65**, 979-991 (2006).

16. Van Kooij,R.J. *et al.* The neutral comet assay detects double strand DNA damage in selected and unselected human spermatozoa of normospermic donors. *Int. J. Androl* **27**, 140-146 (2004).

17. Rudak,E., Jacobs,P.A., & Yanagimachi,R. Direct analysis of the chromosome constitution of human spermatozoa. *Nature* **274**, 911-913 (1978).

18. Lee,J.D., Kamiguchi,Y., & Yanagimachi,R. Analysis of chromosome constitution of human spermatozoa with normal and aberrant head morphologies after injection into mouse oocytes. *Hum. Reprod.* **11**, 1942-1946 (1996).

19. Rybouchkin,A., Dozortsev,D., De Sutter,P., Qian,C., & Dhont,M. Intracytoplasmic injection of human spermatozoa into mouse oocytes: a useful model to investigate the oocyte-activating capacity and the karyotype of human spermatozoa. *Hum. Reprod.* **10**, 1130-1135 (1995).

20. Fiorenza,M.T., Bevilacqua,A., Bevilacqua,S., & Mangia,F. Growing dictyate oocytes, but not early preimplantation embryos, of the mouse display high levels of DNA homologous recombination by single-strand annealing and lack DNA nonhomologous end joining. *Dev. Biol.* **233**, 214-224 (2001).

21. Rogakou,E.P., Pilch,D. R., Orr,A.H., Ivanova,V.S., & Bonner,W.M. DNA double-stranded breaks induce histone H2AX phosphorylation on serine 139. *J. Biol. Chem.* **273**, 5858-5868 (1998).

22. Fernandez-Capetillo,O., Lee,A., Nussenzweig,M., & Nussenzweig,A. H2AX: the histone guardian of the genome. *DNA Repair (Amst)* **3**, 959-967 (2004).

23. Derijck,A.A. *et al.* gamma-H2AX signalling during sperm chromatin remodelling in the mouse zygote. *DNA Repair (Amst)* **5**, 959-971 (2006).

24. van der Heijden,G.W. *et al.* Asymmetry in Histone H3 variants and lysine methylation between paternal and maternal chromatin of the early mouse zygote. *Mech. Dev.* **122**, 1008-1022 (2005).

25. Stalf,T. *et al.* Influence of motility and vitality in intracytoplasmic sperm injection with ejaculated and testicular sperm. *Andrologia* **37**, 125-130 (2005).

26. Ramos,L. & Wetzels,A.M. Low rates of DNA fragmentation

in selected motile human spermatozoa assessed by the TUNEL assay. *Hum. Reprod.* **16**, 1703-1707 (2001).

27. World Health Organization *WHO laboratory manual for the examination of human semen and sperm-cervical mucus interaction*(Cambridge University Press,1999).

28. Friedler,S. *et al.* Factors influencing the outcome of ICSI in patients with obstructive and non-obstructive azoospermia: a comparative study. *Hum. Reprod.* **17**, 3114-3121 (2002).

29. Tournaye,H. *et al.* No differences in outcome after intracytoplasmic sperm injection with fresh or with frozen-thawed epididymal spermatozoa. *Hum. Reprod.* **14**, 90-95 (1999).

30. de Boer,P., Searle,A.G., van der Hoeven,F.A., de Rooij,D.G., & Beechey,C.V. Male pachytene pairing in single and double translocation heterozygotes and spermatogenic impairment in the mouse. *Chromosoma* **93**, 326-336 (1986).

31. Baart,E.B. *et al.* Reduced oocyte activation and first cleavage rate after ICSI with spermatozoa from a sterile mouse chromosome mutant. *Hum. Reprod.* **19**, 1140-1147 (2004).

32. Kimura,Y. & Yanagimachi,R. Intracytoplasmic sperm injection in the mouse. *Biol. Reprod.* **52**, 709-720 (1995).

33. Chohan,K.R., Griffin,J.T., Lafromboise,M., De Jonge,C.J., & Carrell,D.T. Comparison of chromatin assays for DNA fragmentation evaluation in human sperm. *J. Androl* **27**, 53-59 (2006).

34. van der Heijden,G.W. *et al.* Transmission of modified nucleosomes from the mouse male germline to the zygote and subsequent remodeling of paternal chromatin. *Dev. Biol.* **298**, 458-469 (2006).

35. McManus,K.J. & Hendzel,M. J. ATM-dependent DNA Damage-independent Mitotic Phosphorylation of H2AX in Normally Growing Mammalian Cells. *Mol. Biol. Cell* **16**, 5013-5025 (2005).

36. Bench,G.S., Friz,A.M., Corzett,M.H., Morse,D.H., & Balhorn,R. DNA and total protamine masses in individual sperm from fertile mammalian subjects. *Cytometry* **23**, 263-271 (1996).

37. Aravindan,G.R., Bjordahl,J., Jost,L.K., & Evenson,D.P. Susceptibility of human sperm to in situ DNA denaturation is strongly correlated with DNA strand breaks identified by single-cell electrophoresis. *Exp. Cell Res.* **236**, 231-237 (1997).

38. Vendrell,J.M. *et al.* Meiotic abnormalities and spermatogenic parameters in severe oligoasthenozoospermia. *Hum. Reprod.* **14**,

375-378 (1999).

39. Suganuma,R., Yanagimachi,R., & Meistrich,M.L. Decline in fertility of mouse sperm with abnormal chromatin during epididymal passage as revealed by ICSI. *Hum. Reprod.* **20**, 3101-3108 (2005).

40. Shoukir,Y., Chardonnens,D., Campana,A., & Sakkas,D. Blastocyst development from supernumerary embryos after intracytoplasmic sperm injection: a paternal influence? *Hum. Reprod.* **13**, 1632-1637 (1998).

41. Loutradi,K.E. *et al.* The effects of sperm quality on embryo development after intracytoplasmic sperm injection. *J. Assist. Reprod. Genet.* **23**, 69-74 (2006).

42. Sun,J.G., Jurisicova,A., & Casper,R.F. Detection of deoxyribonucleic acid fragmentation in human sperm: correlation with fertilization in vitro. *Biol. Reprod.* **56**, 602-607 (1997).

43. Morris,I.D., Ilott,S., Dixon,L., & Brison,D.R. The spectrum of DNA damage in human sperm assessed by single cell gel electrophoresis (Comet assay) and its relationship to fertilization and embryo development. *Hum. Reprod.* **17**, 990-998 (2002).

44. Seli,E., Gardner,D.K., Schoolcraft,W.B., Moffatt,O., & Sakkas,D. Extent of nuclear DNA damage in ejaculated spermatozoa impacts on blastocyst development after in vitro fertilization. *Fertil. Steril.* **82**, 378-383 (2004).

45. Virro,M.R., Larson-Cook,K.L., & Evenson,D.P. Sperm chromatin structure assay (SCSA) parameters are related to fertilization, blastocyst development, and ongoing pregnancy in in vitro fertilization and intracytoplasmic sperm injection cycles. *Fertil. Steril.* **81**, 1289-1295 (2004).

46. Zini,A. *et al.* Potential adverse effect of sperm DNA damage on embryo quality after ICSI. *Hum. Reprod.* **20**, 3476-3480 (2005).

47. Evenson,D.P. *et al.* Utility of the sperm chromatin structure assay as a diagnostic and prognostic tool in the human fertility clinic. *Hum. Reprod.* **14**, 1039-1049 (1999).

48. Tomlinson,M.J. *et al.* Interrelationships between seminal parameters and sperm nuclear DNA damage before and after density gradient centrifugation: implications for assisted conception. *Hum. Reprod.* **16**, 2160-2165 (2001).

49. Duran,E.H., Morshedi,M., Taylor,S., & Oehninger,S. Sperm DNA quality predicts intrauterine insemination outcome: a prospective cohort study. *Hum. Reprod.* **17**, 3122-3128 (2002).

50. Larson-Cook,K.L. *et al.* Relationship between the outcomes of assisted reproductive techniques

and sperm DNA fragmentation as measured by the sperm chromatin structure assay. *Fertil. Steril.* **80**, 895-902 (2003).

51. Tesarik,J., Greco,E., & Mendoza,C. Late, but not early, paternal effect on human embryo development is related to sperm DNA fragmentation. *Hum. Reprod.* **19**, 611-615 (2004).

52. Lewis,S.E. & Aitken,R.J. DNA damage to spermatozoa has impacts on fertilization and pregnancy. *Cell Tissue Res.* **322**, 33-41 (2005).

53. Spano,M., Seli,E., Bizzaro,D., Manicardi,G.C., & Sakkas,D. The significance of sperm nuclear DNA strand breaks on reproductive outcome. *Curr. Opin. Obstet. Gynecol.* **17**, 255-260 (2005).

54. Tesarik,J., Mendoza,C., & Greco,E. Paternal effects acting during the first cell cycle of human preimplantation development after ICSI. *Hum. Reprod.* **17**, 184-189 (2002).

55. Bizzaro,D., Manicardi,G., Bianchi,P.G., & Sakkas,D. Sperm decondensation during fertilisation in the mouse: presence of DNase I hypersensitive sites in situ and a putative role for topoisomerase II. *Zygote.* **8**, 197-202 (2000).

56. Rybouchkin,A., Benijts,J., De,S.P., & Dhont,M. Disintegration of chromosomes in dead sperm cells as revealed by injection into mouse oocytes. *Hum. Reprod.* **12**, 1693-1698 (1997).

57. Sotolongo,B., Huang,T.T., Isenberger,E., & Ward,W.S. An endogenous nuclease in hamster, mouse, and human spermatozoa cleaves DNA into loop-sized fragments. *J. Androl* **26**, 272-280 (2005).

58. Ward,M.A. & Ward,W.S. A model for the function of sperm DNA degradation. *Reprod. Fertil. Dev.* **16**, 547-554 (2004).

59. Wright,S.J. Sperm nuclear activation during fertilization. *Curr. Top. Dev. Biol.* **46**, 133-178 (1999).

60. Staessen,C., Janssenswillen,C., Devroey,P., & Van Steirteghem,A. C. Cytogenetic and morphological observations of single pronucleated human oocytes after in-vitro fertilization. *Hum. Reprod.* **8**, 221-223 (1993).

61. Palermo,G. *et al.* Sperm characteristics and outcome of human assisted fertilization by subzonal insemination and intracytoplasmic sperm injection. *Fertil. Steril.* **59**, 826-835 (1993).

62. Van,S.A. *et al.* Use of assisted fertilization. *Hum. Reprod.* **8**, 1784-1785 (1993).

63. Kaufman,M.H. *Early Mammalian Development: Parthenogenetic Studies*(Cambridge University

Press,1983).

64. Taylor,A.S. & Braude,P.R. The early development and DNA content of activated human oocytes and parthenogenetic human embryos. *Hum. Reprod.* **9**, 2389-2397 (1994).

65. Sultan,K.M., Munne,S., Palermo,G.D., Alikani,M., & Cohen,J. Chromosomal status of uni-pronuclear human zygotes following in-vitro fertilization and intracytoplasmic sperm injection. *Hum. Reprod.* **10**, 132-136 (1995).

66. Staessen,C. & Van Steirteghem,A.C. The chromosomal constitution of embryos developing from abnormally fertilized oocytes after intracytoplasmic sperm injection and conventional in-vitro fertilization. *Hum. Reprod.* **12**, 321-327 (1997).

67. Barton,S.C., Ferguson-Smith,A.C., Fundele,R., & Surani,M.A. Influence of paternally imprinted genes on development. *Development* **113**, 679-687 (1991).

68. Longo,F.J. Fertilization: a comparative ultrastructural review. *Biol. Reprod.* **9**, 149-215 (1973).

69. Devriendt,K. Hydatidiform mole and triploidy: the role of genomic imprinting in placental development. *Hum. Reprod. Update.* **11**, 137-142 (2005).

70. Gras,L. & Trounson,A.O. Pregnancy and birth resulting from transfer of a blastocyst observed to have one pronucleus at the time of examination for fertilization. *Hum. Reprod.* **14**, 1869-1871 (1999).

71. Dasig,D., Lyon,J., Behr,B., & Milki,A.A. Monozygotic twin birth after the transfer of a cleavage stage embryo resulting from a single pronucleated oocyte. *J. Assist. Reprod. Genet.* **21**, 427-429 (2004).

72. Kornberg,R.D. & Lorch,Y. Twenty-five years of the nucleosome, fundamental particle of the eukaryote chromosome. *Cell* **98**, 285-294 (1999).

73. Nightingale,K.P., O'neill,L. P., & Turner,B.M. Histone modifications: signalling receptors and potential elements of a heritable epigenetic code. *Curr. Opin. Genet. Dev.* **16**, 125-136 (2006).

74. Fischle,W., Wang,Y., & Allis,C. D. Histone and chromatin cross-talk. *Curr. Opin. Cell Biol.* **15**, 172-183 (2003).

75. Kouzarides,T. Chromatin modifications and their function. *Cell* **128**, 693-705 (2007).

76. Arney,K.L., Bao,S., Bannister,A.J., Kouzarides,T., & Surani,M.A. Histone methylation defines epigenetic asymmetry in the mouse zygote. *Int. J. Dev. Biol.*

46, 317-320 (2002).

77. Cowell,I.G. *et al.* Heterochromatin, HP1 and methylation at lysine 9 of histone H3 in animals. *Chromosoma* **111**, 22-36 (2002).

78. Kourmouli,N. *et al.* Heterochromatin and tri-methylated lysine 20 of histone H4 in animals. *J. Cell Sci.* **117**, 2491-2501 (2004).

79. Lepikhov,K. & Walter,J. Differential dynamics of histone H3 methylation at positions K4 and K9 in the mouse zygote. *BMC. Dev. Biol.* **4**, 12 (2004).

80. Santos,F., Peters,A.H., Otte,A. P., Reik,W., & Dean,W. Dynamic chromatin modifications characterise the first cell cycle in mouse embryos. *Dev. Biol.* **280**, 225-236 (2005).

81. Huisman,G.J., Fauser,B.C., Eijkemans,M.J., & Pieters,M.H. Implantation rates after in vitro fertilization and transfer of a maximum of two embryos that have undergone three to five days of culture. *Fertil. Steril.* **73**, 117-122 (2000).

82. Hohmann,F.P., Macklon,N. S., & Fauser,B.C. A randomized comparison of two ovarian stimulation protocols with gonadotropin-releasing hormone (GnRH) antagonist cotreatment for in vitro fertilization commencing recombinant follicle-stimulating hormone on cycle day 2 or 5 with the standard long GnRH agonist protocol. *J. Clin. Endocrinol. Metab* **88**, 166-173 (2003).

83. Hunt,P., LeMaire,R., Embury,P., Sheean,L., & Mroz,K. Analysis of chromosome behavior in intact mammalian oocytes: monitoring the segregation of a univalent chromosome during female meiosis. *Hum. Mol. Genet.* **4**, 2007-2012 (1995).

84. Baart,E.B., de Rooij,D.G., Keegan,K.S., & de Boer,P. Distribution of Atr protein in primary spermatocytes of a mouse chromosomal mutant: a comparison of preparation techniques. *Chromosoma* **109**, 139-147 (2000).

85. Loppin,B. *et al.* The histone H3.3 chaperone HIRA is essential for chromatin assembly in the male pronucleus. *Nature* **437**, 1386-1390 (2005).

86. Schultz,R.M. The molecular foundations of the maternal to zygotic transition in the preimplantation embryo. *Hum. Reprod. Update.* **8**, 323-331 (2002).

87. Braude,P., Bolton,V., & Moore,S. Human gene expression first occurs between the four- and eight-cell stages of preimplantation development. *Nature* **332**, 459-461 (1988).

88. Van Blerkom J., Davis,P., Merriam,J., & Sinclair,J. Nuclear and cytoplasmic dynamics of

sperm penetration, pronuclear formation and microtubule organization during fertilization and early preimplantation development in the human. *Hum. Reprod. Update.* **1**, 429-461 (1995).

89. Krukowska,A. & Tarkowski,A. K. Mouse zygotes with one diploid pronucleus formed as a result of ICSI can develop normally beyond birth. *Mol. Reprod. Dev.* **72**, 346-353 (2005).

90. Tesarik,J. & Mendoza,C. Spermatid injection into human oocytes. I. Laboratory techniques and special features of zygote development. *Hum. Reprod.* **11**, 772-779 (1996).

91. Rienzi,L. *et al.* Relationship between meiotic spindle location with regard to the polar body position and oocyte developmental potential after ICSI. *Hum. Reprod.* **18**, 1289-1293 (2003).

92. Lim,A.S., Goh,V.H., Su,C. L., & Yu,S.L. Microscopic assessment of pronuclear embryos is not definitive. *Hum. Genet.* **107**, 62-68 (2000).

93. Sakkas,D. *et al.* Sperm chromatin anomalies can influence decondensation after intracytoplasmic sperm injection. *Hum. Reprod.* **11**, 837-843 (1996).

94. Flaherty,S.P., Payne,D., Swann,N.J., & Mattews,C.D. Aetiology of failed and abnormal fertilization after intracytoplasmic sperm injection. *Hum. Reprod.* **10**, 2623-2629 (1995).

95. Edwards,R.G. *et al.* Pronuclear, cleavage and blastocyst histories in the attempted preimplantation diagnosis of the human hydatidiform mole. *Hum. Reprod.* **7**, 994-998 (1992).

96. Petignat,P. *et al.* Molar pregnancy with a coexistent fetus after intracytoplasmic sperm injection. A case report. *J. Reprod. Med.* **46**, 270-274 (2001).

97. Bomar,J., Moreira,P., Balise,J.J., & Collas,P. Differential regulation of maternal and paternal chromosome condensation in mitotic zygotes. *J. Cell Sci.* **115**, 2931-2940 (2002).

98. Dozortsev,D. *et al.* Nucleoli in a pronuclei-stage mouse embryo are represented by major satellite DNA of interconnecting chromosomes. *Fertil. Steril.* **73**, 366-371 (2000).

99. Lachner,M., O'Carroll,D., Rea,S., Mechtler,K., & Jenuwein,T. Methylation of histone H3 lysine 9 creates a binding site for HP1 proteins. *Nature* **410**, 116-120 (2001).

Section 5

Summarized findings and the IVF clinic, drawing parallels between mouse and man

Summarized findings

1.
The sex chromosomes undergo extensive nucleosome replacement during male meiosis, which eventually results in the sole presence of histone H3.3 as H3 variant and facilitates the resetting of histone modifications in the sex chromatin. This nucleosome replacement is a reaction to unsynapsed chromatin present during pachytene and therefore a feature of MSCI and MSUC. The biological significance of this in scale unprecedented chromatin mobility is likely a role in MSCI which is a prerequisite for normal spermiogenesis **(Section 2.1)**.

2.
Sperm nucleosomal chromatin is transmitted and contributes to paternal chromatin in mouse and human zygotes. In mouse sperm, nucleosomal chromatin that carries histone H4K8ac and H4K12ac, is enriched in the constitutive heterochromatin. Since human sperm retains a large fraction of nucleosomal chromatin, there is the potential of epigenetic paternal programs. This aspect may well be enhanced in ART as chromatin remodeling problems during spermiogenesis are more manifest among in- and subfertile males **(Section 2.2, 2.3)**.

3.
Protamines are shed from sperm DNA prior to chromatin decondensation after gamete fusion **(Section 2.4)**.

4.
In the early zygote the paternal chromatin is characterized by the presence of histone H3.3, as sole H3 variant, and absence of most histone lysine methyl modifications. The H3 asymmetry is partly reduced during S-phase, when histone H3.1 and H3.2 are deposited **(Section 2.4)**.

5.
Histone 3 and 4 N-tail methyl posttranslational modifications are strikingly different between male and female G1 pronuclei. Male chromatin only shows the H3K4 - and H4K20 monomethylated states **(Section 2.4)**.

6.
Prior to formation of the pronucleus in recondensing chromatin, the paternal chromosomes are characterized by histone modifications that play a role in DNA repair (H2AX-S139ph), chromatin condensation (H3S10ph) and, presumably, DNA-histone interaction (H3ac H4ac) **(Section 2.2, 2.4, 3.1)**.

7.
The evolutionary conserved DSB signaling mechanism, operating via histone H2AX phosphorylation at serine 139, is functional throughout the zygotic cell cycle and already active during chromatin remodeling of sperm chromatin **(Section 3.1, 3.2)**.

8.
The number of γH2AX foci in recondensing male chromatin, approximately 80 minutes post gamete fusion, shows a dose-response relation with the amount of irradiation induced DSBs in sperm **(Section 3.1)**.

9.
The ooplasm influences both the spontaneous and IR induced level of γH2AX foci in recondensing male chromatin **(Section 3.1, 3.2)**, a rise is mainly observed in a DNA-PK_{cs} hypomorphic background.

10.
In scid oocytes, transient paternal DNA breaks that are not detected by PIKK family members ATM and ATR, are converted into full-blown γH2AX positive DSBs, implicating a role for DNA.PK_{cs} in paternal chromatin remodeling **(Section 3.2)**.

11.
γH2AX foci in recondensing male chromatin predict the number of chromosome type abnormalities at first cleavage division in NHEJ proficient strains **(Section 3.2)**.

12.
Zygotic DNA repair analyzed by γH2AX foci kinetics is similar to that of somatic cells for both NHEJ pro- and deficient zygotes. Kinetic analysis of γH2AX foci after Etoposide or Bleomycin treat-

ment suggests a difference in repair proficiency between male and female derived chromatin during early G1 **(Section 3.1, 3.2)**.

13.
The male pronucleus during late G1 shows a proclivity for spontaneous DSB formation, especially in a DNA-PK_{cs} hypomorphic background **(Section 3.2)**.

14.
The interplay between NHEJ and HR during repair of DSBs, as described in somatic cells, also exists in the zygote. At chromatin remodeling and progression through G1, NHEJ plays an important role. During S-phase, a preference for HR mediated repair of IR induced DSBs might exist **(Section 3.2)**.

15.
Active HR is demonstrated by the formation of ionizing radiation induced foci that harbor HR related repair factors such as Rad51 and Brca1 and by the fact that HR deficient zygotes are extremely sensitive to genotoxic compounds interfering with DNA replication, possibly indicating an increased sensitivity for replication fork stalling and/or demise at the onset of embryonic life **(Section 3.2)**.

16.
Unresolved DNA damage can be visualized as γH2AX foci in chromosomes at the first cleavage division and usually is not associated with a chromosome abnormality. By all evidence, these zygotes will progress further into pre-implantation development **(Section 3.2)**.

17.
Genetic instability of expanded simple tandem repeats (ESTR) later in development is induced by irradiated sperm as evidenced by an increased mutation rate in sperm and bone marrow **(Section 3.3)**.

18.
An altered NHEJ activity in the ooplasm by the scid DNA-PK_{cs} allele reduces induced ESTR instability to close to zero **(Section 3.3)**, via an unknown mechanism. This might be due to the interplay of DSB repair pathways in the zygote, a reduced NHEJ activ-

ity demands higher HR activity **(Section 3.2)**. Arguably an altered balance between NHEJ and HR leads to enhanced homologous recombination.

19.
As ESTR mutations occur as a delayed radiation response, the absence of it after a "maternal effect" reduction in NHEJ (by scid), would suggest a more permanent upregulation of HR in this particular genetic background in which the paternal DNA.PK allele is the BALB/c hypomorph **(Section 3.3)**.

20.
In the HIGH assay (for heterologous ICSI and γH2AX assay) heterologous insemination is combined with the most sensitive form of DSB detection currently known. It allows detection and quantification of such lesions after chromatin remodeling in human sperm nuclei **(Section 4.1)**.

21.
Using this assay on 5 probands, the frequency of DSB was not different between normozoospermic and oligo- astheno- teratozoospermic (OAT) men. However, the incidence of affected sperm was higher in the subfertiles **(Section 4.1)**.

22.
The use of ejaculated immotile sperm for artificial reproduction is highly debatable as approximately 70% show DNA degradation at chromatin remodeling with the HIGH assay **(Section 4.1)**.

23.
Injection of immotile sperm resulting in aberrant male γH2AX staining, showed an all-over γH2AX reaction in the female chromosome complement in 70% (10/14) of the cases, possibly indicating early cross-talk between male and female chromatin upon sperm entry **(Section 4.1)**.

24.
The single pronucleus of monopronuclear zygotes obtained after IVF is predominantly due to fusion of the two parental chromatin

domains. When obtained after ICSI the pronucleus more likely only contains maternal or paternal chromatin **(Section 4.2)**.

25.
At a comparable incidence to human IVF, biparental monopronuclear zygotes are also found in mouse IVF, where a genetic component was discovered, raising the incidence in the C.B17 strain **(Section 4.2)**.

The IVF clinic, drawing parallels between mouse and man

Transmission of chromatin

In **section 2.2** and **2.3** we show that sperm derived nucleosomal chromatin contributes to the zygotic paternal chromatin. Potentially, the transmission of DNA in a nucleosomal conformation affects the transcriptional activity of these sequences in the early embryo. This brings the question whether an increased amount of nucleosomes in sperm could have negative effects on embryonic development. In round spermatids, protamination has not yet started and the DNA is solely packed in nucleosomes. The practice of round spermatid nucleus injection (ROSNI) is therefore the most extreme case utilizing male gametes with a shifted nucleosome/protamine ratio for obtaining offspring via reproductive techniques. At present, in depth studies on the effects of ROSNI on embryonic development are predominantly carried out in mice. Analysis of a subset of genes has demonstrated that the expression profile of certain genes is altered in embryos generated via ROSNI[1, 2]. In addition, a clear disruption of the demethylation of the paternal DNA that occurs in the zygote, was observed[3, 4]. Both these aberrations are likely caused by the transmission of paternal DNA in a nucleosomal conformation (as discussed in **section 2.2**), but do these effects also occur when the distortion of the nucleosome/protamine ratio is less severe? Again data obtained in the mouse showed that after injection of elongated spermatids, the distortion of paternal DNA methylation removal is apparent, however less severe[5]. This does not exclude the possibility of a physiological effect in subsequent embryonic development.

In **section 2.4** we have studied whether a specific category of histone modifications (histone lysine methylation) are transmitted via mouse sperm. These modifications are powerful regulators of transcription. We did not find transmission of such marks but more sensitive techniques should be employed to obtain a definite answer. If the increased presence of nucleosomes in sperm, however, results in the transmission of such modifications we now know that they will contribute to the paternal zygotic chromatin. Further research will have to establish whether this has potential detrimental consequences for embryonic development but also for onset of disease later in life.

DNA repair in the zygote

DNA damage arises in many different cell types at various moments of the cell cycle and may result in lasting mutations. When viewing the cycle of life, mutations that occur shortly after gamete fusion deserve special attention as these are fixed in the germline and passed on to future generations when present in cells forming the inner cell mass of the blastocyst. Considering that de novo translocations are often of male descent [5], several findings of our studies shed a new light on the paternal contribution to heritable chromosome mutations:

i) DSBs arise during post fusion chromatin remodeling and are elevated 35-150 fold (depending on ooplasm genotype) compared to the number of spontaneous DSBs in somatic G1 cells as measured by γH2AX foci **(Section 3.1, 3.2)**.
ii) DSBs found in recondensed male chromatin are more likely to convert to lasting chromosome type abnormalities **(Section 3.2)**.
iii) Depending on the ooplasm, male pronuclei show spontaneous break induction before S-phase, possibly related to DNA demethylation **(Section 3.2)**.
iv) Unresolved DSBs found at first cleavage division are more often of male descend **(Section 3.2)**.
v) DNA replication is easily hampered in the absence of homologous recombination repair and prone to the induction of chromosome rearrangements in the male PN after genotoxic treatment **(Section 3.2)**.
vi) Unresolved DSBs labeled by Rad51 at end S-phase after DSB induction at onset of S-phase are more numerous in the male pronucleus, especially in repair hampered zygotes **(Section 3.2)**.

Repair deficiencies have a greater impact on the male pronucleus, indicative for a more demanding nature of the male complement during S-phase with regard to DNA repair.
Sperm populations from infertile patients have an increased number of DNA damaged sperm[6-8]. Sperm selection singles out sperm with little DNA damage [9], however an increased incidence of DSBs at chromatin remodeling after gamete fusion was found in selected sperm derived from OAT patients **(Section 4.1)**. This increase can not account for the effects of OAT semen on preimplantation de-

velopment that have been described **(Section 4.1)**. However, this does not eliminate the fact that an increase in de novo chromosome abnormalities after ICSI has been reported [10].
Zygote development adheres to a strict timing and the onset of first mitotic cleavage has predictive values for the developmental competence of the embryo and pregnancy rate [11, 12]. The analysis of zygotes derived from HR defective oocytes has shown that this repair pathway plays a major role during DNA replication **(Section 3.2)** and might be considered the Achilles heel of the zygote. We postulate that prolongation of the first cell cycle occurs when DNA replication is hampered. Reciprocal quadrivalent chromosome aberrations (the so-called quadriradials) are formed during S-phase in the male pronucleus and will segregate at first mitotic cleavage, producing blastomeres with a reciprocal translocation (among normal and unbalanced complements). Hence, the contribution of the zygotic S-phase to male derived chromosome abnormalities should be reconsidered.
Extending on this, a lot of effort has been put recently into the assessment of risk factors in cancer predisposition. Several single nucleotide polymorphisms (SNPs) for HR genes, associated with an increased likelihood for certain types of cancer, have been described [13-21]. Human preimplantation embryos start transcription at the 4- to 8-cell stage[22] and are likely susceptible to a similar maternal effect on DNA repair as described in mouse **(Section 3.2)**. The effects of hypomorphic SNPs for vital repair genes in oocytes might pose a risk in IVF that needs to be addressed, especially in combination with gametes from infertile men which have an intrinsic increase in DNA damage.

Present-day assays for measuring sperm DNA damage are multifarious and several, like TUNEL and SCSA, are very suitable for routine analysis which has made them widely used in clinical practice **(BOX 2, Section 1)**. Most of these techniques however, have one or several of the following downsides:

i) indirect measurement with an arbitrary output
ii) output based on population of cells
iii) insensitive, only measuring non-physiological amounts of DNA damage
iv) artificial measurement outside of biological context

For a better understanding of the molecular phenomena underlying infertility, more accurate techniques need to be applied. In relation to chromatin structure, electron microscopy is a good example[23] that could be used more often in combination with in situ detection techniques.
Assays based on heterologous insemination provide means to mimic biological context and enable analysis of sperm chromosomes at the first cleavage division [24, 25]. The HIGH assay **(Section 4.1)** introduces new options for analysis of human sperm by heterologous insemination, several advantages being:

i) processing of sperm after gamete fusion similar to normal fertilization
ii) direct measurement of DSBs
iii) quantitative analysis of DSBs with high sensitivity (down to 1 break per nucleus)
iv) sensitive for alterations in chromatin remodeling
v) high reactivity towards aberrant sperm nuclei

The main disadvantage is the need for mouse ICSI which is known for being labor intensive and difficult to perform [26] due to the sensitivity of the mouse oocyte for membrane rupture. Regarding the special qualities of the HIGH assay, several points can be discussed in the light of future research and clinical application.
The HIGH assay measures two types of DSBs, those already present in the mature sperm before gamete fusion **(Section 3.1, 3.2)** and those arising during male chromatin remodeling **(Section 3.1, 3.2)**. The ooplasm influences the number of DSBs detected **(Section 3.2)**. Oocytes with a DNA-PK$_{cs}$ hypomorph are likely more sensitive for DNA damage that negatively influences chromatin remodeling resulting in DSBs **(Section 3.2)**. Using such, scid oocytes, the HIGH assay may become an even more sensitive assay. Alternatively, a combination of HR defective *mRad54*$^{-/-}$*mRad54B*$^{-/-}$ oocytes and the analysis of residual DSBs (and possible PN stalling) at first mitotic cleavage **(Section 3.2)** with the HIGH assay could open up opportunities for the analysis of paternal effects on replication delay. Finally, combining classic cytogenetic analysis of human sperm after heterologous ICSI[25] in the oocyte strain of choice with the HIGH read-out (in the same oocyte background) could result in a regression curve for estimating chromosome abnormalities **(Sec-**

tion 3.2). The delicate mouse ICSI procedure is restricted to oocytes from specific genetic backgrounds, thus mouse strains suitable for this purpose will have to be specifically bred. A possible route to circumvent this problem is the use of inhibitors of DNA repair enzymes, like the DNA-PK$_{cs}$ inhibitor NU7026 [27].
The etiology of the aberrant γH2AX patterns in immotile human sperm used for the HIGH assay is likely due to high amounts of DNA damage from Topoisomerase IIB and an epididymal factor [28-30] **(Section 4.1)**. Using sperm derived from *HR6B*$^{-/-}$ mice in the HIGH assay, 100% abnormal γH2AX staining and fragmentation of chromatin at nuclear remodeling was found (31/31 cells) (unpublished data in collaboration with Dr WM Baarends, department of Reproduction and Development, Erasmus University Medical Centre). *HR6B*$^{+/-}$ sperm showed no such reaction (13/13 cells). *HR6B*$^{-/-}$ mice have a marked but variable reduction of testis weight and sharply reduced sperm counts. Defective spermiogenesis during the elongation stage results in asthenozoo- and teratozoospermia with over 90% of mature sperm showing an abnormal head morphology [31]. Further evidence that the HIGH assay is sensitive for sperm chromatin alterations comes from ICSI using sperm from the fully fertile T(1;13)70H homozygous translocation mouse (Figure 1).

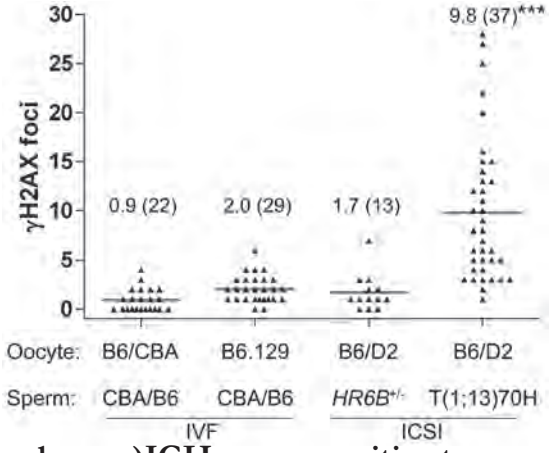

Figure 1 H(omologous)IGH assay sensitive to sperm chromatin aspects γH2AX foci at chromatin remodeling after fusion of gametes from indicated strains. In ICSI morphologically normal, progressively motile sperm were used. Foci average and (number of zygotes) are indicated. *** $p<0.001$ to all other groups.

Untreated sperm from two different backgrounds (CBA/B6 or C57Bl/6, *HR6B*$^{+/-}$) fused with three different oocyte genotypes resulted in similar amounts of γH2AX positive DSBs. The homozygous T70H mouse had an increase that surpassed the level of γH2AX foci found after fusion of 4 Gy irradiated CBA/B6 sperm with B6/CBA oocytes **(Section 3.1)**. Although the origin of this aberrant γH2AX foci level is presently unknown and more research is needed, it implies that the HIGH assay also measures transient DSBs that seemingly leave fertility unaffected. These findings underline the context sensitive nature of the HIGH assay, setting it apart from all currently used assays. Clinical questions on human sperm chromatin and DNA quality in need for highly sensitive "proof of principle" experiments could benefit from the HIGH assay. The use of oral antioxidant intake in the reduction of sperm DNA damage serves as a good example [32].

If we think about the ESTR mutation rate as a secondary effect that merely visualizes an alteration of DNA metabolism, the implications of transgenerational ESTR instability are far-reaching. First of all, an acquired ESTR instability will influence the affected generation and those to come. Second, if the altered DNA metabolism also has a bearing on global changes in gene expression, even more cellular processes can be subtly affected. Third, a global alteration in DNA metabolism relates to a variable degree of cancer predisposition. The understanding of epigenetic forms of cancer is dawning [33]. Here we found an increase in ESTR mutation rate after sperm ionizing radiation. ESTR instability is also induced by certain chemical compounds. Hence, it would be intriguing to test whether sperm with an intrinsic increase in DNA damage, i.e. by hampered spermiogenesis, in possible interaction with a long sojourn in the epididymis, increases ESTR mutation rate. If the outcome of this thought experiment would show an increase in ESTR mutation rate, the risk of using gametes from sparse semen samples should be revisited.

Nederlandse samenvatting

In Nederland werd in 2005 ongeveer 1 op de 40 kinderen via kunstmatige bevruchting verwekt. De belangrijkste reden om in vitro bevruchting toe te passen ligt voor de hand: infertiliteit voorkomt (en subfertiliteit bemoeilijkt) natuurlijke bevruchting. De oorzaken van sub- en infertiliteit zijn talrijk en kunnen zowel afkomstig zijn van de man, de vrouw of beide. Bij onderzoek is gevonden dat zaadcellen van mannen die sub- of infertiel zijn een verhoogd niveau van DNA beschadigingen hebben en dikwijls een afwijkende chromatine configuratie laten zien (het totaal van eiwitten en DNA waaruit een chromosoom bestaat heet chromatine). De consequenties van het gebruik van dit zaad voor het embryo en het nageslacht van dit embryo wanneer het volwassen is, zijn onduidelijk. De beantwoording van deze vraag wordt pas mogelijk wanneer er meer kennis is van de biologie van chromatine en DNA herstel in de vroege embryonale stadia. Het onderzoek beschreven in deze dissertatie heeft als doel om meer inzicht te krijgen in processen die zich afspelen nadat de zaadcel is versmolten met de eicel. De aandacht richtte zich vooral op chromatine veranderingen en herstel van dubbel strengs DNA breuken in de genetische bijdrage van de vader.
Chromatine veranderingen treden op tijdens de spermatogenese (het proces van zaadcel vorming) en in de zygote (het "1-cellig embryo"). Het hier beschreven onderzoek heeft geleid tot nieuwe inzichten in dit omvangrijke gebied.
Tevens is gekeken hoe en wanneer dubbel strengs DNA breuken in de zygote worden gerepareerd en wat deze breuken betekenen voor de genetische stabiliteit van het nageslacht van zygotes voortgekomen uit sperma met door ionizerende straling beschadigd DNA. Tijdens het onderzoek is grotendeels gebruik gemaakt van de muis als model systeem. In een aantal gevallen zijn humane zaadcellen en afwijkende embryo's, ongeschikt voor humane voortplanting, benut.

Hieronder volgt een puntsgewijze opsomming van de belangrijkste bevindingen van dit onderzoek.

1.
De geslachtschromosomen vervangen hun nucleosomen tijdens de mannelijke meiose. Nucleosomen zijn de basisstructuren die het DNA in de kern verpakken en die een rol spelen bij het "aan of uit zetten" van genen. Ze zijn een belangrijk onderdeel van het chromatine. De vervanging resulteert uiteindelijk in een unieke verpakking gekenmerkt door nucleosomen met alleen histon H3.3. Door dit proces worden histon modificaties (chemische wijzigingen van nucleosomen, betrokken bij het "aan of uit zetten" van genen) in het sex chromatine gewijzigd. De chromatineverandering, die op deze schaal nog niet bekend was, speelt waarschijnlijk ook een rol bij een tijdelijke stillegging van de genactiviteit van de geslachtschromosomen. Dit proces is noodzakelijk voor het normale verloop van de spermatogenese **(Sectie 2.1)**.

2.
Het meeste DNA van de zaadcel is verpakt door middel van protamine eiwitten, die in de zygote weer verdwijnen. De zaadcel brengt echter ook DNA verpakt in nucleosomaal chromatine over naar de zygote. De nucleosomen worden niet vervangen en dragen bij aan het paternale chromatine van zowel mens als muis. Omdat humane zaadcellen in tegenstelling tot de muis een significante hoeveelheid nucleosomaal chromatine mee brengen, en de histonen door modificaties (zie boven) boodschappen voor gebruik van genen kunnen bevatten, bestaat de mogelijkheid dat dit de ontwikkeling van het vroege (preimplantatie) embryo beinvloedt. Dit aspect kan versterkt zijn bij gebruik van zaadcellen van sub- of infertiele mannen voor kunstmatige voortplanting, omdat tijdens de zaadcelvorming bij deze mannen de vervanging van nucleosomen door protamines minder volledig is **(Sectie 2.2, 2.3)**.

3.
In het 1-cellige embryo onderscheidt het chromatine van de vader zich van dat van de moeder door de aanwezigheid van histon H3.3 als nagenoeg enige H3 variant en de afwezigheid van de meeste histon lysine modificaties. Wanneer het DNA wordt verdubbeld veran-

dert deze situatie **(Sectie 2.4)**.

4.
De speciale nucleosoom-bouwsteen histon H2AX ondergaat een chemische verandering (aangegeven met γH2AX) als de DNA keten (de dubbele helix) breekt. Zo "weet" de cel waar reparatie plaats moet vinden. Dit in de evolutie geconserveerde principe is ook actief in het 1-cellige embryo, zelfs al zeer kort na het samensmelten van zaadcel en eicel **(Sectie 3.1, 3.2)**.

5.
Door γH2AX signalen in de kern van de zaadcel zo'n 80 minuten na het begin van de bevruchting te tellen, kan het aantal dubbel strengs DNA breuken in het sperma worden bepaald. Deze breuken waren deels al voor de bevruchting aanwezig en zijn deels ontstaan tijdens de chromatine verandering, van protamine naar nucleosomen kort na de versmelting van zaadcel en eicel **(Sectie 3.1)**.

6.
Het 1-cellig embryo is voor alle noodzakelijke processen die het moet volbrengen aangewezen op factoren in de eicel. De eicel beïnvloedt de hoeveelheid γH2AX signalen kort na bevruchting en stuurt het herstel van DNA breuken in het 1-cellige embryo **(Sectie 3.1, 3.2)**.

7.
De γH2AX signalen in de kern van de zaadcel kort na bevruchting, voorspellen het ontstaan van chromosoom afwijkingen die worden doorgegeven aan het 2-cellige embryo **(Sectie 3.2)**.

8.
Het herstel van DNA breuken in sperma wordt voltrokken door factoren opgeslagen in de eicel. Twee belangrijke herstelprocessen die gericht zijn op dubbel strengs DNA breuken, en die bekend zijn van lichaamscellen, zijn ook in de zygote actief. De beide processen vervullen ieder hun rol in verschillende trajecten van de ontwikkeling van het 1-cellige embryo **(Sectie 3.2)**.

9.
De genetische stabiliteit van een bepaald stuk DNA, met de structuur van een veelvuldig herhaald simpel basismotief (een zogeheten "ESTR"), is verstoord in nageslacht uit bestraald sperma **(Sectie 3.3)**.

10.
Door de ontwikkeling van de HIGH-meting, voor heterologe ICSI en gamma-H2AX (γH2AX), is een zeer gevoelige bepaling van het aantal dubbel strengs DNA breuken in humaan sperma mogelijk **(Sectie 4.1)**.

11.
De HIGH-meting is gebruikt voor de vergelijking van de hoeveelheid dubbel strengs DNA breuken in sperma van een klein aantal fertiele en subfertiele mannen. Er was geen verschil in de gemiddelde hoeveelheid breuken per zaadcelkern. De fractie cellen met tenminste 1 een dubbel strengs DNA breuk was echter verhoogd in de subfertiele mannen **(Sectie 4.1)**.

12.
De HIGH-meting toonde aan dat onbeweeglijk sperma in 70% van de gevallen direct in de eicel uiteenvalt door de hoge mate van DNA schade dat het bij zich draagt **(Sectie 4.1)**.

13.
Het 1-cellige embryo kenmerkt zich door het bezit van 2 kernen, een van vader en een van moeder. Bij IVF worden echter ook 1-cellige embryo's aangetroffen met maar 1 kern. Deze 1-kernige embryo's ontstaan doordat het chromatine van de vader en de moeder vroegtijdig samensmelten. Bij 1-kernige embryo's na ICSI is deze of van de vader of van de moeder afkomstig **(Sectie 4.2)**.

14.
Het aantal 1-kernige 1-cellige embryo's bij muis IVF is vergelijkbaar met dat gevonden bij mens. In de muis zijn er aanwijzingen voor een genetische factor bij het ontstaan van dit soort embryo's **(Sectie 4.2)**.

References

1. Hayashi,S., Yang,J., Christenson,L., Yanagimachi,R., & Hecht,N.B. Mouse Pre-implantation Embryos Developed from Oocytes Injected with Round Spermatids or Spermatozoa Have Similar but Distinct Patterns of Early mRNA Expression. *Biol. Reprod.*(2003).

2. Ziyyat,A. & Lefevre,A. Differential gene expression in pre-implantation embryos from mouse oocytes injected with round spermatids or spermatozoa. *Hum. Reprod.* **16**, 1449-1456 (2001).

3. Kishigami,S. *et al.* Epigenetic abnormalities of the mouse paternal zygotic genome associated with microinsemination of round spermatids. *Dev. Biol.* **289**, 195-205 (2006).

4. Yamazaki,T., Yamagata,K., & Baba,T. Time-lapse and retrospective analysis of DNA methylation in mouse preimplantation embryos by live cell imaging. *Dev. Biol.* **304**, 409-419 (2006).

5. Olson,S.B. & Magenis,R.E. Preferential paternal origin of de novo structural chromosome rearrangements in *The Cytogenetics of Mammalian Autosomal Rearrangements* 583-599 (Alan R. Liss, Inc., 1988).

6. Spano,M., Seli,E., Bizzaro,D., Manicardi,G.C., & Sakkas,D. The significance of sperm nuclear DNA strand breaks on reproductive outcome. *Curr. Opin. Obstet. Gynecol.* **17**, 255-260 (2005).

7. Lewis,S.E. & Aitken,R.J. DNA damage to spermatozoa has impacts on fertilization and pregnancy. *Cell Tissue Res.* **322**, 33-41 (2005).

8. Zini,A. & Libman,J. Sperm DNA damage: importance in the era of assisted reproduction. *Curr. Opin. Urol.* **16**, 428-434 (2006).

9. Ramos,L. & Wetzels,A.M. Low rates of DNA fragmentation in selected motile human spermatozoa assessed by the TUNEL assay. *Hum. Reprod.* **16**, 1703-1707 (2001).

10. Bonduelle,M. *et al.* Prenatal testing in ICSI pregnancies: incidence of chromosomal anomalies in 1586 karyotypes and relation to sperm parameters. *Hum. Reprod.* **17**, 2600-2614 (2002).

11. Fenwick,J., Platteau,P., Murdoch,A.P., & Herbert,M. Time from insemination to first cleavage predicts developmental competence of human preim-

plantation embryos in vitro. *Hum. Reprod.* **17**, 407-412 (2002).

12. Sakkas,D., Shoukir,Y., Chardonnens,D., Bianchi,P.G., & Campana,A. Early cleavage of human embryos to the two-cell stage after intracytoplasmic sperm injection as an indicator of embryo viability. *Hum. Reprod.* **13**, 182-187 (1998).

13. Kuschel,B. *et al.* Variants in DNA double-strand break repair genes and breast cancer susceptibility. *Hum. Mol. Genet.* **11**, 1399-1407 (2002).

14. Han,J., Colditz,G.A., Samson,L.D., & Hunter,D.J. Polymorphisms in DNA double-strand break repair genes and skin cancer risk. *Cancer Res.* **64**, 3009-3013 (2004).

15. Kadouri,L. *et al.* A single-nucleotide polymorphism in the RAD51 gene modifies breast cancer risk in BRCA2 carriers, but not in BRCA1 carriers or noncarriers. *Br. J. Cancer* **90**, 2002-2005 (2004).

16. Seedhouse,C., Faulkner,R., Ashraf,N., Das-Gupta,E., & Russell,N. Polymorphisms in genes involved in homologous recombination repair interact to increase the risk of developing acute myeloid leukemia. *Clin. Cancer Res.* **10**, 2675-2680 (2004).

17. Auranen,A. *et al.* Polymorphisms in DNA repair genes and epithelial ovarian cancer risk. *Int. J. Cancer* **117**, 611-618 (2005).

18. Poplawski,T. *et al.* DNA damage and repair in gastric cancer--a correlation with the hOGG1 and RAD51 genes polymorphisms. *Mutat. Res.* **601**, 83-91 (2006).

19. Ryk,C., Kumar,R., Thirumaran,R.K., & Hou,S. M. Polymorphisms in the DNA repair genes XRCC1, APEX1, XRCC3 and NBS1, and the risk for lung cancer in never- and ever-smokers. *Lung Cancer* **54**, 285-292 (2006).

20. Thirumaran,R.K. *et al.* Single nucleotide polymorphisms in DNA repair genes and basal cell carcinoma of skin. *Carcinogenesis* **27**, 1676-1681 (2006).

21. Zienolddiny,S. *et al.* Polymorphisms of DNA repair genes and risk of non-small cell lung cancer. *Carcinogenesis* **27**, 560-567 (2006).

22. Braude,P., Bolton,V., & Moore,S. Human gene expression first occurs between the four- and eight-cell stages of preimplantation development. *Nature* **332**, 459-461 (1988).

23. Prisant,N. *et al.* Ultrastructural nuclear defects and increased chromosome aneu-

ploidies in spermatozoa with elongated heads. *Hum. Reprod.* **22**, 1052-1059 (2007).

24. Rudak,E., Jacobs,P.A., & Yanagimachi,R. Direct analysis of the chromosome constitution of human spermatozoa. *Nature* **274**, 911-913 (1978).

25. Lee,J.D., Kamiguchi,Y., & Yanagimachi,R. Analysis of chromosome constitution of human spermatozoa with normal and aberrant head morphologies after injection into mouse oocytes. *Hum. Reprod.* **11**, 1942-1946 (1996).

26. Yoshida,N. & Perry,A.C. Piezo-actuated mouse intracytoplasmic sperm injection (ICSI). *Nat. Protoc.* **2**, 296-304 (2007).

27. Veuger,S.J., Curtin,N.J., Richardson,C.J., Smith,G.C., & Durkacz,B.W. Radiosensitization and DNA repair inhibition by the combined use of novel inhibitors of DNA-dependent protein kinase and poly(ADP-ribose) polymerase-1. *Cancer Res.* **63**, 6008-6015 (2003).

28. Sotolongo,B., Huang,T. T., Isenberger,E., & Ward,W. S. An endogenous nuclease in hamster, mouse, and human spermatozoa cleaves DNA into loop-sized fragments. *J. Androl* **26**, 272-280 (2005).

29. Shaman,J.A., Prisztoka,R., & Ward,W.S. Topoisomerase IIB and an Extracellular Nuclease Interact to Digest Sperm DNA in an Apoptotic-Like Manner. *Biol. Reprod.*(2006).

30. Yamauchi,Y., Shaman,J.A., & Ward,W.S. Topoisomerase II-Mediated Breaks in Spermatozoa Cause the Specific Degradation of Paternal DNA in Fertilized Oocytes. *Biol. Reprod.* **76**, 666-672 (2007).

31. Roest,H.P. *et al.* Inactivation of the HR6B ubiquitin-conjugating DNA repair enzyme in mice causes male sterility associated with chromatin modification. *Cell* **86**, 799-810 (1996).

32. Greco,E. *et al.* ICSI in cases of sperm DNA damage: beneficial effect of oral antioxidant treatment. *Hum. Reprod.* **20**, 2590-2594 (2005).

33. Ting,A.H., McGarvey,K. M., & Baylin,S.B. The cancer epigenome--components and functional correlates. *Genes Dev.* **20**, 3215-3231 (2006).

List of shared publications

Motile human normozoospermic and oligozoospermic semen samples show a difference in double-strand DNA break incidence.
Derijck AA, **van der Heijden GW**, Ramos L, Giele M, Kremer JA, de Boer P.
Human Reproduction, June 2007, featured on cover

Chromosome-wide nucleosome replacement and H3.3 incorporation during mammalian meiotic sex chromosome inactivation.
van der Heijden GW, **Derijck AA**, Posfai E, Giele M, Pelczar P, Ramos L, Wansink DG, van der Vlag J, Peters AH, de Boer P.
Nature Genetics, February 2007

Maternal effects of the scid mutation on radiation-induced transgenerational instability in mice.
Hatch T, **Derijck AA**, Black PD, **van der Heijden GW**, de Boer P, Dubrova YE.
Oncogene, Januari 2007

Transmission of modified nucleosomes from the mouse male germline to the zygote and subsequent remodeling of paternal chromatin.
van der Heijden GW, **Derijck AA**, Ramos L, Giele M, van der Vlag J, de Boer P.
Developmental Biology, October 2006

gammaH2AX signalling during sperm chromatin remodelling in the mouse zygote.
Derijck AA, **van der Heijden GW**, Giele M, Philippens ME, van Bavel CC, de Boer P.
DNA Repair, August 2006

Asymmetry in histone H3 variants and lysine methylation between paternal and maternal chromatin of the early mouse zygote.
van der Heijden GW, Dieker JW, **Derijck AA**, Muller S, Berden JH, Braat DD, van der Vlag J, de Boer P.
Mechanisms of Development, September 2005

Additional publications AHAA Derijck

Partitioning and plasticity of repressive histone methylation states in mammalian chromatin.
Peters AH, Kubicek S, Mechtler K, O'Sullivan RJ, **Derijck AA**, Perez-Burgos L, Kohlmaier A, Opravil S, Tachibana M, Shinkai Y, Martens JH, Jenuwein T.
Molecular Cell, December 2003

Suv39h-mediated histone H3 lysine 9 methylation directs DNA methylation to major satellite repeats at pericentric heterochromatin.
Lehnertz B, Ueda Y, **Derijck AA**, Braunschweig U, Perez-Burgos L, Kubicek S, Chen T, Li E, Jenuwein T, Peters AH.
Current Biology, 2003 July 2003

Additional publications GW van der Heijden

Fen1 does not control somatic hypermutability of the (CTG)(n)(CAG)(n) repeat in a knock-in mouse model for DM1.*
van den Broek WJ, Nelen MR, **van der Heijden GW**, Wansink DG, Wieringa B.
FEBS Letters, October 2006

Reduced oocyte activation and first cleavage rate after ICSI with spermatozoa from a sterile mouse chromosome mutant.
Baart EB, **van der Heijden GW**, van der Hoeven FA, Bakker R, Cooper TG, de Boer P.
Human Reproduction, May 2004

Alwin Derijck was born on the 22nd of August 1978 in Roosendaal and Nispen, The Netherlands. He finished secondary school at the "Katholieke Scholengemeenschap Etten-Leur" in 1996. He started his studies at the "Biologie en medische laboratorium opleiding (HLO)" at the "Hogeschool Brabant". During an internship at the Erasmus University Rotterdam at the department of Cell Biology and Genetics, prof. J.H.J. Hoeijmakers raised his interests in DNA repair mechanisms. After finishing his Bachelor of Science in Biotechnology with honours in 2000, he continued studying Biology at the Wageningen University. From 2001 to 2002 he joined the group of dr. T. Jenuwein at the Research Institute for Molecular Pathology, Vienna, working on embryonic stem cells and histone methyltransferases, guided by dr. A.H.F.M. Peters. After obtaining a Master of Science degree in Cell Biology with distinction in 2002 he started his Ph.D. project at the Department of Obstetrics and Gynaecology of the Radboud University Nijmegen Medical Centre under supervision of dr. P. de Boer. In a joined effort with Godfried van der Heijden he worked on zygotic double stranded DNA break repair and inheritance of histones and their modifications, as described in this thesis. In June 2007, he switched research fields by joining the laboratory of dr. R.J. Pasterkamp at the Department of Pharmacology and Anatomy, Rudolf Magnus Institute for Neuroscience, University Medical Center Utrecht, as a postdoctoral fellow. His postdoctoral work involves the signaling of axon guidance molecules and embryonic stem cell treatment for Parkinson's Disease.

Alwin Derijck, geboren op 22 augustus 1978 in Roosendaal en Nispen, voltooide in 1996 het VWO aan de Katholieke Scholengemeenschap Etten-Leur. Hij startte zijn studie, Biologie en medische laboratorium opleiding (HLO), aan de Hogeschool Brabant. Tijdens een stage aan de Erasmus Universiteit Rotterdam, afdeling Celbiologie en Genetica, wekte prof. J.H.J. Hoeijmakers zijn interesse in DNA herstel mechanismen. Na het met lof behalen van zijn ingenieurs (ing) diploma Biotechnologie in 2000, continueerde hij met de studie Biologie aan de Wageningen Universiteit. Van 2001 tot 2002 maakte hij deel uit van de groep van dr. T. Jenuwein in het Research Institute of Molecular Pathology te Wenen, werkend aan embryonale stamcellen en histon methyltransferases onder begeleiding van dr. A.H.F.M. Peters. Na het met lof behalen van het ingenieurs (IR) diploma Celbiologie in 2002 startte hij zijn junior- onderzoeker project bij de afdeling Verloskunde en Gynaecologie aan het Medisch Centrum van de Radboud Universiteit Nijmegen onder begeleiding van dr. P. de Boer. In samenwerking met Godfried van der Heijden werkte hij aan zygotisch herstel van dubbelstrengs DNA breuken en vererving van histonen en hun modificaties, als beschreven in dit proefschrift. In 2007 werd hij post-doc in de groep van dr. R.J. Pasterkamp in het Rudolf Magnus Instituut voor Neurowetenschappen, Universitair Medisch Centrum Utrecht. Hier betrad hij een nieuw onderzoeksveld, signaaltransductie van axon sturende moleculen en therapie voor de ziekte van Parkinson met behulp van embryonale stamcellen.

Godfried Willibrord van der Heijden was born on May 9th 1977 in Geldrop, The Netherlands. In 1996 he graduated from secondary school at the Philips van Horne Scholengemeenschap in Weert. From 1996 to 2002 he studied Bioprocess Engineering at Wageningen University. The major subject, cell biology, included three training periods, in Wageningen, Boston and Nijmegen. The research in Wageningen was supervised by dr. Peter de Boer and was aimed at induction of premature chromosome condensation and characterization of the sperm chromosomes following mouse ICSI. In the laboratory of dr. David Page, at the Massachusetts Institute of Technology in Boston, he worked on evolution rates of testis expressed genes and the characterization of a novel testis expressed gene under supervision of dr. Jeremy Wang. His third training period was at the Department of Obstetrics and Gynaecology of the Radboud University Nijmegen Medical Centre, again under supervision of dr. Peter de Boer. This project segued into his Ph.D. research project, a joined effort with Alwin Derijck on zygotic inheritance of histones and their modifications and double stranded DNA break repair, as described in this thesis. In 2007 he moved to Baltimore, USA, to join the group of dr. Alex Bortvin, at the Carnegie Institute of Embryology, to continue research on the germ line and pre-implantation development.

Godfried Willibrord van der Heijden werd op 9 mei 1977 te Geldrop geboren. Van 1989 tot 1996 zat hij op de Philips van Horne Scholengemeenschap in Weert en doorliep daar achtereenvolgens de HAVO en het VWO. Na het behalen van dit laatste diploma begon hij de studie Bioprocestechnologie aan de Wageningen Universiteit. Tijdens zijn studie koos hij voor de cellulaire/moleculaire specialisatie. Drie onderzoeks stages, in Wageningen, Boston en Nijmegen, maakten deel uit van deze specialisatie. Het onderzoek in Wageningen stond onder begeleiding van dr. Peter de Boer en had als doel een manier te vinden om premature chromosoom condensatie te induceren na muis ICSI. In het laboratorium van dr. David Page, op het Massachusetts Institute of Technology in Boston, bestudeerde hij onder begeleiding van dr. Jeremy Wang de evolutie snelheid van genen die specifiek in de testis tot expressie komen en de functie van een dergelijk gen. De derde onderzoeksstage vond plaats op de afdeling Verloskunde en Gynaecologie aan het Medisch Centrum van de Radboud Universiteit Nijmegen, wederom onder begeleiding van dr. Peter de Boer. Dit onderzoek mondde uiteindelijk uit in zijn junior-onderzoeker project met als focus de vererving van histonen en hun modificaties en zygotisch herstel van dubbelstrengs DNA breuken. De resultaten van dit project, dat is uitgevoerd in samenwerking met Alwin Derijck, zijn beschreven in dit proefschrift. In April 2007 verhuisde hij naar Baltimore in de Verenigde Staten en voegde hij zich bij de onderzoeksgroep van dr. Alex Bortvin op het Carnegie Institute. Hier zet hij zijn onderzoek aan de kiembaan en pre-implantatie embryogenese voort.

Om en nabij 6 jaar geleden initieerde de pijler voortplantingsgeneeskunde fundamenteel onderzoek naar de zygote. In het kader hiervan werden twee AIO projecten opgestart. Met de afronding van dit proefschrift komt er een eind aan deze projecten. Wij, de twee desbetreffende AIOs, hebben voor ons promotie-onderzoek zeer intensief samengewerkt. Daarom hebben we besloten er een dubbelpromotie van te maken. Ongebruikelijk, maar in ons geval eigenlijk vanzelfsprekend. Tijdens de vijf jaar die verstreek tussen het eerste experiment en de laatste printopdracht zijn er veel mensen intensief, zijdelings of rakelings, betrokken geweest bij het hier beschreven onderzoek.

Peter, als kapitein van ons onderzoeksbootje heb je ons de vrijheid gegeven om overstag te gaan wanneer we dat zeer graag wilden. Drieste ideeën mochten vaak getest worden en onverwachte bevindingen verkend. Maar altijd heb je het uiteindelijke doel in het vizier gehouden en gezorgd dat we daar aankwamen. Hoe moeilijk dat is wordt pas duidelijk als de trossen gelegd zijn en de lading gelost is. Hartelijk bedankt.

Jan, ook al lag ons onderzoeksgebied veelal ver van de kliniek en patiënt, je bleef altijd enthousiast, geïnteresseerd en kritisch. Dank hiervoor.

De soms wat bovenmatige zucht naar data werd veraangenaamd en vermenselijkt door Maud Giele en Liliana Ramos. Maud, je bent er zowat vanaf het begin bij geweest. Dank voor al het werk dat je hebt verzet en de verlevendiging. Liliana, dank voor de goede samenwerking, de gezellige diners bij je thuis en de koffie momenten bij de cilinder. Dank ook voor het opfleuren van het AIO bestaan met verhalen uit de wereldse kliniek.

Zoals te zien is aan alle namen boven de secties is er veel samengewerkt met mensen uit andere groepen. Esther Baart en Ilse van de Berg, Eszter Posfai en Antoine Peters, dank hiervoor. Marielle Phillipens, zonder jouw steun en toewijding was dit proefschrift de helft dunner geweest. Vele avonden was ik (Alwin) al wandelend door de catacomben van het Radboud met een obscuur verhulde bak op weg naar jouw domein bij Radiotherapie waar jij me immer enthousiast begroette. Voor de vele vrijwillige uren zijn wij je zeer dankbaar. Lars van Bolderen, als complementerend steunpilaar van de afdeling Radiotherapie was jouw bijdrage onmisbaar. We also would like to thank Professor Yuri Dubrova and Timothy Hatch for their fruitful collaboration. Frank Wagener, de samenwerking was minder vruchtbaar dan we hadden gehoopt, maar in ieder geval zeer prettig, bedankt. Een zeer waardevolle en intensieve samenwerking is ontstaan met het Laboratorium Nierziekten. Zonder Jürgen Dieker maar vooral Johan van der Vlag was het een geheel ander proefschrift geworden. Bedankt!

In het bijzonder willen wij professor Bé Wieringa en professor Henk Stunnenberg bedanken. Het onbaatzuchtig openstellen van jullie onderzoeksgroepen (en voorraad antilichamen) was onmisbaar voor het slagen van dit project. Veel tijd hebben we doorgebracht met de mensen van deze afdelingen, hoewel we feitelijk buitenstaanders waren, hebben we ons er altijd thuis gevoeld. Nu kan er een lange lijst van namen komen maar dat is een uitnodiging tot onvolledigheid. Daarom, iedereen van de 6de (ook afdeling Moleculaire Dierfysiologie) en de 3de, hartelijk dank.

Toch nog even uitlichten: Huib Croes en Jack Fransen, altijd bereid om "onze" microscoop weer haarscherp af te stellen. Rick Wansink voor het naar een taalkundig hoger plan tillen van enkele van onze manuscripten. We herinneren ons Wilma Peters en voelen haar afwezigheid.
Henk Jongsma, hartelijk dank voor het ontwikkelen van de onmisbare "mouse database". Anneke Punt, dank voor de adviezen omtrent muis IVF bij de aanvang van ons project. Iedereen van het klinische lab van voortplantingsgeneeskunde, waar de cake altijd werd gedeeld, bedankt.
De radertjes van onze soepel lopende machine zouden krakend tot stilstand zijn gekomen zonder de hulp van Emiel Lindeman. Dank voor je ondersteuning bij het op peil houden van onze voorraden.
In de beginjaren passeerden enkele studenten de revue die ieder hun sporen hebben nagelaten. In chronologische volgorde: Christian Boschker, Debby Melissen, Noortje Bax, Sabine de Brouwer en Casandra van Bavel. Dank voor jullie medewerking en uithoudingsvermogen.
Wilma Janssen en Connie Verbaas, de eerste jaren in het pijpenla-lab waren wat krap, maar dankzij jullie inschikkelijkheid werkte het. Onze dank hiervoor.
Veel muizen zijn verwerkt in dit proefschrift. Hun verzorging was in professionele en behulpzame handen van de mensen werkzaam in het CDL. Hartelijk dank hiervoor.
Het werken met zygotes is verre van praktisch. Om de gewenste proeven mogelijk te maken was een "custom made" CO_2 stoof noodzakelijk. Jos Evers en Theo Arnoldussen, bedankt. Zonder jullie hulp was onze "diamant" er nooit gekomen.
Als "ICT-manager" van de "de Boer groep" (Alwin), was het dirigeren van onze datastromen een taaie klus geworden zonder de hulp van Wim Abma, Benny Hendriks en Marcus Hendriks. Bedankt.
Dankwoord Alwin
Edwin Commandeur, je snelle "on demand" hulp met statistische vragen was fenomenaal. Je motiverende persoonlijkheid wist me soepel te houden tijdens Capoeira, en bovendien positief. Obrigado!
Aan alle betrokken familieleden en vrienden en in het bijzonder pap en mam, bedankt.
Als er iemand is wie me met name in het laatste traject van deze onderneming er doorheen heeft weten te slepen, dan kan dat maar een persoon zijn. Ilse, ik dank je voor je unieke steun.
Dankwoord Godfried
De afgelopen jaren lieten familie en vrienden mij steevast realiseren dat er wel degelijk meer was dan Histone H3.3 en dergelijke. Vader, moeder, broers, zussen, neefjes & nichtjes maar zeker ook vrienden, bedankt.
Querida linda Adrianita, que suerte hayas venido a Holanda. Gracias por todo lo que has hecao para mi estos años y por nuestra bonita amistad.
Dragi Ozrene, Bilo mi je jako drago kad si do šao u Bottendaal. Hvala ti za sva dobra sjećanja i za tvoje prijateljstvo. Rock on.